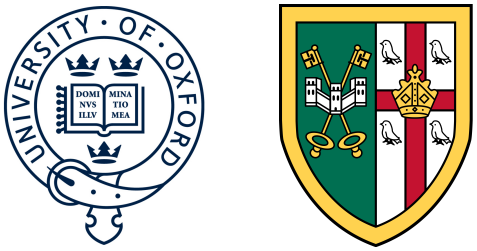
Investigating the role of BRCA2 in the maintenance of chromosomal stability



Lucia Rampazzo
St. Peter's College Oxford
University of Oxford

A thesis submitted for the degree of
Doctor of Philosophy

Michaelmas Term 2021

Alla mia *famiglia*
e a *Luca*.

Declaration

I declare that the work presented in this thesis is my own work, unless otherwise stated in the text. Davide Torre, a Master's student from the University of Bologna, joined the laboratory of Dr. Fumiko Esashi from February 2019 to December 2019. DT worked on the HAC project (Chapter 3) under my supervision. DT performed the experiments presented in Figures 3.21, 3.22, 3.23, 3.24, 3.25, 3.26, 3.27, 3.28, 3.29.

Abstract

Genetic information is preserved across cell divisions by the faithful transmission of chromosomes. Mutations in the *BRCA2* gene predispose individuals to breast and ovarian cancers. BRCA2-deficient cells are characterised by an aberrant structure and number of chromosomes. The former phenotype has been generally explained by the BRCA2 function in the DNA repair, through the homologous recombination (HR) pathway mediated by RAD51 recombinase. However, it is not fully understood how BRCA2 deficiency leads to an abnormal number of chromosomes. Proper chromosome segregation in mitosis requires the orderly assembly of kinetochore components at specific DNA regions of chromosomes, called centromeres. Due to their complex structure, centromeres are particularly susceptible to DNA damage, which in turn can lead to abnormal chromosomal rearrangements. Despite the importance of maintaining centromere integrity, the mechanism protecting centromeric DNA remains largely unknown. Throughout my research, I explored the function that BRCA2 may play in the protection and formation of centromeres.

In this thesis, the role of BRCA2 at centromeres was investigated using three experimental approaches. Firstly, I utilised a previously established human HT1080 cell line carrying a small extra-chromosome, called the alphoid^{tetO} HAC, engineered from synthetic centromeric alphoid DNA arrays. Using this system, I showed that BRCA2 is important for the faithful transmission of the HAC during the cell division, whereas the same conclusion could not be drawn for other HR factors, such as RAD51. Interestingly, however, I observed that tethering the RAD51 binding motif of BRCA2, BRC4, to the HAC negatively impacted on the HAC maintenance. Secondly, the impact of BRCA2 depletion on endogenous centromeres was investigated in HeLa cells. Using immunofluorescence experiments, I found no clear evidence that BRCA2 protects centromeric DNA from damage, but unexpectedly observed that the removal of BRCA2 changed the chromatin status and the centromeres formation. Lastly, I generated CRISPR-modified HCT116 cell lines, in which endogenous BRCA2 is tandem tagged with a fluorescent protein and an auxin-inducible degron (AID). This cell line is a novel tool to study the localisation and functions of BRCA2 at every stage of the cell cycle. Using this system, I observed that BRCA2 partially localised at kinetochores and centromeres in interphase.

Based on the results presented in this thesis, I propose that BRCA2 may have a DNA-repair independent function at centromeres. BRCA2 may be important for chromatin remodelling, which can affect the centromere and kinetochore formation. These findings shed light on the BRCA2 function and suggest new ways by which BRCA2 may promote chromosome maintenance.

Contents

Acronyms ix

1 Introduction 1
- 1.1 Genome instability . . . 1
  - 1.1.1 Sources of DNA breaks . . . 3
  - 1.1.2 DNA damage response . . . 4
  - 1.1.3 DNA repair mechanisms . . . 5
    - 1.1.3.1 Double-strand break repair . . . 6
    - 1.1.3.2 Repair mechanisms after replication stress . . . 9
- 1.2 BRCA2 . . . 12
  - 1.2.1 Implications of BRCA2 in cancer and genome stability . . . 12
  - 1.2.2 BRCA2 structure . . . 14
  - 1.2.3 BRCA2 functions . . . 16
    - 1.2.3.1 Homologous recombination (HR) . . . 16
    - 1.2.3.2 Replication fork protection (FP) . . . 17
    - 1.2.3.3 Transactivation activity . . . 17
    - 1.2.3.4 Mitotic function . . . 18
    - 1.2.3.5 Cell cycle regulation of BRCA2 functions . . . 20
  - 1.2.4 Open questions . . . 21
- 1.3 Centromeres and kinetochores . . . 24
  - 1.3.1 Centromere structure and function . . . 24
  - 1.3.2 CENP-A deposition . . . 26
  - 1.3.3 Kinetochore structure and formation . . . 29
  - 1.3.4 Spindle Assembly Checkpoint . . . 32
- 1.4 Research aim . . . 35

2 Materials and Methods 37
- 2.1 Tables of materials . . . 38
  - 2.1.1 Mammalian cell lines . . . 38
  - 2.1.2 Plasmids . . . 42
  - 2.1.3 Oligonucleotides . . . 43
  - 2.1.4 Antibodies . . . 46
  - 2.1.5 siRNAs . . . 48
  - 2.1.6 Buffers and solutions . . . 49
  - 2.1.7 List of materials used . . . 50
- 2.2 DNA analysis techniques . . . 54
  - 2.2.1 Genomic DNA extraction . . . 54
  - 2.2.2 Agarose gel electrophoresis . . . 54
  - 2.2.3 Restriction enzyme digestion . . . 55
  - 2.2.4 Polymerase chain reaction (PCR) . . . 55

2.2.5 DNA plasmid cloning . . . 56
2.2.6 Gibson Assembly . . . 57
2.2.7 Colony PCR . . . 58
2.2.8 Sanger sequencing . . . 58
2.2.9 Generation of tetR-constructs . . . 58
2.3 Bacterial techniques . . . 65
2.3.1 Heat-shock transformation . . . 65
2.3.2 Bacterial cultures . . . 65
2.3.3 Glycerol stock . . . 65
2.3.4 Extraction of DNA plasmid . . . 65
2.4 Mammalian cell culture techniques . . . 67
2.4.1 Cell culture propagation and storage . . . 67
2.4.2 Preparation of conditioned culture medium . . . 67
2.4.3 Transfections . . . 68
2.4.4 Generation of stable cell lines . . . 69
2.4.5 Generation of CRISPR-modified cell lines . . . 69
2.5 Protein analysis techniques . . . 71
2.5.1 Western blot (WB) . . . 71
2.5.2 Immunoprecipitation . . . 72
2.5.3 Chromatin fractionation . . . 73
2.6 Cell analysis techniques . . . 74
2.6.1 Analysis of the cell cycle profile by propidium iodide staining . . . 74
2.6.2 Analysis of the mitotic index by flow cytometry . . . 74
2.6.3 Analysis of cell proliferation by dye dilution assay . . . 75
2.6.4 Analysis of cell proliferation by growth curve . . . 75
2.6.5 Cell viability assay . . . 76
2.6.6 Metaphase preparation . . . 77
2.6.7 Fluorescence In Situ Hybridization (FISH) . . . 77
2.6.8 Immunofluorescence (IF) . . . 78
2.6.9 Live-cell imaging . . . 79
2.6.10 EdU labelling . . . 80
2.6.11 Analysis of the mitotic stage . . . 80
2.6.12 Analysis of mitotic defects . . . 81
2.6.13 Proximity Ligation Assay (PLA) . . . 81
2.6.14 Analysis of the nuclear actin filaments . . . 82
2.6.15 HAC stability assay after drug treatment . . . 82
2.6.16 HAC stability assay after siRNA treatment . . . 83
2.6.17 HAC stability assay after tethering of tetR-constructs . . . 83
2.7 Data analysis techniques . . . 85
2.7.1 Sequencing data analysis . . . 85
2.7.2 Imaging data analysis . . . 85
2.7.3 Flow cytometry data analysis . . . 85
2.7.4 Statistics . . . 85

3 The role of genotoxic stress and HR factors in chromosome inheritance: exploiting the Human Artificial Chromosome as a model system 88
3.1 Introduction . . . 89
3.1.1 The development of the alphoid^{tetO} HAC . . . 90
3.1.2 The HAC loss assay using the alphoid^{tetO} EGFP-HAC . . . 92

3.2 Results . . . 95
3.2.1 Effect of replication stress on HAC stability using the alphoid^{tetO} EGFP-HAC . . . 95
3.2.2 Effect of HR proteins on HAC stability using the alphoid^{tetO} HAC-dGFP . . . 99
3.2.2.1 Optimisation of the HAC loss assay . . . 102
3.2.2.2 Effect of HR proteins depletion on HAC stability . . . 104
3.2.2.3 Cell cycle arrest upon BRCA2 and RAD51 depletion . . . 111
3.2.2.4 Effect of BRCA2 depletion in combination with PALB2 and RAD51 knockdown on HAC stability . . . 113
3.2.2.5 BRCA2 and RAD51 protect the HAC from replication stress . . . 118
3.2.3 Effect of HR factors on HAC stability using tetO-tetR system . . . 122
3.2.3.1 Generation of stable cell lines . . . 123
3.2.3.2 Validation of the tetR-mCherry constructs . . . 128
3.2.3.3 Tethering of the BRC4 wild-type to the HAC increases HAC loss . . . 131
3.3 Discussion . . . 138
3.3.1 Effect of replication stress and B02 treatment on the HAC stability using the alphoid^{tetO} EGFP-HAC . . . 138
3.3.2 Technical considerations affecting the HAC loss assay . . . 139
3.3.3 BRCA2 depletion increases HAC loss in a HR independent manner in unperturbed cells . . . 142
3.3.4 The effect of the tetR-mCherry expressing cell line on the HAC stability . . . 145

4 Investigating the role of BRCA2 at endogenous centromeres 148
4.1 Introduction . . . 149
4.2 Results . . . 152
4.2.1 BRCA2 depletion increases mitotic defects in HeLa cells . . . 152
4.2.2 Effect of replication stress and BRCA2 depletion on centromeric DNA stability . . . 158
4.2.3 Chromatin changes upon BRCA2 depletion . . . 169
4.3 Discussion . . . 182
4.3.1 Investigating the role of BRCA2 in centromere DNA stability during replication . . . 182
4.3.2 Depletion of BRCA2 leads to chromatin movement, senescence-like phenotype and abnormal centromere formation . . . 184

5 Investigating the role of BRCA2 at kinetochores 188
5.1 Introduction . . . 189
5.1.1 The challenge of detecting BRCA2 . . . 194
5.2 Results . . . 196
5.2.1 Generation of CRISPR-modified cell lines for BRCA2 tagging . . . 196
5.2.2 BRCA2 localisation with kinetochore and centromere components during the cell cycle . . . 204
5.2.3 Effect of BRCA2 depletion on kinetochore recruitment at centromeres . . . 206
5.3 Discussion . . . 209

5.3.1 A new system to study BRCA2 localisation in time and space . . 211

6 Discussion and Conclusions **213**
6.1 Summary of thesis 213
6.1.1 BRCA2 regulated RAD51-mediated recombination at centromeres 214
6.1.2 Proposed function of BRCA2 as a chromatin linker and structural nuclear protein 215
6.1.3 BRCA2, kinetochores and centromeres 218
6.1.4 Development of CRISPR-modified cells for BRCA2 tagging . . . 218
6.2 Concluding remarks 219

A Supplementary information **220**
A.1 Macros for image analysis 222
A.1.1 Micronuclei counting 222
A.1.2 PLA foci counting 222
A.1.3 Colocalisation analysis 222

Acknowledgements **224**

Bibliography **226**

List of Figures

1.1 Initiation of the DNA damage response . . . 5
1.2 Double-strand break repair mechanisms . . . 8
1.3 Mechanisms of DNA repair at replication fork . . . 11
1.4 BRCA2 structure . . . 14
1.5 Schematic representation of BRCA2 phosphorylated sites . . . 21
1.6 Centromere structure . . . 25
1.7 Kinetochore structure . . . 30
1.8 The Spindle Assembly Checkpoint . . . 34

2.1 Generation of pJETY3-tetR-EYFP-BRC4/B2.8/WD40 plasmids . . . 60
2.2 Generation of pJETY3-tetR-mCherry plasmids . . . 62
2.3 Generation of pJETY3-tetR-mCherry-IRES-Puro plasmids . . . 64

3.1 The HAC loss assay using the alphoid^{tetO} EGFP-HAC . . . 94
3.2 Cell viability assay in HT1080 alphoid^{tetO} EGFP-HAC cells in presence of aphidicolin (APH), hydroxyurea (HU) and RAD51 inhibitor (B02) . . . 96
3.3 Effect of replication stress and RAD51 inhibitor on HAC stability . . . 98
3.4 The HAC loss assay using the alphoid^{tetO} HAC-dGFP . . . 101
3.5 Dye dilution assay using Far Red Cell Trace . . . 103
3.6 Table of Division Indexes (DI) . . . 104
3.7 Time course of the GFP level in HT1080 HAC-dGFP cells upon siRNA treatments . . . 106
3.8 Western blot showing the level of protein depletion in HT1080 HAC-dGFP cells upon siRNA treatments . . . 107
3.9 Dye dilution assay after siRNA treatment . . . 108
3.10 HAC loss after BRCA2, PALB2 and RAD51 depletion by siRNAs . . . 110
3.11 Cell cycle Profile upon BRCA2 and RAD51 depletion . . . 112
3.12 Mitotic index upon BRCA2 depletion . . . 113
3.13 Western blot showing the level of protein depletion in HT1080 HAC-dGFP cells upon combined siRNA treatments . . . 114
3.14 Dye dilution assay after combined siRNA treatment . . . 115
3.15 Analysis of the HAC loss at 72 h after siRNA treatment . . . 117
3.16 Cell cycle profile 72 h after siRNA treatment and aphidicolin treatment . . . 119
3.17 Cell cycle Profile upon BRCA2 and RAD51 depletion upon aphidicolin treatment . . . 120
3.18 Analysis of the HAC loss at 72 h after siRNA treatment . . . 121
3.19 The BRC4, B2.8 and WD40 fragments . . . 122
3.20 Generation of HT1080 HAC-dGFP cells expressing WD40 constructs . . . 125
3.21 Generation of HT1080 HAC-dGFP cells expressing BRC4 constructs . . . 127

3.22 BRCA2 binding to tetR-mCherry-WD40 constructs . . . 128
3.23 RAD51 binding to tetR-mCherry-BRC4 constructs . . . 129
3.24 Localisation of tetR-mCherry-constructs to the tetO-HAC upon doxycycline removal . . . 130
3.25 HAC loss analysis with the tetR-mCherry expressing cells . . . 131
3.26 Growth curves of HT1080 HAC-dGFP cells expressing tetR-mCherry-BRC4 constructs . . . 133
3.27 Analysis of the HAC loss at 96 h after seeding . . . 134
3.28 Growth curves of HT1080 HAC-dGFP cells expressing tetR-mCherry-WD40 constructs . . . 136
3.29 Analysis of the HAC loss at 96 h after seeding . . . 137
3.30 Diagram for the HAC loss analysis . . . 141

4.1 Centromere abnormalities upon HR protein depletion. . . . 151
4.2 Mitotic index upon BRCA2 depletion in HeLa cells . . . 153
4.3 Mitotic defects upon BRCA2 depletion in HeLa cells . . . 155
4.4 Micronuclei formation upon BRCA2 depletion in HeLa cells . . . 157
4.5 Immunofluorescence (IF) of γH2AX and CENP-C in the presence and absence of BRCA2 . . . 160
4.6 Manders' Colocalisation Coefficient (MCC) between CENP-C and γH2AX in the presence and absence of BRCA2 and APH treatment . . . 161
4.7 Immunofluorescence (IF) of γH2AX and CENP-B in the presence and absence of BRCA2 . . . 162
4.8 Manders' Colocalisation Coefficient (MCC) between CENP-B and γH2AX in the presence and absence of BRCA2 and APH treatment . . . 163
4.9 Proximity Ligation Assay (PLA) between CENP-C and γH2AX in the the presence and absence of BRCA2 . . . 165
4.10 Proximity Ligation Assay (PLA) between CENP-B and γH2AX in the presence and absence of BRCA2 . . . 166
4.11 Cell cycle profile upon BRCA2 depletion and APH treatment in HeLa cells. . . . 168
4.12 p53 and p21 expression upon BRCA2 depletion in HeLa cells . . . 169
4.13 Nuclear expansion upon BRCA2 depletion and APH treatment in HeLa cells . . . 171
4.14 DNA content upon BRCA2 depletion and APH treatment in HeLa cells . 172
4.15 Nuclear actin filaments (NAFs) formation upon BRCA2 depletion and APH treatment in HeLa cells . . . 174
4.16 CENPs foci formation upon BRCA2 depleteion and APH treatment in HeLa cells . . . 176
4.17 CENP-A and CENP-B foci formation upon BRCA2 depletion in HeLa cells 177
4.18 Cellular fractionation analysis upon BRCA2 depletion in HeLa cells . . . 178
4.19 Acetyl-Lysin and H3K9me3 intensity upon BRCA2 depletion in HeLa cells 180
4.20 HP1 intensity upon BRCA2 depletion in HeLa cells . . . 181

5.1 BRCA2 interactome . . . 191
5.2 BRCA2 binding partners in synchronised culture . . . 193
5.3 Imaging analysis of HeLa Kyoto NFLAP-BRCA2 cells . . . 195
5.4 Generation of CRISPR-modified HCT116 mAID-Halo-BRCA2 cell line . 197

5.5 Generation of CRISPR-modified HCT116 mAID-mNeonGreen-BRCA2 cell line 200
5.6 mNeonGreen-BRCA2 localisation in the presence and absence of HU . . 201
5.7 Localisation of mNeonGreen-BRCA2 with DNA damage marker during the cell cycle 203
5.8 Localisation of mNeonGreen-BRCA2 with MIS12 complex during the cell cycle 205
5.9 Localisation of mNeonGreen-BRCA2 with centromeres during the cell cycle 206
5.10 Effect of BRCA2 depletion on DSN1 recruitment at centromeres during the cell cycle 208

6.1 Proposed Model 2: BRCA2 acts as a chromatin linker and a structural nuclear protein 217

A.1 Diagram for the HAC loss analysis 221

List of Tables

2.1 Mammalian cell lines used in this thesis . . . 39
2.2 Stable cell lines generated in this thesis . . . 40
2.3 CRISPR-modified cell lines generated in this thesis . . . 41
2.4 Plasmids used in this thesis . . . 42
2.5 Oligonucleotides used in this thesis . . . 43
2.6 Oligonucleotides used in this thesis . . . 44
2.7 Oligonucleotides used in this thesis . . . 44
2.8 Oligonucleotides used in this thesis . . . 45
2.9 FISH probes used in this thesis . . . 45
2.10 List of primary antibodies used in this thesis . . . 46
2.11 List of secondary antibodies used in this thesis . . . 47
2.12 List of siRNAs . . . 48
2.13 Buffers and solutions . . . 49
2.14 List of reagents used in this thesis . . . 50
2.15 List of reagents used in this thesis . . . 51
2.16 List of reagents used in this thesis . . . 52
2.17 List of drugs, antibiotics, kits and enzymes used in this thesis . . . 53
2.18 PCR reactions/protocols . . . 56
2.19 Sizes and volumes of cell culture dishes used in this thesis . . . 68

3.1 Doubling times of tetR-mCherry BRC4 constructs. . . . 132
3.2 Doubling times of tetR-mCherry WD40 constructs. . . . 135

Acronyms

γH2AX Histone H2AX phosphorylated at serine 139.

53BP1 TP53-binding protein 1.

APC/C Anaphase-promoting complex/cyclosome.

ATM Ataxia telangiectasia mutated.

ATR Ataxia telangiectasia and Rad3-related protein.

ATRIP ATR-interacting protein.

BAC Bacterial artificial chromosome.

BER Base-excision repair.

BIR Break-induced replication.

BRCA1 Breast cancer type 1 susceptibility protein.

BRCA2 Breast cancer type 2 susceptibility protein.

BSA Bovine Serum Albumin.

CCAN Constitutive-centromere associated network.

CDC20 Cell division cycle 20.

CDK Cyclin-dependent kinase.

CENP-A Centromere protein A.

CENP-B Centromere protein B.

CENP-C Centromere protein C.

ChIP Chromatin immunoprecipitation.

CHK1 Checkpoint kinase 1.

CHK2 Checkpoint kinase 2.

CIN Chromosomal instability.

CRISPR Clustered Regularly Interspaced Short.

CtIP CtBP-interacting protein.

dH$_2$O Distilled water.

DBD DNA binding domain.

DDR DNA damage response.

dHJ double Holliday junction.

DMEM Dulbecco's Modified Eagle Medium.

DNA Deoxyribonucleic acid.

dNTPs Deoxynucleoside triphosphates.

DSB Double-strand break.

DSS1 Deleted in split hand/split foot.

FISH Fluorescence In-Situ Hybridization.

FRAP Fluorescence recovery after photobleaching.

GCRs Gross chromosomal rearrangements.

GFP Green fluorescent protein.

GIN Genome instability.

H3K36me2 Dimethylation of histone H3 at lysine 36.

H3K4me2 Dimethylation of histone H3 at lysine 4.

H3K9me3 Trimethylation of histone H3 lysine 9.

HAC Human artificial chromosome.

HDR Homology-directed repair.

HJURP Holliday junction recognition protein.

HORs Higher-order repeats.

HP1 Heterochromatin protein 1.

HR Homologous recombination.

HU Hydroxyurea.

IF Immunofluorescence.

IR Ionising Radiation.

KMN KNL1 complex, MIS12 complex and NDC80 complex.

LIG4 Ligase 4.

MCC Mitotic checkpoint complex.

MEFs Mouse embryonic fibroblasts.

MIS18 MIS18α, MIS18β, MIS18BP1 complex.

MMC Mitomycin C.

MMCT Microcell-mediated chromosome transfer.

MMR Mismatch repair.

MMS Methyl methanesulfonate.

MRN MRE11, RAD50 and NBS1 complex.

mRNA Messenger ribonucleic acid.

MSI Microsatellite instability.

n-CIN Numerical chromosomal instability.

NEB New England Biolabs.

NES Nuclear export signal.

NHEJ Non-homologous end joining.

NLSs Nuclear localization signals.

o/n overnight.

OB Oligonucleotide/oligosaccharide binding.

P/CAF P300/CBP-associated factor.

PALB2 Partner and localiser of BRCA2.

PBS Phosphate Buffered Saline.

PCR Polymerase Chain Reaction.

PFA Paraformaldehyde.

PLK1 Polo-like kinase 1.

RAD51 RAD51 recombinase.

RPA Replication protein A.

RT Room temperature.

s-CIN Structural chromosomal instability.

SAC Spindle assembly checkpoint.

SD Standard Deviation.

SDSA Synthesis-dependent strand annealing.

siRNA small interfering RNA.

SOB Super Optimal Broth.

SSA Single-strand annealing.

ssDNA single-stranded DNA.

TAE Tris Acetate EDTA.

TBE Tris Borate EDTA.

TLS Translesion synthesis.

UFBs Ultrafine anaphase bridges.

UV Ultraviolet.

WB Western Blot.

WT Wild-type.

Chapter 1

Introduction

Maintenance of genetic information encoded by DNA and its faithful transmission across generations is fundamental for lifelong health and well-being. However, correct preservation of genetic information can be impaired by DNA replication infidelity and chromosome mis-segregation. These events determine genomic instability, which in turn can lead to catastrophic events, such as cell death or malignant aberrations. To alleviate these detrimental consequences, cells have developed multiple mechanisms to sense and tackle these challenges. It remains to be fully elucidated how such mechanisms are regulated and function. This is critical in order to understand the progression of certain diseases and cancer.

1.1 Genome instability

Genome instability (GIN) consists of a range of genetic abnormalities, such as point mutations and chromosome rearrangements and aneuploidy, which arises from incorrect repair of DNA lesions and chromosomes segregation. Different types of GIN have been described based on the type of genetic abnormalities generated: microsatellite instability (MSI), which is characterised by the expansion or contraction of DNA repeats;

mutations, such as nucleotide substitutions, deletions or insertions; and chromosomal instability (CIN), which refers to structural and numerical changes of chromosomes [1] [2].

Among all types of GIN, CIN is one of the most frequent and harmful form of genomic instability observed in cancer cells [2]. The association between CIN and cancer was first proposed in the early 20^{th} century by the German zoologist Theodor Boveri [3] [4]. He observed that the double-fertilisation of sea urchin eggs led to abnormal chromosome division, and the sea urchin embryos generated from this fertilisation were highly abnormal [5] [6]. CIN is particularly harmful to the cells because it can lead to the gain or loss of entire chromosomes or rearrangements of large chromosome regions that can alter the expression of hundreds of genes and disturb a vast series of cellular processes [7]. Furthermore, mis-segregation of entire chromosomes or chromosome fragments during mitosis can generate micronuclei, small nuclei that are not incorporated into the nucleus of the daughter cells. These structures are particularly vulnerable to DNA damage resulting in chromosome shattering [8] [9]. This mutational process, called chromothripsis, leads to numerous chromosome rearrangements in a confined genomic region and is quite common in cancer cells [10]. Due to its harmful consequences, CIN in cancer cells is often associated with poor prognosis in cancer patients and therapeutic resistance [11] [12] [13] [14] [15] [16] [17] [18].

The causes of structural CIN (s-CIN) and numerical CIN (n-CIN) are thought to be different [19]. s-CIN, which refers to the presence of large chromosome rearrangements, such as inversion, deletion and translocations, arises from defective DNA repair [2] [17]. By contrast, n-CIN refers to the loss or gain of whole chromosomes and the causes of this are considered to be linked mainly with defective mitotic events, such as Spindle Assembly Checkpoint (SAC) signalling, chromosome cohesion, centrosome amplification or kinetochore-microtubule attachment [7] [17]. However, emerging evidence suggests that replication stress can be a leading cause for both structural and numerical CIN [20] [19]. Additionally, a recent study conducted by Kabeche et al. has shown that proteins involved in DNA damage signalling are important in activating

the signalling pathway necessary to correct the microtubule-kinetochore attachments [21]. Together, it appears that accurate chromosome inheritance may depend on the fidelity of replication and the DNA repair machinery.

The main aim of my doctoral research project was to elucidate the causes of s- and n-CIN upon depletion of a well-recognised DNA repair protein, Breast Cancer Protein 2 (BRCA2), which I will discuss in the following sections. To this end, I initially focused on outlining the causes of DNA lesions as well as the DNA repair mechanisms in which BRCA2 is involved.

1.1.1 Sources of DNA breaks

GIN arises from DNA breaks that can occur as the result of DNA exposure to exogenous sources (e.g. ionising radiation (IR), ultraviolet (UV) light, chemicals) and endogenous stress (e.g. metabolic free radicals, replication defects) [22]. Overall, it has been estimated that each cell can undergo approximately 10^5 spontaneous DNA lesions per day [22]. Most of the lesions are single-strand DNA (ssDNA) breaks, which can be generated during metabolism by oxidative stress. If this persists after replication, ssDNA breaks can become double-strand DNA breaks (DSBs), which can be much more harmful for the cell [23].

In proliferating cells, replication is one of the major sources of DNA breaks [24]. To replicate DNA, the replisome first assembles at the multiple genomic replication origins and subsequently initiates DNA synthesis. This process generates a structure called the replication fork, where two strands of parental DNA are unwound and the synthesis of new DNA strands takes place. DNA replication forks can be frequently challenged and arrested by various lesions leading to stalled replication forks or replication fork collapse [1] [24]. Transient slowing or stalling of replication forks can be caused by different types of replication stress, such as DNA lesions, unusual DNA secondary structures, tightly bound protein-DNA complexes or repetitive sequences [25]. Replication stalling usually results in extended stretches of single-stranded DNA (ss-

DNA). ssDNA is rapidly coated by the ssDNA-binding replication protein A (RPA). RPA-coated ssDNA generates a signalling platform to recruit a number of replication stress-responsive proteins, which stabilise the stalled fork and ensure the rapid resumption of DNA synthesis [25] [24]. However, if forks fail to restart, they collapse into one-ended double-strand breaks (DSBs) through the digestion of stalled fork by nuclease.

1.1.2 DNA damage response

After DNA damage, the cell must rapidly respond to survive. In proliferating cells, cell cycle checkpoints are activated to arrest cell cycle progression and allow the repair of the DNA damage. The principal components of the DNA damage response (DDR) are ataxia-telangiectasia-mutated (ATM) and ataxia telangiectasia and Rad3-related (ATR) proteins. ATM and ATR are recruited at different sites of damage: ATM responds to DSBs and it is recruited through the MRN complex (MRE11-RAD50-NBS1), whereas ATR senses the ssDNA at the stalled replication forks (Figure 1.1). The extended ssDNA, which is rapidly coated by RPA, is recognised by ATRIP, which recruits ATR at ssDNA [26] [24]. However, resection at DSBs also leads to ATR recruitment [27]. When ATM and ATR are recruited to the sites of damage, they generate a cascade of phosphorylation events that recruit other proteins for the repair of the DNA lesion and arrest the cell cycle progression. In particular, ATM and ATR phosphorylate the checkpoint kinases CHK2 and CHK1, respectively. These promote cell cycle arrest by inhibiting the cyclin-dependent kinase (CDK) activity, which coordinates the cell cycle progression [28] [22].

At DSBs and stalled replication forks, ATM and ATR phosphorylate histone H2AX at serine 139 (γH2AX) [29] [30]. This signal is spread for several megabases around the breaks [31]. γH2AX is one of the initial events that mark the site of damage and lead to the recruitment of other DNA repair factors, such as MRN, 53BP1, BRCA1, which subsequently start the DNA repair process [28] [22].

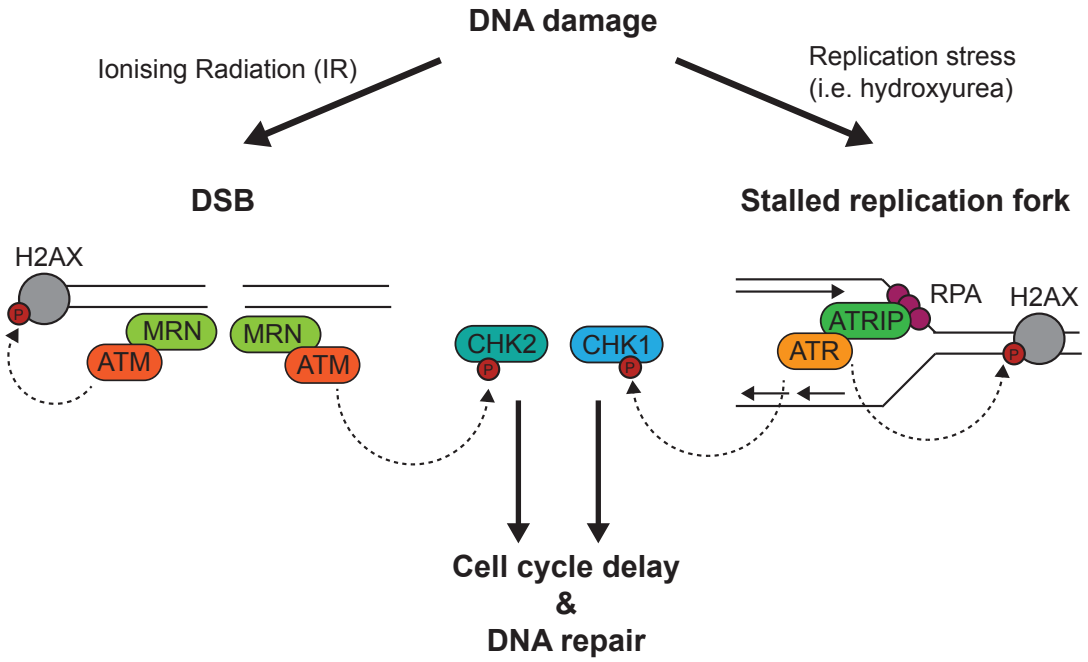


Figure 1.1: **The DNA damage response.** Ionising radiation (IR) treatment leads to the formation of DSBs, which recruit the MRN/ATM complex at DNA damaged sites. Activation of the ATM kinase leads to the phosphorylation of CHK2 and H2AX, which leads to the recruitment of DSB repair factors as described in the section 1.1.3.1. DNA damage induced by replication stress, such as hydroxyurea (HU), leads to the stalling of the replication fork and the accumulation of RPA on ssDNA. This recruits the ATR/ATRIP complex. Activation of ATR leads to CHK1 and H2AX phosphorylation as described in the section 1.1.3.1. Modified from Ciccia and Elledge [22]

1.1.3 DNA repair mechanisms

DNA lesions can be repaired by various DNA repair pathways according to the type of DNA damage and the phase of the cell cycle [28]. For example, base mismatches that are generated during replication are repaired by the mismatch repair (MMR) pathway, which acts mainly in the S phase [28]. Chemical alterations of nucleotide bases (e.g. oxidation, alkylation and deamination) or nucleotide substitutions (e.g. uracil incorporation) can be repaired by base-excision repair (BER) [28]. DSBs, which can be generated by IR, metabolic free radicals and collapsed replication forks, can be repaired by non-homologous end joining (NHEJ) in G1, whereas they can be repaired by both NHEJ and homologous recombination (HR) in S and G2 phases [28].

1.1.3.1 Double-strand break repair

Double-strand breaks (DSBs) are repaired by two primary pathways, NHEJ and HR (Figure 1.2). NHEJ is the fastest and easiest way to repair the DNA, by which the two broken ends are rejoined together to seal the break. In this process, KU70-KU80 heterodimer is loaded onto the DSB ends, which in turn recruits the catalytic subunit of DNA-dependent protein kinase (DNA-PKcs). DNA-PKcs phosphorylates ARTEMIS, which processes the DSB ends to generate blunt ends. Then a complex of XRCC4, XLF and ligase 4 (LIG4) ligates the broken ends to complete the repair (Figure 1.2). NHEJ provides immediate repair of DNA breaks but it can lead to small deletions of nucleotides, accumulating alterations of genetic information. By contrast, HR can repair DSBs with high fidelity using a homologous template, which originates from the replicated sister chromatid. In this way, HR can restore the genetic sequence of the broken DNA with no loss of genetic information [28] [22].

The key step in HR is the end resection of the DSB: the MRN complex, composed of RAD50, NBS1 and MRE11 with 3'-5' nuclease activity, together with CtIP and BRCA1, stimulates the initiation of the end resection of DSBs generating short single-strand (ss) ends (Figure 1.2). The nucleases exonuclease 1 (EXO1) and DNA replication ATP-dependent helicase/nuclease 2 (DNA2) and the helicase Bloom syndrome protein (BLM) are recruited to the short newly synthesised ssDNA to further extend the ssDNA [32]. The 3' overhanging ssDNA is coated by RPA, and subsequently replaced by the RAD51 recombinase. This process is facilitated by breast cancer associated protein 2 (BRCA2). The RAD51 nucleoprotein filament mediates the strand invasion into the sister chromatid to search for homology and to form the displacement loop (D-loop) structure (Figure 1.2). Finally, the invading 3'-strand is extended by DNA polymerase [28] [22].

The D-loop structures can be resolved through synthesis-dependent strand annealing (SDSA), where the extended 3'-strand is displaced from the D-loop and re-anneals to the other end of the break (Figure 1.2). Alternatively, the second end of the broken DNA can be incorporated by the D-loop (a process called 'second-end capture') to

form a double Holliday junction (dHJ) structure (Figure 1.2). The dHJ structure can be dissolved by helicases (BLM and TOPOIIIa) to form a non-crossover or cleaved by endonucleases (GEN1, MUS81/EME1, SLX1/SLX4), which can induce crossover events (Figure 1.2).

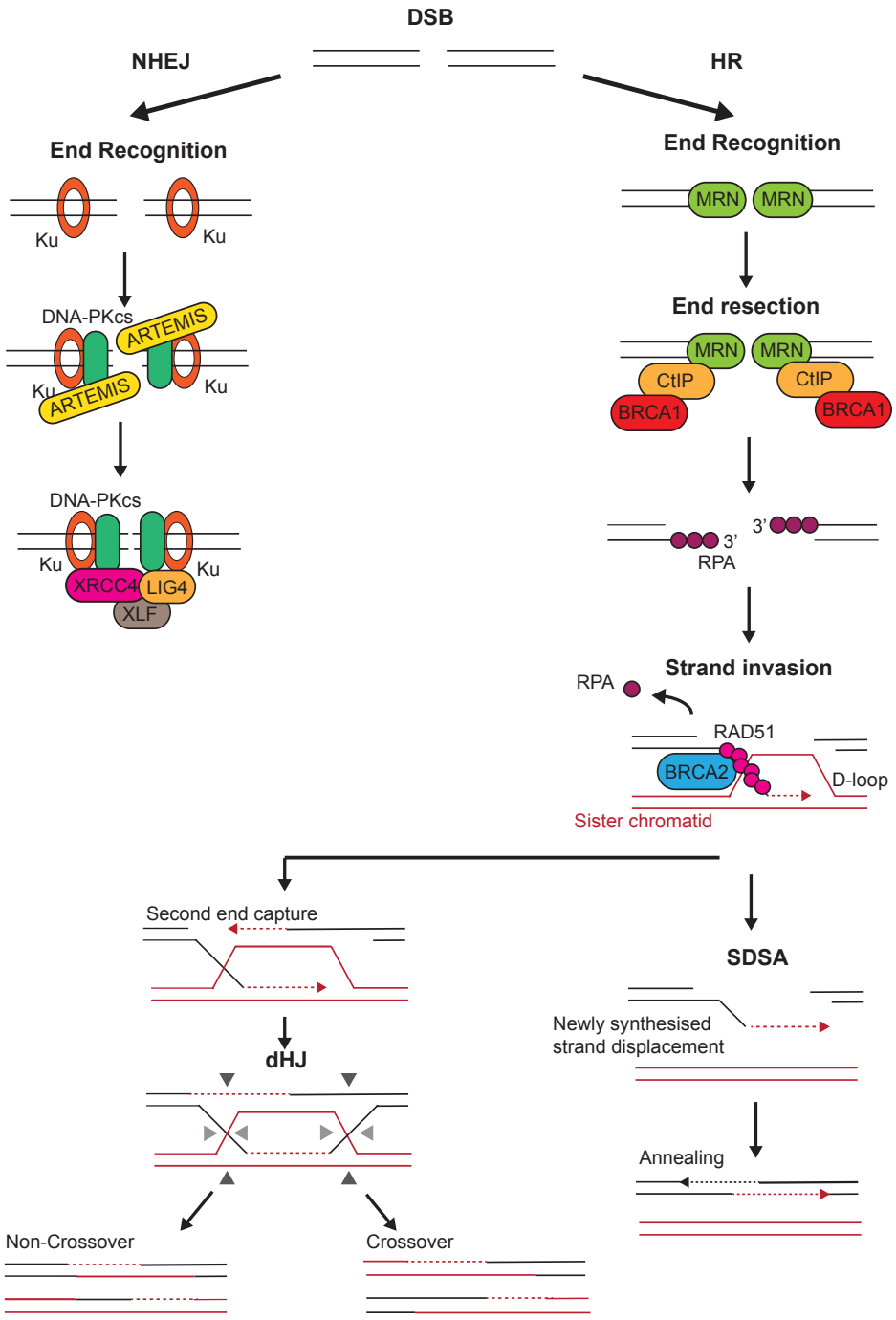


Figure 1.2: **Double-strand break (DSB) repair mechanisms**. DSBs are repaired through two primary pathways: non-homologous end joining (NHEJ) and homologous recombination (HR). In NHEJ, the broken ends are rejoined together as described in section 1.1.3.1. In HR, the two key steps are the end resection and the strand invasion. The former is mediated by MRN-CtIP and BRCA1 complex, the latter is mediated by RAD51 recombinase, which is loaded onto 3'-overhang strands by BRCA2. The displacement loop (D-loop) structure, which is formed after the strand invasion into the sister chromatid, can be resolved through synthesis-dependent strand annealing (SDSA) or through the formation of the double Holliday junction (dHJ) as described in section 1.1.3.1. Non-crossover results from cleavage at dark or light gray arrows, crossover results from cleavage at dark gray arrows on one side and at light gray arrows on the other side. Modified from Ciccia and Elledge [22] and Moynahan and Jasin [33]

Due to the presence of a homologous template, HR is generally considered to be an error-free repair pathway compared to NHEJ, which is more prone to errors. However, crossover events can also lead to genetic rearrangements, which may be deleterious: crossing over between sister chromatids restores the same genetic information at the site of break, but crossing over between homologous chromosomes can lead to translocation of long regions and loss of genetic information (loss of heterozygosity) [33]. Crossover events between homologous chromosomes are rare events in somatic cells [34] [35] [36] [33]; nevertheless, they can play an important role in the development of tumours. For example, in hereditary retinoblastoma, crossover between homologous chromosomes leads to the loss of the wild-type RB1 gene [37] [33]. The contribution of crossover events between homologous chromosomes in the development of other types of tumours is still unknown [33]. Furthermore, crossover events can occur between repetitive regions in non-homologous chromosomes [33]. These can potentially lead to translocations [33]. Studies conducted in mouse embryonic cells where DSBs were induced in proximity to Alu elements, the most common repetitive element in the human genome, have shown that DSBs at these regions are preferentially repaired by other DNA repair pathways, such as single-strand annealing (SSA) or NHEJ [38] [33].

Although HR is considered to be an accurate DNA repair pathway, the resolution of HR structures can lead to gross chromosome rearrangements. Therefore, the regulation of HR across the genome is important to prevent deleterious chromosome structures.

1.1.3.2 Repair mechanisms after replication stress

If the DNA lesion persists from the G1 phase or arises during replication, it can stall replication and can generate other types of damage, leading to harmful consequences for the cell. Upon replication fork stalling, cells are equipped with mechanisms to restart DNA synthesis. DNA lesions can either be bypassed to ensure that the replication continues or it can pause until the lesion is removed (Figure 1.3). To ensure that the

replication continues, DNA lesions on the leading-strands can be bypassed using specialised polymerases, called translesion synthesis (TLS) polymerases, such as POLH, POLK, POLI, REV1, POLQ, POLN, REV3L-REV7 [24]. These allow the resumption of DNA replication, although they have low-fidelity [24]. Alternatively, DNA synthesis can restart beyond the lesion, a process called repriming, which is mediated by PrimPol polymerase [39] [40] [41]. This process leaves a ssDNA gap behind the resumed DNA synthesis, which can be repaired by homology-directed repair (HDR) [24] [42]. However, if the gaps or unreplicated regions remain in mitosis, they can generate aberrant mitotic structures and DSBs [24].

Alternatively, stalled forks can reverse and form a four-way structure, called the chicken-foot structure (Figure 1.3). These structures were widely detected by electron microscopy in mammalian cells extracts after various treatments with genotoxic agents [43] [44]. The formation of the chicken-foot structure is mediated by several factors, such as the DNA translocases SMARCAL1, ZRAMB3, HLTF, and RAD51 [45] [46] [47] [44]. Furthermore, RAD51, together with BRCA2, at stalled forks has the function to protect the replication forks from the nuclease activity of MRE11, a nuclease implicated in the end-processing at DSB, which can lead to fork collapse [48] [49]. Subsequently, the reversed forks can either restart after the DNA lesion is removed or it can activate an HDR-like mechanism in which the 3'-overhang of the reversed arm coated by RAD51 mediates the invasion into the DNA duplex ahead of the fork [24].

Prolonged stalled forks or failure to restart DNA synthesis can lead to fork collapse and the formation of one-ended DSBs [24]. DSBs can be repaired by break-induced replication (BIR) (Figure 1.3). BIR starts with the strand-invasion into the donor molecule and continues to copy hundreds of kilobases of DNA. However, the problem of BIR is that it is an error-prone repair pathway, which can lead to frequent chromosome rearrangements and microhomology-based template switching, especially at repetitive regions [50][51] [24] [52] [53].

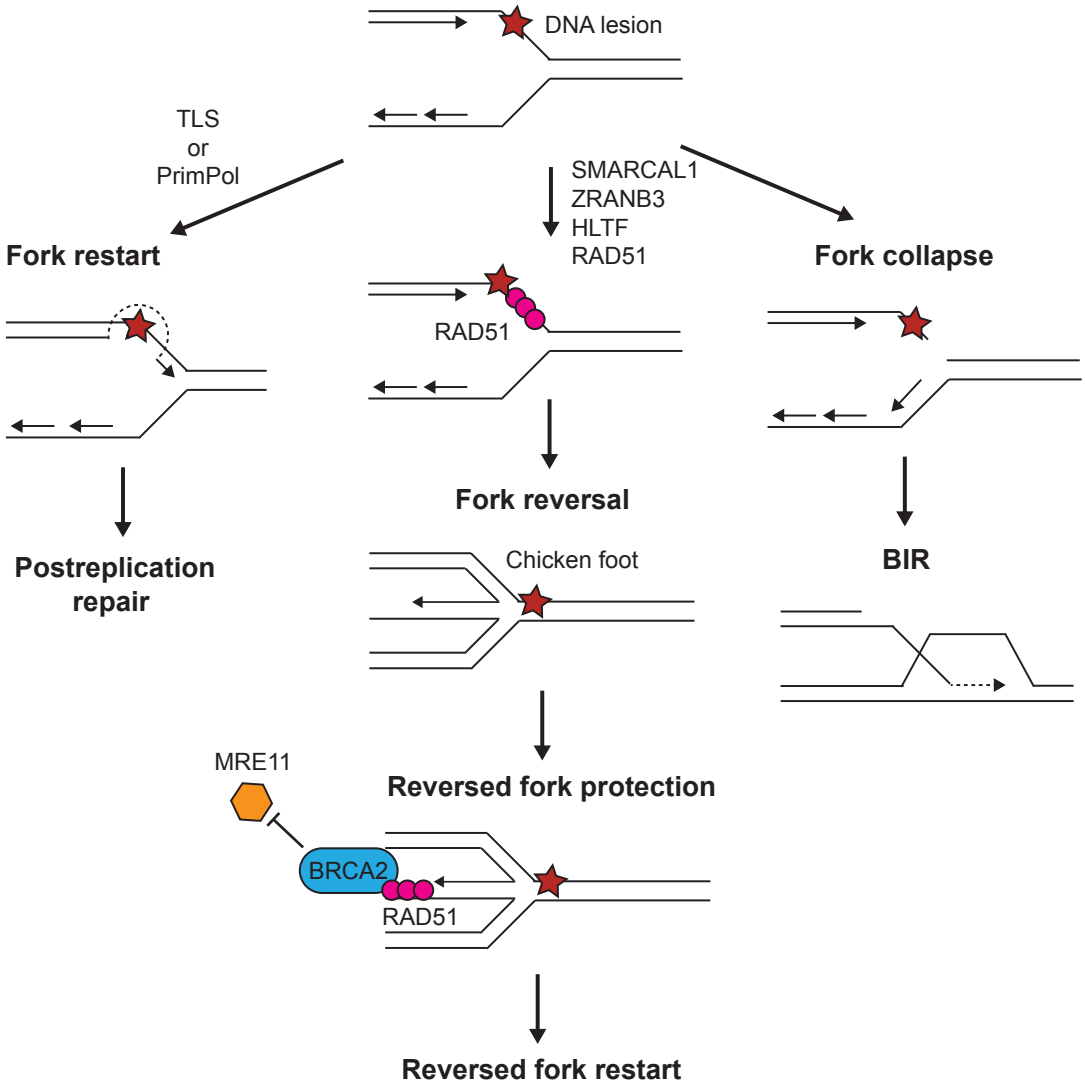


Figure 1.3: **Mechanisms of DNA repair at replication fork**. Stalled replication forks can be processed through three mechanisms. From the left, DNA lesions can be bypassed with translesion synthesis (TLS) polymerases or PrimPol polymerase, which mediates fork restart after the lesion. This process leaves DNA gaps behind the fork that are subsequently repaired as described in section 1.1.3.2. Alternatively, fork reversal is mediated by several DNA translocases (i.e. SMARCAL1, ZRANB3, HLTF) and RAD51 recombinase. Reversed forks are subsequently protected by BRCA2 and RAD51 from the MRE11 endonuclease activity. Protracted stalled forks lead to fork collapse and formation of DSB that can be repaired through the process of break-induced replication (BIR) as described in section 1.1.3.2. Modified from Berti and Virdigni [24]

1.2 BRCA2

In 1990, the first Breast Cancer 1 gene (*BRCA1*) was discovered as a gene mutated in breast cancer patients with family history [54]. Following studies showed that a large subset of breast cancer patients did not have *BRCA1* mutations, suggesting that other genes were responsible for breast cancer susceptibility [55]. Soon after, in 1994, the Breast Cancer 2 gene, *BRCA2*, was discovered as the second gene mutated in breast cancer patients and subsequently, its hereditary mutations were also shown to be associated with other types of cancer, such as ovarian cancer [56] [57]. While monoallelic mutations of *BRCA2* increase the risk of developing breast and ovarian cancer up to 80% and 20%, respectively [58] [59] [60]; mutations on both alleles predispose to a much more severe syndrome, called Fanconi anemia (FA), a rare disease that is characterised by developmental disorders, bone marrow failures and susceptibility to the development of several types of tumours [61]. FA cells with BRCA2 loss are characterised by hypersensitivity to DNA cross-linking agents, such as mitomycin C and cisplatin [61], and show increase chromosome breakage [62], implying its importance to preserve genome stability. Understanding the molecular mechanism by which BRCA2 prevents these diseases is critical in order to develop new therapeutic strategies.

1.2.1 Implications of BRCA2 in cancer and genome stability

Breast cancer is the most common tumour in the female population. Approximately 10% of the total cases of breast cancer are associated with hereditary mutations of specific genes. Among these, *BRCA2* mutations account for about 20% of the familial breast cancer cases [63] [64]. Nonetheless, *BRCA2* mutations are also associated with other types of tumours, such as ovarian cancer in females [65] and breast and prostate cancer in males [66] [67], pancreatic cancer in both female and male [68]. While the *BRCA2* gene is expressed in all tissues, it is still not fully understood why *BRCA2* mutations lead to cancer development in specific tissues. Recent studies using an HDR assay with a GFP-reporter gene in mice have shown that an hypomorphic mutation

of *BRCA2*, which lacks the C-terminal region of the protein, reduced HDR events in several tissues; however, highly proliferative mammary gland tissue in pubertal and pregnant mice presented a higher level of HDR events compared to the other tissues [69]. Therefore, they suggested that the association between *BRCA2* mutations and the development of breast cancer may be due to the high dependency of the mammary gland in HDR during the proliferation in puberty and pregnancy, rather than due to *BRCA2* mutations per se [69]. However, since *BRCA2* mutations also lead to other types of tumours, it is possible that several factors may affect tumour development, such as the level of cell proliferation and the cell turnover.

While monoallelic and biallelic mutations of *BRCA2* gene predispose to increased risk of cancers and Fanconi anemia respectively, the complete loss of BRCA2 function leads to embryonic lethality in mice [70] [71]. Cell death in BRCA2-null cells is associated with p53-dependent checkpoint activation [71], where p53 is a tumour suppressor protein that negatively regulates cell growth in response to several cellular stresses. It is only in the absence of functional p53, that BRCA2-null cells are able to proliferate and promote tumour development [72].

Chromosomal instability is a common feature of BRCA2-deficient cells. CIN in BRCA2-deficient cells, which carry a truncation of the C-terminal region of the protein, consists of gross chromosomal rearrangements (GCRs) such as translocations and deletions (observed by karyotype analysis), aberrant chromosome structure such as chromosome breaks, triradial and quadriradial structures, and abnormal chromosome numbers [73] [62] [74]. Mouse embryonic fibroblasts (MEFs), with an homozygous mutation on the amino acid (aa) 1492, that lead to a half-truncated protein, exhibited increased sensitivity to IR and genotoxic stress, such as mitomycin C (MMC), a DNA cross-linking agent, and methyl methanesulfonate (MMS), an alkylating agent [62]. These stresses were known to induce DSBs. Therefore, these observations provided evidence that BRCA2 was involved in mechanisms for sensing and repairing DNA damage [62].

1.2.2 BRCA2 structure

The human *BRCA2* gene is located in chromosome 13 and it encodes for a large protein of 3418 aa. Due to its large size, its complete structure has not been fully resolved and the exhaustive characterisation of its functions has proved challenging. In 2010, full-length human BRCA2 protein was purified from HeLa cells carrying a bacterial artificial chromosome (BAC) with the *BRCA2* gene and a FLAP tag at 5'- or 3'-end used for protein purification [75]. The 3D reconstitution of full-length human BRCA2 by electron microscopy showed that BRCA2 was predominantly present as a dimer and had a high affinity to bind ssDNA [75] [76]. These studies contributed to the understanding of its interaction with RAD51, the most well-characterised BRCA2 binding partner [70]. Furthermore, to date, BRCA2 has not been shown to have an enzymatic activity but it is proposed to act as a scaffold protein to recruit and regulate the activity of its numerous binding partners.

BRCA2 is a nuclear protein. It harbours two nuclear localization signals (NLSs) at the C-terminal region [77], which allow the localisation of the protein in the nuclear compartment (Figure 1.4). Indeed, CAPAN-1 cells, a pancreatic cancer cell line that expresses a truncated form of BRCA2 lacking the NLS, present a cytoplasmic localisation of BRCA2 [78].

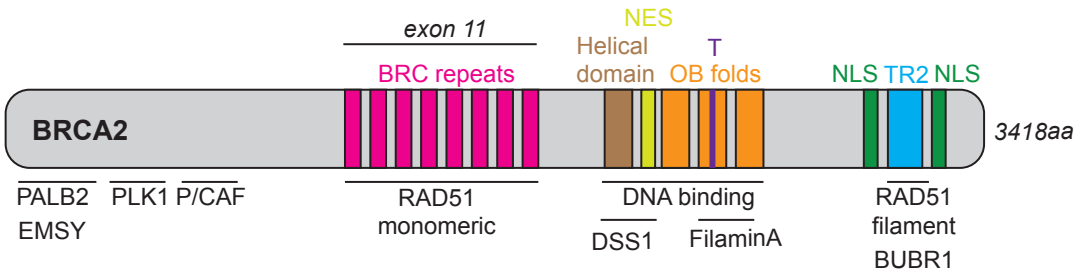


Figure 1.4: **BRCA2 structure**. Schematic representation of the structural domains of BRCA2 and its binding partners. Modified from Martinez et al. [79] and Fradet-Turcotte et al. [80]

In the central region, encoded by the exon 11, BRCA2 harbours eight BRC motifs, each

of which binds RAD51 [81] (Figure 1.4). The BRC motifs bind the monomeric form of RAD51 in solution and facilitate the loading of RAD51 onto the ssDNA, which in turn catalyses the strand invasion during the homology search [82]. However, each BRC motif has a different affinity of interaction for RAD51 interaction. The first BRC motifs 1-4 have high affinity to bind monomeric RAD51 [83]. These are essential in order to stabilise RAD51-ssDNA complex and allow DNA strand exchange activity *in vitro* [82]. In particular, BRC4 binds RAD51 three times stronger than BRC1 [84]. BRC4 blocks RAD51 ATPase activity, and in this way, it can promote the assembly of RAD51 onto the ssDNA to allow the strand invasion during HR [85] [86]. However, the over-expression of BRC4 leads to the inability to form RAD51 foci upon IR [84]. Biochemically, at high concentrations, BRC3 and BRC4 block RAD51-DNA filament formation, suggesting that their impacts are dose-dependent [87]. By contrast, BRC5-8 have lower affinity for monomeric RAD51 but a high affinity to RAD51-ssDNA [82]. BRC5 and BRC6 showed no interaction with free RAD51 [81]. However, BRC5-8 improve DNA strand pairing mediated by RAD51 [88].

BRCA2 interacts with the DNA through a DNA binding domain (DBD), which is composed of three oligonucleotide/oligosaccharide binding (OB) folds, an α-helical domain and a tower domain (T) [89] (Figure 1.4). The DBD allows the interaction of BRCA2 with ssDNA, which is essential for the recognition and repair of the DSB [89]. Through the DBD, BRCA2 also interacts with DSS1 (deleted in split hand/split foot) [90] (Figure 1.4), which is essential for the BRCA2 and RAD51 nuclear localisation [91]. BRCA2 has a highly conserved nuclear export signal (NES) motif within the DSS1-binding region [91] (Figure 1.4). In wild-type BRCA2, the NES is masked by DSS1 interaction allowing the BRCA2 nuclear localisation [91]. By contrast, mutations that impair BRCA2-DSS1 interaction lead to cytoplasmic localisation of BRCA2 and also affect RAD51 nuclear localisation [91]. Furthermore, DSS1 binds RPA and it is essential to recognise RPA-ssDNA. DSS1 removes RPA from ssDNA to allow RAD51 loading [92]. Thus, DSS1 acts as a DNA mimic to reduce RPA affinity to the ssDNA.

At the carboxyl-terminal (C-terminal) region, BRCA2 has a second site of interaction

with RAD51, called the TR2 domain (Figure 1.4). TR2 binds the filament of RAD51 and it is essential for stabilising the nucleoprotein filament of RAD51 [93] [94]. Furthermore, the TR2 presents a site of phosphorylation (serine 3291; S3291), which is phosphorylated by cyclin-dependent kinases (CDKs) in mitosis [95]. S3291 phosphorylation prevents RAD51 binding in mitosis and it is important for regulating HR activity during the cell cycle [95] [96].

Another well-characterised binding partner of BRCA2 is PALB2 (Partner and localiser of BRCA2) (Figure 1.4). The amino-terminal (N-terminal) region of BRCA2 interacts with the WD40 domain of PALB2 [97]. PALB2 depletion reduces BRCA2 localisation inside the nucleus, abrogates BRCA2 localisation at sites of DNA damage upon ionising radiation, reduces HR efficiency and increases sensitivity to mitomycin C [97]. Furthermore, it has been shown that PALB2 bridges BRCA1-BRCA2 interaction [98]. Through its coiled-coil domain at the N-terminal region, PALB2 interacts with BRCA1, one of the first proteins recruited at DSBs (see section 1.1.3.1), and allows the recruitment of BRCA2 to the sites of DNA damage [98]. Thus, PALB2 acts as a linker between BRCA2 and BRCA1.

1.2.3 BRCA2 functions

1.2.3.1 Homologous recombination (HR)

Increased sensitivity to genotoxic stress and gross chromosome rearrangements in BRCA2-deficient cells provided some evidence to support BRCA2 function in DNA repair [62] [73]. Initially, BRCA2 was found to interact with RAD51, the essential recombinase of HR [81]. Subsequently, BRCA2-deficient CAPAN-1 cells were shown to have reduced RAD51 foci formation upon IR treatment [99]. This observation supported the idea that BRCA2 had a function in mediating RAD51 foci formation. Furthermore, using an HDR-assay in human and mouse cells, where a GFP-reporter gene is reconstituted upon DSB and HR repair, it has been shown that BRCA2-deficient cells had reduced

HR activity, demonstrating its direct importance in DNA repair through HR [100]. In particular, at double-strand breaks (DSBs), BRCA2 facilitates the loading of RAD51 onto the ssDNA to allow the process of strand invasion into the sister chromatid [64]. To exert its repair function, BRCA2 is localised by PALB2 at the sites of DNA damage. Once it is recruited, BRCA2 binds the DNA through its DBD domain. The binding to DSS1 allows the displacement of RPA from the ssDNA and the loading of RAD51. In the progressive formation of the nucleoprotein filament of RAD51, the C-terminal region of BRCA2 stabilises the RAD51 filaments and regulates RAD51 activity during the cell cycle [95] [93] [94] [79] [101].

1.2.3.2 Replication fork protection (FP)

Upon replicative stress induced by hydroxyurea (HU), BRCA2-deficient cells, which lack the C-terminal region, exhibited increased DSBs at stalled forks [102]. This observation led to the suggestion that BRCA2 was important in protecting the nascent DNA at stalled forks [102]. The following studies characterised the function of BRCA2 in the protection of the replication forks (FP). At reversed forks, BRCA2 stabilises RAD51 nucleoprotein filaments and protects the nascent strand from resection by the MRE11 nuclease [48] [49]. Interestingly, FP is a separate function from BRCA2's HDR function. It has been shown that cells carrying S3219A mutation at the C-terminal region, which prevents RAD51-filament binding, were able to restore HR in BRCA2-deficient cells but not the FP function. Thus, it has been proposed that BRCA2 C-terminal region was dispensable for the HR function, while it is essential for the FP [48] [49].

1.2.3.3 Transactivation activity

Soon after its discovery, BRCA2 exon 3 was found to present transactivation activity of a reporter gene [103]. However, its targets inside the cells are still mostly unknown. The interest in this region was supported by the fact that mutations in exon 3 were identified in germlines of patients with breast and ovarian cancer [104]. Further studies

showed that the N-terminal region of BRCA2 binds the acetyltransferase P/CAF and through this interaction BRCA2 promotes acetyltransferase activity [105] (Figure 1.4). Furthermore, exon 3 also binds the transcriptional repressor EMSY, which silences its transactivation activity [106] (Figure 1.4). EMSY is localised at sites of DNA damage and binds chromatin-remodelling proteins, such as HP1 [106], suggesting a function of BRCA2 and EMSY in the chromatin remodelling, which may occur at sites of DNA damage.

1.2.3.4 Mitotic function

BRCA2-deficient cells exhibited unequal chromosome segregation (aneuploidy) [62]. BRCA2-deficient mouse cells showed >4N DNA content and aneuploidy is also observed in BRCA2-deficient cancer cells [74]. These observations generated interest in identifying mitotic functions of BRCA2. Furthermore, depletion of BRCA2 leads to the formation of small DNA-containing bodies, called micronuclei, as a result of chromosome mis-segregation [107]. In the same studies, BRCA2-deficient MEFs cells were found to undergo centrosome amplification [107]. Centrosome amplification can lead to unbalanced attachment of microtubules to chromosomes and generates mis-segregated chromosomes [108]. Later studies showed that BRCA2 localised at centrosomes thanks to the presence of a centrosomal localisation signal (CLS)[109] and its function at centrosome has been further described in following studies [110][111] [112].

Time-lapse experiments of MEF cells showed that BRCA2-deficient cells have longer cytokinesis and increased cytokinesis abnormalities (i.e. binucleation of cells) [113]. In this study, BRCA2 was found to localise at the midbody; however, the specificity of the antibody was questioned. Indeed, cells expressing GFP-BRCA2 on a bacterial artificial chromosome (BAC) vector failed to show the localisation of BRCA2 at the midbody [114]. A later study, however, showed that BRCA2 is recruited by Filamin A, an actin-binding protein, at the midbody and it allows the recruitment of the proteins of the endosomal sorting complex (ESCRT) involved in the proper abscission of the

daughter cells [115] (Figure 1.4), providing further evidences for BRCA2's function in mitosis. However, the importance of the BRCA2's function during cytokinesis still remains controversial , since BRCA2 depletion does not result in delayed cytokinesis abscission [114].

Another study identified an interaction of the C-terminal region of BRCA2 with BubR1 [116], a critical component of the Spindle Assembly Checkpoint (SAC) (see section 1.3.4) (Figure 1.4). In this study, they propose that BRCA2 acts as a scaffold protein to bring P/CAF acetyltransferase and BubR1 in close proximity and facilitates BubR1 acetylation, which in turn activates the SAC. However, despite the described functions of BRCA2 in mitosis, it is still not fully understood how BRCA2 deficiency leads to chromosome mis-segregation. Choi et al. have shown that conditional deletion of BRCA2 exon 11 in mice led to lagging chromosomes even though this region does not directly interact with the previously described mitotic BRCA2 binding partners [116].

More recent studies have suggested that chromosome mis-segregation associated with BRCA2 depletion was linked to its HR function in the S-G2 phase, which leads to under-replicated DNA before mitotic entry, resulting in abnormal mitotic structures, such as anaphase bridges and lagging chromosomes [117]. In this study, BRCA2 depletion has been associated with increased mitotic DNA synthesis (detected by the incorporation of the thymidine analogue 5-ethynyl-2'-deoxyuridine (EdU) in early mitotic cells), a process that has been described to allow the completion of DNA synthesis at difficult-to-replicate regions before anaphase onset [118]. This result suggested that BRCA2 may be important to complete the replication at specific regions in early mitosis. If under-replicated regions remain after anaphase, they can originate a specific type of anaphase bridges, called ultrafine anaphase bridges (UFBs) [119]. These are not detectable with conventional DNA staining such as DAPI staining but they can be detected with BLM and PICH, two helicases that are associated with these structures and are important for their resolution [120] [121] [119]. Indeed, it has been shown that BRCA2 depleted cells increased the formation of UFBs, and these originated from under-replicated regions detected by FANCD2 foci, a marker of uncom-

pleted replication [117]. This study suggested that mis-segregation defects in BRCA2 depleted cells were due to its function during replication. However, it remains to be understood where under-replicated regions are specifically mapped in the genome in BRCA2-depleted cells and whether this event can cause whole-chromosome loss.

1.2.3.5 Cell cycle regulation of BRCA2 functions

BRCA2 functions are regulated during the cell cycle by cyclin-dependent kinases (CDKs). Serine 3291 at the C-terminal region is phosphorylated by CDKs in mitosis. This phosphorylation is responsible for RAD51 disassembly from DNA to prevent aberrant recombination events during mitosis [95] [96] (Figure 1.5). At the N-terminal region of BRCA2, CDK1 and CDK2 phosphorylate threonine 77 in G2/M phase. This phosphorylation facilitates the interaction with the mitotic polo-like kinase 1 (PLK1) [122] (Figure 1.5). BRCA2-PLK1 interaction has been shown to be important to recruit RAD51 at stalled forks: BRCA2 facilitates PLK1-mediated RAD51 phosphorylation at serine 14 and this phosphorylation has been shown to be important to recruit RAD51 at stalled replication forks after HU treatment [123] [122]. Even if the role of PLK1 is well documented in mitosis, some studies have also reported that PLK1 interacts with components of the replicative helicase, the Mcm complex, in S-G2 phase and have proposed a PLK1 function outside mitosis [124] [125] [126]. However, in unperturbed conditions the phosphorylation of RAD51 peaks in G2-M phase, rather than in S phase, which is when the replication is predominantly executed. Thus, the function of the PLK1-mediated RAD51 phosphorylation in the G2-M phase remains to be seen in unperturbed conditions. Furthermore, in M phase S3291 phosphorylation prevents RAD51 interaction; thus, it is still unclear how BRCA2 coordinates RAD51 activity during the cell cycle.

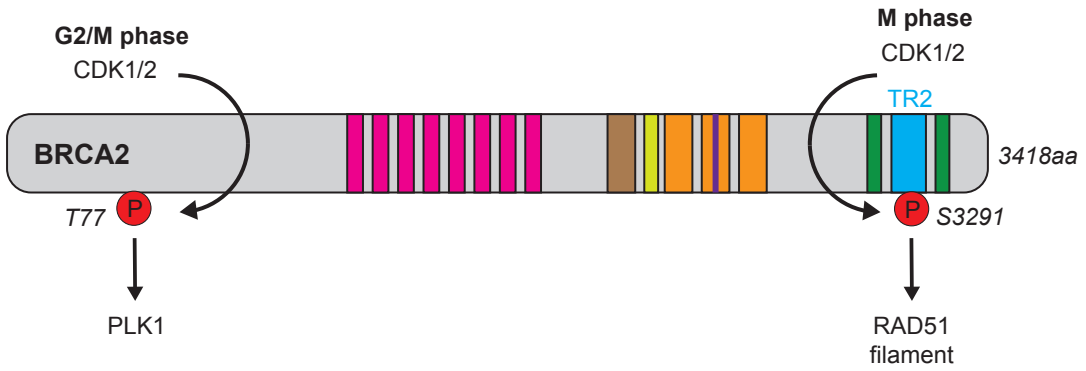


Figure 1.5: **Schematic representation of BRCA2 phosphorylated sites**. Sites of phosphorylation (P) during the cell cycles. Phosphorylation of serine 3291 (S3291) prevents RAD51 binding. Phosphorylation of threonine 77 (T77) allows PLK1 interaction. Modified from Fradet-Turcotte et al. [80]

1.2.4 Open questions

Despite 25 years of studies on BRCA2, there are still several questions that remain unanswered regarding its functions.

• *Why are BRCA2-mutations predominantly associated with certain types of cancer?*

BRCA2 is expressed in all human tissues; however, it is still not fully understood why *BRCA2* mutations predispose individuals to specific types of cancer, such as breast, ovarian, prostate and pancreatic cancers. It has been proposed that mammary gland tissue relies more on HDR compared to other tissues, such as the small intestine [69]. The reason why mammary gland cells have such high levels of HDR is proposed to be associated to the fast cell proliferation during puberty and pregnancy [69]. However, it is not fully understood why BRCA2-mutations lead to breast cancer in males, which do not undergo similar levels of proliferation. Furthermore, testis and lymphoid tissues express the highest level of BRCA2 mRNA [127], although these tissues are not predominantly affected by the BRCA2-deficiency.

• *How does BRCA2 facilitate RAD51 loading onto the DNA during the HR?*

BRCA2 binds RAD51 through two regions: the BRC motifs and the TR2 motif. BRC

repeats bind monomeric RAD51. The overexpression of BRC4 in cells or high doses of BRC4 *in vitro* have been shown to prevent RAD51 focus formation and RAD51 nucleoprotein filament formation onto dsDNA, respectively [84] [87] [93]. At the same time, it has been shown that BRC4 facilitates RAD51 assembly onto the ssDNA and facilitates the DNA strand exchange *in vitro* [86]. Thus, it has been proposed that the BRC motifs may play a dose-dependent function for the loading and disassembly of RAD51 onto the DNA [94]. The C-terminal region of BRCA2, TR2, binds the RAD51 nucleoprotein filament. This has been shown to stabilise the RAD51 filament onto the DNA and it has been proposed to facilitate recombination [94]. However, following studies have also proposed that the C-terminal region of BRCA2 was important for the disassembly of RAD51 filament rather than the completion of the recombination[96]. The molecular mechanism by which BRCA2 controls HR, hence, requires further investigation.

• *How does BRCA2-deficiency lead to n-CIN?*

BRCA2-deficient cells show chromosomal instability (CIN) characterised by structural and numerical CIN (s-CIN and n-CIN) [74] [62]. s-CIN in BRCA2-deficient cells can be explained by the impaired function of BRCA2 in DNA repair: in the absence of functional BRCA2, HR is inhibited and DNA breaks can be repaired by error-prone DNA repair mechanisms (e.g. NHEJ), which can lead to translocations, deletions and nucleotide mutations. In contrast, the aberrant number of chromosomes observed in BRCA2-deficient cells cannot be explained explicitly by its DNA repair function. While several BRCA2 functions have been proposed in mitosis (as described in section 1.2.3), it is still not fully understood how and why BRCA2-deficient cells exhibit chromosome mis-segregation. MEFs with conditional depletion of exon 11, which binds RAD51, showed lagging chromosomes, albeit this region has not been associated with a BRCA2 function in mitosis [116]. Thus, while BRCA2 appears to be important for the accurate segregation of chromosomes during mitosis, the mechanism which drives this process remains to be understood.

• *What is the importance of BRCA2 transactivation activity?*

The N-terminal region of BRCA2 interacts either with PALB2 or EMSY [128]. While

the interaction between BRCA2 and PALB2 has been shown to be important to recruit BRCA2 at sites of DNA damage [97], the function of BRCA2-EMSY interaction has yet to be fully understood. Additionally, BRCA2 has been shown to exhibit a transactivation activity [103] [105], which is inhibited by the binding with EMSY [106]. However, the true importance of this function is still not fully understood.

• *Does BRCA2 have a function beyond DNA damage repair?*

The localisation of BRCA2 and its function has been well described at sites of DNA damage under conditions of genotoxic stress, such as IR [97] [129]. However, its functions beyond DNA damage repair and in undamaged conditions remain understudied. It is possible that BRCA2 exerts different functions in different moments of the cell cycle.

1.3 Centromeres and kinetochores

Faithful chromosome segregation is essential in order to preserve the genetic information encoded in our genome. Accurate chromosome segregation relies on the presence of a specific region present on each chromosome, called the centromere. Centromeres are the platform for the kinetochore machinery, which is composed of large protein complexes that assemble at centromeres and allow the attachment of spindle microtubules (Figure 1.6). Centromeres and kinetochores are pivotal structures for chromosome segregation, and defects in their formation can result in the development of diseases and cancer [7] [130] [131].

1.3.1 Centromere structure and function

In most eukaryotes, centromeres are defined in a region of highly repetitive sequences [132]. This is different in some organisms, such as nematodes (*Caenorhabditis elegans*), where the centromere is diffused along the whole chromosome, a characteristic called holocentricity [130]. In eukaryotes, there are two types of monocentric centromeres: "point centromeres" are defined by a short sequence of 125 bp of DNA and found in budding yeast, "regional centromeres" are highly repetitive regions that span several kilobases or megabases of DNA and found from fission yeast to humans [132]. However, centromeric sequences are not conserved between species [132]. Mammalian centromeres are composed of long arrays of tandem repeats (171 base pair), known as α-satellite DNA (Figure 1.6). Clusters of α-satellite repeats are highly organised head-to-tail and form higher-order repeats (HORs) (Figure 1.6). HORs are repeated several times to form the centromere core, which is several Mb long [130] [133]. The centromere core is flanked by heterochromatic regions, called the pericentromere, which contains less ordered DNA repeats [130] (Figure 1.6). However, the centromere identity is not defined by repetitive sequences, but by the presence of an epigenetic marker, the histone H3 variant CENP-A [134] [135] [136]. Centromeres are characterised by the presence of nucleosomes containing CENP-A interspersed with histone H3-containing

nucleosomes [130] [132]. CENP-A is conserved through species and it is essential for cell survival [137][132].

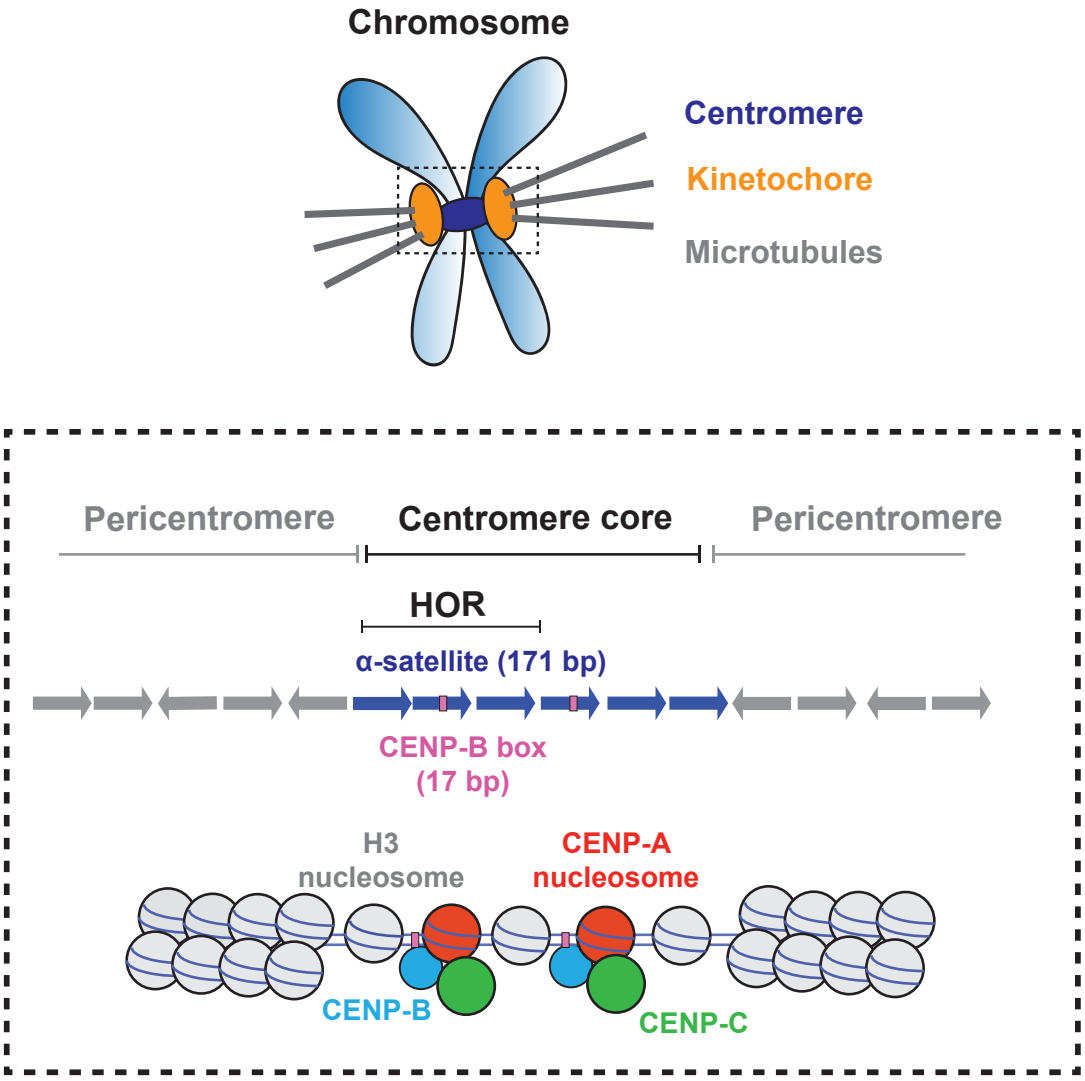


Figure 1.6: **Centromere structure**. Schematic representation of the centromere structure. This is composed by α-satellite DNA repeats (171 bp) that are organised head-to-tail to form higher order repeats (HORs). HORs are repeated up to several Mb to form the centromere core. The centromere core is flanked by the pericentromere, which is composed of less ordered repeats. Some of the α-satellite DNA repeats contain a CENP-B box (17 bp), which is the site of CENP-B binding. Modified from McKinley and Cheeseman [130].

Within the centromere core, some of the repeats contain the CENP-B box [138]. This is a conserved 17 bp sequence between rodents and primates [130]. The CENP-B box recruits the DNA-binding CENP-B protein [139] [140]. CENP-B interacts both with

CENP-A at nucleosomes and the kinetochore protein CENP-C [132] [130]. These interactions are essential in order to stabilise CENP-A and CENP-C at centromeres. The disruption of CENP-B/CENP-C interaction leads to cell cycle delays, chromosome missegregation and reduced CENP-C recruitment at centromeres [141] [142]. Furthermore, using an artificial mini-chromosome made by arrays of α-satellite DNA sequences (Human Artificial Chromosome, HAC) Ohzeki and colleagues have shown that the CENP-B box was essential for the *de novo* deposition of CENP-A and the formation of functional centromeres [143]. Despite its linker role between centromeric chromatin and the kinetochore, the importance of CENP-B (and consequently the CENP-B box) remains uncertain. Indeed, CENP-B knockout mice are viable [144] [145] [146] and CENP-B (and the CENP-B box) is not present in the Y chromosome [147] [139]. Furthermore, the presence of CENP-B was not reported at neocentromeres, which are functional centromeres formed outside the canonical α-satellite DNA regions [148] [149]. The discovery of the neocentromeres [148] was the first evidence that suggested that centromere identity was not defined by the repetitive DNA sequences. Neocentromeres were defined by the presence of the epigenetic marker CENP-A but not CENP-B [130] [150]. The deposition of new CENP-A allows the formation of functional kinetochores, microtubule attachment and chromosome segregation [151] [152] [153].

1.3.2 CENP-A deposition

Centromere transmission is an essential requirement to allow appropriate chromosome segregation. The CENP-A deposition is fundamental for the appropriate formation of kinetochores. In human cells, deposition of new CENP-A occurs in G1 phase [154] [155]. Its deposition is mediated by two main factors: the Holliday junction recognition protein (HJURP) and the MIS18 complex (MIS18α, MIS18β, MIS18BP1), which direct the CENP-A deposition at the right time and space [156] [157] [158] [159]. HJURP is the CENP-A histone chaperone that is necessary for CENP-A deposition [156] [157]. HJURP is recruited at centromeres in early G1 and its localisation is regulated by the MIS18 complex. MIS18BP1 is recruited at centromeres in mitosis, followed by

MIS18α and MIS18β at the end of mitosis [158]. CENP-C facilitates the CENP-A loading through its binding with MIS18BP1 [160] [161].

At the end of G1, the CENP-A deposition machinery is disassembled from the chromatin thanks to the CDK activity which inhibits MIS18 localisation, assembly and HJURP recruitment. Subsequently, during replication, the DNA strands are duplicated and the CENP-A nucleosomes are diluted into the replicating strand, while the gaps on the other strand are replaced by histone H3.3-containing nucleosomes [162] [130]. This half-maximal CENP-A occupancy is maintained until telophase when new CENP-A is subsequently re-incorporated [154] [130]. Furthermore, recent studies have proposed that replication acts as a correction mechanism to remove CENP-A ectopically integrated into the chromosome arms during G1 [163]. Using chromatin immunoprecipitation (ChIP) they mapped CENP-A incorporation before and after replication and they observed that CENP-A signal is partially enriched at transcriptionally active regions outside centromeres before replication. After replication, the ectopic CENP-A signal is removed from chromosome arms but it is retained at centromeres where the other proteins of the kinetochore complex (CCAN complex, explained below) are assembled [163].

CENP-A deposition is also affected by the surrounding chromatin environment. At epigenetic level, the core centromere is characterised by transcriptionally permissive marks, such as dimethylation of histone H3 at lysine 4 (H3K4me2) and dimethylation of histone H3 at lysine 36 (H3K36me2) [164] [165] [130] [133]. By contrast, chromatin of the pericentromere is heterochromatic, containing heterochromatin markers trimethylation of histone H3 lysine 9 (H3K9me3) and heterochromatin protein 1 (HP1). Using the artificial chromosome HAC system it has been shown that increased heterochromatinisation at the α-satellite repeats reduces CENP-A loading, whereas increased euchromatinisation promotes *de novo* CENP-A loading [166] [133]. Further studies suggested that CENP-B plays a critical role in the formation of the chromatin environment to allow and stabilise CENP-A deposition [167] [133]. In this study, a BAC carrying human α-satellite DNA was transfected in MEFs cells with wild-type CENP-B or CENP-

B-deficient. In CENP-B expressing cells, HAC was formed and stably maintained as extra-chromosome. Using chromatin immunoprecipitation coupled with quantitative PCR (ChIP-qPCR) analysis, it was observed that CENP-A was enriched at α-satellite DNA in the extra-chromosomal HAC. By contrast, CENP-A was not associated to α-satellite DNA if it was ectopically integrated in the chromosome arms in CENP-B proficient. At chromosome-integrated HAC, increased heterochromatinisation (detectable by the presence of H3K9me3) was reported in CENP-B proficient cells, whereas reduced H3K9me3 was reported in CENP-B deficient cells, suggesting that methylation of α-satellite DNA was CENP-B dependent. Thus, it was proposed that CENP-B plays a dual role at α-satellite repeats: at centromeres, it is essential for the *de novo* CENP-A assembly, whereas at sites of ectopic integration of the α-satellite repeats, it may enhance heterochromatinisation and prevents CENP-A deposition [167]. Therefore, based on the chromatin context, CENP-B can facilitate or antagonise CENP-A loading. However, it is still not fully understood how CENP-B recognises the different chromatin context and how it can induce heterochromatin or euchromatin formation. A recent study has shown that CENP-B can bind different chromatin modifiers, such as the H3K9 methylase SUV39H1, HP1 and the H3K36 methylase ASHL1, which may promote the heterochromatinisation or open chromatin formation at α-satellite DNA and affect the CENP-A deposition [168].

The presence of transcriptionally permissive marks at the core centromere is associated with transcriptional activity in this region. It has been proposed that transcriptional activity plays an important function in the CENP-A deposition. RNA polymerase II was identified at centromeres in mitosis and its inhibition reduced CENP-C kinetochore binding [169]. Subsequent studies have shown that centromeric transcripts associate to HJURP and CENP-C and facilitate the CENP-A loading [170] [171]. Consistent with these results, removal of transcription permissive marks at core centromere caused a failure to recruit HJURP and was associated with reduced CENP-A level at the HAC centromeres [172]. Together, these results suggest that CENP-A loading may be a transcription-mediated process. However, it is still unclear what is the function of transcription at centromeres.

1.3.3 Kinetochore structure and formation

Functional centromeres recruit kinetochore components, which are essential for the attachment of the microtubules of the mitotic spindle. The kinetochore machinery forms complex structures composed of different units of two complexes: the inner kinetochore complex formed by the constitutive-centromere associated network (CCAN), and the outer kinetochore complex, called KMN complex, consisting of the KNL1 complex, the MIS12 complex and the NDC80 complex (Figure 1.7).

The CCAN is composed of 16 CENP proteins that are close to the CENP-A nucleosome. These are divided into five subcomplexes: CENP-C, the CENP-L-N complex, the CENP-H-I-K-M complex, the CENP-O-P-Q-U-R complex and the CENP-T-W-S-X complex [173] [130] [174] [175]. In the CCAN, CENP-C is the 'keystone' protein that links centromeres with kinetochores [174] [175]. On one hand, CENP-C binds CENP-A nucleosomes through its central domain and the CENP-C motif, and stabilises CENP-A nucleosomes at centromeres [176] [177] [178] . On the other hand, it interacts with the MIS12 complex, which is essential for the recruitment of the outer-kinetochore proteins [179] [180] [181] [182]. In human cells, depletion of CENP-C reduces centromeric CENP-A, recruitment of outer kinetochore components and leads to chromosome mis-segregation [176] [179]. CENP-C and CENP-T recruit the proteins of the KMN network through independent pathways [183] [184] [185]. CENP-C recruits the NDC80 complex through its interaction with MIS12 and KNL1 complexes, whereas CENP-T binds directly to two NDC80 complexes and one MIS12-KNL1 complex, which subsequently recruits another NDC80 complex [185] [184] [186] (Figure 1.7).

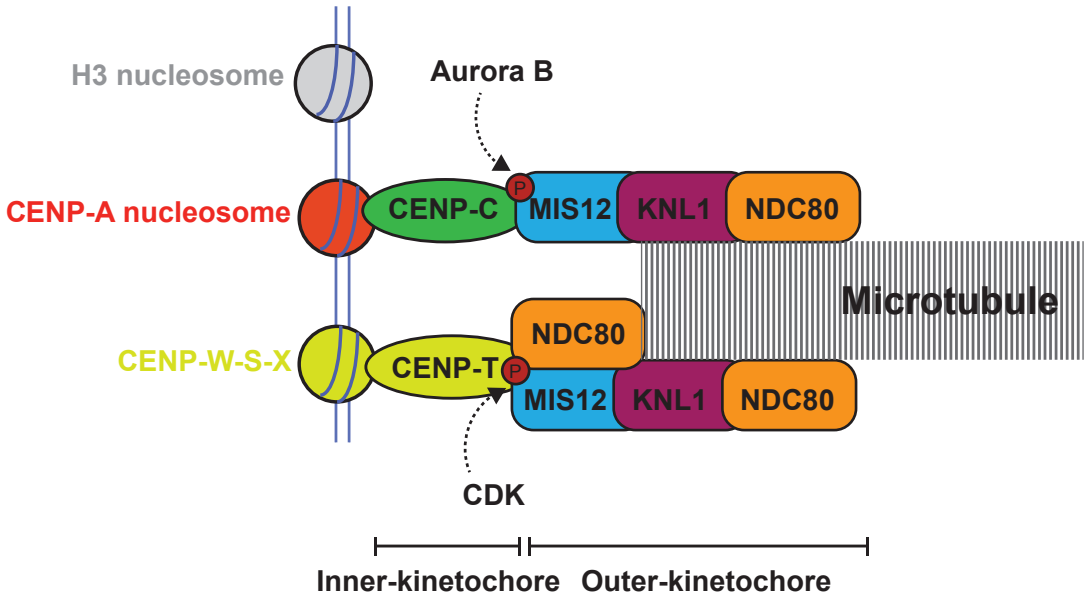


Figure 1.7: **Kinetochore structure**. Schematic representation of the kinetochore structure, which allowed the attachment of the microtubule spindle to the centromere. This figure represents the contribution of the CENP-C and CENP-T pathways for the recruitment of the kinetochore at centromere. Modified from McKinley and Cheeseman [130].

The KMN network is composed of three subcomplexes. The MIS12 complex contains the MIS12, PMF1, NSL1, DSN1 subunits, while the KNL1 complex contains KNL1 and ZWINT subunits. Finally, the NDC80 complex contains the NDC80, NUF2, SPC24, and SPC25 subunits, which are responsible for the microtubule binding [174] [187].

The KMN network has a dual role: it is the platform for microtubule attachment and it is essential for Spindle Assembly Checkpoint (SAC) signalling. On one hand, MIS12 is the complex that licenses the kinetochore formation at centromeres and links the CCAN with the other complexes of the outer-kinetochore [182]. Inhibition of MIS12 leads to the reduction of multiple kinetochore components and chromosome misalignment [188]. Furthermore, the MIS12 complex interacts with the pericentromere to stabilise the kinetochore establishment: MIS12 interacts with ZWINT and forms a stable complex with the centromeric heterochromatin through the binding with the heterochromatin protein 1 (HP1) [189]. HP1 depletion reduces MIS12 localisation at centromeres [189]. On the other hand, the KNL1 complex links the structural kinetochore

components with SAC signalling. ZWINT interacts and localises the ZW10 protein at centromere [190] [191]. This interaction is essential in stabilising the components of SAC signalling, such as MAD1 and MAD2, at unattached kinetochores [192]. KNL1 and NDC80 generate strong affinity for the microtubule binding [193][194].

All kinetochore proteins are well orchestrated to associate with the centromeres at the correct time during the cell cycle to ensure equal chromosome segregation. In human cells, the CCAN proteins are associated with centromere throughout the cell cycle [173]. The proteins of the outer-kinetochore are recruited during the S-G2 and M phase. In particular, MIS12 and KNL1, which are localised inside the nucleus, start to associate with centromeres in the S phase. By contrast, NDC80, which is localised in the cytoplasm during interphase, is recruited at centromeres after the nuclear envelope breakdown when cells enter into mitosis [195]. Fluorescence recovery after photobleaching (FRAP) experiments, used to assess the mobility of kinetochore and centromeres components in human cells, have shown that CENPs and MIS12 proteins have higher mobility during interphase but they are stably associated to the chromatin during mitosis [196]. When cells exit from mitosis, kinetochore proteins start to dissociate from centromeres, while the proteins for the CENP-A loading (i.e. MIS18) start to associate with centromeres. The temporal regulation of the assembly and disassembly of the kinetochore at centromeres is coordinated by cyclin-dependent kinases (CDKs) and the mitotic kinase Aurora B [195]. CENP-C binding with the MIS12 complex is facilitated by DSN1 phosphorylation mediated by Aurora B, whereas CENP-T interaction with NDC80 and MIS12 complexes is regulated by the CDK-dependent phosphorylation of CENP-T [185] [197] [182] [186] (Figure 1.7). Despite the observation that both pathways have been shown to be important to recruit kinetochore components, it is still not fully understood whether one pathway is more important than the other in recruiting kinetochores at centromeres. Single depletion of CENP-C in chicken DT40 cells showed mitotic delays: cells can progress to the next cell cycle, but its long term depletion leads to cell death [198]. Depletion of CENP-T in DT40 cells showed strong mitotic arrest and hypercondensed chromosomes, which failed to align in metaphase [199]. Double-depletion of CENP-C and CENP-T pathways leads to a rapid cell death,

suggesting that both pathways are involved in allowing appropriate chromosome segregation [199].

1.3.4 Spindle Assembly Checkpoint

To ensure the appropriate chromosome segregation, cells have developed regulatory mechanisms to sense the attachment of the kinetochore to the mitotic spindle. Once the kinetochore-microtubule attachment is established, the chromosomes are pulled towards the two opposite poles of the cells. The spindle assembly checkpoint (SAC), the mitotic checkpoint signalling that monitors the kinetochore-microtubule attachment, is activated in the presence of unattached kinetochores or defective kinetochore-microtubule attachment. SAC activation delays the mitotic exit to ensure that the kinetochore-microtubule attachment is satisfied at all chromosomes [173]. If the SAC is inhibited, cells enter anaphase without appropriate kinetochore-microtubule attachments, leading to chromosome mis-segregation [7] [187].

The proteins involved in this mechanism are MAD1, MAD2, BUBR1, BUB1, BUB3 and MPS1 [173]. These proteins act in concert to inactivate CDC20, a factor of the E3 ubiquitin ligase APC/C (anaphase-promoting complex/cyclosome). When kinetochores are unattached to microtubules, the CDC20 is in a complex with MAD2, BUB3 and BUBR1, called the mitotic checkpoint complex (MCC). This complex prevents the binding of APC/C ^{CDC20} with Cyclin B and Securin inhibiting their ubiquitination and proteolysis (Figure 1.8). In this way, the SAC is activated (SAC ON) and microtubules have enough time to bind kinetochores. When the kinetochore-microtubule attachment is established, the SAC is satisfied (SAC OFF) and the MCC complex is removed from CDC20 (Figure 1.8). The APC/C ^{CDC20} binds Cyclin B and Securin and promotes their ubiquitination. The degradation of Securin liberates Separase, which cleaves the cohesion ring that holds the centromeres together and allows chromosome segregation. At the same time, the degradation of Cyclin B inactivates CDK1 and allows mitotic exit [173] [200] (Figure 1.8). The initiation of the SAC signalling occurs at unattached kine-

tochores where MPS1 kinase phosphorylates KNL1. This phosphorylation is essential for the recruitment of the MCC proteins and the assembly of the complex [201]. In fission yeast, mutations of KNL1, which prevent MPS1 phosphorylation, inhibit SAC function [187]. However, it is still unclear whether the MCC complex can form entirely or partially at kinetochores [201]. Likely, the MCC complex can subsequently diffuse inside the cells to inactivate the APC/C complex [201]. Indeed, this has been reported to localised in several cellular compartments, such as centrosomes, microtubules, kinetochores and chromosomes during mitosis [202].

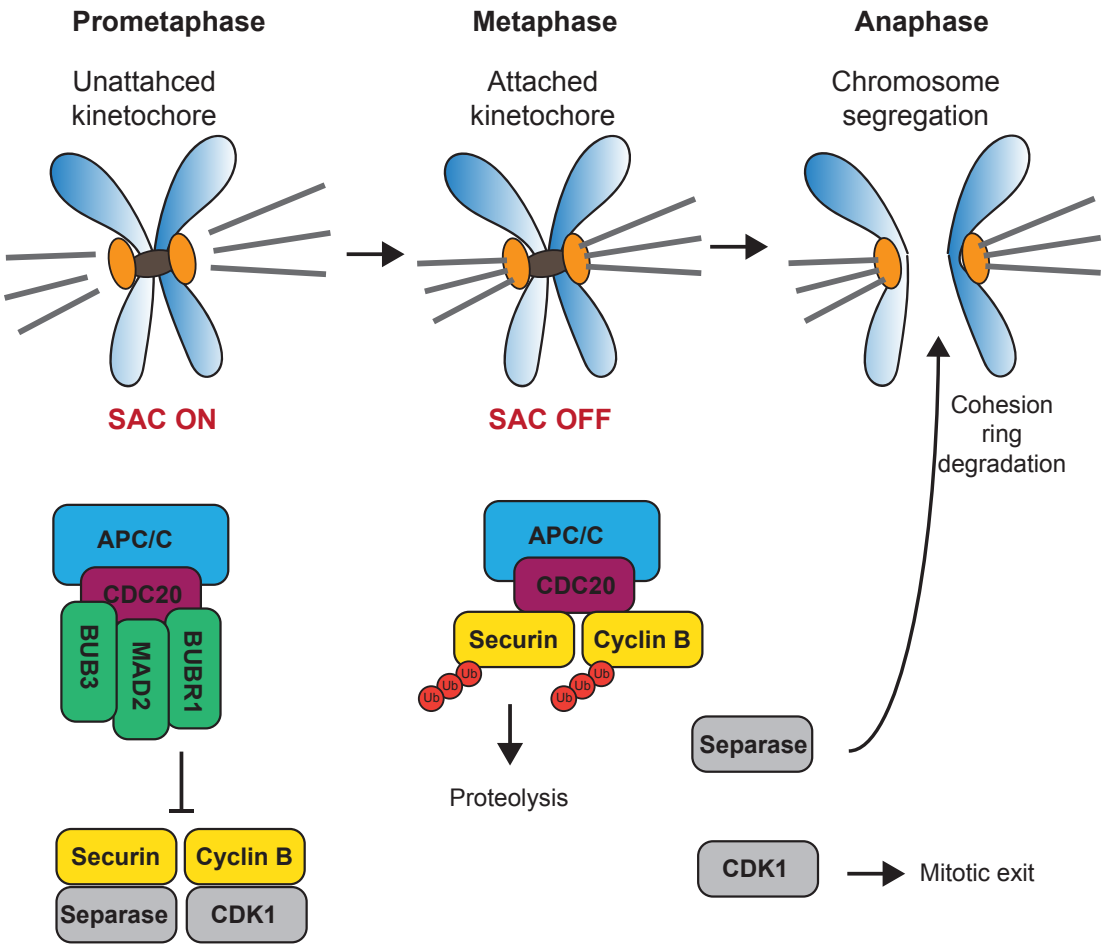


Figure 1.8: **The Spindle Assembly Checkpoint**. Schematic representation of the spindle assembly checkpoint (SAC). When kinetochores are unattached, the CDC20 is in complex with MCC complex (BUBR1, MAD2 and BUB3), preventing Securin and Cyclin B degradation (SAC ON). Once microtubule-kinetochore attachment is established, MCC complex is removed and the APC/C ^{CDC20} complex promotes the degradation of the Securin and Cyclin B. In this way, Separase and CDK1 are released. This leads to the degradation of the cohesin ring, which allows the separation of chromosomes and mitotic exit. Modified from Foley and Kapoor [187] and Holland and Cleveland [7].

1.4 Research aim

Since the causes of numerical CIN (n-CIN) in BRCA2-deficient cells are not fully explained by the current knowledge about the functions of BRCA2 (section 1.2.4), I decided to investigate the mechanisms underlying this phenotype. In particular, I took the decision to investigate the function of BRCA2 at centromeres, which are the pivotal regions for chromosome segregation. To the best of my knowledge, the role of BRCA2 in centromeric DNA repair and protection has not been explored in previous research studies.

In this thesis, three hypotheses have been investigated to assess the function of BRCA2 at centromeres to prevent n-CIN:

1. *BRCA2 may protect or repair centromeres from DNA damage.* The function of BRCA2 has been well-characterised in DNA repair and protection. At the same time, centromeres can be prone to DNA damage due to their complex DNA structures, which can be difficult to resolve during replication. In this context, BRCA2 may promote HR (or fork protection) to prevent the formation of harmful DNA breaks at centromeres.

2. *BRCA2 may assist kinetochore assembly.* Recent proteomics studies conducted in the laboratory of Dr. Fumiko Esashi showed that BRCA2 interacts with kinetochore-associated proteins (see Chapter 5). The accurate establishment of kinetochore machinery at centromeres is essential for accurate chromosome segregation during mitosis. In this context, BRCA2 may regulate kinetochore assembly at centromeres.

3. *BRCA2 may affect chromatin remodelling.* BRCA2 binds chromatin-remodelling factors (section 1.2.3.3). At the same time, centromere formation is affected by the surrounding chromatin organisation. Thus, BRCA2 may modulate the chromatin status to support the centromere formation.

The results of this study are presented in three chapters. In Chapter 3, n-CIN has been examined using the HAC system to investigate the function of HR proteins at centromeric DNA. In Chapter 4, CIN has been investigated for endogenous chromosomes upon BRCA2 depletion. In this context, the functions of BRCA2 in DNA repair at centromeres and chromatin remodelling have been assessed. In Chapter 5, the function of BRCA2 in kinetochore assembly has been explored.

Chapter 2

Materials and Methods

2.1 Tables of materials

2.1.1 Mammalian cell lines

Cell line	Parental	Origin	Karyotype	Medium	Antibiotics
HT1080 EGFP-HAC [203]	HT-1080	Fibrosarcoma	Pseudodiploid (44-48)	DMEM	5 μg/ml blasticidin
HT1080 HAC-dGFP [204]	HT-1080	Fibrosarcoma	Pseudodiploid (44-48)	DMEM	15 μg/ml blasticidin
HeLa Kyoto NFLAP-BRCA2 [114]	HeLa	Adenocarcinoma	Polyploid (70-164)	DMEM	400 μg/ml geneticin
HCT116	-	Colorectal carcinoma	Diploid (46)	McCoy's 5A	-
HCT116 CMV-OsTIR1 [205]	HCT116	Colorectal carcinoma	Diploid (46)	McCoy's 5A	1 μg/ml puromycin
HCT116 tet-OsTIR1 [205]	HCT116	Colorectal carcinoma	Diploid (46)	McCoy's 5A	1 μg/ml puromycin

Table 2.1: Mammalian cell lines used in this thesis

Cell line	Parental	Gene expression	Plasmid	System	Antibiotics
HT1080 HAC-dGFP tetR-mCherry*	HT1080 HAC-dGFP	tetR-mCherry	pJETY3 tetR-mCherry	constitutive expression	15 μg/ml blasticidin 0.5 μg/ml puromycin 1 μg/ml doxycyline
HT1080 HAC-dGFP tetR-mCherry-BRC4 WT**	HT1080 HAC-dGFP	tetR-mCherry BRC4 (wild-type)	pJETY3 tetR-mCherry BRC4 WT	constitutive expression	15 μg/ml blasticidin 0.5 μg/ml puromycin 1 μg/ml doxycyline
HT1080 HAC-dGFP tetR-mCherry-BRC4 M5**	HT1080 HAC-dGFP	tetR-mCherry BRC4 M5	pJETY3 tetR-mCherry BRC4 M5	constitutive expression	15 μg/ml blasticidin 0.5 μg/ml puromycin 1 μg/ml doxycyline
HT1080 HAC-dGFP tetR-mCherry-WD40 WT*	HT1080 HAC-dGFP	tetR-mCherry WD40 (wild-type)	pJETY3 tetR-mCherry WD40 WT	constitutive expression	15 μg/ml blasticidin 0.5 μg/ml puromycin 1 μg/ml doxycyline
HT1080 HAC-dGFP tetR-mCherry-WD40 A1025R*	HT1080 HAC-dGFP	tetR-mCherry WD40 A12025R	pJETY3 tetR-mCherry WD40 A1025R	constitutive expression	15 μg/ml blasticidin 0.5 μg/ml puromycin 1 μg/ml doxycyline

Table 2.2: Stable cell lines generated in this thesis. Generated by L. Rampazzo (*). Generated by L. Rampazzo and D.Torre (**)

Cell line	Parental	Mutation	Medium	Antibiotics
HCT116 CMV-OsTIR1 mAID-Halo-BRCA2*	HCT116 CMV-OsTIR1 [205]	N-terminal mAID-Halo-tag BRCA2	McCoy's 5A	1 μg/ml puromycin 700 μg/ml geneticin
HCT116 mAID-mNeonGreen-BRCA2**	HCT116	N-terminal mAID-mNeonGreen-tag BRCA2	McCoy's 5A	100 μg/ml hygromycin
HCT116 CMV-OsTIR1 mAID-mNeonGreen-BRCA2**	HCT116 CMV-OsTIR1 [205]	N-terminal mAID-mNeonGreen-tag BRCA2	McCoy's 5A	1 μg/ml puromycin 100 μg/ml hygromycin

Table 2.3: CRISPR-modified cell lines generated in this thesis. Generated by L. Rampazzo, X. Saayman and F. Esashi (*). Generated by L. Rampazzo (**)

2.1.2 Plasmids

Name	Purpose
pJETY3 [166]	Generation of pJETY3 plasmids
pcDNA-DEST mCh-B2.4 #1	PCR amplification of BRC4 (wild-type)
pcDNA-DEST53 PALB2 WT	PCR amplification of WD40 (wild-type)
pcDNA-DEST53 PALB2 A1025R	PCR amplification of WD40 A1025R
pDEST17 B.8 WT #2	PCR amplification of B2.8 (wild-type)
pcDNA-DEST53 B2.8 S3149A #2	PCR amplification of B2.8 S3149A
pcDNA-DEST53 B2.8 T3193A #2	PCR amplification of B2.8 T3193A
pcDNA-DEST53 B2.8 S/T #2	PCR amplification of B2.8 S3149A/T3193A
pH2B_mCherry-IRES-Puro	PCR amplification of mCherry
Flag-HA-USPII [206]	PCR amplification of IRES-Puro
pJETY3 tetR-mCherry-IRES-Puro	Generation of HT1080 HAC-dGFP
	tetR-mCherry stable cell lines
pJETY3 tetR-mCherry-BRC4 WT-IRES-Puro	Generation of HT1080 HAC-dGFP
	tetR-mCherry-BRC4 WT stable cell lines
pJETY3 tetR-mCherry-BRC4 M5-IRES-Puro	Generation of HT1080 HAC-dGFP
	tetR-mCherry-BRC4 M5 stable cell lines
pJETY3 tetR-mCherry-WD40 WT-IRES-Puro	Generation of HT1080 HAC-dGFP
	tetR-mCherry-WD40 WT stable cell lines
pJETY3 tetR-mCherry-WD40 A1025R-IRES-Puro	Generation of HT1080 HAC-dGFP
	tetR-mCherry-WD40 A1025R stable cell lines
pX458pSpCas9(BB)2A-GFP-BRCA2-gRNA	Generation of CRISPR-modified cell lines
pMK341-neoR-mAID-HaloTag-BRCA2	Generation of CRISPR-modified cell lines
pMK341-hygR-mAID-mNeonGreenTag-BRCA2	Generation of CRISPR-modified cell lines

Table 2.4: Plasmids used in this thesis

2.1.3 Oligonucleotides

Name	Sequence 5′-3′	Purpose
XhoI_BRC4-WT_F	ATA CTC GAG AAA GAA	PCR amplification
	CCT ACT CTA TTG	BRC4-WT fragment
XhoI_BRC4-M5_F	ATA CTC GAG AA AGA	PCR amplification
	ACC TAC TCT ATT GGG	BRC4-M5 fragment
	TTT TCA TGC **G***CA TAG	
	CGG	
BRC4_STOP_NotI_R	TAT GCG GCC GC*T CA*T	PCR amplification
	TGC TCT TTT TCA TC	BRC4 fragments
XhoI_B2.8_F	ATA CTC GAG GCT AAC	PCR amplification
	AGT ACT CGG CC	B2.8 fragments
B2.8_WT_STOP_NotI_R	TAT GCG GCC GC*T CA*G	PCR amplification
	TCT TTA GTT GGG GTG G	B2.8 fragments
B2.8_T3193A_STOP_NotI_R	TAT GCG GCC GC*T CA*G	PCR amplification
	TCT TTA GTT GGG GCG G	B2.8 T3193A fragment
XhoI_WD40_F	ATA CTC GAG TCC GTC	PCR amplification
	GAA CAG ACT G	WD40 fragment
WD40_STOP_NotI_R	TAT GCG GCC GC*T CA*T	PCR amplification
	GAA TAG TGG TAT ACA	WD40 fragment
	AAT ATA TTT CC	
B2.8_5′end_R	ATC CAG ATG ATG TCT	Validation of B2.8 construct
	TCT CCA TCC	by Sanger sequencing
B2.8_3′end_F	GTG GCG ACC AGA ATC	Validation of B2.3 construct
	CAA ATC AGG	by Sanger sequencing
WD40_5′end_R	TTC GCA AGC AGT TAT	Validation of WD40 construct
	GAT ACA TGG	by Sanger sequencing
WD40_3′end_F	TGC AGC AGC AAT CTT	Validation of WD40 construct
	GAC TTC TGG	by Sanger sequencing

Table 2.5: Oligonucleotides used in this thesis for the generation of pJETY3-tetR-EYFP constructs in the first step of cloning described in section 2.2.9. Restriction sites (underlined). Start and stop codons (italic). Asterisk (*) indicates a site-specific of mutagenesis: Threonine (ACA) is replaced with an Alanine (**G***CA)

Name	Sequence 5′-3′	Purpose
AfeI-mCherry_F1	TAT GCA AGC GCT ACC	PCR amplification
	GGT CGC CAC C*AT* GGT	mCherry fragment
	GAG CAA GGG CGA GGA	
mCherry-EcoRV_R1	TAT GCA GAT ATC TTC TTG TAC A	PCR amplification
	GCT CGT CCA T	mCherry fragment
tetR_F	GAG GAG CAA GCA ACA	Validation of tetR-mCherry clones
	AAC CAG ATA G	by colony PCR
mCherry_R	GGC TTC TTG GCC TTG	Validation of tetR-mCherry clones
	TAG GTG G	by colony PCR

Table 2.6: Oligonucleotides used in this thesis for the generation of pJETY3-tetR-mCherry constructs in the second step of cloning described in section 2.2.9. Restriction sites (underlined). Start and stop codons (italic).

Name	Sequence 5′-3′	Purpose
F-BamHI-IRES	AGA GAG GGA TCC GGA	PCR amplification
	ATT CCG CCC CTC TCC	IRES-Puro fragment
	CTC CCC CCC CCC TAA	
	CGT TAC TGG CC	
R-SpeI-STOP-Puro	CTC TCT ACT AGT *TCA*	PCR amplification
	GGC ACC GGG CTT GCG	IRES-Puro fragment
	GGT	
R_IRES	TGT TTG TCT TCA AGA	Validation of IRES-Puro construct
	AGC TTC CAG	by Sanger sequencing
F_Puro	TCT GGG CAG CGC CGT	Validation of IRES-Puro construct
	CGT GCT	by Sanger sequencing

Table 2.7: Oligonucleotides used in this thesis for the generation of pJETY3-tetR-mCherry-IRES-Puro constructs in the third step of cloning described in section 2.2.9. Restriction sites (underlined). Start and stop codons (italic).

Name	Sequence 5′-3′	Purpose
Vector_F	TCG AGC TCA AGC TTC GAT GCC TAT TGG ATC CAA AGA GAG GCC AAC ATT	PCR amplification of the vector used for Gibson assembly
Vector_R	CCT CCT CGC CCT TGC TCA CCA TGC CAG ATC CGG CGC CTG C	PCR amplification of the vector used for Gibson assembly
CRISPR_Nterm	GCC CTT TTG TCT CTG CCA AC	PCR amplification of genomic DNA (Validation of CRISPR cell lines)
BRCA2genDNA_F		
CRISPR_Cterm	TGG GTA TGA GGA ACA TGT GGA C	PCR amplification of genomic DNA (Validation of CRISPR cell lines)
BRCA2genDNA_R		
CRISPR_Hyg_R	AAC TTC TCG ACA GAC GTC GC	PCR amplification of genomic DNA (Validation of CRISPR cell lines)
CRISPR_mNG_R	AGG CTG TTG GTC ATC ACA GG	PCR amplification of genomic DNA (Validation of CRISPR cell lines)
CRISPR_pMK431backbone_F	TGT AAA ACG ACG GCC AGT GA	PCR amplification of genomic DNA (Validation of CRISPR cell lines)

Table 2.8: Oligonucleotides used in this thesis for the generation of CRISPR modified cell lines as described in section 5.2.1. Overlap region for Gibson assembly (underlined).

Name	Sequence 5′-3′	Supplier
tetO-probe [203]	[FITC-OO]-ACC ACT CCC TAT CAG	Panagene
CENP-B-Cy5 probe	ATT CGT TGG AAA CGG GA	PNA bio

Table 2.9: FISH probes used in this thesis.

2.1.4 Antibodies

Antibody	Supplier	Application	Dilution
BRCA2	Millipore (OP95)	WB	1:1000
RAD51	Biogenes [122] (7946)	WB	1:5000
PALB2	Biorbyt (orb412704)	WB	1:1000
LaminA	Sigma Aldrich (L1293)	WB	1:10000
Histone H3 (phospho-S10)	Millipore (06-570)	FC	1:1000
Histone H3	Bethyl Laboratories (A300- 823A-T)	WB	1:2000
mCherry	GeneTex (GTX128508)	WB	1:1000
α-Tubulin (DM1A)		WB	1:1000
CENP-A	Abcam (ab13939)	IF, WB	1:1000
CENP-C	Millipore (ABE1957)	IF, WB	1:2000
CENP-B	Bethyl Laboratories (IHC-00064-T)	IF, WB	1:1000
ACA (anti-centromere)	Antibodies incorporated	IF	1:2000
ZWINT	GeneTex (GTX107155)	WB	1:500
CASC5/KNL1	Bethyl Laboratories (A300-805A-T)	WB	1:500
DSN1 (N3C3)	GeneTex (GTX120402)	WB	1:500
HP1 alpha (EPR5777)	Abcam (ab109028)	WB, IF	1:1000
Acetylated lysine (Ac-K2-100)	Cell Signalling Technology	WB, IF	1:1000, 1:250
Histone H3 (tri methyl K9)	Abcam (ab8898)	IF, WB	1:500, 1:1000
HaloTag	Promega (G9211)	WB	1:1000
p21 (12D1)	Cell Signalling Technology	WB	1:1000
p53 (pAb122)	Abcam (ab90363)	WB	1:1000
γH2AX (clone JBW301)	Millipore	IF	1:1000
Cyclin B1 (GNS1)	Santa Cruz (sc-245)	IF	1:500
DSN1	Yanagida's Laboratory	IF	1:20

Table 2.10: List of Primary antibodies used in this thesis. Western Blot (WB), Immunofluorescence (IF). Flow cytometry (FC)

Antibody	Supplier	Application	Dilution
Goat anti-rabbit HRP	Dako (PO448)	WB	1:2000
Goat anti-mouse HRP	Dako (PO447)	WB	1:1000
Alexa-Fluor 647	Thermo Fisher Scientific (A-21235)	IF	1:500
	Thermo Fisher Scientific (A-21244)	IF, FC	1:500, 1:100
Alexa-Fluor 555	Thermo Fisher Scientific (A-21422)	IF	1:500
	Thermo Fisher Scientific (A-21428)		
Alexa-Fluor 488	Thermo Fisher Scientific (A-11001)	IF	1:500
	Thermo Fisher Scientific (A-11008)	IF	1:500

Table 2.11: List of secondary antibodies used in this thesis. Western Blot (WB), Immunofluorescence (IF). Flow cytometry (FC)

2.1.5 siRNAs

Name	Sequence 5′-3′	Supplier
siCTR (scr-1)*	GAACAACCUCACAAACUAAUU	Invitrogen
siCTR (scr-2)*	GGCAAACGCAUCAUCACGUUU	Invitrogen
BRCA2 (1) [123]	CAACAAUUACGAACCAAAC	Invitrogen
BRCA2 (2) [123]	CUGAGCAAGCCUCAGUCAA	Invitrogen
RAD51 (1) [123]	GACUGCCAGGAUAAAGCUU	Invitrogen
RAD51 (2) [123]	GUGCUGCAGCCUAAUGAGA	Invitrogen
PALB2 (1) [98]	GGAAAGAGCCGGUUGUAAAdTdT	Sigma
PALB2 (2) [98]	GGAGAAAUUAGCAUUCUUGdTdT	Sigma
STK38* [204]	CCUUAUCGCUCAACAUGAAdTdT	Dharmacon
STK38 [204]	CCUUAUCGCUCAACAUGAAdTdT	Invitrogen
GFP* [204]	GCAAGCUGACCCUGAAGUUC	Dharmacon
GFP [204]	GCAAGCUGACCCUGAAGUUCdTdT	Invitrogen

Table 2.12: siRNAs used in this thesis. (*) Used in Exp.1 of Figures 3.7 and 3.10

2.1.6 Buffers and solutions

Name	Composition
1× Phosphate Buffered Saline (PBS)	136.9 mM NaCl, 2.7 mM KCl,
pH 7.4	17.2 mM Na_2HPO_4, 1.76 mM KH_2PO_4
NETN150 lysis buffer	50 mM Tris-HCl pH 8.0, 150 mM NaCl, 2 mM EDTA pH 8,
	0.5 % NP-40, 1× Sigma protease inhibitors,
	10 mM Benzamide Hydrochloride, 20 mM NaF,
	1 mM Na_3VO_4, 20 mM Na-β- Glycerophosphate
Tris Acetate EDTA (TAE) buffer	1.25 mM EDTA, 40 mM Tris, 5.7 % acetic acid
Tris Borate EDTA (TBE) buffer	
Genomic DNA extraction buffer	10 mM Tris-HCl pH 8.0, 1 mM EDTA pH 8,
	25 mM NaCl, 200 μg/ml Proteinase K
PTEMF fixation buffer	20 mM PIPES pH 6.5, 0.2 % Triton X-100, 10 mM EGTA
	1 mM EGTA, 4 % Formaldehyde

Table 2.13: Buffers and solutions used in this thesis

2.1.7 List of materials used

Item	Supplier
DNA Loading dye (6×)	New England Biolabs
DNA ladders (100 bp, 1 kb)	New England Biolabs
Ethidium bromide	Sigma Aldrich
Ultra Pure Agarose	Invitrogen
Calf Intestinal Alkaline Phosphatase (CIP)	New England Biolabs
One Shot^{TM} TOP10 *E. coli* cells	Thermo Fisher Scientific
Ampicillin	Melford
LB agar	Merck
LB broth	Merck
SOB	Fisher BioReagents
NEB Buffer 3.1 (10*times*)	NEB
CutSMART buffer (10×)	NEB
Gateway LR Clonase enzyme mix	Thermo Fisher Scientific
Dulbecco's Modified Eagle Medium (DMEM)	GIBCO
Heat Inactivated FBS Fetal Bovine Serum (EU approved)	GIBCO
Trypsin (Tryple Express Enzyme)	GIBCO
Penicillin-Streptomycin	GIBCO
McCoy's 5A (Modified) Medium	GIBCO
Opti-MEM I (1×) Reduced Serum Medium	GIBCO
Lipofectamine RNAiMAX reagent	Thermo Fisher Scientific
DharmaFECT1 transient reagent	GE Dharmacon
1× PBS	
Triton X-100 (10 %)	Sigma Aldrich

Table 2.14: Reagents used in this thesis.

Item	Supplier
Bovine Serum Albumin (BSA)	Sigma Aldrich
RNAse A	Sigma Aldrich
Formaldehyde (37%)	Sigma Aldrich
Paraformaldehyde (16%)	Thermo Fisher Scientific
Mowiol mounting media	
Hoechst	Sigma Aldrich
5-ethynyl-2′-deoxyuridine (EdU)	Life Technologies
Dimethyl sulfoxide (DMSO)	Sigma Aldrich
Tween-20	Sigma Aldrich
10 % NP-40 detergent solution	Thermo Fisher Scientific
Benzamidine Hydrochloride hydrate	Sigma Aldrich
Benzonase Nuclease	EMD Millipore
Protease inhibitor cocktail	Sigma Aldrich
Nitrocellulose membrane (Amersham Protan)	GE Healthcare Life Sciences
Dried skimmed milk	Marvel
NuPAGE 4-12 % Bis-Tris protein gels	Thermo Fisher Scientific
BlueEasy Pre-stained protein ladder	Geneflow
NuPAGE LDS sample buffer	Thermo Fisher Scientific
ECL Western Blotting detection reagents	GE Healthcare
Bradford protein assay	Bio-Rad
Dithiothreitol (DTT)	Sigma Aldrich
Ponceau	Sigma Aldrich
Re-Blot Plus Mild Solution	EMD Millipore
Duolink™ proximity ligation assay(PLA®)	Sigma Aldrich
Alexa Fluor™ 647 Phalloidin	Thermo Fisher Scientific

Table 2.15: Other reagents used in this thesis.

Item	Supplier
Cell Counting Kit-8	
B02 (RAD51 inhibitor)	Calbiochem
CellTrace™ Far Red Cell Proliferation Kit	Thermo Fisher Scientific
MISSION® siRNA Universal Negative Control #1	Sigma Aldrich
DRAQ7	Abcam
Propidium Iodide	Sigma Aldrich
DAPI	Molecular Probes
ProLong™ Gold Antifade Mountant	Life Technologies
ProLong™ Gold Antifade Mountant with DAPI	Life Technologies
RFP-TrapA	Chromotek
Formamide (100%)	Sigma Aldrich
Destran sulfate	Sigma Aldrich
PCRBio HiFi Polymerase	PCR Biosystems
PCRBio HiFi buffer	PCR Biosystems
Q5 High-Fidelity DNA polymerase	New England BioLabs
NEBuilder® HiFi DNA Assembly Cloning Kit	New England BioLabs
NEB 5-alpha competent *E. coli* cells	New England BioLabs
Auxin	Sigma Aldrich
siR-DNA	Spirochrome
Proteinase K	Sigma Aldrich
Alexa Fluor™ 647 Azide	Thermo Fisher Scientific
HaloTag ligand Janelia Fluor™ 549	Lavis Lab
HaloTag ligand Janelia Fluor™ 646	Lavis Lab
HaloTag Ligand TMR-Direct	Promega
HaloTag Ligand Oregon Green	Promega
CELLview™ Dish with Glass Bottom (35 mm)	Greiner Bio-One

Table 2.16: Reagents and various items used in this thesis.

Drugs	**Supplier**
Aphidicolin	Santa Cruz
Hydroxyurea	Sigma Aldrich
Taxol	
RO3306	Axon Medchem
Nocodazole	Calbiochem
Antibiotics	**Supplier**
Blasticidin	Invivogen
Puromycin	Invivogen
Doxycycline	Sigma Aldrich
G418 disulfate salt (geneticin)	Sigma Aldrich
Kits	**Supplier**
Quiaquick Gel extraction Kit 50	Qiagen
Quiaquick PCR purification kit	Qiagen
GeneJET Plasmid Miniprep Kit	Thermo Fisher Scientific
GeneJET Genomic DNA Purification Kit	Thermo Fisher Scientific
DNA Ligation kit	Takara
Restriction enzymes	**Supplier**
XhoI	New England Biolabs
NotI	New England Biolabs
AfeI	New England Biolabs
EcoRV	New England Biolabs
BamHI	New England Biolabs
SpeI	New England Biolabs

Table 2.17: Drugs, antibiotics, kits and enzymes used in this thesis.

2.2 DNA analysis techniques

2.2.1 Genomic DNA extraction

Genomic DNA was extracted from mammalian cells and used as a DNA template for PCR reactions. This method was used to test the integration of Hyg-mAID-mNeonGreen tag at the N-terminus of the endogenous *BRCA2* gene in CRISPR-modified cell lines (section 5.2.1). Starting from a confluent 6-well, cells were collected by trypsinisation as described in section 2.4.1. The cell pellet was washed once in PBS, frozen in liquid nitrogen and stored at -80 °C until genomic DNA extraction was performed. All samples were analysed within a month. At the time of the analysis, 400 μl of Genomic DNA extraction buffer was added to 10-20 mg of cell pellet. The homogenised cell pellet was incubated at 65 °C for 30 min followed by incubation at 95 °C for 2 min to inactivate Proteinase K. DNA content was measured using a spectrophotometer.

2.2.2 Agarose gel electrophoresis

Agarose gel electrophoresis was used to separate DNA fragments according to their size. DNA is negatively charged and migrates to the anodes and the velocity of migration depends on the size of the fragment: small DNA fragments migrate faster, whereas large DNA fragments migrate slower on the gel. DNA samples were run on 1-2 % (w/v) agarose gels based on the size of the expected fragments (i.e. 2 % was used to separate small-size fragments <200 bp). Agarose was dissolved in 1× TBE or TAE buffer for 2-3 min in the microwave. DNA fragments are better separated with TBE buffer but the borate in the TBE buffer can inhibit enzymatic activity; therefore, TBE was preferred for endpoint analysis to check the size of the DNA fragments. By contrast, TAE was favoured when DNA fragments were used for subsequent enzymatic applications (i.e. ligation). After cooling down, 0.25 μg/ml of ethidium bromide was added to the agarose solution and a gel was poured into the gel stamp. Ethidium bromide was used as an intercalating DNA agent to detect the DNA using UV light. DNA

samples were prepared with 1× DNA Loading dye and loaded into the gel. 100 bp and 1 kb DNA ladders were used to verify the size of the DNA fragments. Electrophoresis was performed at 80 V. DNA fragments were visualised under UV light.

2.2.3 Restriction enzyme digestion

Digestion of DNA fragments and DNA plasmids with different DNA restriction enzymes was performed according to the manufacturer's procedures (NEB). Generally, the digestion mix contains 1 μg DNA, 1× reaction buffer, 20 U of restriction enzyme, dH_2O up to a final volume of 50 μl. Typically digestion was performed at 37 °C for 1 h.

2.2.4 Polymerase chain reaction (PCR)

PCR was used to amplify DNA fragments starting from DNA plasmids or genomic DNA of cultured cell lines. Amplified DNA fragments were used for cloning of DNA plasmids and the screening process of newly generated cell lines.
Each PCR reaction mix contains the DNA template, two oligonucleotides (primers) at the 5' and 3' ends of the DNA fragment, forward (F) and reverse (R) primers, dNTPs and the DNA polymerase for the DNA synthesis. The PCR reaction has three steps: the initial denaturation of the double-stranded DNA, the annealing of the primers to the complementary DNA sequence and the extension, or DNA synthesis, of the DNA fragment, executed by the DNA polymerase. Each step is performed at different temperatures: the DNA is denaturated at 95 °C, primers annealing is performed at 55-65 °C (varies based on the primer set), 72 °C for the DNA synthesis. The duration of the extension step depends on the length of the DNA fragment that is amplified. The three steps of the PCR reaction are repeated 20-35 times to allow DNA amplification. In this thesis, PCR reactions were prepared as described in table 2.18 using PCRBio HiFi Polymerase according to the manufacturer's procedures.

Reaction mix	**Programme**	**Application**
1X PCRBio Reaction Buffer (5×)	95 °C × 1 min	Amplification
0.4 μM Forward primer (F)	95 °C × 15 sec *	from plasmid DNA
0.4 μM Reverse primer (R)	55-65 °C × 15 sec *	
10 ng Template DNA	72 °C × 30 sec per kb *	
1 U PCRBio Hifi polymerase	* *repeat for 25 cycles*	
dH_2O up to 50 μl of final volume	72 °C × 5 min	
1X PCRBio Reaction Buffer (5×)	95 °C × 1 min	Amplification
0.4 μM Forward primer (F)	95 °C × 15 sec *	from genomic DNA
0.4 μM Reverse primer (R)	55-65 °C × 15 sec *	
100-300 ng genomic DNA	72 °C × 30 sec per kb *	
1 U PCRBio Hifi polymerase	* *repeat for 30 cycles*	
dH_2O up to 20 μl of final volume	72 °C × 5 min	

Table 2.18: PCR reactions/protocols

2.2.5 DNA plasmid cloning

Insert preparation

PCR was performed to amplify the desired DNA fragment from plasmid DNA using the appropriate set of primers. 10 % of the PCR product was used for agarose gel electrophoresis to check the amplification of the correct DNA fragment. The remaining 90 % of the PCR product was purified using the Quiaquick PCR purification kit according to the manufacturer's procedures. The purified PCR product was subsequently

digested using restriction enzymes and used for ligation 2.2.5.

Vector preparation

DNA plasmid was digested using restriction enzymes. The digestion mix was supplemented with 4 U of Calf Intestinal Alkaline Phosphatase (CIP) to prevent vector re-ligation. Digested vector was run into an agarose gel. The appropriate band was excised and purified using the Quiaquick Gel extraction kit according to the manufacturer's procedures. Purified vector was used for ligation 2.2.5.

Ligation

50 ng of the purified vector was used for each ligation reaction. Vector was mixed with the insert at 1:3 molar ratio vector: insert and 1× volume of DNA Ligation mix (Takara) was added to the ligation mix. Ligation was performed at 16 °C o/n. Ligated constructs were subsequently used for transformation in bacteria 2.3.1.

2.2.6 Gibson Assembly

Gibson assembly was used to generate the DNA plasmid pMK341-hygR-mAID-mNeonGreenTag-BRCA2. Vector amplification from pMK341-neoR-mAID-HaloTag-BRCA2 plasmid was performed by PCR using Q5 HiFi DNA polymerase according to the manufacturer's procedures. The amplified vector was run into an agarose gel and purified using the Quiaquick Gel extraction kit according to the manufacturer's procedures. Purified vector was used for Gibson Assembly. Gibson assembly was performed using NEBuilder® HiFi DNA Assembly Cloning Kit according to the manufacturer's procedures. Briefly, the vector was mixed with the insert at 1:2 molar ratio vector:insert. 10 μl of Gibson Assembly Master Mix was added to the vector-insert mixture and dH_2O was added to a final volume of 20 μl. Gibson Assembly reaction mix was incubated at

50 °C for 60 min. The DNA was transformed performed into NEB 5-alpha competent *E. coli* cells according to the manufacturer's procedures.

2.2.7 Colony PCR

Colony PCR consists of a PCR reaction as described in section 2.2.4 using a bacterial colony instead of plasmid DNA as a DNA template. This technique was used after transformation to screen bacterial colonies. This method allows a fast screening without prior expansion of the bacterial colonies and extraction of the DNA plasmid. Bacterial colonies were picked with a toothpick or a sterile pipette tip and swirled into the PCR reaction mix. Colony PCR reaction mix was prepared as described in section 2.2.4 and dH_2O was added up to a final volume of 10 μl.

2.2.8 Sanger sequencing

All plasmids generated in this thesis were validated by Sanger sequencing. Sequencing was performed by Source BioScience UK Ltd and Eurofins Genomics.

2.2.9 Generation of tetR-constructs

The tetR-mCherry-BRC4/B2.8/WD40 constructs were generated with three steps of cloning. In the first step, the BRC4 WT, B2.8 WT, B2.8 S3149A, B2.8 T3193, B2.8 S3149A/T3193A, WD40 WT and WD40 A1025R were PCR-amplified from plasmids, using the corresponding primers (Table 2.5) with an XhoI restriction site at the 5'-end and NotI at the 3'-end (Figure 2.1A). BRC4-M5 mutation was introduced in the BRC4 construct using a 5'-end primer with a single nucleotide mutation: an adenine was substituted with a guanine in the 5'-end primer in order to replace the threonine 10 with alanine. The XhoI-insert-NotI constructs were cloned into the XhoI/NotI digested pJETY3 vector containing tetR sequence and an EYFP gene. The integration of the constructs was

validated by enzymatic digestion with XhoI and NotI restriction enzymes: clones with the right insert showed a band at around 1277 bp for B2.8 construct and 1056 bp for WD40 constructs. In this gel, the BRC4 constructs (115 bp) ran off the gel (Figure 2.1B). All BRC4 clones and the positive B2.8 and WD40 clones were sequenced by Sanger sequencing with either the amplification primers or primers designed ∼150 bp downstream the 5′-end and 3′-end to sequence the extremity of the constructs. WT and mutant clones were generated for each construct by sequencing (Figure 2.1C).

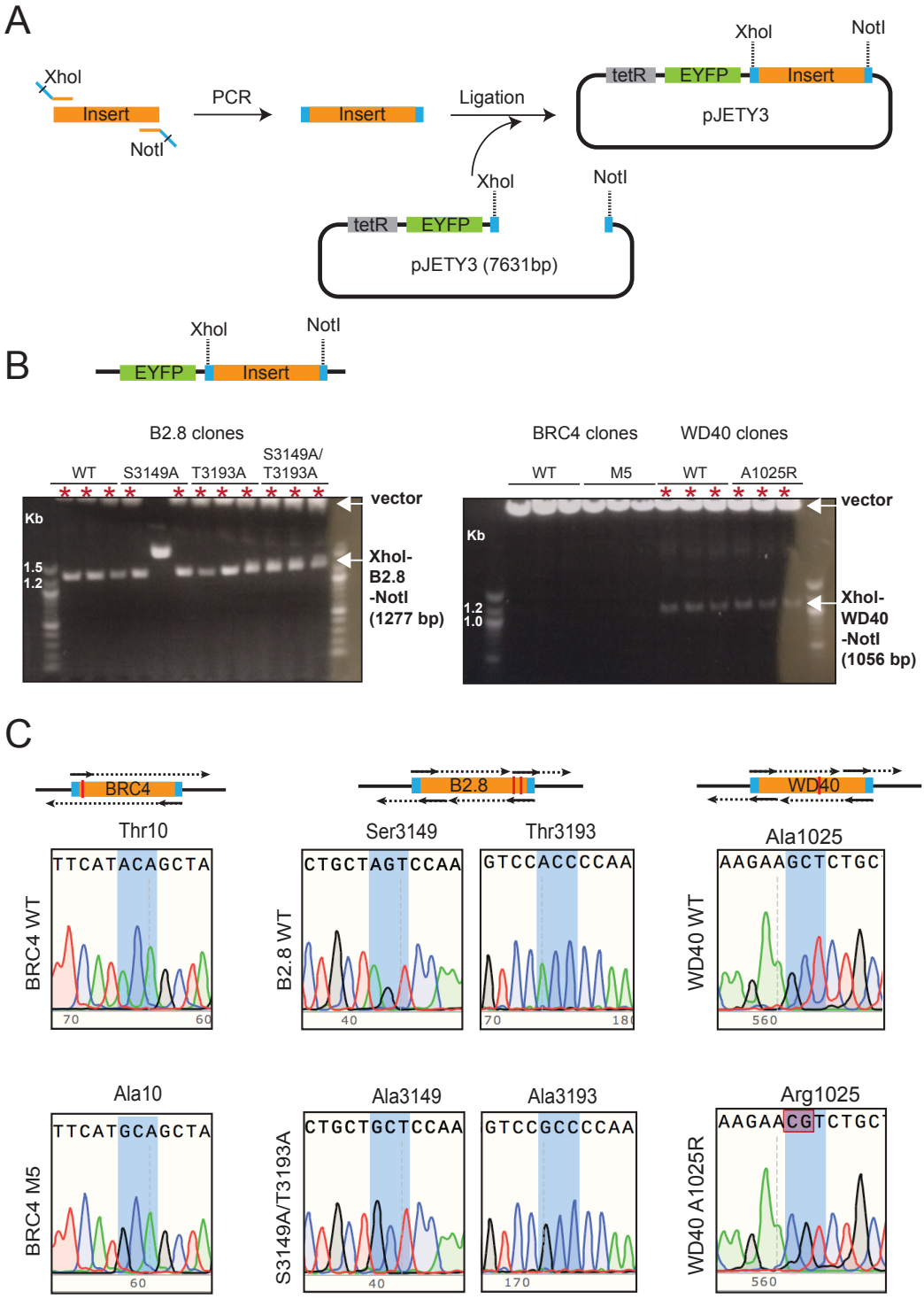


Figure 2.1: **Generation of pJETY3-tetR-EYFP-BRC4/B2.8/WD40 plasmids.** (**A**) Schematic representation of the cloning steps. Inserts (BR4 WT, BRC4 M5, B2.8 S3149A, B2.8 T3193A, B2.8 S3149A/T3193A, WD40 WT, WD40 A1025R) were PCR-amplified and introduced into the pJETY3 vector after XholI/NotI digestion. (**B**) Enzymatic digestion of the generated construct with with Xhol and NotI restriction enzymes. Positive clones (red asterisk) (**C**) Schematic representation of the primers used for Sanger sequencing (black continuous arrows). Position of the mutations of each construct are highlighted in red. Electropherogram of one representative clone for each construct. WT sequences and mutated sequences are highlighted in blue. Cloning was performed in collaboration with Chris Ralf and Xanita Saayman: LR generated B2.8 constructs, XS generated BRC4 and WD40 constructs, CR helped LR and XS in the experimental design.

In the second step of cloning, the EYFP gene was replaced with mCherry to enable detection of the fusion protein separately from the EGFP expressed from the HAC. The mCherry was PCR-amplified from a plasmid, using the corresponding primers (Table 2.6) with an AfeI restriction site at 5′-end and EcoRV at 3′-end. The AfeI-mCherry-EcoRV was cloned into the AfeI/EcoRV digested pJETY3 vectors (Figure 2.2A). Colonies screening was initially performed by colony PCR using a forward primer on the tetR sequence and a reverse primer on the mCherry sequence (Figure 2.2B): positive clones showed a PCR product around 465 bp. The positive clones were digested with AfeI and EcoRV restriction enzymes to validate the integration of the full length mCherry construct: positive clones showed a band around 747 bp for the insert and the around 7000 bp for the vectors (Figure 2.2C). Finally, the positive clones were sequenced by Sanger sequencing using the forward amplification primer and a tetR-primer or an internal reverse primer to sequence the extremity of the construct (Figure 2.2D).

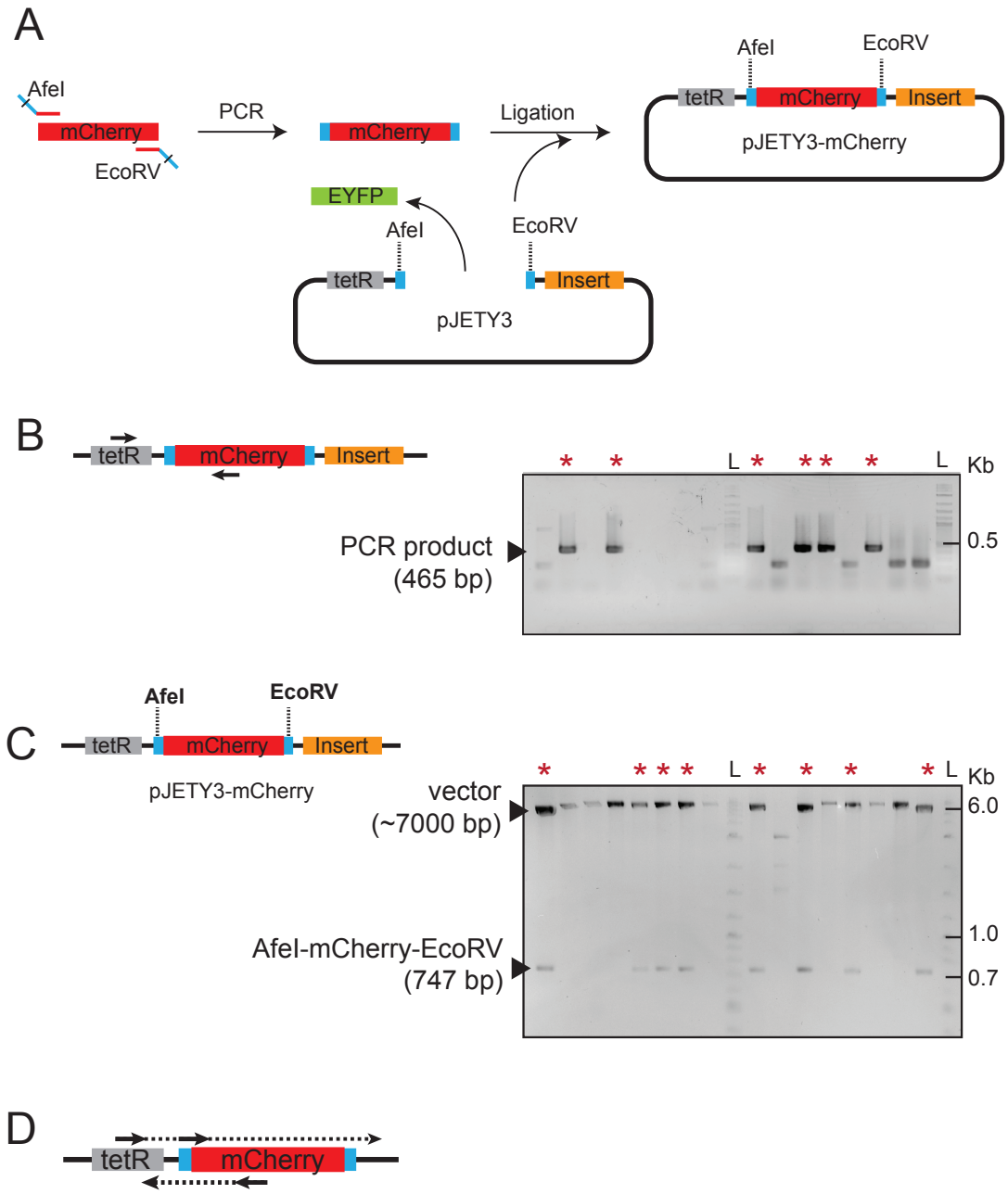


Figure 2.2: **Generation of pJETY3-tetR-mCherry plasmids.** (**A**) Schematic representation of the cloning steps. EYFP gene on pJETY3 vectors was replaced with mCherry gene. mCherry gene was PCR-amplified and introduced into the pJETY3 vector after AfeI/EcoRV digestion. Validation of the clones was done in three steps: colony PCR (**B**), enzymatic digestion with AfeI and EcoRV restriction enzymes(**C**) and Sanger sequencing (**D**). Primers used for each step (black arrows). Positive clones marked with a red asterisk (*). 1Kb Ladder (L). Cloning was performed in collaboration with Nicholay Goncharov and Mikhail Liskovykh: LR generated tetR-mCherry constructs, NG contributed at the screening of the clones by colony PCR, ML helped LR in the experimental design.

In the last step of cloning, the hygromicin (Hyg) resistance gene was replaced with a puromycin resistance gene. This step was performed in order to select cells expressing tetR-mCherry-constructs in HAC/dGFP expressing cells. In order to co-express the tetR-mCherry-construct and the resistance gene separately, an internal ribosomal entry sequence (IRES) was introduced between the tetR-mCherry-constuct and the puromycin resistance gene. The IRES-Puro was PCR-amplified from plasmid, using the corresponding primers (Table 2.7) with a BamHI restriction site at the 5'-end and SpeI at the 3'-end. BamHI-IRES-Puro-SpeI was cloned into the BamHI/SpeI digested pJETY3 vectors (Figure 2.3A) . The integration of the construct has been validated by enzymatic digestion with BamHI and SpeI restriction enzymes: positive clones showed a band around 1200 bp for the insert and a band around 700 bp for the vectors. Finally, all constructs were sequenced using the primers of the initial amplification step and two internal primers to sequence the extremities of the construct (Figure 2.3B-C).

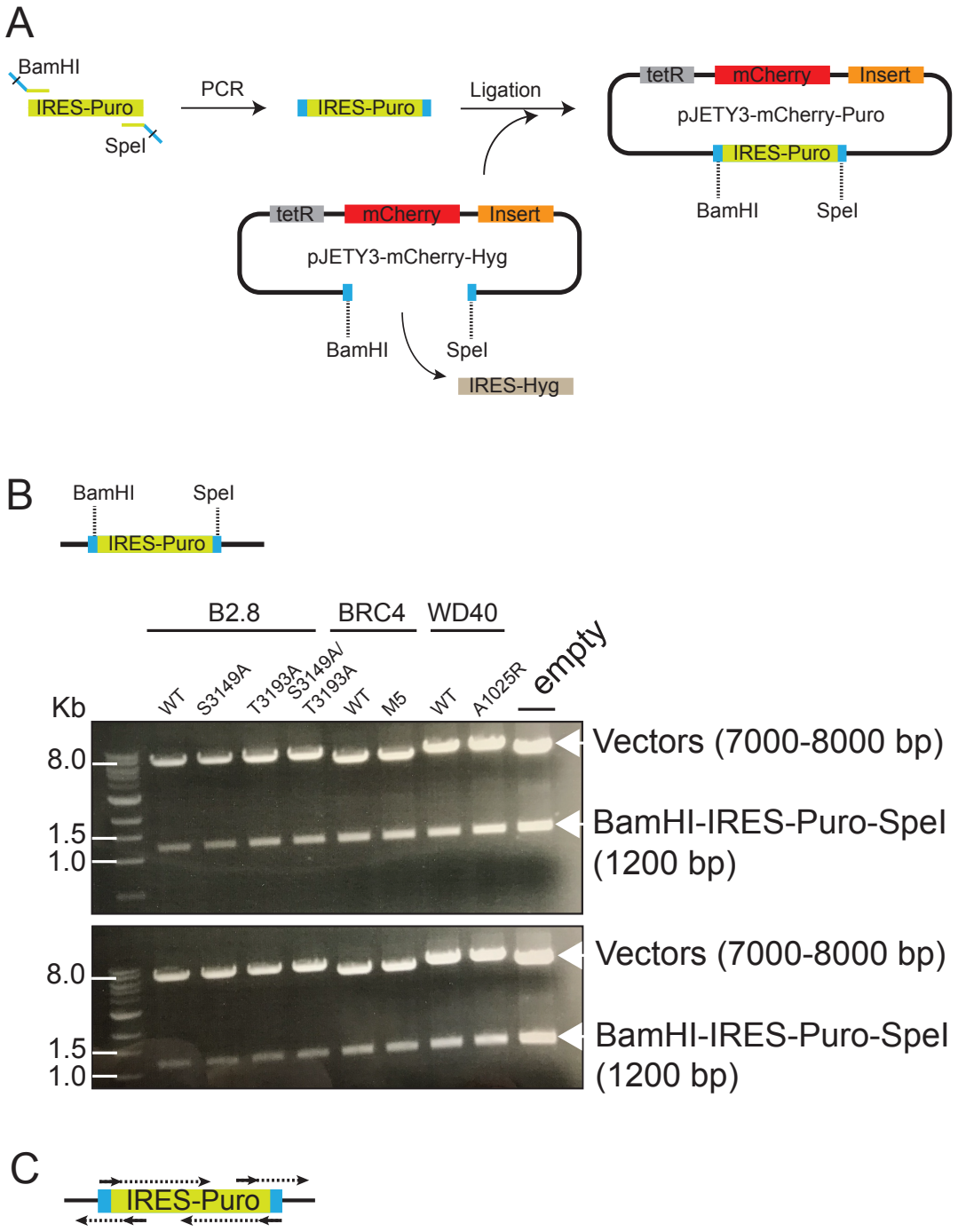


Figure 2.3: **Generation of pJETY3-tetR-mCherry-IRES-Puro plasmids. A**: Schematic representation of the cloning steps. IRES-Hygromicin (Hyg) gene on pJETY3 vectors was replaced with IRES-Puromycin (Puro) gene. IRES-Puro was PCR-amplified and introduced into the pJETY3 vector after BamHI/SpeI digestion. Validation of the clones was done by enzymatic digestion and Sanger sequencing. (**B**) Representative gel with clones after enzymatic digestion with BamHI and SpeI restriction enzymes. Positive clones showed a band at around 1200 bp. (**C**) Schematic representation of the primers used for Sanger sequencing (black arrows). Cloning was performed in collaboration with Chris Ralf. LR generated the IRES-Puro constructs. CR contributed at the screening of the clones by enzymatic digestion and helped LR in the experimental design.

2.3 Bacterial techniques

2.3.1 Heat-shock transformation

Transformation in bacterial cells was performed to amplify plasmid DNA. TOP10 *E. coli* competent cells were used for the transformation. Approximately 50 ng of plasmid DNA was added to 100 μl of thawed competent cells, mixed by tapping gently and incubated for 30 min on ice. The mixture was incubated at 42 °C for 30 sec and subsequently placed on ice for 2 min. 500 μl of pre-warmed (37 °C) SOB medium supplemented with 20 mM glucose was added to the cells and incubated at 37 °C for 1 h with constant shaking. Transformed cells were collected by centrifugation for 5 min at 200 g. The cell pellet was resuspended in 100-200 μl of remaining supernatant and cells are plated in LB agar plates with corresponding antibiotic selection (e.g. Ampicillin 100 μg/ml). Plates were incubated at 37 °C o/n to allow the growth of bacterial colonies.

2.3.2 Bacterial cultures

Bacterial colonies were inoculated into 5 ml of LB broth containing the appropriate antibiotic (e.g. Ampicillin 100 μg/ml). Bacterial cultures were grown at 37 °C o/n.

2.3.3 Glycerol stock

500 μl of bacterial culture was added to 500 μl of 50 % glycerol and stored at -80 °C.

2.3.4 Extraction of DNA plasmid

DNA plasmids were extracted from bacterial cultures using GeneJet Plasmid Miniprep kit (small scale plasmid DNA extraction) according to the manufacturer's procedures.

DNA plasmid was subsequently used for transfection in mammalian cells (2.4.3).

2.4 Mammalian cell culture techniques

2.4.1 Cell culture propagation and storage

All cell lines were cultured at 37 °C and 5% CO_2 in the Galaxy 170R cell incubator in the corresponding cell culture medium with 10% FBS, 1% penicillin/streptomycin, and the additional antibiotics as listed in section 2.1.1. Cells were passaged at ca. 80-90% confluency. Before trypsinization, the cell culture was washed with PBS. Cells were incubated with trypsin for 5 min at 37 °C until cells detach. The medium was subsequently added to inactivate trypsin. For cell storage, cells were harvested by trypsinization, centrifugated for 5 minutes at 500g at 4 °C. Then, the cell pellet was resuspended in FBS with 10% DMSO, transferred in a Cryo tube vial, and placed in a Cryo freezing container containing 2-propanol before storing at -80 °C. To revive frozen stocks, cells were thawed at 37 °C for 1-2 min, resuspended in 5 ml of complete medium to remove DMSO, centrifugated (500g, 5 min), and plated in complete medium. Selective antibiotics were added 24 h after defrosting to allow cell recovery and expression of resistance genes. Any centrifugation was performed at 500 g for 5 min unless differently stated.

2.4.2 Preparation of conditioned culture medium

Cells were grown for 48 h until ca. 50-80 % confluency. Then, the culture medium was collected and filtered through 0.33 μm cell strainer. Conditioned medium was stored at 4 °C for maximum one week.

2.4.3 Transfections

DNA transfection

Cells were seeded at a density of 2.5 x 10^5 cells/well in 6-well plate a day before the transfection. Cells were transfected using Lipofectamine LTX (Thermo Fisher Scientific) according to the manufacturer's procedures. 9 μ of Lipofectamine LTX and 3.5 μg of DNA was used for each transfection. The transfection mixture was applied for 24 h before changing the medium.

siRNA transfection in HT1080 HAC-dGFP cells

HT1080 HAC-dGFP cells were initially transfected with siRNA as described in [204]. Under these conditions, high cell death was observed 24 h after transfection. Thus, the protocol was optimised as follow to reduce the cell toxicity. Briefly, cells were seeded at a density of 10 000 cells/well in 24-well plate a day before the experiment. Cells were transfected using Lipofectamine RNAiMAX (Thermo Fisher Scientific) according to the manufacturer's procedures with 17 nM siRNA for siCTR, siBRCA2, siRAD51, siGFP, siSTK38 and 41.5 nM siRNA for siPALB2. The transfection mixture was applied for 5 h before changing the medium. Then cells were grown in medium until the day of the analysis. To scale up the experiment, the corresponding amount of cells was seeded as described in Table 2.19.

Size	Cells seeded	Volume	Purpose
6-well plate	50 000	2 ml	HAC loss with flow cytometry, cell cycle profile
10-cm dish	500 000	10 ml	FISH, cell proliferation

Table 2.19: Sizes and volumes of cell culture dishes used in this thesis

siRNA transfection in HeLa Kyoto NFLAP-BRCA2

Cells were seeded at a density of 1.5 x 10^5 cells in 6-well plates and then transfected the following day with siBRCA2 (100 nM) or control siSCR (scramble) with DharmaFECT1 reagent (Dharmacon) according to the manufacturer's procedures. Cells were incubated for 24-48 h before the analysis. For immunofluorescence (IF) experiments (2.6.8), 24 h after transfection, 50 000 cells were trypsinised and seeded on coverslips. Where indicated, 24 h after seeding, cells were treated with aphidicolin (0.4 μM) for 18-19 h before fixation.

2.4.4 Generation of stable cell lines

After transfection as described in section 2.4.3, cells were grown in the selective medium for about one week to select transfected cells. To generate clonal cell lines, transfected cells were sorted based on the fluorescent signal expressed by the tagged-protein. Single cells were plated in 96-well plate after Fluorescence-activated cell sorting (FACS) and they were grown for approximately ten days in complete medium supplemented with selective drugs and 20% of conditioned medium. Once clones started to grow, they were expanded in 24-well plate and subsequently 6-well plate for further analysis. Validation of clones was performed by flow cytometry to check the intensity of the fluorescent signal and by western blot to check the level of protein expression.

2.4.5 Generation of CRISPR-modified cell lines

Cells were transfected as described in section 2.4.3 using 3 μg of DNA (1 μg of Cas9 and 2 μg of repair template). Then, clonal cell lines were generated as described in section 2.4.4 by single-cell sorting and the validation of clones was performed by microscopy and flow cytometry to check the intensity of the fluorescent signal; by western blot (section 2.5.1) to check the level of protein expression and by PCR (section 2.2.4) to check the integration of the construct using the primers listed in Table 2.8. Optimised

condition for PCR: annealing temperature of primers 65 °C, extension time 120 sec.

2.5 Protein analysis techniques

2.5.1 Western blot (WB)

Preparation of whole-cell lysates

Starting from about 1-0.5 x 10^6 cells, cells were harvested by trypsinization, centrifugated for 5 min at 500g at 4 °C and washed once in ice-cold PBS. The cell pellet was resuspended in NETN150 lysis buffer with 125 U/ml Benzonase (15-20 μl per 10 mg of cells) and incubated for more than 30 min on ice. The cell lysate was centrifugated for more than 15 minutes at 16100g at 4 °C to pellet cell debris. The supernatant was collected as 'Whole Cell Extract' (WCE). Protein concentration was measured by the Bradford protein assay (Bio-Rad) according to the manufacturer's instructions.

SDS-PAGE of proteins

Samples were prepared for protein electrophoresis or SDS-PAGE (Sodium Dodecyl Sulphate - Polyacrylamide Gel Electrophoresis) with 1× NuPAGE LDS sample buffer and 25 mM DTT. Samples were boiled for 5 min at 80-85 °C to allow protein denaturation. Protein separation was performed in 1× MOPS-SDS running buffer (0.2 mM MOPS 0.2 mM Tris, 0.1% SDS, 4mM EDTA) at 100-120V using NuPAGE 4-12% Bis-Tris gels.

Blotting

Protein transfer was performed onto nitrocellulose membranes using 15% methanol in Transfer Buffer (100 mM Tris, 767 mM Glycine) at 10V o/n or 70V for 3 hours in a Mini Trans-Blot system. The membrane was stained with Ponceau staining solution (0.1% Ponceau in 5% acetic acid) until transferred protein became visible, then the Ponceau

staining was removed thoroughly by washing the membrane several times in water. At this point, the membrane was cut into sections to be treated with different antibodies. Subsequently, the membrane was blocked for 30 min in Blocking buffer (PBS with 5% milk and 0.05% Tween-20). Primary antibodies were diluted in Blocking buffer at the corresponding concentration (Table 2.10) and they were applied for 2-3 hours at room temperature or o/n at 4 °C. The membrane was washed in PBS with 0.05% Tween-20 buffer three times for 5 min, followed by incubation with corresponding secondary antibodies diluted in Blocking buffer for approximately 1 h at room temperature (Table 2.11). After three washes in PBS with 0.05% Tween-20 buffer for 5 min each, proteins were detected using a 1:1 mixture of ECL Western Blotting detection reagent 1 and 2 and an image was obtained on photographic film. The blot was developed using a Curix 60 tabletop processor. To test different antibodies the membrane was treated with Re-Blot Plus Mild Solution (Millipore) before incubating with another antibody.

2.5.2 Immunoprecipitation

Starting from at least 1 x 10^6 cells, immunoprecipitation of mCherry-tagged proteins was performed using the RFP-TrapA system (Chromotek) according to the manufacturer's procedures. Briefly, for each sample 20 μl of bead slurry was initially equilibrated with two washes in NETN150 buffer. Then, beads were blocked in 0.5 ml of NETN150 with 5 mg/ml of BSA for 1 h at 4 °C on the rotator. Beads were collected by centrifugation (2500g, 2 min, 4 °C) and resuspended in 100 μl of NETN150. The cell lysate was obtained as described in section 2.5.1, and 50 μl was saved for the input. The remaining cell lysate was diluted to 1 mg/ml in NETN150 and incubated with blocked beads for 1 h at 4 °C on the rotator. After immunoprecipitation, beads were collected by centrifugation (2500g, 2 min, 4 °C) and 50 μl of supernatant were saved for the flow-through. After three washes in NETN150 the cross-linked complex was eluted from the beads in 2X NuPAGE LDS sample buffer and 10 mM DTT and boiled at 85 °C for 15 min. Subsequently, the eluted sample was used for SDS-PAGE and Western Blot as described in sections 2.5.1 and 2.5.1.

2.5.3 Chromatin fractionation

Cell fractionation was performed as described in [207]. Briefly, starting from about 8 x 10^6 cells, cells were harvested by trypsinization and washed once in ice-cold PBS. Approximately 1/6th of the cells were used for whole-cell lysates as described in section 2.5.1. The remaining cells were used to perform cell fractionation as described in [207]. Briefly, the cytoplasmic fraction was extracted in Sucrose buffer ((10 mM Tris pH 7.5, 20 mM KCl, 250 mM Sucrose, 2.5 mM MgCl2, 10 mM Benzamidine Hydrochloride and protease inhibitor cocktail (Sigma); the nuclear fraction was extracted in NETN150 with 200 mM of NaCl and the chromatin fraction was extracted in NETN150 buffer with 5 mM MgCl2 and 125 U/ml Benzonase.

2.6 Cell analysis techniques

2.6.1 Analysis of the cell cycle profile by propidium iodide staining

Starting from approximately 1x10^6 cells per sample, cells were harvested by trypsinization, washed once in PBS and resuspended in 150 μl of PBS. Resuspended cells were fixed adding 350 μl of 100 % ice-cold ethanol dropwise with gentle agitation on the vortex for about 30 sec. Then, cells were stored at -20 °C for at minimum 1 h.
After fixation, cells were centrifugated (1000g, 5 min) and resuspended in 50 μl of residual ethanol. Then, cells were incubated in 0.5 ml of propidium iodide staining solution (PBS, 0.1 % BSA, 0.1 mg/ml RNAse A, 2 μg/ml propidium iodide) for 30 minutes at room temperature in the dark. Cells were collected by centrifugation (1000g, 5 min) and resuspended in 1 ml of PBS. Cells were analysed using a Cytek DxP8 Flow cytometer.

2.6.2 Analysis of the mitotic index by flow cytometry

Cells were harvested and fixed as described in section 2.6.1. After fixation, cells were centrifugated (1000g, 5 min) and resuspended in 0.5 ml of PBS with 0.1 % Triton X-100, 1 % BSA for 15 minutes in ice for permeabilization. Cells were collected by centrifugation (1000g, 5 min) and washed twice in 0.5 ml of PBST-BSA (PBS, 0.1 % Tween-20, 1 % BSA). Then, cells were incubated with Histone H3 (phospho-S10) antibody in 100 μl of PBST-BSA for 45-60 min on the shaker. Cells were washed twice in 0.2 ml of PBST-BSA and incubated with corresponding secondary antibody in 50 μl of PBST-BSA for 30 min on the shaker in the dark. Cells were washed twice in 0.2 ml of PBST-BSA. Propidium iodide staining and flow cytometry analysis were performed as described in section 2.6.1.

2.6.3 Analysis of cell proliferation by dye dilution assay

HT1080 HAC-dGFP cells were stained following the manufacturer's protocol (CellTrace™ Far Red Cell Proliferation Kit). Briefly, starting from 1x10^6 cells, cells were incubated in 1 ml of Cell Trace Far Red staining solution (PBS, 0.5 μM Cell Trace Far Red solution) for 20 min at 37°C. After centrifugation (500g, 5 min), cells were resuspended in 4 volumes of complete medium and incubated for 5 min at 37°C to absorb unbound dye. After centrifugation (500g, 5 min), the unbound dye was removed, and 500 000 cells were seeded in fresh complete medium in a 10-cm dish. Untreated cells were harvested by trypsinization 24h after seeding to determine the undivided population. After treatment, cells were harvested by trypsinization to assess the number of cell divisions. Cells were washed once in PBS and resuspended in 0.3 ml of PBS with 50 ng/ml of DAPI to distinguish live and dead cells. Cells were analysed using a Cytek DxP8 Flow cytometer. The obtained proliferation curve was fitted using FlowJo analysis software (version 10.5.3). Parameters were fixed at 0.5 Peak Ratio, 8 Number of peaks and Peak CV was based on the undivided population as analysed at 24h.

2.6.4 Analysis of cell proliferation by growth curve

HT1080 HAC-dGFP cells expressing tetR-constructs were seeded at a density of 1.5 x 10^5 cells in 10-cm dish. Cellular growth was analysed every 24 h for four days. Cells were harvested by trypsinization, resuspended in 10 ml of complete medium and counted three times using the hemocytometer.

The doubling time, τ, is defined by the following equation:

$$N(t) = N_0 \cdot 2^{t/\tau} \tag{2.1}$$

where $N(t)$ is the number of cells at time t and N_0 is the number of cells at time $t = 0$. To measure τ, a linear fit, of the form $y = a + b \cdot x$, is performed on equation 2.1 after

being linearised:

To measure τ, the equation 2.1 was linearised:

$$\log_2(N(t)) = \log_2(N_0) + \frac{1}{\tau} \cdot t \tag{2.2}$$

The equation 2.2 was fitted with a line $y = a + b \cdot x$ where $y = \log_2(N(t))$, $a = \log_2(N_0)$, $x = t$ and $b = 1/\tau$. Therefore, $\tau = 1/b$. The number of cell divisions at time t, $CD(t)$, is calculated as $CD(t) = t/\tau$

2.6.5 Cell viability assay

Cell viability was measured using the WST-8 tetrazolium cell viability assay (Cell counting Kit-8). This is a colorimetric assay that is based on the cleavage of a water soluble tetrazolium salt (WST-8), by mitochondrial dehydrogenases to form orange formazan in viable cells. The greater the number of viable, metabolically active cells, the greater the amount of formazan produced following the addition of WST-8. The number of viable cells is proportional to the amount of formazan produced. Briefly, 4000 HT1080 cells were seeded in 96-well plate with 100 μl of complete medium. 24h after seeding, cells were treated with different drugs as indicated for 24h. Then, cells were washed three times in complete medium (5 min at 37 °C for each washing step) and incubated for 2 days to allow cell recovery. Finally, 10 μl of Cell counting Kit-8 Solution Reagent was added to each well and cells were incubated at 37 °C for 2.5 hours. Cell viability was determined by measuring the absorbance af orange formazan at 450 nm using a VersaMAX microplate reader.

2.6.6 Metaphase preparation

500 000 cells were seeded in a 10-cm dish and transfected as described in section 2.4.3. 72h after transfection, metaphase cells were obtained by adding colcemid to a final concentration of 0.1 μg/ml and incubating them for 5h. Cells were harvested by trypsinization and washed once in PBS. The cell pellet was resuspended in 100 μl of PBS by tapping carefully. Then, 10 ml of pre-warmed (37 °C) hypotonic solution (75 mM KCl in distilled water) was added to the cells drop-by-drop while agitating gently. Cells were incubated for 20 min at 37 °C. A pre-fixation step was performed by adding 10 drops of fixative solution (75 % methanol 25 % acetic acid) to the cells resuspended in hypotonic solution and gently mixed by flipping the tube upside down for 4-5 times. Cells were fixed with three washes of fixative solution. Between each wash, cells were pelleted by centrifugation at 150 g for 5 min, the cell pellet was resuspended by tapping carefully and 1 ml of fixative solution was added. After the final wash, metaphases were resuspended in 1 ml of fixative solution and stored at -20 °C or spread on a microscope slide where the fixative solution evaporated over water.

2.6.7 Fluorescence In Situ Hybridization (FISH)

Dry slides were rehydrated with PBS for 15 min, and fixed in 4 % formaldehyde for 2 min, followed by three washes of 5 min with PBS and ethanol series (of 70%, 90% and 100%) dehydration (5 min for each step). Slides were dried for 10-15 min. 30 μl of hybridization buffer (distilled water with 10 mM Tris-HCl, pH 7.2-7.5, 70% Formamide, 5% Dextran sulfate, 0.25 μM PNA-FITC-tetO, 0.25 μM PNA-CENPB-Cy5) was applied to the slides and slides were covered with a glass slide. The denaturation step was performed at 80 °C for 3 min followed by hybridization for 2 hr at RT in the dark. Cover slides were removed and slides were washed twice in formamide washing solution (distilled water with 70% formamide, 10 mM Tris pH 7.2, 0.1% BSA) followed by three washes of 5 min with TBS-T (PBS with 0.08% Tween-20). Slides were washed twice with PBS for 2 min and incubated in DAPI solution (PBS with 1 μg/ml of DAPI)

for 30min. Then, slides were washed once in PBS for 2min and dehydrated gradually with a series of 70%, 90% and 100% ethanol washes and mounted. Images were captured using an Olympus Microscope FV1000. For each metaphase, a Z-stack of 10 images was acquired. Images were analysed using ImageJ analysis software (version 2.0.0-rc-69/1.52p).

2.6.8 Immunofluorescence (IF)

50000-100000 cells were seeded on coverslips. Soluble proteins were pre-extracted before fixation by incubation for 2 min in 0.1 % (vol/vol) Triton X-100 in 1× PBS. Cells were fixed for 15 min in PBS + 4% paraformaldehyde (PFA) the incubated for 5 min with 125 mM glycine in PBS to quench PFA fixation. Subsequently, cells were permeabilised for 5 min in 0.5 % Triton X-100 in 1× PBS. Cells were blocked for 1 h in 3 % BSA in 1× PBS. Primary antibodies were applied o/n at 4 °C at the dilution listed in 2.10. Coverslips were washed 3× 5 min in 0.05 % (vol/vol) Triton X-100 in 1× PBS and secondary antibodies conjugated with fluorophores were applied for 1 h at RT in the dark. After 3× 5min washes in 0.05 % (vol/vol) Triton X-100 in 1× PBS, coverslips were mounted with ProLog Gold reagent with DAPI on glass slides. Slides were stored at 4 °C and analysed within a month. Images were captured using an Olympus FV1000 or FV1200.

Immunofluorescence for outer-kinetochore proteins

Cells were simultaneously fixed and permeabilised using PTEMF fixation buffer for 15 min. After two washes in PBS, cells were blocked in PBS containing 3 % BSA and 0.1 % Triton X-100 for 30 min. Primary antibodies were applied for 1 h at RT at the dilution listed in table 2.10. Coverslips were washed 3× 5 min in 0.05 % (vol/vol) Triton X-100 in 1× PBS, secondary antibody conjugated with fluorophores were applied for 1 h at RT in the dark. The secondary antibody solution was supplemented with 20 μM Hoechst to stain the nuclei. Coverslips were washed 2× 5 min in PBS, and one time in

dH_2O to remove remaining salt. Slides were air-dried for 1 h at RT and subsequently mounted using 9 μl Mowiol mounting medium. Slides were air-dried for 1 h at RT before imaging analysis.

Immunofluorescence with mNeonGreen-BRCA2

The immunofluorescence protocol for HCT116 mAID-mNeonGreen-BRCA2 was optimised as follows. All steps described below were performed in the dark. 50000-100000 cells were seeded on coverslips. Cells were washed twice with pre-warmed PBS at 37 °C and subsequently fixed in PTEMF fixation buffer at pH 7.5 and containing 2 % formaldehyde for 15 min then quenched for 5 min with 125 mM Glycine in PBS. After 2 washes in PBS, cells were blocked for 30 min with blocking solution containing PBS with 3 % BSA and 0.1 % Triton X-100. Primary antibodies were applied for 1 h at RT at the dilution listed in 2.10. Coverslips were washed 3× 5 min in 0.05 % (vol/vol) Triton X-100 in 1× PBS and secondary antibodies conjugated with fluorophores were applied for 1 h at RT in the dark. The secondary antibody solution was supplemented with 20 μM Hoechst to stain the nuclei. Coverslips were washed 2× 5 min in PBS, and one time in dH_2O to remove remaining salt. Slides were air-dried for 1 h at RT and subsequently mounted using 9 μl Mowiol mounting medium. Slides were cured for 1 h at RT before imaging analysis. Slides were analysed within 2 days. Images were captured using Olympus FV1200.

2.6.9 Live-cell imaging

Live-cell imaging of CRISPR-modified mNeonGreen-BRCA2 expressing cell lines

HCT116 mAID-mNG-BRCA2 cells were used to detect BRCA2 in live cell imaging. 100 000 - 200 000 cells were seeded on 35 mm bottom glass dish and let recover for 48 h. To induce DSBs, cells were treated with 2 mM hydroxyurea (HU) for 16 h. Before image capture, cell medium was replaced with phenol red-free complete medium to reduce

background fluorescence and supplemented with 100 nM siR-DNA to stain the nuclei.

Live-cell imaging with HaloTag ligand

5×10^4 HCT116 mAID-Halo-BRCA2 cells were seeded on 35 mm glass bottom dish and left to recover for 48 h. Subsequently, cells were incubated with HaloTag Ligand according to the manufacturer's procedures and several HaloTag Ligands were tested for imaging analysis. Briefly, cells were incubated with 100 nM TMR-Direct o/n at 37 °C, 1 μM Oregon Green for 15 min at 37 °C, 200-500 nM Janelia Fluor™ 549 or Janelia Fluor™ 646 for 30 min - 1 h. Cells were washed 3 times with PBS to remove unbound ligand. Ligand-containing medium was replaced with phenol red-free complete medium to reduce background fluorescence.

2.6.10 EdU labelling

5-ethynyl-2'-deoxyuridine (EdU) incorporation was used to visualise replicating cells. EdU is a nucleotide analogue, which is incorporated into the newly synthesised DNA strand. EdU is visualised using the "Click-IT" reaction, where a fluorescently labelled azide binds the alkyne (EdU). 10 μM EdU was added to the medium for 10 min. Subsequently, cells were fixed, permeabilised and blocked as described in section 2.6.8. After blocking, cells were incubated with Click-IT reaction mixture containing 2 mM $CuSO_4$, 10 mM sodium ascorbate and 10 μM Alexa Fluor 647 Azide for 45 min at RT in the dark. Click-IT reaction mixture was subsequently removed, cells were washed once in PBS and incubated with antibodies as described in section 2.6.8.

2.6.11 Analysis of the mitotic stage

HT1080 HAC-dGFP cells were transfected as described in section 2.4.3. After fixation (section 2.6.8), coverslips were mounted with ProLong™ Gold Antifade Moun-

tant with DAPI on glass slides. Cells were separated into three categories based on the DAPI stain: cells in interphase, early mitosis or late mitosis.

2.6.12 Analysis of mitotic defects

To enrich the number of cells in mitosis, cells were synchronised with single thymidine block and release. HeLa Kyoto NFLAP-BRCA2 cells were transfected as described in section 2.4.3. 24 h after transfection, 10^5 cells were seeded on coverslips in 24-well plates in complete medium. The day after, cells were treated with 2 mM thymidine, an inhibitor of DNA synthesis, for 18 h to arrest cells in S phase. Then, cells were washed twice in PBS are released in normal medium for 10 h before fixation in 4% PFA (see section 2.6.8). After thymidine release, cells enter mitosis in synchrony. After fixation, coverslips were mounted in slides using ProLong™ Gold Antifade Mountant with DAPI to detect nuclei. Pictures were captured using Olympus FV1200. 20-30 Z-stacks were taken for each picture. Images were analysed using ImageJ using a Z-projection. Mitotic defects such as lagging chromosomes, anaphase bridges, multipolar spindle cells were identified based on DAPI staining.

2.6.13 Proximity Ligation Assay (PLA)

PLA was performed according to the manufacturer's procedures Duolink PLA (Sigma-Aldrich). Incubation with primary antibody was performed at the concentrations described in table 2.10 at 4 °C o/n. Pictures were taken with Olympus FV1000. 10-20 Z-stacks were taken for each picture. Images were analysed using ImageJ using a Z-projection. To count the number of foci inside the nuclei, a nuclear mask was initially defined based on the DAPI stain. "Find Maxima" was applied to count the foci. (See Supplementary Information A.1.2).

2.6.14 Analysis of the nuclear actin filaments

Nuclear actin filaments were detected using Alexa Fluor™ 647 Phalloidin. Phalloidin is a toxin isolated from the *Amanita phalloides* mushroom, which has a high affinity for F-actin. HeLa Kyoto NFLAP-BRCA2 cells were transfected with siRNA as described in section 2.3.1. 72h after transfection cells were fixed and stained with Alexa Fluor™ 647 Phalloidin according to the manufacturer's procedures. Briefly, cells are fixed in 3.7 % PFA for 10min, permeabilisation was performed in 0.1 % Triton X-100 for 4 min, blocking was performed in 1 % BSA for 20 min. Finally, incubation with Alexa Fluor™ 647 Phalloidin (0.165 μM) was performed for 20 min at RT. After washes, coverslips were mounted with ProLog Gold reagent with DAPI on glass slides.

2.6.15 HAC stability assay after drug treatment

HAC stability assay upon drug treatment was carried out as described [208]. After 24 hr of drug treatment, the drug was removed by performing three consecutive medium washes, and the cells were subsequently grown without blasticidin selection for 13 days. Then, cells were collected after trypsinization, washed once in PBS and analysed by flow cytometry to detect the proportion of cells that preserve EGFP signal. Cells were analysed using a Cytek DxP8 Flow cytometer and data were analysed using FlowJo analysis software (version 10.5.3). The rate of HAC loss after drug treatment was calculated using the formula:

$$R_{drug} = 2 - 2 \cdot \left[\frac{\frac{P_{drug}}{P_0}}{\left(\frac{2-R_{norm}}{2}\right)^{n_3}} \right] \tag{2.3}$$

where R_{drug} is the rate of HAC loss after drug treatment; P_{drug} is the percentage of EGFP+ cells after drug treatment; P_0 is the percentage of EGFP+ cells at the beginning of the experiment in cells cultured with blasticidin, R_{norm} is the natural rate of spontaneous HAC mis-segregation; n_3 is the number of cell divisions after drug removal

[203].

2.6.16 HAC stability assay after siRNA treatment

HAC stability assay upon siRNA treatment was carried out as described in [204]. Cells were transfected as described in section 2.4.3. Where indicated, 24h after transfection, cells were treated with aphidicolin (APH) (0.4 μM) for 24h. Then, cells were grown without blasticidin for an additional 24 h. At 72 h after transfection, cells were collected by trypsinization, washed once in PBS and resuspended in PBS with 0.3 μM DRAQ7 to distinguish live and dead cells. Cells were analysed using a Cytek DxP8 Flow cytometer and data were analysed using FlowJo analysis software (version 10.5.3). For the analysis, single cells were selected using parameters of light scattering, and the proportion of GFP+/Live cells was used to calculate the rate of HAC loss. The rate of HAC loss after siRNA treatment was calculated using the formula:

$$R_{si} = 2 - 2 \cdot \left(\frac{P_{si}}{P_0} \right)^{\frac{1}{n}} \tag{2.4}$$

where R_{si} is the rate of HAC loss after siRNA treatment; P_{si} is the percentage of EGFP+ cells after drug treatment; P_0 is the percentage of EGFP+ cells at the beginning of the experiment in cells cultured with blasticidin; n is the number of cell divisions at the time of the analysis [204].

2.6.17 HAC stability assay after tethering of tetR-constructs

For the HAC stability assay, HT1080 HAC-dGFP cells expressing tetR-mCherry constructs were seeded at a density of 1.5 x 10^5 cells in 10-cm dish in presence or absence of DOX for 96 h. At the end of the experiment, cells were harvested by trypsinization,

washed once in PBS and resuspended in PBS with 0.3 μM DRAQ7 to distinguish live and dead cells. Cells were analysed using a BDX Fortessa X20 Flow cytometer and data were analysed using FlowJo analysis software (version 10.5.3). For the analysis, single cells were initially gated using parameters of light scattering, then live cells were gated and mCherry positive cells were gated. The proportion of GFP+ cells was used to calculate the rate of HAC loss. The rate of HAC loss after siRNA treatment was calculated using the formula 3.1. To assess the effect of the tethering of the construct on the HAC stability, the rate of HAC loss in the absence of DOX (tethering) was normalised for the rate of HAC loss in presence of DOX (no tethering).

2.7 Data analysis techniques

2.7.1 Sequencing data analysis

Sequencing analysis and primers' design was performed using SnapGene software (version 5.1.4.1)

2.7.2 Imaging data analysis

Imaging analysis was performed using ImageJ software (version 2.0.0-rc-69/1.52p).

2.7.3 Flow cytometry data analysis

Analysis of flow cytometry data was performed using FlowJo software (version 10.5.3).

2.7.4 Statistics

Statistical analysis was performed to determine whether differences between two (or more) groups originate from different treatments or they are simply due to biological variability. To do that, the p-value is calculated using statistical tests. The p-value is the probability (from 0 to 1) of observing a difference between two groups that is at least as large as the difference observed, given that the null hypothesis is true. Given two groups (i.e. control vs treatment), the null hypothesis is that the two groups derive from the same distribution (i.e. the difference observed between the two groups is due to biological variability and not to the treatment). Therefore, a small p-value indicates that it is unlikely to observe that difference between the two groups, given that they come from the same distribution. Conventionally, p-values < 0.05 denote statistical significance. Therefore, if the p-value is < 0.05 the null hypothesis is discarded (i.e. the two groups come from different distributions). By contrast, if the p-value > 0.05

the null hypothesis can not be discarded. Different statistical tests were chosen according to the types of data analysed. If the different treatments (e.g., control, treatment 1, treatment 2) were handled in parallel, paired tests (e.g., paired Student t-test and repeated measure (RM) one-way ANOVA) were used to calculate the p-values. The paired tests compare the means of matched groups. If different treatments were not handled in parallel in all experiments, unpaired (e.g., one-way ANOVA) tests were used to calculate the p-values. The unpaired tests compare the means of unmatched groups. Below are listed the statistical tests used in this thesis.

Comparison between two groups

To compare the mean values of a variable between two groups (i.e. control vs treatment), statistical analysis was performed using the paired two-tailed Student t-test.

Comparison between more than two groups

To compare the mean value of a variable between more than two groups, statistical analysis was performed using repeated measure (RM) one-way ANOVA. The null-hypothesis tested with ANOVA is that all groups come from the same distribution. Therefore, the p-value of the ANOVA test only tells whether the groups come from the same distribution or not. To compare differences between pairs of samples (i.e. control vs treatment 1, control vs treatment 2, etc.) the Tukey and Dunnett's *post hoc* tests were used. Tukey test compares every mean with every other mean, Dunnett's test compares the mean of the control sample with every other means.

Excel and GraphPad PRISM software (version 7) were used for data analysis and statistical analysis, following the GraphPad Statistics Guide [209]. Data were expressed as mean and ± SD. Each experiment was performed N times, from one to four times, as reported in the caption of each figure. *n* represents the total number of cells (or events) analysed. If experiments wee performed one time (e.g. Figure 4.1C, Figure 4.17, Figure

4.20B) statistical analysis could not be performed. In this case, the mean and the SD of the population of the single experiment is reported on the graph. If more then one experiment is performed, the mean and SD of the independent experiments is represented on the graph. P-values < 0.05 denote statistical significance. Levels of statistical significance were represented as follows: $p \leqslant 0.05$ (*), $p \leqslant 0.01$ (**), $p \leqslant 0.001$ (***), $p \leqslant 0.0001$ (****).

Chapter 3

The role of genotoxic stress and HR factors in chromosome inheritance: exploiting the Human Artificial Chromosome as a model system

3.1 Introduction

Chromosomal instability (CIN) is a hallmark of cancer cells [2]. BRCA2-deficient cancer cells show structural CIN, such as chromosome breaks, translocations and chromosome rearrangements, and numerical CIN, i.e., gain or loss of whole chromosomes [74]. While structural CIN in BRCA2-deficient cells is explained by the function of BRCA2 in DNA repair [62], it remains contentious how BRCA2 deficiency leads to numerical CIN, i.e., abnormal chromosome number (aneuploidy). Aneuploidy arises from abnormal chromosome segregation in mitosis [7]. Mitotic abnormalities, such as lagging chromosomes, anaphase bridges, and micronuclei formation were associated with BRCA2 deficiency [107] [113] [116] [115] [117], and functions of BRCA2 in centrosome amplification [107], cytokinesis [113] [115] and regulation of the spindle assembly checkpoint [116] have been proposed, as outlined in section 1.2.3.4. Conversely, Choi et al. [116] reported that mitotic defects could be found in mice harboring a conditional in-frame deletion of BRCA2 exon 11, therefore expressing a BRCA2 variant lacking only the central RAD51 interacting region, which has not been described in having a mitotic function. A more recent study also suggested that the chromosome mitotic abnormalities associated to BRCA2 depletion are linked to its RAD51-mediated HR function in S-G2 phase [117]. Namely, depletion of BRCA2 led to under-replication, which could remain after mitotic entry; if replication was not completed before entry into anaphase, this could result in abnormal mitotic structures, such as lagging chromosomes and anaphase bridges [117]. In this study, increased formation of UFBs was observed in BRCA2-deficient cells as a consequence of under-replicated regions in mitosis. However, it has not been addressed whether UFBs could be one of the cause of whole-chromosome loss in BRCA2-deficient cells or can only cause the loss of small chromosome regions. Therefore, despite these observations, evidence that supports the direct role of BRCA2 in preventing numerical CIN is still missing.

Accurate chromosome segregation requires a distinctive chromosomal region, called the centromere, which is late replicating and susceptible to DNA damage [210] [131]. Centromeres are composed of highly repetitive DNA sequences, named alphoid DNA

repeats, which can adopt unusual conformation and form complex DNA structures [211] [212] [25] [213]. These structures can be difficult to resolve during replication, and if left unresolved, lead to fork stalling or fork collapse. Using a genome-wide approach to map DNA breaks, the enrichment of DSBs was observed at centromeres upon mild replication stress induced by a DNA polymerase inhibitor aphidicolin, corroborating that these regions are particularly susceptible to DNA breakage when exposed to replicative stress [214]. Furthermore, centromeres are actively transcribed and, as the result of collisions between the transcription and replication machinery, replication fork can be stalled, which in turn can trigger DNA breaks [215] [216][25]. At the same time, transcription at centromeres generates RNA transcripts, and if they hybridise with the complementary DNA sequence, they can generate RNA:DNA hybrids, also called R-loops. Stable R-loops can interfere with the replication machinery, leading to fork stalling or collapse [25] [217]. These properties of centromeres may cause DNA breaks during replication, leading to mis-segregation of chromosomes if they are not properly repaired before chromosome segregation. In this scenario, it is conceivable that the HR factors, such as BRCA2, PALB2 and RAD51, assist accurate and complete replication of centromeric regions and, in this way, ensure the correct chromosome segregation.

In this chapter, I set out the experiments to study how replication stress and HR factors, i.e., BRCA2, RAD51 and PALB2, affect chromosome segregation. To this end, I made use of cells carrying a Human Artificial Chromosome (HAC). The HAC is made from centromeric α-satellite DNA sequences; therefore, it was used as a model to study the impact of the HR factors at centromeres.

3.1.1 The development of the alphoid^{tetO} HAC

The HAC is a small extrachromosomal element made by arrays of alphoid DNA sequences (α-satellite), which was originally developed to deliver large genomic-DNA regions in human cells [218]. After the first HAC was generated [219], many stud-

ies have followed in order to generate new types of HACs and to characterise their structures. The HACs can be generated with two different methods: a top-down or a bottom-up approach [218] [133]. The former consists of the truncation of the chromosome arms of an endogenous chromosome by homologous recombination with telomere sequences [220] [221] [222] [223] [224] [225], the latter consists of the introduction into human cells of natural or synthetic alphoid DNA repeats by transfection or viral infection [226] [227] [228][229] [230] [231] [232]. Several HACs were generated from alphoid DNA of different chromosomes (e.g. chromosome 21, chromosome 17, chromosome X); however, they all share the common feature of being made by arrays of alphoid DNA sequences, which contain CENP-B boxes. Thanks to the presence of a functional centromere, HACs can replicate and segregate appropriately inside human cells as an endogenous chromosome [233] [133].

The development of a new generation of HAC, called the alphoid^{tetO} HAC [234] brought a significant contribution to the research field of centromere biology because it allowed researches to study the function of chromatin modifiers on centromere formation (reviewed in [133]). The alphoid^{tetO} HAC generated by Nakano et al. [234], and used in this thesis, consists of a synthetic dimer of alphoid DNA sequences, where one monomer originates from chromosome 17 and contains a CENP-B box, while the other is synthetically generated and the CENP-B box is replaced with the tetracycline operator (tetO) sequence. The tetO sequence is the binding site of *E. coli* tetracycline repressor (tetR); thus, using this system, tetR-fusion proteins can be artificially tethered to the HAC to study their effect on the centromere formation. The synthetic dimer of alphoid DNA was amplified by rolling circle amplification (RCA) and cloned into a YAC/BAC vector by transformation-associated recombination (TAR) cloning in yeast. The vector has a YAC and BAC cassette with an origin of replication and a mammalian selectable marker, the blastocidin resistance gene (bsr). The BAC was then purified and transfected in HT1080 human fibrosarcoma cells where it was stably maintained, segregated correctly and independently from the other chromosomes. Importantly, HT1080 cells exhibit a reduced level of H3K9 methyltransferase SUV39H1, and this property turned out to be important for the efficient assembly of centromere proteins

to the alphoid DNA, hence alphoid^{tetO} HAC maintenance, as compared to other cell lines, such as HeLa cells, which have higher level of the methyltransferase [133]. The alphoid^{tetO} HAC made it possible to further study the chromatin features of functional centromeres. In agreement with the observation that HT1080 acts as a better host for the alphoid^{tetO} HAC, it was shown that high level of H3K9me3, a marker of heterochromatin, at alphoid DNA reduces the association of centromere proteins and the formation of kinetochores on the HAC [166]. This and further studies have suggested that a correct balance between heterochromatin and euchromatin at centromeres is important for the centromere formation and the HAC maintenance [133]. A few years later, the determination of the structure of the HAC generated by Nakano et al. revealed that the alphoid^{tetO} HAC is made up of an array of 1.1 Mb of α-satellite DNA sequences and it carries a fragment of gene-poor region of chromosome 13 captured during the HAC formation [235].

3.1.2 The HAC loss assay using the alphoid^{tetO} EGFP-HAC

In the laboratory of Dr. Vladimir Larionov, the alphoid^{tetO} HAC was modified to study chromosome instability (CIN). Explicitly, an EGFP transgene cassette was introduced inside the HAC [203] (Figure 3.1A). To introduce the EGFP cassette, the alphoid^{tetO} HAC in HT1080 cells was transfected into chicken DT40 cells by microcell-mediated chromosome transfer (MMCT) [203]. In the DT40 cells, a loxP gene loading site was introduced by homologous recombination [236]. The alphoid^{tetO} HAC with the loxP site was subsequently transferred into hamster CHO (hprt -/-) cells by MMCT. The EGFP cassette was introduced into the alphoid^{tetO} HAC at the loxP site by Cre-mediated recombination and the reconstitution of the HPRT gene, achieved by Cre-LoxP recombination, allowed positive selection using HAT medium. Finally, the HAC was reintroduced into HT1080 cells by MMCT. This system made it possible to detect HAC containing cells based on the EGFP expression: cells that contain the HAC display green fluorescence, while cells that have lost the HAC lose the fluorescent signal. In this way, the transmission of the HAC can be easily monitored by flow cytometry,

making the alphoid-tetO EGFP-HAC a powerful system to study chromosome mis-segregation. Indeed, other methods for studying chromosome mis-segregation, such as karyotype analysis, fluorescence in-situ hybridization (FISH) and micronuclei assay, are laborious and only a limited number of cells can be analysed [237]. Moreover, loss of endogenous chromosomes, which carry essential genes for the cell survival, may lead to cell death and, consequently, to the underestimation of chromosome mis-segregation. By contrast, the HAC does not carry any essential gene for the cell survival; therefore, cells are able to survive even after they lose the HAC. Furthermore, due to its small size, the HAC has a mitotic stability that is about 10-fold lower than a natural chromosome, making the system a sensitive tool to study numerical CIN [203].

In previous publications, the HAC loss assay developed by Lee et al. [203] was used to test the effect of several anticancer drugs on chromosome segregation [208]. In this HAC loss assay, cells were initially seeded in blasticidin containing medium to select the HAC-containing cells, such that almost all cells were EGFP positive at the initial time point (Figure 3.1B). Then, blasticidin was removed from the medium and cells were treated with different drugs for 24 hours. After the drug treatment, cells were grown in blasticidin-free medium for several days before analysis by flow cytometry. The EGFP protein is stable and the green fluorescent signal persists inside the cells for several days after the cells have lost the HAC. For this reason, the analysis was performed several days after drug treatment to allow enough time for the cells to lose the EGFP signal [203]. Finally, the rate of HAC loss was calculated based on the percentage of EGFP positive cells (Figure 3.1C). Specifically, cells grown in the absence of blasticidin can naturally lose the HAC, defined as natural HAC loss. Cells treated with drugs in the absence of blasticidin can either show little change in the proportion of EGFP positive cells if the HAC is maintained (equivalent to the level of natural HAC loss), or a reduction in the EGFP population if the HAC is lost.

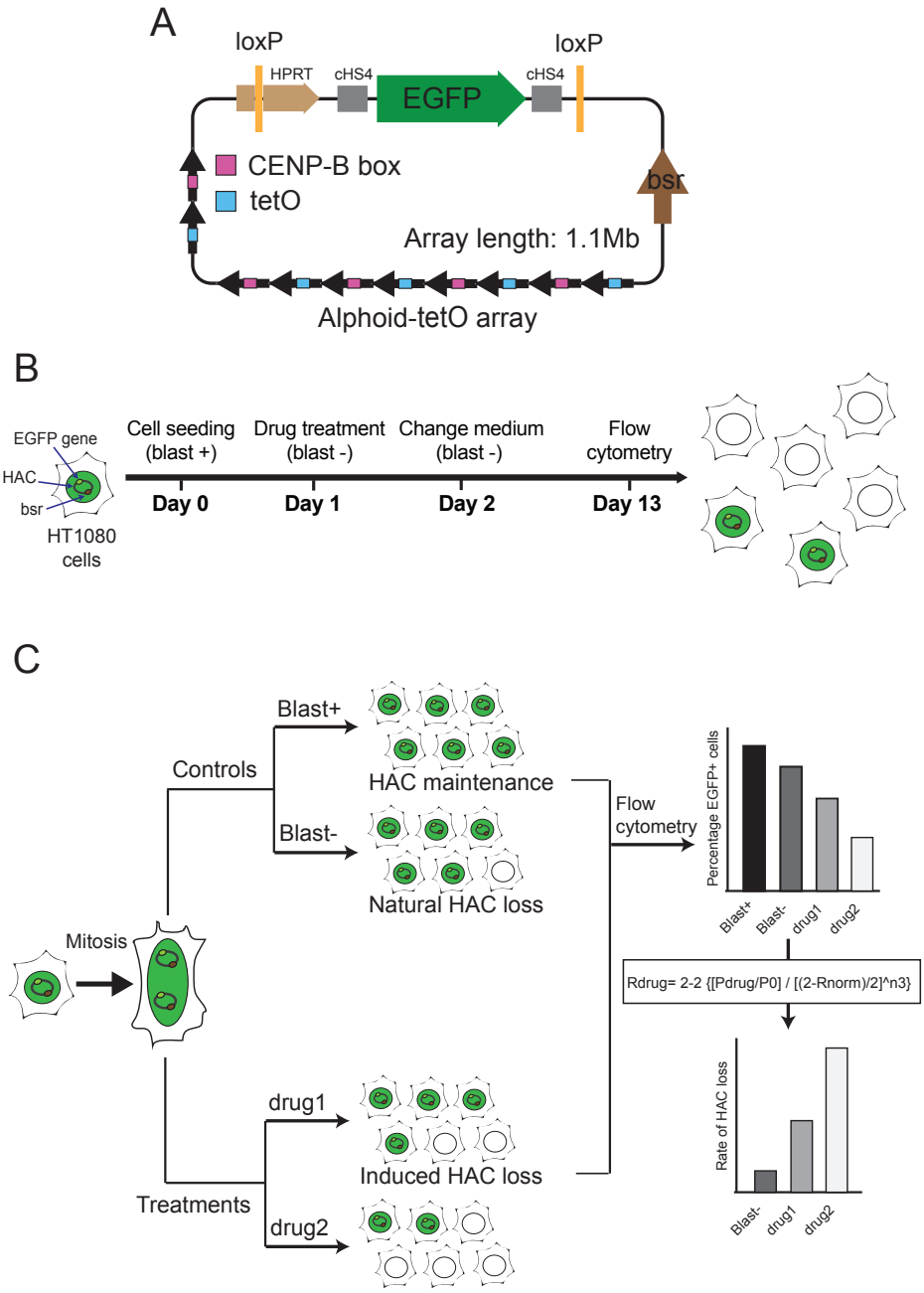


Figure 3.1: **The HAC loss assay using the alphoid^{tetO} EGFP-HAC**. (**A**) Schematic representation of the alphoid^{tetO} EGFP-HAC generated by Lee et al. [203]. The EGFP transgene cassette was introduced into the alphoid^{tetO} HAC by Cre-loxP recombination in hamster CHO cells. Reconstitution of the HPRT gene allows the cell selection in hamster CHO cells, used during the steps of HAC formation. cHS4 insulator sequences flank the EGFP gene to avoid epigenetic silencing of the transgene. Selectable marker blasticidin (bsr). Picture modified from [203]. (**B**) Schematic representation of the protocol of the HAC loss assay after drug treatment. Cells are seeded in blasticidin (blast) containing medium followed by 24 h with drug treatments and subsequently grown for 11 days before flow cytometry analysis. (**C**) Schematic representation of the HAC loss assay. Cells grown in blasticidin containing medium maintain the HAC, cells grown in blasticidin-free medium show natural level of HAC loss, cells treated with drugs show increase HAC loss detected by a reduced level of EGFP positive cells. Rate of HAC loss was calculated as described in section 2.6.15. Picture modified from [208].

3.2 Results

3.2.1 Effect of replication stress on HAC stability using the alphoid^{tetO} EGFP-HAC

In this section, I initially tested the effect of replication stress and HR inhibitors on the HAC stability. To this end, I used the HAC loss assay described in section 3.1.2 to test the effect of a DNA polymerase inhibitor, aphidicolin (APH), a ribonucleotide reductase inhibitor, hydroxyurea (HU), and a RAD51 inhibitor (B02). In order to compare the effect of different drugs on HAC stability, the HAC loss assay was performed at a drug concentration that kills half of the cells, called lethal dose 50 (LD50) [203]. The highest rate of HAC loss was previously demonstrated at the LD50, while higher concentrations increase cell toxicity without increasing HAC loss [203]. Here, the LD50 was determined using a cell viability assay based on the cleavage of a water-soluble tetrazolium salt (WST-8) by mitochondrial dehydrogenases (Figure 3.2A). Increasing concentrations of APH showed a stable 50% of cell viability; however, using a different water-soluble tetrazolium salt (WST-1), increasing cell death was observed at increasing concentrations of drugs (Figure 3.2B). To compare the effect of different drugs on the HAC loss, the LD50 of APH was established at 50 μM; the LD50 of HU at 2-4 mM and the LD50 of B02 treatment around 10 μM.

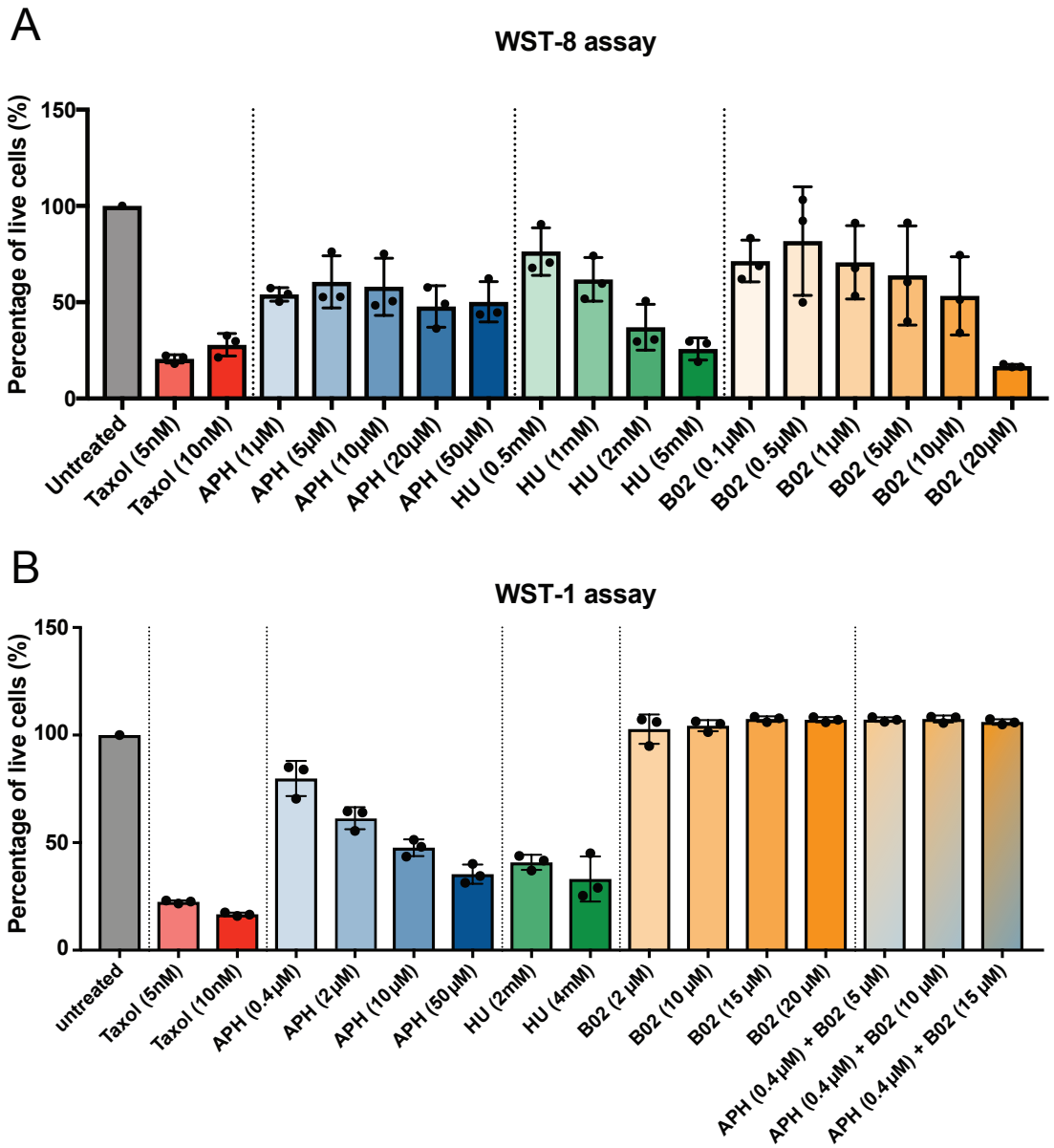


Figure 3.2: **Cell viability assays of HT1080 alphoid^{tetO} EGFP-HAC cells in presence of aphidicolin (APH), hydroxyurea (HU) and RAD51 inhibitor (B02).** (**A**) WST-8 assay. (**B**) WST-1 assay. Results were normalised on the untreated sample, which corresponds to cells grown in blasticidin-free medium. Taxol was used as positive control [208]. Error bars represent the SD of a single experiment, performed in triplicate. Data shown in (A) was generated in collaboration with Dr. Lee Hee-Sheung

Subsequently, the rate of HAC loss was calculated using the proportion of EGFP+ cells 11 days after drug removal (Figure 3.3A). The natural HAC loss was calculated using cells that were not treated with drugs (Figure 3.3B). Taxol, a microtubule stabiliser, which inhibits the microtubule dynamics, was used as a positive control for the HAC

loss assay [208]. Both APH and HU treatments induced a mild increase in HAC loss compared to untreated cells. APH and HU treatments were used in previous work to induce replicative stress repaired by HR factors [48] [49] [238] [239]. Similarly, I tested whether the DNA damage induced by HU treatment requires HR-mediated repair at centromeres to maintain HAC stability. To this end, I combined HU and a RAD51 inhibitor (B02), which inhibits RAD51 binding to ssDNA and prevents its activity of DNA stand exchange [240] [241] [242]. HAC loss was tested upon treatment with a RAD51 inhibitor (B02). Increasing concentrations of B02 (10, 15, 20 μM) did not induce any change in the rate of HAC loss compared to the untreated cells (Figure3.3B). Still, no change was observed in the HAC loss compared to untreated cells in combination with different concentrations of HU (2 and 4 mM). These results may suggest that the B02 treatment had a dominant negative effect that inhibits the effect of the HU treatment, such as a cell cycle arrest before replication occurs.

Overall, the experiments in this section showed that replication stress impairs HAC stability. However, it was not possible to define whether HR was important to protect centromeric DNA from replicative stress due to a possible effect of the B02 treatment on the cell cycle as previously reported [241]. However, I learnt that the effect of different treatments on the cell cycle can affect the results of the HAC loss assay.

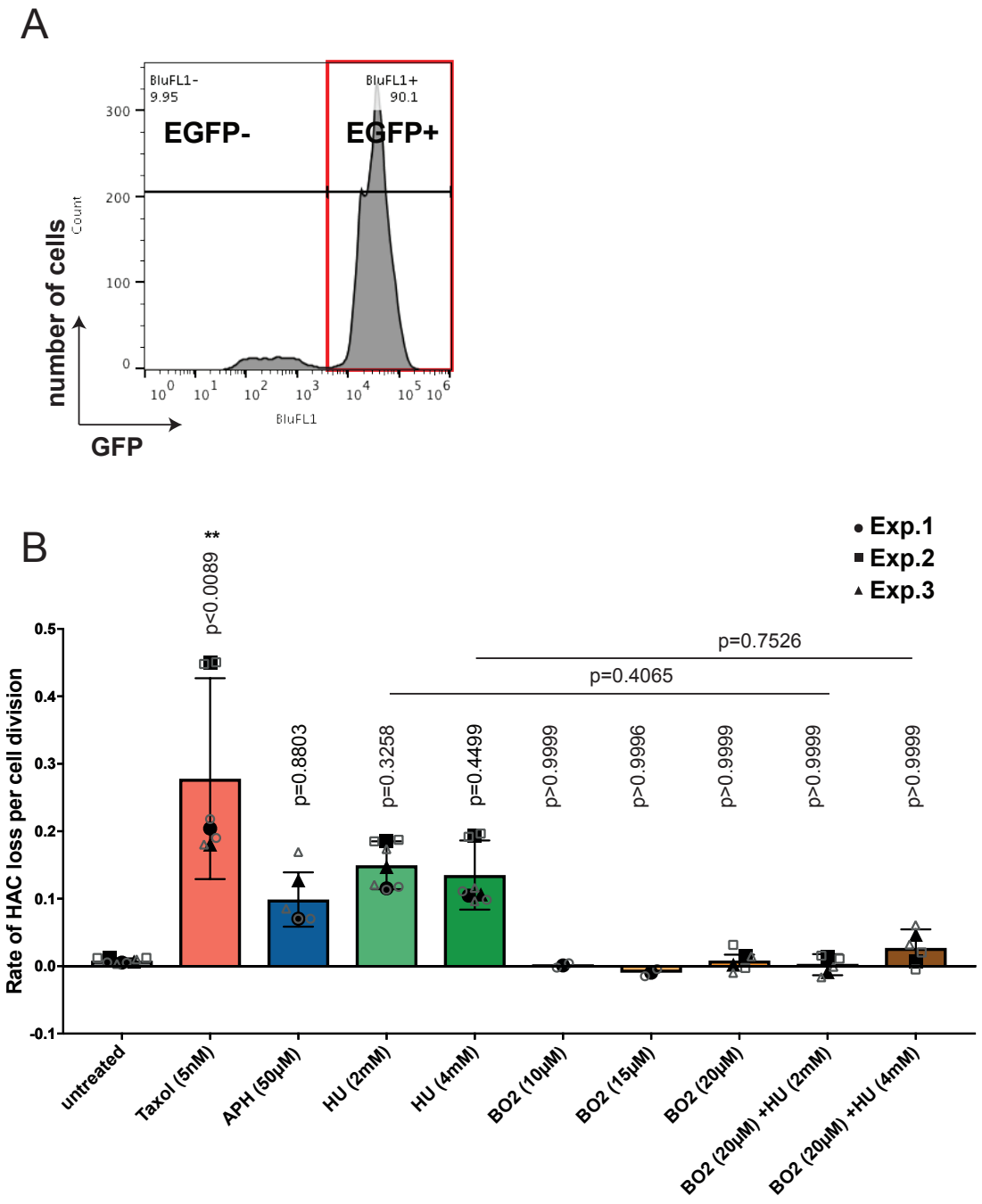


Figure 3.3: **Effect of replication stress and RAD51 inhibitor on HAC stability.** (**A**) Representative flow cytometry histograms to measure the proportion of EGFP+ cells. (**B**) Rate of HAC loss upon drug treatments. Untreated cells represent the natural HAC loss. Taxol (5 nM) was used as a positive control. Error bars represent SD of three independent experiments, each performed in duplicate. Empty symbols represents the values of the single repeats. p-values were calculated using one-way ANOVA with *post hoc* Tukey (**, $p < 0.01$). Data shown in this figure were generated in collaboration with Dr. Lee Hee-Sheung.

3.2.2 Effect of HR proteins on HAC stability using the alphoid^{tetO} HAC-dGFP

In this section, I investigated the involvement of the HR factors on HAC stability using siRNA approach. To this end, I made use of HT1080 fibrosarcoma cells carrying a new generation of alphoid^{tetO} EGFP-HAC, called alphoid^{tetO} HAC-dGFP [204]. This new generation of HAC cells allows the study of HAC loss over a shorter window of time. While the stable nature of the EGFP expressed in the alphoid^{tetO} EGFP-HAC system makes the assessment of the HAC loss difficult over the short-term, the new HAC-dGFP system circumvents this problem by fusing GFP to proteins whose stability are strictly controlled during the cell cycle. Specifically, the HAC-dGFP system expresses two fusions of the GFP transgene (dGFP), i.e., GFP-CDT1 and GFP-GEMININ, targeted for proteolysis in a cell cycle-dependent manner (Figure 3.4A). CDT1 activity is restricted to G1, and the protein is rapidly degraded at the G1-S transition. Conversely, GEMININ is rapidly degraded during mitotic exit (upon anaphase entry), such that its activity is restricted to S-G2 and early M. In this way, the HAC-dGFP system expresses green fluorescence throughout the cell cycle apart from late M; GFP-CDT1 provides the green fluorescence in G1 phase, while GFP-GEMININ provides the green fluorescence in S-G2 and early M. Given the rapid and cell-cycle dependent turnover of both CDT1 and GEMININ, fluorescence is lost rapidly when cells lose HAC, thus allowing the use of the HAC-dGFP system to study the effects of protein depletion within relatively short time periods, such as 72-96 h after siRNA treatment (Figure 3.4B). Using this HAC system, protein kinases involved in chromosome transmission have been previously identified [204]. In this study, the rate of HAC loss was calculated using the proportion of GFP+ cells using the formula:

$$R_{si} = 2 - 2 \cdot \left(\frac{P_{si}}{P_0} \right)^{\frac{1}{n}} \tag{3.1}$$

where R_{si} is the rate of HAC loss after siRNA treatment; P_{si} is the percentage of GFP+ cells after siRNA treatment; P_0 is the percentage of GFP+ cells at the beginning of the

experiment in cells cultured in blasticidin; *n* is the number of cell divisions at the time of the analysis [204] (Figure 3.4C).

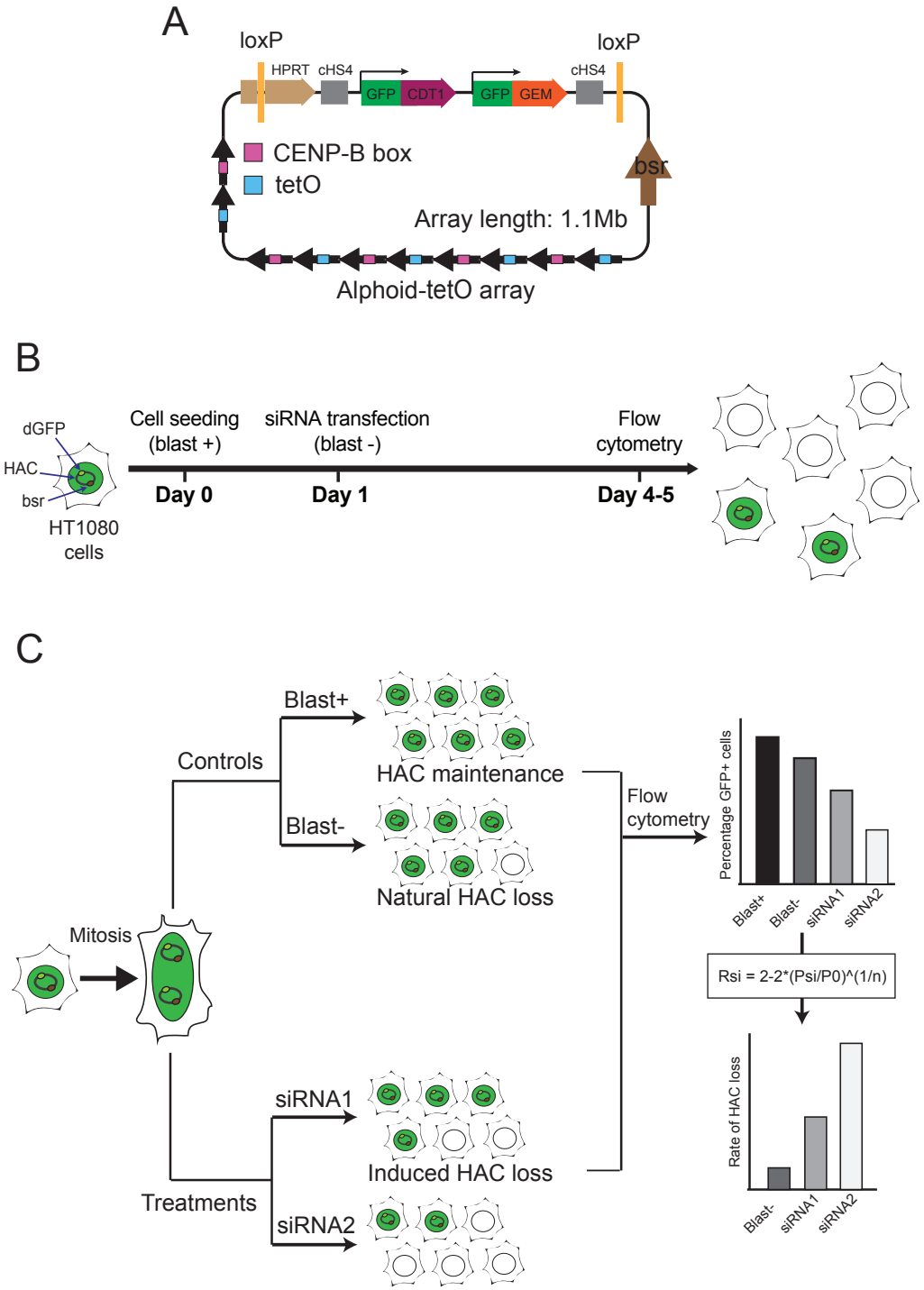


Figure 3.4: **The HAC loss assay using the alphoid^{tetO} HAC-dGFP.** (**A**) Schematic representation of the HAC-dGFP. The GFP-CDT1-GFP-GEMININ (GEM) gene cassette was introduced in the alphoid^{tetO} HAC [234] using a loxP loading site as previously described in section 3.1.2. Selectable marker blasticidin (bsr). Picture modified from [204]. (**B**) Schematic representation of the protocol of the HAC loss assay with siRNA treatment. Cells are seeded in blasticidin (blast) containing medium. 24 h after seeding, cells are transfected in blasticidin-free medium. HAC loss is analysed 72-96 h after siRNA treatment (**C**) Schematic representation of the HAC loss assay. Cells grown in blasticidin containing medium maintain the HAC, cells grown in blasticidin-free medium show natural level of HAC loss, cells treated with siRNAs show increase HAC loss detected by a reduced level of EGFP positive cells. Rate of HAC loss was calculated as described in section 2.6.16.

3.2.2.1 Optimisation of the HAC loss assay

The rate of HAC loss was previously defined as the probability of losing the HAC after *n* cell divisions [204]. In previous studies, *n* was fixed based on the estimated doubling time of the HT1080 cells (18 h) [204], such that *n*=4 at 72 h after siRNA treatment. However, if the protein depletion slows down cell growth, the number of cell divisions is reduced and the rate of HAC loss can be underestimated. Depletion of HR factors may lead to the accumulation of DNA damages that activate the cell cycle checkpoints. This gives the cells more time to repair the damage; and, at the same time, it slows down cell proliferation. To address this problem, *n* was determined using a dye dilution assay (Figure 3.5). In this assay, cells are initially incubated with a fluorescent dye. When cells are then grown in the absence of the dye, the initially incorporated fluorescent dye is diluted in half after each cell division, allowing the estimation of *n* at 72 h after dye exposures (Figure 3.5A). The Division Index (DI), which indicates the average number of cell divisions in the whole population, was measured by flow cytometry as described in section 2.6.3. At 72 h, parental cells showed a DI = 3.62 similar to the estimated number of cell divisions based on the doubling time of HT1080 cells (i.e. DI=4 at 72 h). The slight reduction could be due to an initial adaptation after cell seeding.
In the following experiments, *n* was experimentally determined with the dye dilution assay for each siRNA treatment and the values of DI were incorporated in the calculation of the rate of HAC loss (Table 3.6).

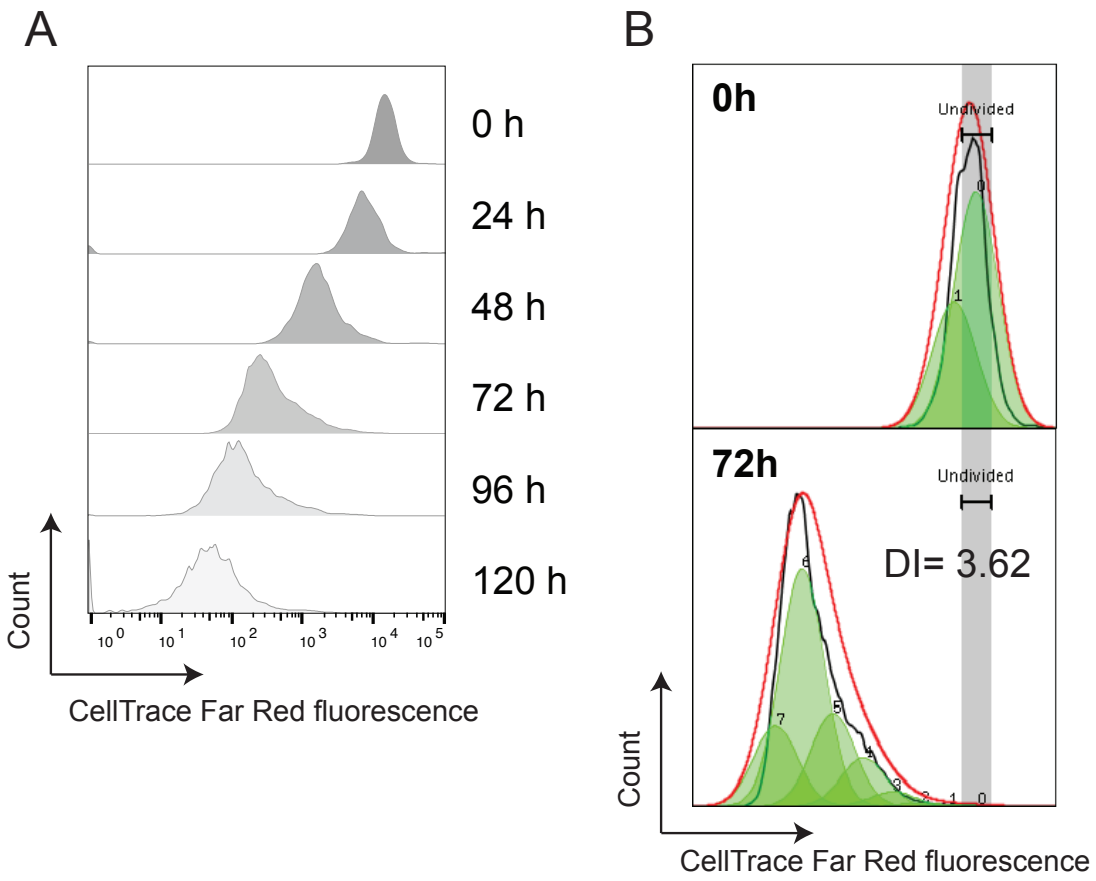


Figure 3.5: **Dye dilution assay using Far Red Cell Trace.** (**A**) Proof of principle of the dye dilution assay. Fluorescent intensity of the CellTrace Far Red dye is progressively diluted every 24 h as the cells grow. (**B**) Proliferation curve fitted using FlowJo proliferation tool. The intensity of the undivided population was determined at 0 h after siRNA treatment. At 72 h, the average number of cell divisions, i.e., division index (DI), was estimated based on the fluorescence intensity.

Sample	Number of peak	Peak CV	Peak Ratio	Division Index	Average DI
HT1080A1_blast+_1	8	5.5	0.5	4.08	
HT1080A1_blast+_2	8	5.5	0.5	3.36	**3.62**
HT1080A1_blast+_3	8	5.5	0.5	3.42	
HT1080A1_blast-_1	8	5.5	0.5	3.67	
HT1080A1_blast-_2	8	5.5	0.5	3.5	**3.63**
HT1080A1_blast-_3	8	5.5	0.5	3.71	
HT1080A1_siBRCA2_1	8	5.5	0.5	3.32	
HT1080A1_siBRCA2_2	8	5.5	0.5	3.41	**3.16**
HT1080A1_siBRCA2_3	8	5.5	0.5	2.75	
HT1080A1_siCTR_1	8	5.5	0.5	3.1	
HT1080A1_siCTR_2	8	5.5	0.5	3.1	**3.33**
HT1080A1_siCTR_3	8	5.5	0.5	3.79	
HT1080A1_siPALB2_1	8	5.5	0.5	3.31	
HT1080A1_siPALB2_2	8	5.5	0.5	3.27	**3.25**
HT1080A1_siPALB2_3	8	5.5	0.5	3.18	
HT1080A1_siRAD51_1	8	5.5	0.5	2.92	
HT1080A1_siRAD51_2	8	5.5	0.5	3.17	**2.80**
HT1080A1_siRAD51_3	8	5.5	0.5	2.31	
HT1080A1_APH	8	6.2	0.5	**3.17**	
HT1080A1_siBRCA2+APH	8	6.2	0.5	**2.61**	
HT1080A1_siRAD51+APH	8	6.2	0.5	**2.56**	
HT1080A1_siBRCA2+siPALB2	8	9	0.5	**2.15**	
HT1080A1_siBRCA2+siRAD51	8	9	0.5	**2.05**	
HT1080A1_siSTK38	8	9	0.5	**2.04**	

Figure 3.6: **Table of Division Indexes (DI)**. Values of DI were used to calculate the rate of HAC loss. DI was determined either from the average of three measures from a single experiment or from one single measure. Parameters were fixed at 0.5 Peak Ratio, 8 Number of peaks and Peak CV was based on the undivided population as analysed at 24h.

3.2.2.2 Effect of HR proteins depletion on HAC stability

Initially, the optimal time point at which to measure HAC loss upon depletion of HR proteins was determined. To this end, time course experiments was performed where the proportion of GFP positive cells were measured every 24 hours by flow cytometry (Figure 3.7). In the flow cytometric analysis, an anthracycline derivative (DRAQ7) was used to monitor cell toxicity [243] and the fraction of GFP+/live cells was selected as previously described in [204] to calculate the rate of HAC loss (Figure 3.7A). As expected, cells grown in HAC-selective medium (blast+) displayed a high and stable level of GFP-HAC, while cells grown in the absence of blasticidin (blast-) exhibited a slight reduction of GFP signal over time (Figure 3.7B). Cells treated with a non-targeting control siRNA (siCTR) showed a similar level of GFP compared to

blasticidin-free treated cells. Knockdown of STK38, a serine/threonine kinase that is important for proper centrosome duplication, alignment of mitotic chromosomes and spindle orientation in mitosis, induced a decreased level of GFP compared to siCTR agreeing with the previous report [204]. In these experiments, siRNA against GFP was also used to assess the transfection efficiency. In all three independent experiments, knockdown of BRCA2 consistently induced a decrease in GFP positive cells compared to siCTR at 72 h. Knockdown of RAD51 reduced the level of GFP positive cells at 48 h and 120 h. PALB2 depletion induced a reduction in GFP positive cells at 48 hours in a single experiment. However, during the experiments, I observed that low level of GFP at initial time points (i.e. 24-48 h) was associated with an increased level of dead cells, which may be due to initial adaptation and/or toxicity after transfection; while, at later time points (i.e. 120-144 h), as cells reached 100% confluency, they were split to allow continue cell growth. At 120 h, many cells formed aggregates and the low level of GFP is associated with a reduced number of cells analysed, which may not be representative of the whole population.

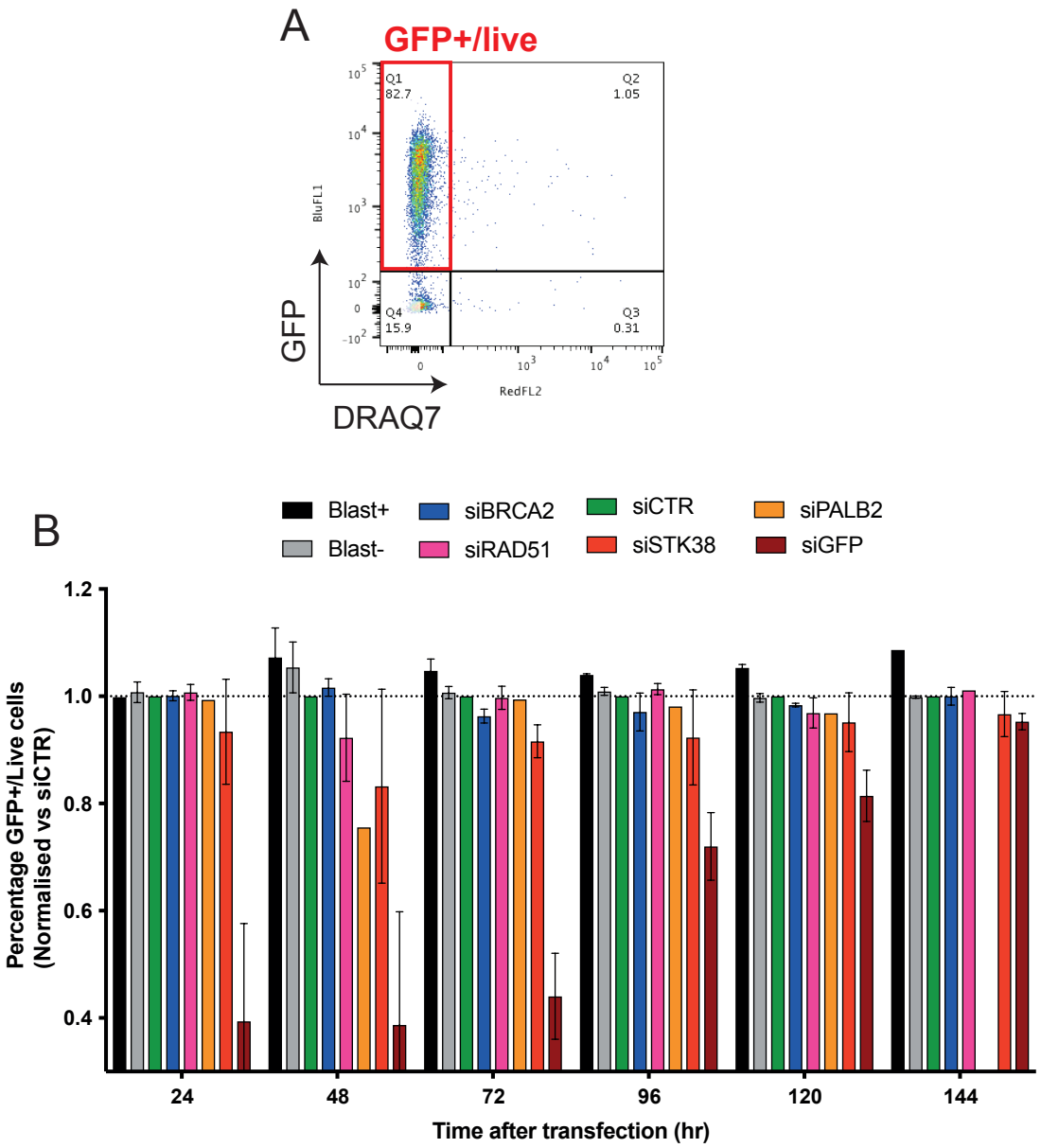


Figure 3.7: **Time course of the GFP level in HT1080 HAC-dGFP cells upon siRNA treatments**. (**A**) Representative flow cytometry graph showing the HAC-dGFP in untreated cells. GFP+/live cells was selected for the HAC loss analysis (red square). (**B**) Percentage of GFP+/Live cells were measured every 24 h after siRNA treatment. Data were normalised with respect to negative control (siCTR). Mean and SD in three independent experiments, except for siRAD51 (two experiments) and siPALB2 (one experiment).

In the meantime, the level of protein expression was also monitored by Western blot over time (Figure 3.8). Cells treated with siBRCA2, siRAD51 and siPALB2 showed almost complete protein depletion at 48 h. As the impact of protein depletion was

expected to influence cellular phenotypes in the next 24 hours, the rate of HAC loss was assessed at 72 h. Similarly, the number of cell divisions was measured at 72 h after siRNA treatment. Knockdown of BRCA2 and PALB2 induced a small reduction of the cell proliferation compared to the siCTR (DI=3.16 and DI=3.25, respectively) (Figure 3.9), whereas RAD51 depletion induced higher reduction of the cell proliferation (DI=2.80)

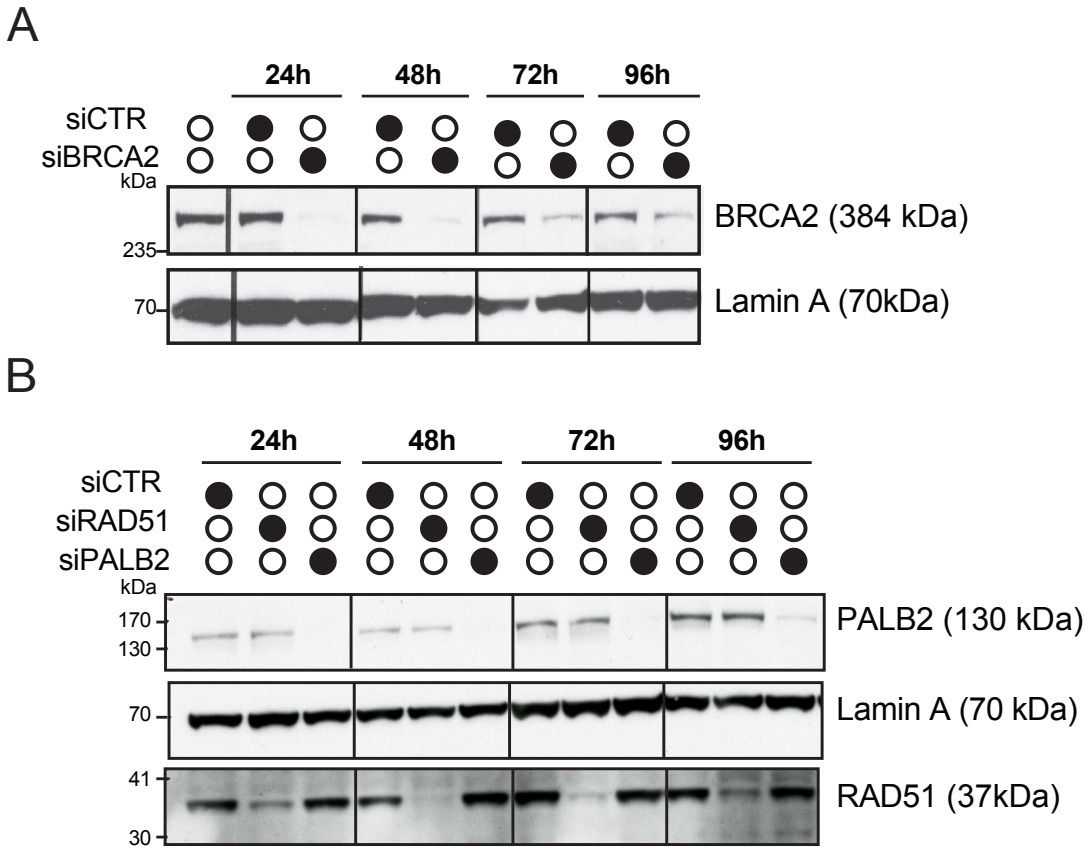


Figure 3.8: **Western blot showing the level of protein depletion in HT1080 HAC-dGFP cells upon siRNA treatments.** (**A**) BRCA2 depletion every 24 h after siRNA treatment. (**B**) RAD51 and PALB2 depletion every 24 h after siRNA treatment. Lamin A was used as a loading control.

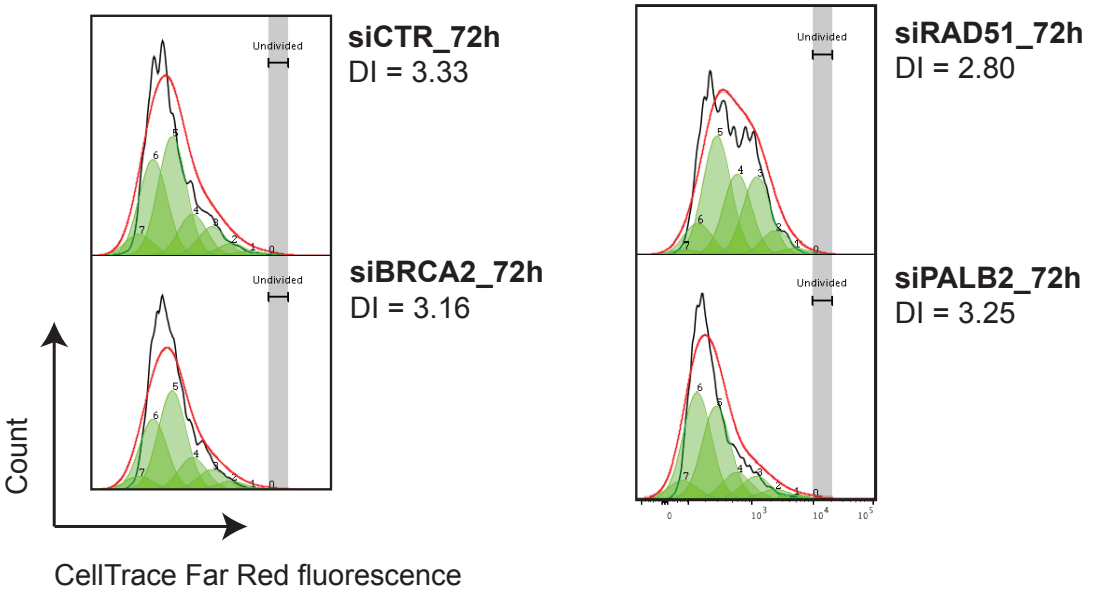


Figure 3.9: **Dye dilution assay after siRNA treatment.** Graphs represent the curves fitted with FlowJo. Average number of cell divisions 72 h after siRNA treatments (DI). DI are the average of one single experiment performed in triplicate.

The rate of HAC loss displayed in the negative control (siCTR) was comparable to the natural HAC loss measured with the blasticidin-free treated cells (blast-). Knockdown of STK38 increased HAC loss, as previously reported [204]. Across three independent experiments, siBRCA2 consistently resulted in increased HAC loss compared to the siCTR (Figure 3.10A). The impact of RAD51 depletion was tested in two independent experiments, which gave widely varying results, while PALB2 depletion did not induce HAC loss compared to siCTR as measured in a single experiment. However, at 72 h after siRNA treatment, the knockdown of BRCA2 showed a slight increased level of dead cells in Exp. 2 and 3, which may lead to overestimate the HAC loss. Similarly, this was observed for the knockdown of RAD51 in Exp. 3.

To further confirm the HAC loss upon siBRCA2 treatment, cells were fixed and the number of cells with and without the HAC was measured by Fluorescence In Situ Hybridization (FISH) analysis (Figure 3.10B). In this way, all cells (live and dead) were taken into consideration and the presence of the HAC was detected using a FISH probe rather than the GFP intensity, which could be affected by the cell viability. After fixation, DNA was hybridised with a FISH probe specific for the tetO sequence to detect

the HAC and a FISH probe specific for the CENP-B box, which detects centromeres. The presence of the HAC was identified by the colocalisation of both FISH signals (Figure 3.10B). Despite the small sample size that would not be sufficient to conclude statistical significance between different treatments, this preliminary result was in line with the results observed by flow cytometry analysis in which BRCA2 depletion increased HAC loss, RAD51 depletion decreased the rate of HAC loss and PALB2 depletion displayed similar level to the siCTR treated cells. Overall, this set of experiments suggested that BRCA2 is important for transmission of the HAC.

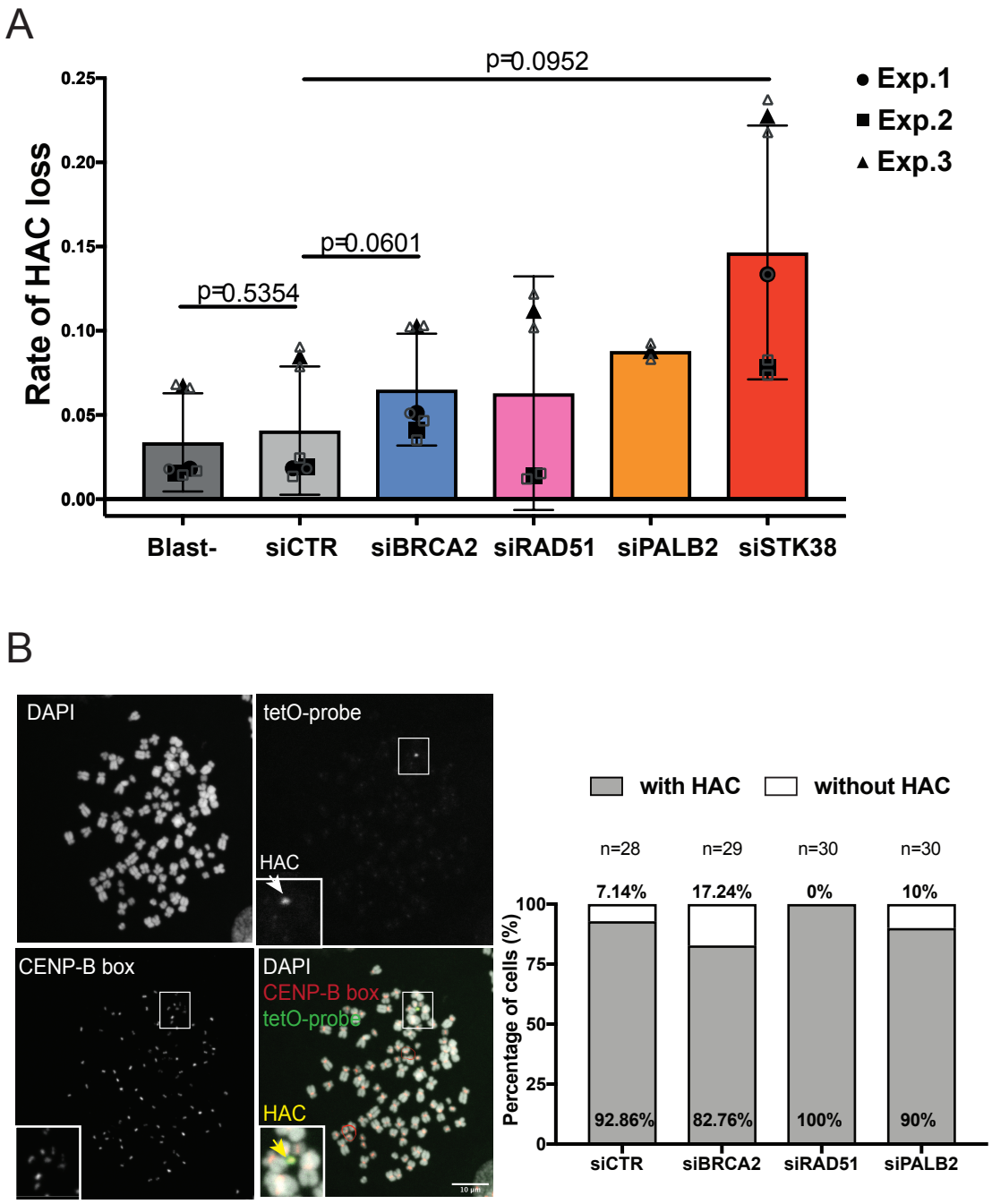


Figure 3.10: **HAC loss after BRCA2, PALB2 and RAD51 depletion by siRNAs**. (**A**) Rate of HAC loss calculated as described in 2.6.16. Cells grown in blasticidin-free medium (blast-) represent the natural HAC loss. siCTR (negative control). siSTK38 (positive control). Error bars represent SD of three independent experiments. Experiment 2 and 3 were performed in duplicate. Empty symbols represents the values of the single repeats. p-values were calculated using RM one-way ANOVA with *post hoc* Dunnet. (**B**) FISH analysis. On the left, representative figure of metaphase spread. Endogenous centromeres were detected with CENP-B-box-probe. HAC was detected with a tetO-probe. n is the number of metaphases analysed for each condition in a single experiment.

3.2.2.3 Cell cycle arrest upon BRCA2 and RAD51 depletion

Cells containing the HAC-dGFP express the GFP signal throughout the cell cycle except the late phase of mitosis [204]. Therefore, if cells are arrested at specific phases of the cell cycle, this can affect the proportion of GFP+ cells. BRCA2 and RAD51-depleted cells exhibited a lower DI compared to siCTR-treated cells (Figure 3.9), suggesting that depletion of these proteins leads to a longer cell cycle. Indeed, given the widely reported role of these proteins in DNA replication [48] [49] [80] [244], it was possible that cells were arrested in S phase. This assumption is in line with previously observed roles of BRCA2 and RAD51 during DNA replication. To assess this possibility, I checked the cell cycle profile upon BRCA2 and RAD51 depletion (Figure 3.11). Cells were stained with propidium iodide (PI) to assess the DNA content: cells in G1 phase have less DNA showing a lower PI signal intensity, while as cells replicate DNA, they shown increasing PI signal intensity (Figure 3.11A). A mitotic marker for chromatin condensation, phosphorylation of histone H3 at serine 10 (pH3S10), was used to distinguish between cells in G2 and M phase. RO-3306, a CDK1 inhibitor, was used to enrich cells in G2 phase (Figure 3.11B) and nocodazole, an inhibitor of microtubule polymerisation, was used to enrich cells in M phase (Figure 3.11C). The analysis of the cell cycle profile at 72 h after siRNA treatment revealed that BRCA2 depletion slightly increased cells in S/G2 compared to the negative control (Figure 3.11D-E), and RAD51 depletion displayed an even higher increase (Figure 3.11F). Thus, it is possible that the reduced rate of HAC loss in siRAD51-treated cells may be due to an increased number of cells arrested in S/G2 phase.

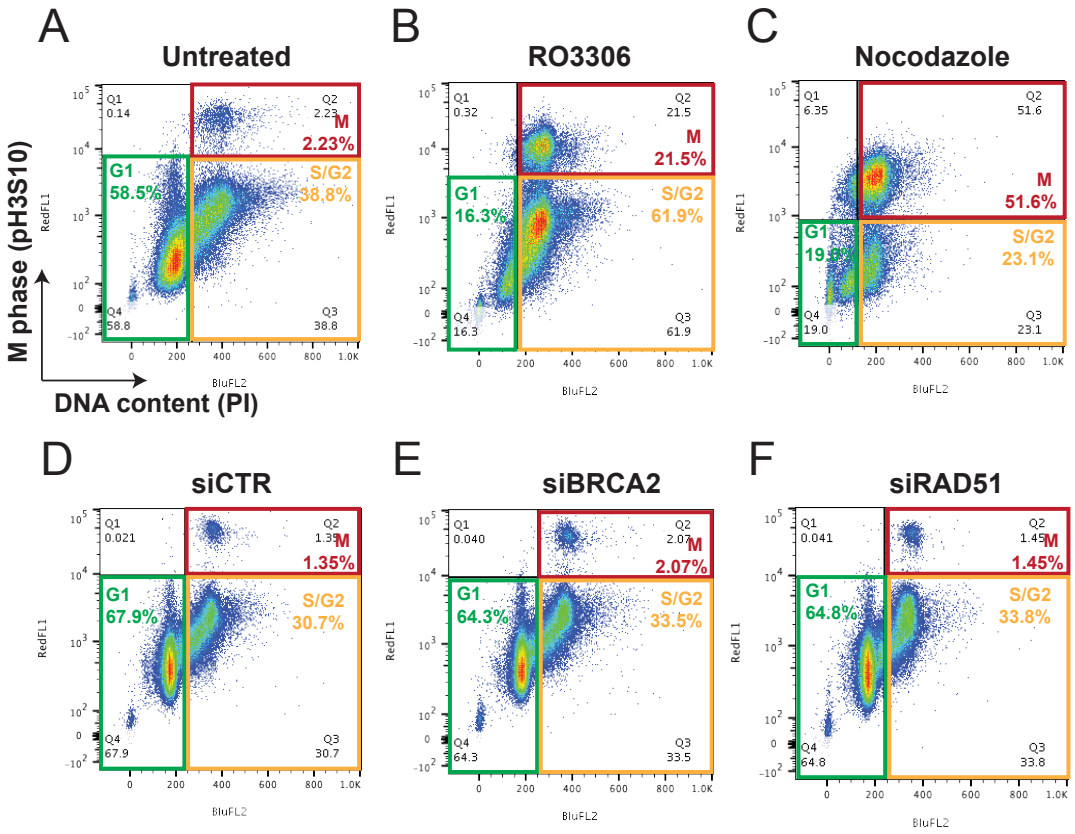


Figure 3.11: **Cell cycle Profile upon BRCA2 and RAD51 depletion.** (**A**) Cells were stained with Propidium iodide (PI) to distinguish between G1 and S/G2 phase based on the amount of DNA content, and pH3S10 antibody as marker of M phase to distinguish between G2/M phase. (**B**) Cells were treated with a RO-3306 (9 μM for 16 h) to enrich cells in G2 phase. (**C**) Cells were treated with a nocodazole (200 nM for 16 h) to enrich cells in M phase. Cells cycle profile was assessed 72 h after siCTR (**D**), siBRCA2 (**E**), and siRAD51 (**F**) treatment.

siBRCA2-treated cells contained slightly more cells in M phase compared to the negative control. Since late mitosis is the time when cells lose the GFP signal, I assessed at which stage of mitosis siBRCA2 treated cells were arrested. Cells were fixed, stained with DAPI and the different cell cycle stages (interphase, early mitosis and late mitosis) were evaluated based on the DNA morphology: in interphase, the nucleus presented a rounded shape with less intense DAPI signal, whilst in mitosis, cells show intense DAPI staining due to chromatin condensation. In early mitosis (prophase and metaphase) all chromosomes are condensed, and in late mitosis (anaphase and telophase), sister chromatids are separate from each other and are segregated into two daughter cells (Figure 3.12A). In the BRCA2 depleted cells, the number of cells in mi-

tosis was almost doubled (4.04%) compared to the negative control (2.1%), and most of the mitotic cells, enriched upon siBRCA2 treatment, were found to be in early mitosis (3.43%). This result suggested that the increased rate of HAC loss observed in BRCA2 depleted cells was unlikely caused by cellular arrest in late mitosis.

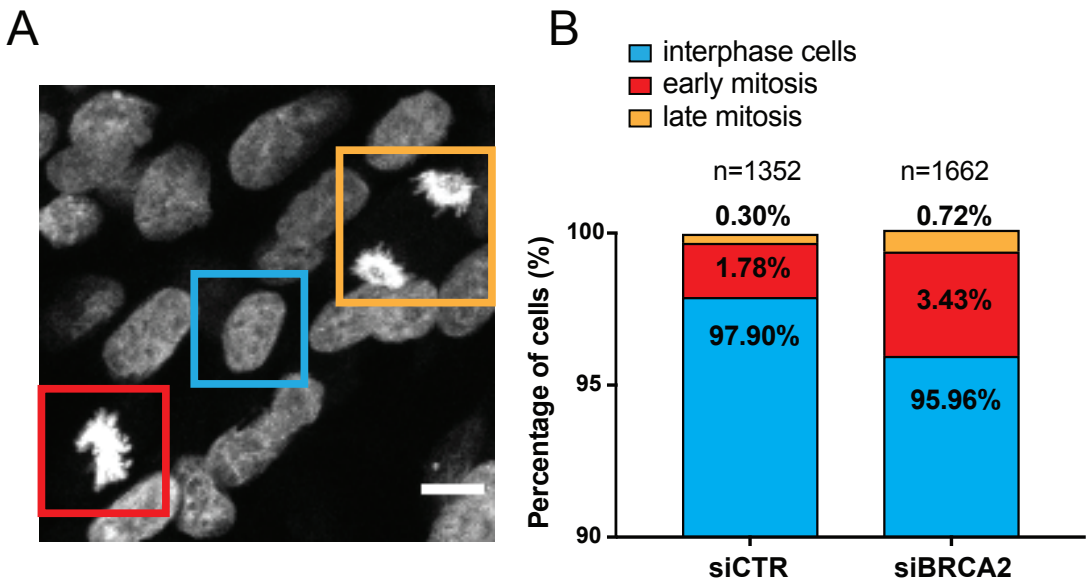


Figure 3.12: **Mitotic index upon BRCA2 depletion.** HT1080 HAC-dGFP cells were treated with siCTR and siBRCA2. 72 h after treatment cells were fixed and stained with DAPI. (**A**) Representative picture of cells in different stages of the cell cycle: interphase (blue), early mitosis (red), late mitosis (yellow). Scale bar: 10 μm. (**B**) Column graph represents the percentage of cells in different stage of cell cycle in control cells (siCTR) and BRCA2-depleted cells (siBRCA2). n is the number of cells analysed for each condition in a single experiment.

3.2.2.4 Effect of BRCA2 depletion in combination with PALB2 and RAD51 knockdown on HAC stability

BRCA2 acts in concert with PALB2 and RAD51 to promote HR [79]. Given that only BRCA2 depletion appeared to increase the rate of HAC loss (section 3.2.2.2), I considered the possibility that BRCA2 acts independently of the other HR proteins to ensure appropriate chromosome transmission. To test this hypothesis, BRCA2 depletion was combined with PALB2 or RAD51 depletion. If PALB2 acted upstream to recruit BRCA2, the depletion of BRCA2 and PALB2 would result in a similar level of HAC

loss compared to single protein depletion. Conversely, if BRCA2 and PALB2 acted in separate pathways, the combined depletion of both proteins should increase the HAC loss compared to single protein depletion. Similarly, this can be applied to test whether BRCA2 acts upstream to recruit RAD51.

Protein depletion was monitored by Western blot (Figure 3.13) and the number of cell divisions was measured by dye dilution assay (Figure 3.14). Knockdown of BRCA2 in combination with PALB2 or RAD51 resulted in a reduced number of cell divisions compared to untreated cell (Figure 3.9) and single siRNA treatment (Figure 3.9).

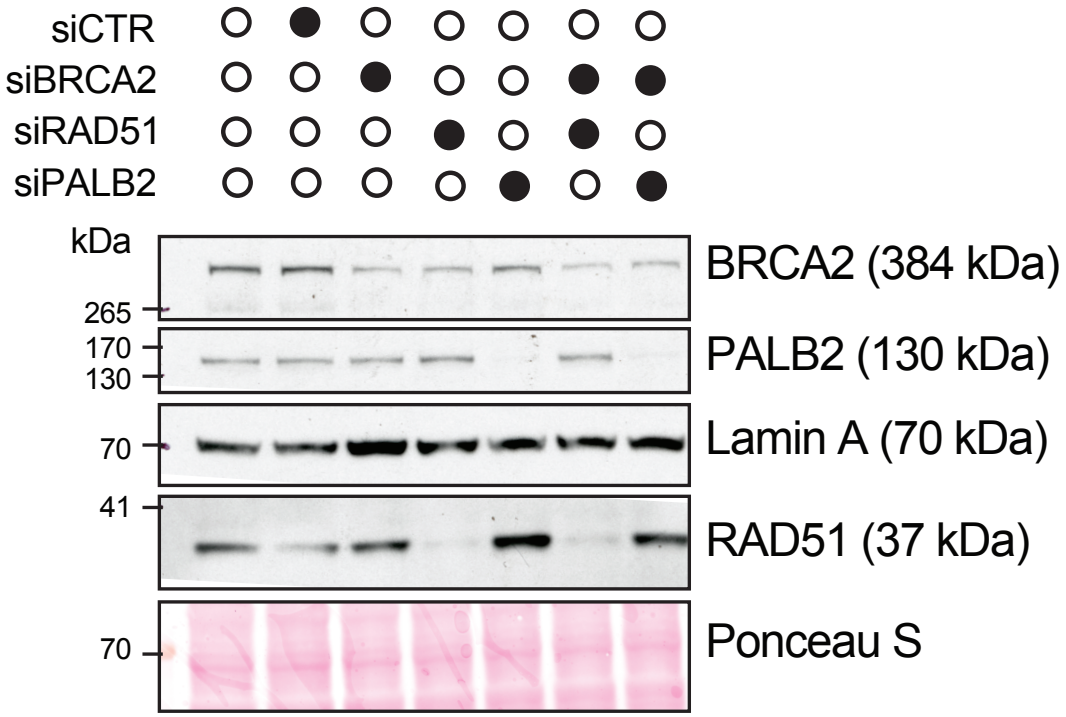


Figure 3.13: **Western blot showing the level of protein depletion in HT1080 HAC-dGFP cells upon combined siRNA treatments.** BRCA2, RAD51 and PALB2 protein expression was detected 48h after siRNA treatment. Lamin A and Ponceau S staining were used as loading controls.

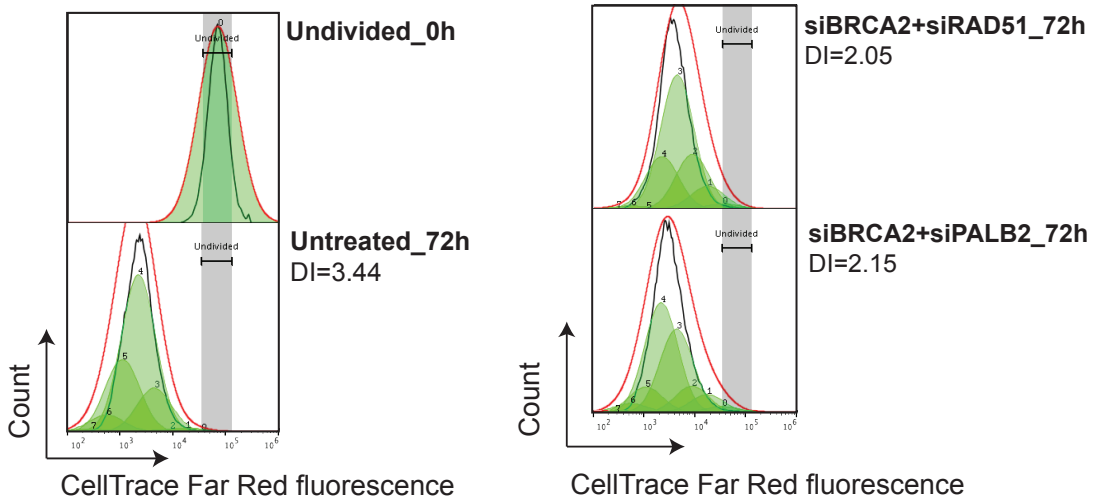


Figure 3.14: **Dye dilution assay after combined siRNA treatment.** Graphs represent the curves fitted with FlowJo. Average number of cell division 72 h after siRNA treatments (DI).

The rate of HAC loss was initially measured taking the fraction of GFP+/live cells in the single cell population as previously described (Figure 3.7A). Under these conditions, siBRCA2 treatment in combination with siPALB2 and siRAD51 increased HAC loss compared to the negative control in four independent experiments (Figure 3.15A). While the level of cell death was reduced upon single siRNA treatment, a much higher level of cell toxicity was observed upon double siRNA treatments (Figure 3.15B). As discussed above, increased cell death reduces the proportion of GFP+/live cells, leading to an apparent increase in the rate of HAC loss. To reduce the effect of cell toxicity, the proportion of GFP+/live cells was assessed in the population of the live cells only (Figure 3.15C). Under these conditions, double depletion of BRCA2 and PALB2 was found to significantly increase the rate of HAC loss compared to single siBRCA2 treatment. Similarly, the depletion of BRCA2 together with siRAD51 treatment increased the HAC loss, albeit not statistically significant, compared to siBRCA2 treatment alone. These results supported the idea that BRCA2 may contribute HAC transmission in a manner independent of PALB2 and RAD51.

Of note, in this set of experiments, siCTR treated cells displayed higher HAC loss compared to the non-siRNA treated cells cultured in blasticidin-free media (Figure 3.15A),

likely due to a high cell toxicity in Exp. 3 and Exp. 4 (Figure 3.15B). Such increase was not seen in earlier HAC loss experiments shown in Figure 3.10A. Indeed, when dead cells are excluded in this analysis, the rate of HAC loss detectable upon siCTR treatment was similar to the blasticidin-free treated cells (blast-) (Figure 3.15C). When this assessment criterion was applied, BRCA2-depleted cells exhibited higher HAC loss in three out of four experiments (Figure 3.15C). The discrepancy between these results might be caused the difference in the efficiency of BRCA2 depletion at 48 h between these experiments (Figure 3.8 and Figure 3.13).

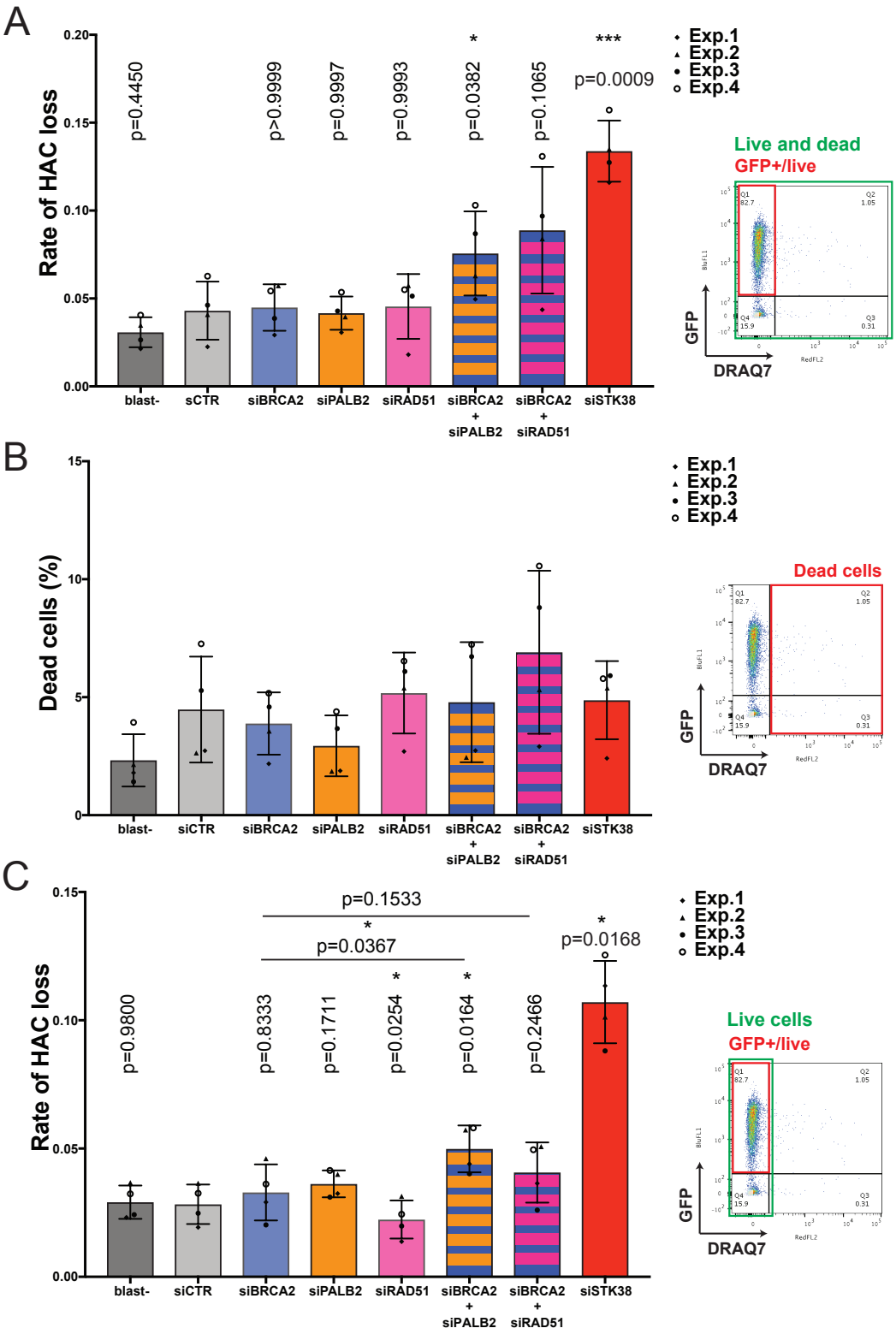


Figure 3.15: **Analysis of the HAC loss at 72 h after siRNA treatment**. (**A**) Rate of HAC loss calculated using GFP+/live cells in the whole single cell population (live and dead) (graph on the right). Cells grown in blasticidin-free medium (blast-) represent the level of natural HAC loss. siCTR (negative control). siSTK38 (positive control) [204]. (**B**) Percentage of dead cell 72 h after siRNA treatment. Dead cells were stained with live/dead marker (DRAQ7) (graph on the right). (**C**) Rate of HAC loss at 72 h calculated using the GFP+/live cells in the live cells only (graph on the right). Error bars represent SD of four independent experiments. p-values were calculated using RM one-way ANOVA with *post hoc* Tukey (*, $p<0.05$; ***, $p<0.001$).

3.2.2.5 BRCA2 and RAD51 protect the HAC from replication stress

Replication stress induced by aphidicolin and hydroxyurea treatments led to increased HAC loss in alphoid-tetO EGFP-HAC cells (Figure 3.3). In order to understand whether depletion of HR factors exacerbates replication stress at centromeric DNA, aphidicolin (APH) treatment was combined with siRNA-mediated BRCA2 and RAD51 depletion. In this set of experiments, a low dose of APH (0.4 μM) was added at 24 h after siRNA treatment to induce replication stress. This concentration partially inhibits DNA polymerase allowing the cells to continue to divide [245]. Under these conditions, APH treatment slightly increased the level of cells in S/G2 phase (Figure 3.16A), whilst depletion of BRCA2 or RAD51 followed by APH treatment increased the cellular population in G1 phase (Figure 3.16B) and in S/G2 phase (Figure 3.16C), respectively. Moreover, the dye dilution assay showed that double treatment with siBRCA2 and siRAD51 together with APH slowed the cellular growth compared to siCTR treated cells (Figure 3.17).

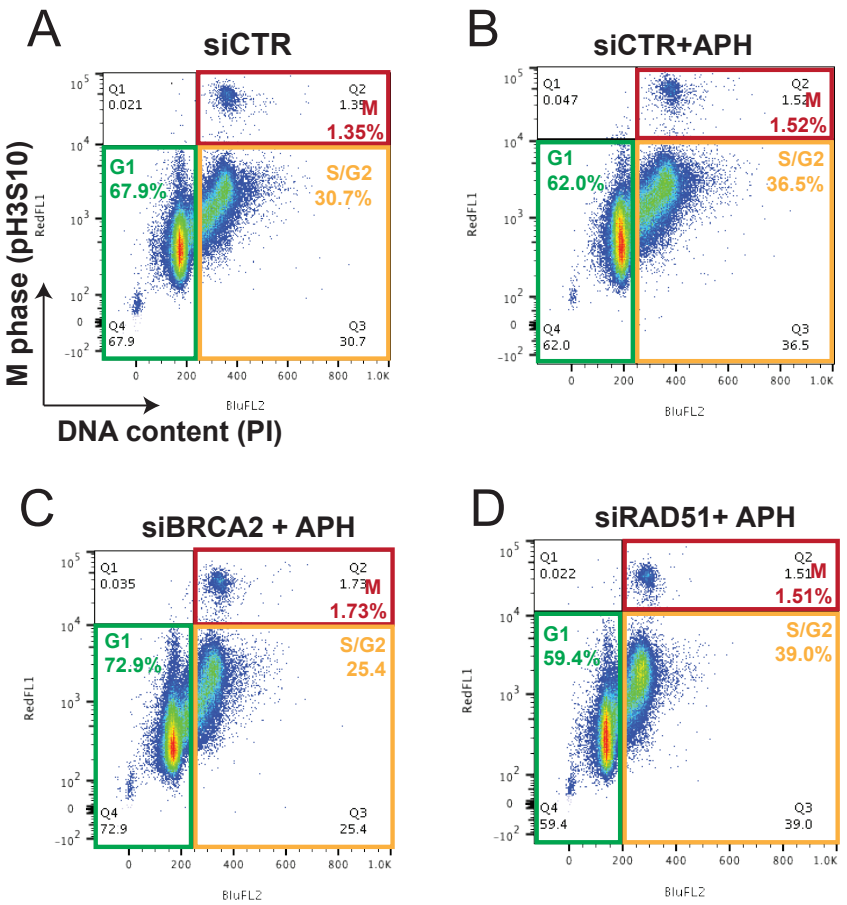


Figure 3.16: **Cell cycle profile 72 h after siRNA treatment and aphidicolin treatment.** Cells were stained with Propidium iodide (PI) to assess the DNA content and with antibody for pH3S10 (marker of M phase) to distinguish different phases of the cell cycle. HT1080 HAC-dGFP cells were treated with siRNAs followed by 24 h of aphidicolin (APH) treatment (0.4 μM). Cells were analysed 72 h after siRNA treatment with non-targeting siRNA (siCTR) (**A-B**), siBRCA2 (**B**), siRAD51 (**C**).

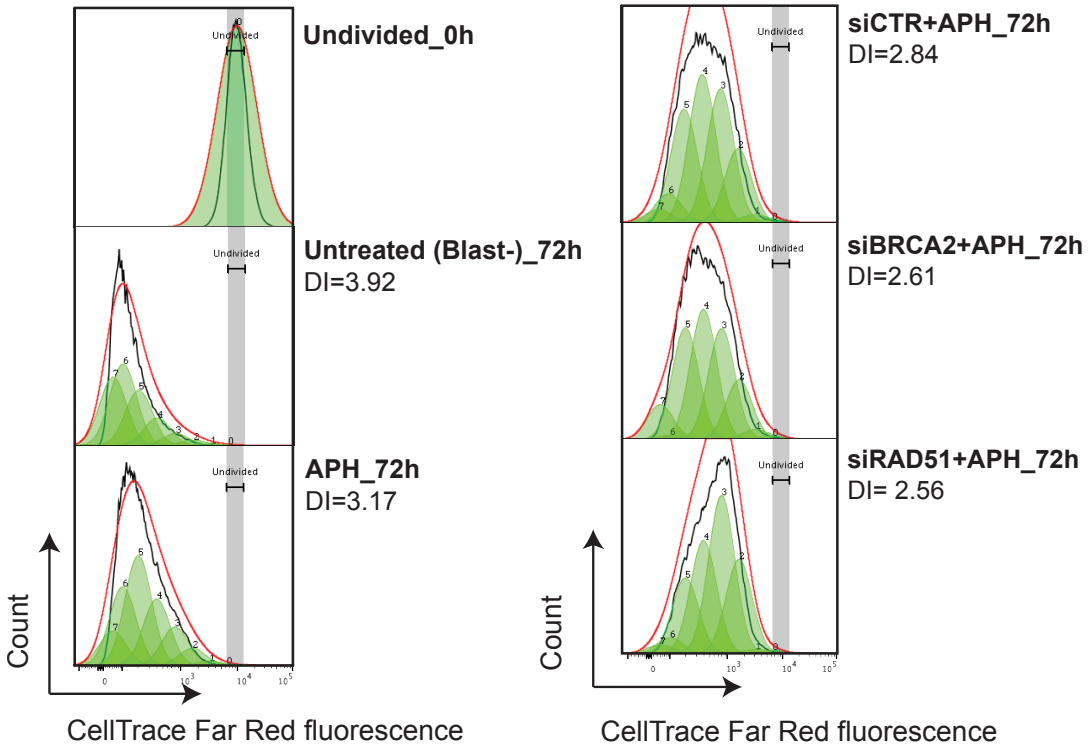


Figure 3.17: **Cell cycle Profile upon BRCA2 and RAD51 depletion upon aphidicolin treatment.** HT1080 HAC-dGFP cells were treated with siRNAs followed by 24 h of aphidicolin (APH) treatment (0.4 μM). Cells were analysed 72 h after siRNA treatment with non-targeting siRNA (siCTR), siBRCA2, and siRAD51. Graphs represent the curves fitted with FlowJo. Average number of cell division 72 h after siRNA treatments (DI).

APH treatment alone showed an increased rate of HAC loss compared to untreated cells. Depletion of BRCA2 or RAD51 in combination with APH further increased the HAC loss compared to single APH treatment (Figure 3.18A). However, given that, increased level of cell death was also observed upon APH treatment (Figure 3.18B). Thus, the HAC loss was re-calculated using the population of live cells only (Figure 3.18C). APH treatment alone consistently increased the rate of HAC loss in three independent experiments. The rate of HAC loss was further increased upon BRCA2 or RAD51 depletion in all three independent experiments. These results suggested that RAD51 and BRCA2 are both important for the HAC maintenance upon exposure to mild replication stress.

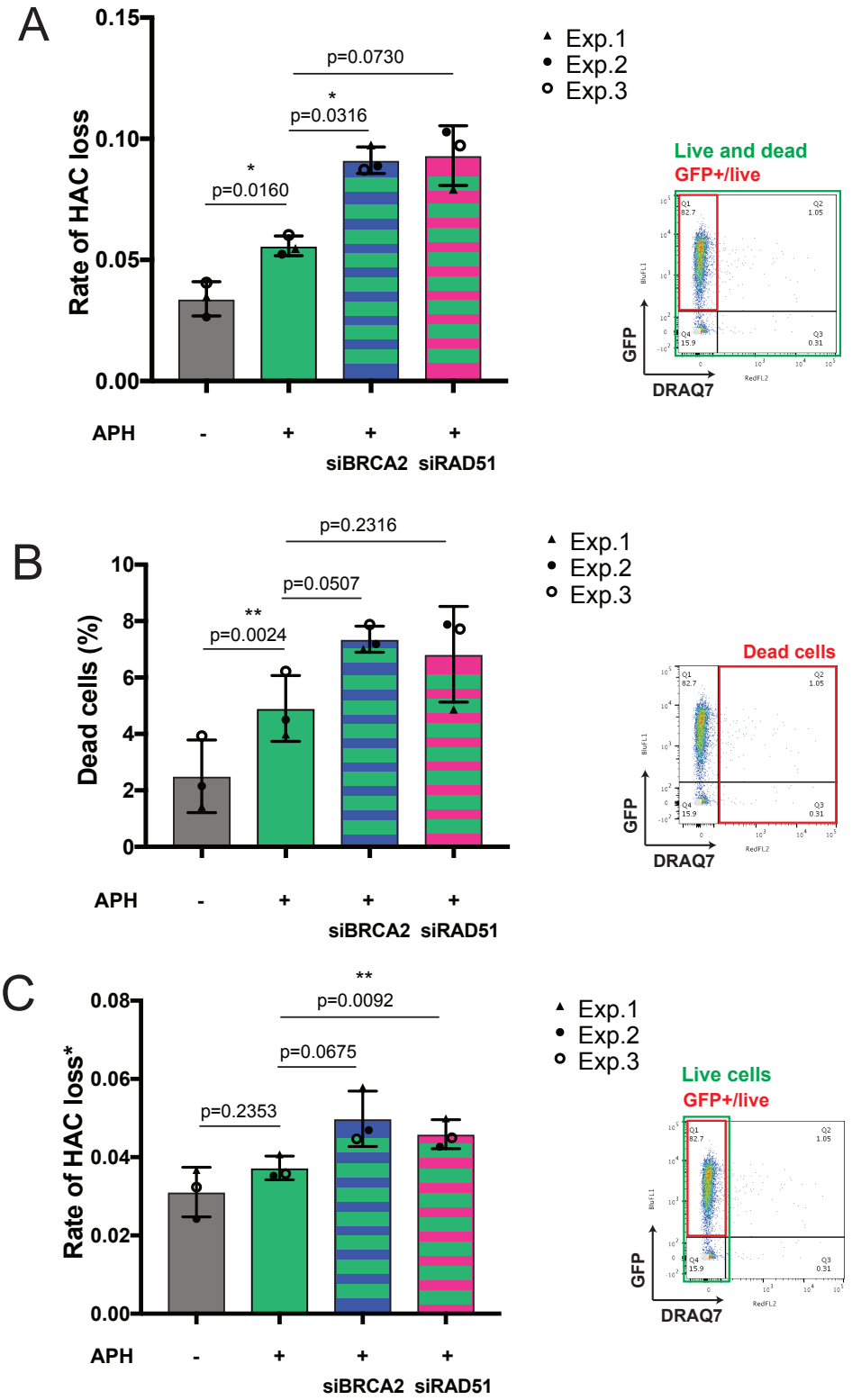


Figure 3.18: **Analysis of the HAC loss at 72 h after siRNA treatment**. (**A**) Rate of HAC loss calculated using the GFP+/live cells in the whole single cell population as described in 3.2.2.2. Cells grown in drug-free medium represent the level of natural HAC loss (graph on the right). (**B**) Level of cell death 72 h after siRNA treatment. Dead cells were stained with live/dead marker (DRAQ7) (graph on the right). (**C**) Rate of HAC loss at 72 h calculated using the GFP+/live cells in the live cells only (graph on the right). Error bars represent SD of three independent experiments. p-values were calculated using RM one-way ANOVA with *post hoc* Dunnet (*, $p < 0.05$; **, $p < 0.01$).

3.2.3 Effect of HR factors on HAC stability using tetO-tetR system

Results in section 3.2.2.2 suggested that BRCA2 is important for the HAC stability. BRCA2 is a large protein of 3418 amino acids and through different regions it mediates different functions [79]. Here, I aimed to assess which region of BRCA2 was important to preserve the HAC stability. To this end, I generated stable cell lines expressing tetR-mCherry-fusion constructs constructs to enrich a fragment of or a full length BRCA2 and tested their effect on the HAC stability. Given that tetR-fusion proteins bind the tetO regions within the alphoid-DNA arrays of the HAC, this system can be used to artificially tether proteins of interest and assess their effect on the HAC stability.

Three different constructs were initially generated: tetR-mCherry-BRC4, tetR-mCherry B2.8 and tetR-mCherry-WD40 (Figure 3.19A-B).

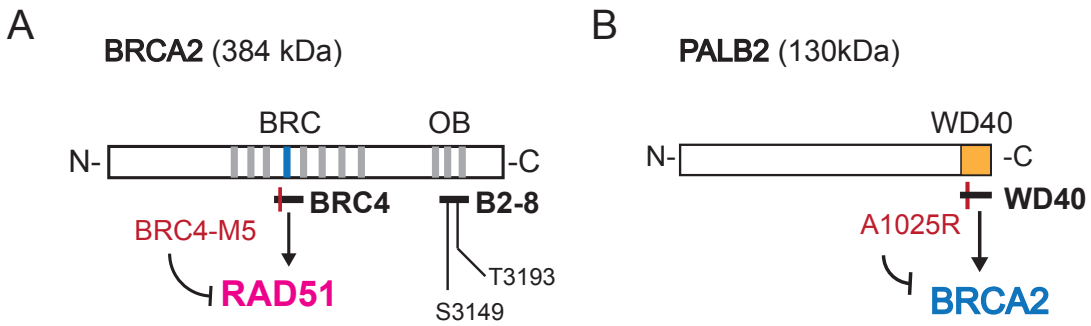


Figure 3.19: **The BRC4, B2.8 and WD40 fragments.** (**A**) Schematic representation of BRCA2 fragments, BRC4 and B2.8. BRC4 wild-type binds RAD51. BRC4-M5 (T1526A) prevents RAD51 binding. B2.8 presents two potential CDK-target sites, serine (S) 3149 and theonine (T) 3193. (**B**) Schematic representation of PALB2 fragment, WD40. WD40 wild-type binds BRCA2. WD40 A1025R prevents BRCA2 binding.

Through the BRC repeats, BRCA2 binds RAD51 and mediates recombination [246] [85] (Figure 3.19A). BRC4 is the fourth BRC repeat of BRCA2 that binds RAD51 with high affinity [84]. This fragment was used to assess whether BRCA2 function in RAD51-mediated HR was essential to preserve the HAC stability. The B2.8 fragment is a C-terminal fragment (from amino acid 2780 to 3197) harboring the single strand DNA binding OB (oligonucleotide/oligosaccharide-binding) fold motifs and where predicted

CDK target residues were identified [122] (Figure 3.19A). Moreover, preliminary experiments in the laboratory of Dr. Fumiko Esashi found that this region interacts with ZWINT, a kinetochore component. This observation suggested an interesting possibility that BRCA2, through this region, may influence kinetochore assembly. The WD40 is the C-terminal region of PALB2 that binds BRCA2 [128] (Figure 3.19B). Due to the large size of BRCA2 and the difficulty to transfect big vectors inside cells, this domain was used to recruit the full-length BRCA2 to the HAC. For each construct, wild-type (WT) and mutated variants were generated. In the BRC4, theonine 1526 was replaced with an alanine to prevent RAD51 binding [84] (Figure 3.19A). In the B2.8 fragment, two potential CDK-target sites, serine 3149 and threonine 3193, were replaced with alanines to prevent CDK-mediated phosphorylations. In total, three mutants were generated for the B2.8 fragment: S3149A, T3193A and S3149A/T3193A. In the WD40 fragment alanine 1025 was replaced with arginine (A1025R) to perturb BRCA2 binding [128] (Figure 3.19A). Moreover, an empty vector with tetR-mCherry only was generated as a negative control. The tetR-mCherry constructs were generated as described in section 2.2.9.

3.2.3.1 Generation of stable cell lines

Stable cell lines expressing the WD40 and BRC4 constructs were initially generated. The WD40 constructs generated in section 2.2.9 were transfected in HT1080 HAC-dGFP cells (Figure 3.20A). After transfection, cells were transferred to a 10-cm dish at high dilution with selective medium. Then, around 10-20 colonies were picked for each construct and expanded in 24-well plates. Subsequently, FACS was used to validate the expression of the mCherry-constructs in these clones : 13 clones were tested for the WD40 A1025R construct, 9 for the WD40 WT and 12 for the empty vector. Clones homogeneously expressing high levels of both mCherry and GFP+ positive cells were selected. Overall, it was possible to identify 3 clones for the WD40 A1025R construct, 1 clone for the WD40 WT construct, 7 clones for the empty vector. The expression of the expected fusion proteins was also confirmed by Western blotting (Figure 3.20F).

Clones expressing WD40 constructs showed a band around 87 kDa, and clones expressing the empty vector showed a band at 48 kDa. In all cases, degraded protein products, detected as lower bands, were also observed. For each cell line, one clone was selected for further experiments. Clones with similar levels of GFP/mCherry co-expression were chosen in order to obtain comparable results. Clone 3 was selected for WD40 A1025R and clone 9 was selected for tetR-mCherry, where co-expression of GFP/mCherry was detectable in 91.0% and 90.6% of cells respectively (Figure 3.20B-C-E). Among 9 clones harboring WD40 WT, clone 2 showed the highest percentage of GFP/mCherry co-expression (87.4%). This clone, therefore, was used for further experiments (Figure 3.20D).

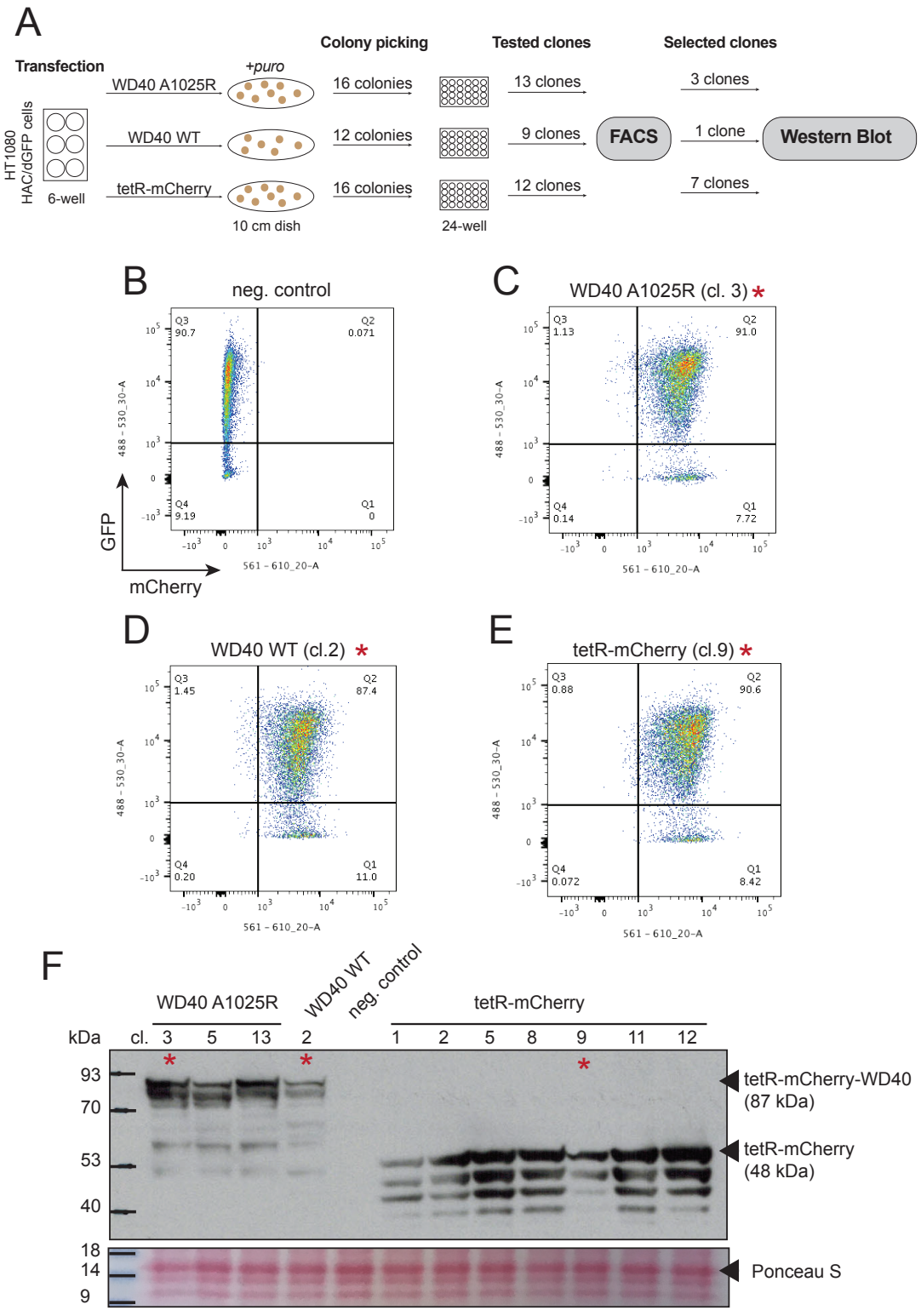


Figure 3.20: **Generation of HT1080 HAC-dGFP cells expressing WD40 constructs.** (**A**) Schematic representation of the protocol for the generation of clonal cell lines. Clones used for further experiments (red asterisks) were tested by FACS and Western Blot. (**B-C-D-E**) FACS analysis of selected clones. (**F**) Western blot of the selected clones. tetR-mCherry constructs were detected with antibody against mCherry. Ponceau S was used as a loading control.

In parallel, HT1080 HAC-dGFP cell lines harboring BRC4 constructs were generated by Davide Torre, a Master's student who joined the laboratory of Dr. Fumiko Esashi for a ten-month internship. Davide contributed to this project under my supervision, most notably in generating the BRC4 cell lines, validating the clones and conducting the HAC loss assay. Since a very limited number of clones were obtained for the WD40 WT construct using the "colony picking" method, single cell sorting of the GFP/mCherry positive cells was used to improve the chances of getting positive clones that express BRC4-fusion (Figure 3.21A). After transfection, GFP/mCherry positive cells were sorted in 96-well plates in selective media. Then, colonies were expanded and tested by flow cytometry (Figure 3.21B-C) and Western blotting (Figure 3.21D). Overall, 12 clones for the BRC4 WT construct and 22 clones for the BRC4-M5 construct were obtained. One clone from each cell line with a high level of GFP/mCherry co-expression was selected for further experiments. Clone 10 was selected for BRC4 WT and clone 3 for BRC4-M5, co-expressing 96.9% and 96.5% GFP/mCherry cells respectively (Figure 3.21B-C). The multiple lower bands observed on the Western blot were partially due to protein degradation following freezing of the cell pellet; indeed, when cells were processed without freezing most of the bands disappeared. However, one lower band was still observed. To assess whether this band was a result of endogenous protein degradation, cells were treated with a proteasome inhibitor (MG-132) at different times of incubation and concentrations. However, the lower band was still present even at high concentrations of MG-132 and long time of incubations (Figure 3.21E). Therefore, it is possible that these constructs either generate a second transcript or part of the protein is rapidly cleaved after synthesis.

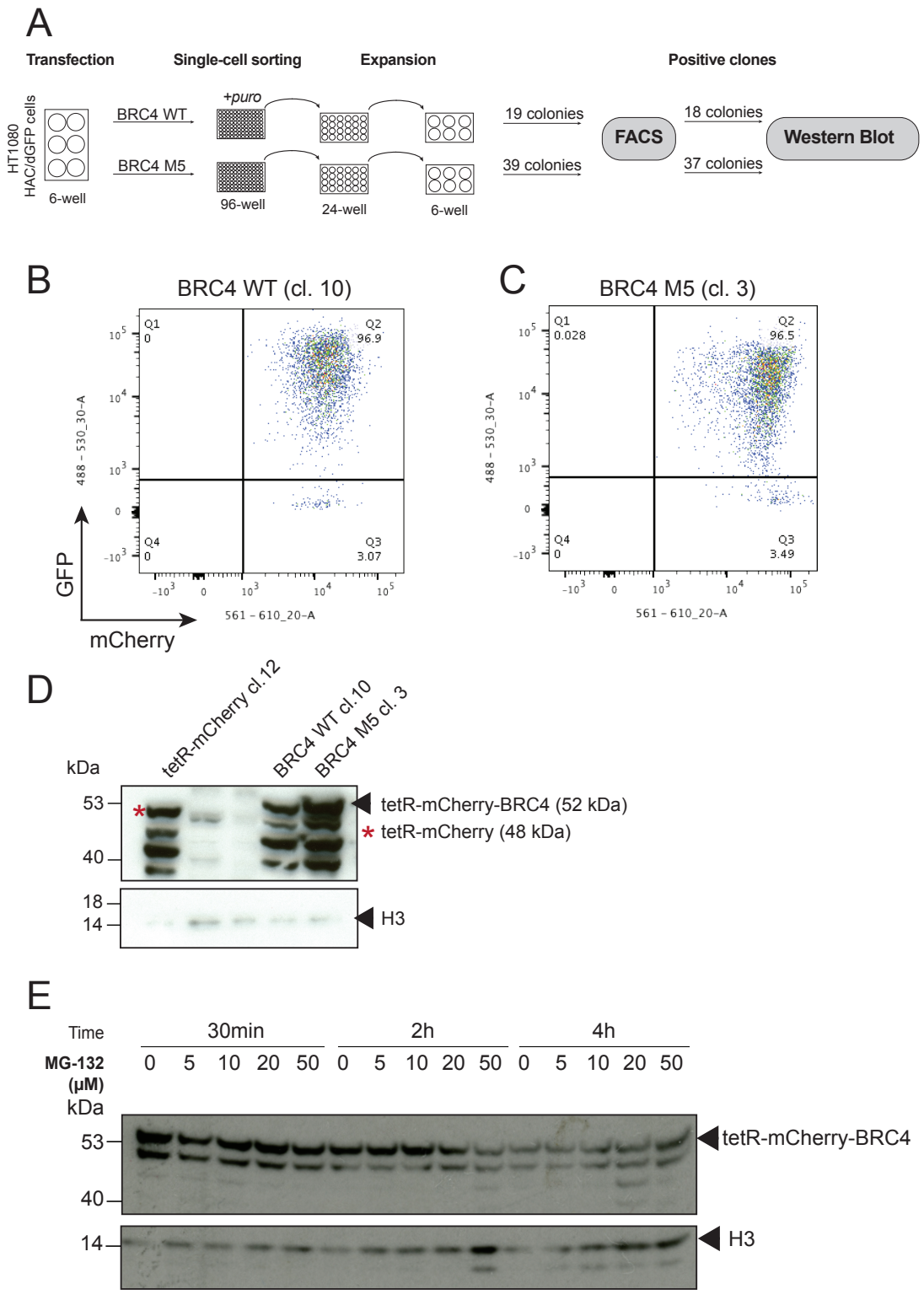


Figure 3.21: **Generation of HT1080 HAC-dGFP cells expressing BRC4 constructs.** (**A**) Schematic representation of the protocol for the generation of the clonal cell lines. Clones used for further experiments were tested by FACS and Western blot. (**B-C**) FACS analysis of selected clones. (**D**) Western blot of the selected clones. (**E**) Western blot with tetR-mCherry-BRC4 expressing cells. Proteasome inhibitor (MG-132) was added at different concentrations and times of incubation. tetR-mCherry construct was detected with an antibody against mCherry. Experiments in B,C,D,E were performed by Davide Torre.

3.2.3.2 Validation of the tetR-mCherry constructs

The interaction between the WD40 construct and endogenous BRCA2 was then tested by Western blot after mCherry pull-down in WD40-expressing cells (Figure 3.22). mCherry pull-down was performed using RFP-Trap and its interaction with BRCA2 was detected using BRCA2 antibody. As expected, tetR-mCherry WD40 WT showed a strong interaction with BRCA2. Conversely, BRCA2 interaction was not detectable with tetR-mCherry and tetR-mCherry-WD40 A1025R constructs. Similarly, the interaction between BRC4 construct and endogenous RAD51 was tested in the BRC4-expressing cells (Figure 3.23). The interaction with RAD51 was detected using RAD51 antibody. Again, as expected, tetR-mCherry BRC4 WT showed a strong interaction with RAD51, whereas tetR-mCherry BRC4-M5 showed a weak interaction with RAD51.

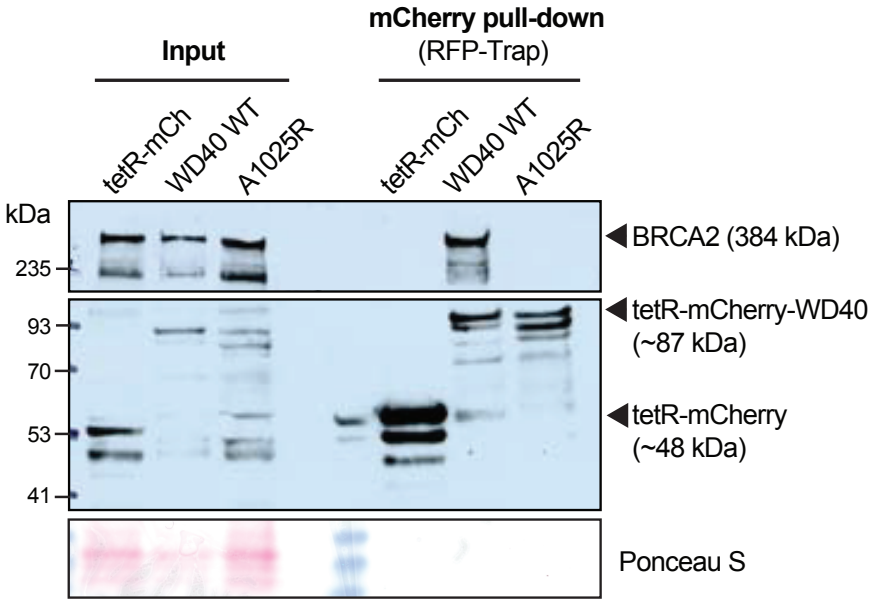


Figure 3.22: **BRCA2 binding to tetR-mCherry-WD40 constructs.** mCherry pull down using RFP-Trap. tetR-mCherry constructs were detected using mCherry antibody. Experiment was performed by Davide Torre.

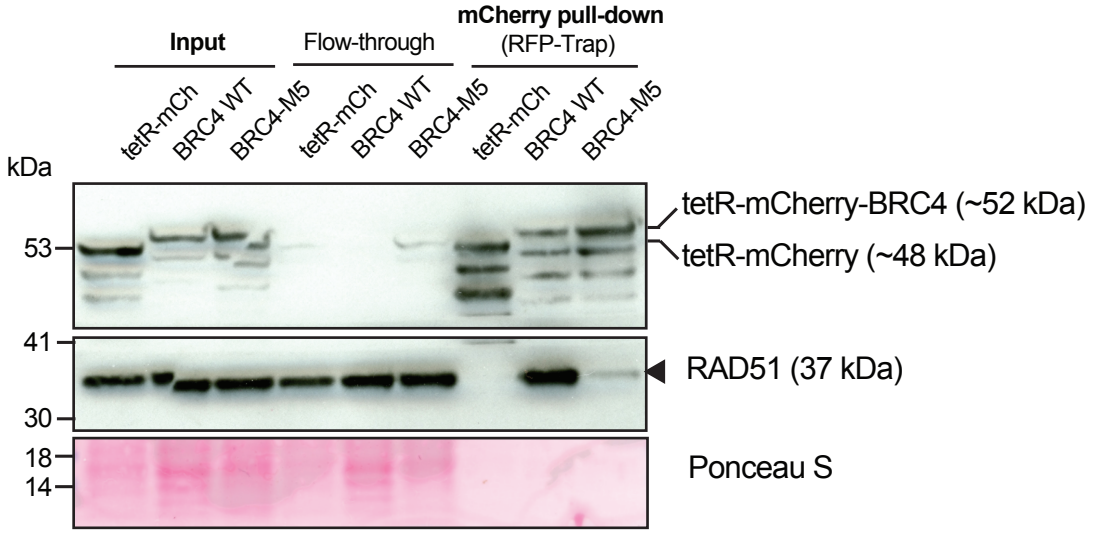


Figure 3.23: **RAD51 binding to tetR-mCherry-BRC4 constructs.** mCherry pull down using RFP-Trap. tetR-mCherry constructs were detected using mCherry antibody. Experiment was performed by Davide Torre.

To test whether the tetR-constructs were indeed tethered to the HAC, the enrichment of the mCherry signal at the HAC was examined by live cell imaging upon doxycycline removal. Of note, during the generation of the cell lines, cells were maintained in medium containing doxycycline (DOX) to prevent the tetR binding to the tetO-HAC. Removal of DOX from the medium would allow the binding of tetR to tetO sequence, hence the localisation of tetR-fusion constructs at the HAC (Figure 3.24A-B). Two representative clones were tested for the localisation of the tetR-mCherry construct: the empty vector (tetR-mCherry cl.9) (Figure 3.24C) and tetR-mCherry-BRC4 WT cl.10 (Figure 3.24D). Cells were grown for 96 h in presence or absence of DOX. Cells grown in DOX (1μg/ml) showed diffused mCherry signal inside the nucleus. When DOX was removed from the medium, the mCherry signal was enriched at the HAC. Some cells showed two dots in one nucleus, likely due to the HAC mis-segregation.

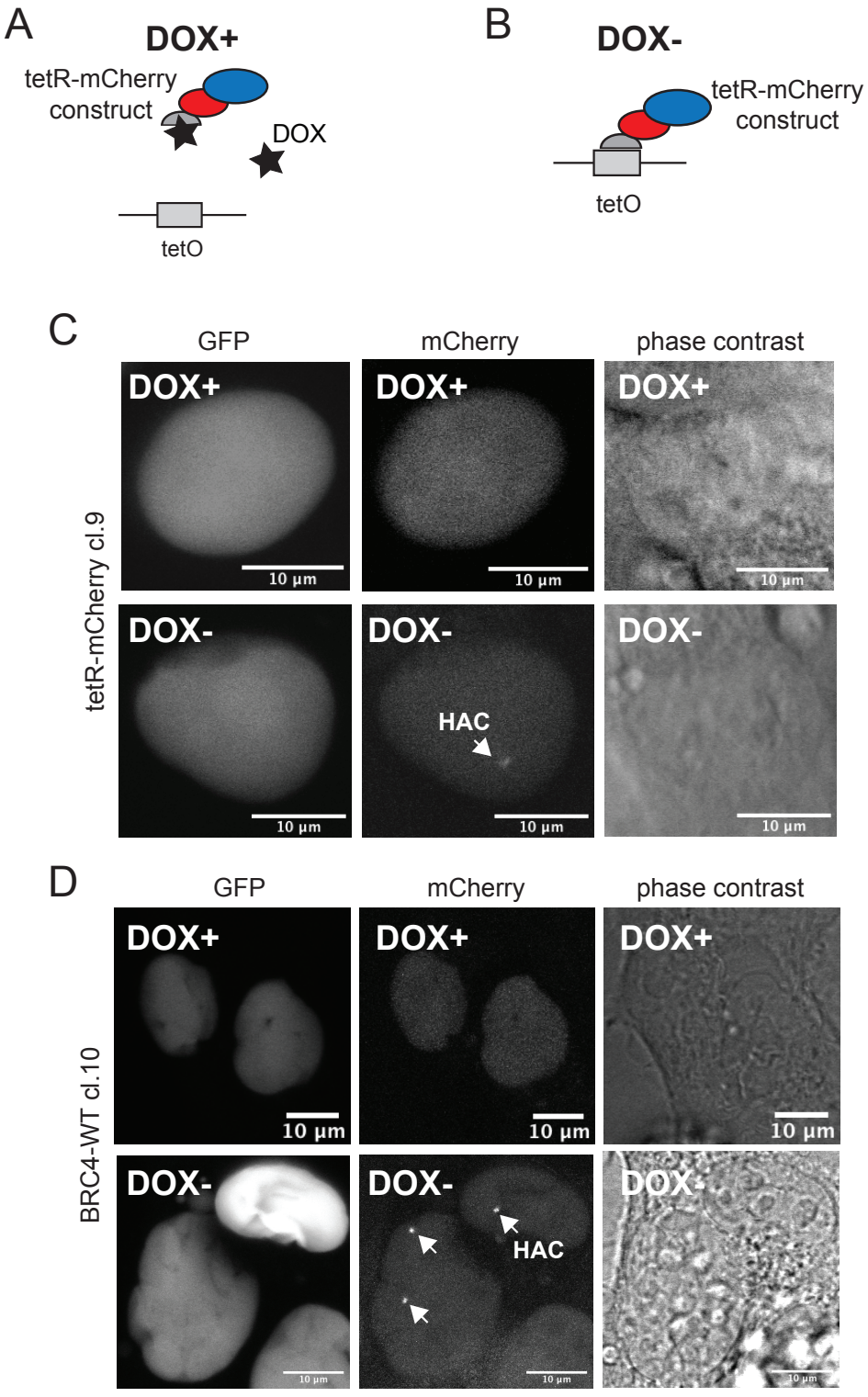


Figure 3.24: **Localisation of tetR-mCherry-constructs to the tetO-HAC upon doxycycline removal**. Schematic representation of the localisation of tetR-mCherry-construct in presence (**A**) and absence of doxycycline (DOX) (**B**) the presence of DOX prevents tetR-tetO binding. (**C**) Live cell imaging of tetR-mCherry cl.9. (**D**) Live cell imaging of tetR-mCherry-BRC4 WT cl.10. Representative image of cells grown 96 h in presence or absence of DOX. Scale bar = 10 μm. Data shown in these figures were generated by Davide Torre.

3.2.3.3 Tethering of the BRC4 wild-type to the HAC increases HAC loss

The effect of BRC4 constructs on HAC stability was tested by the HAC loss assay. The rate of HAC loss was measured 96 h after seeding in presence or absence of DOX (Figure 3.25A). This time point was established in order to combine this assay with the siRNA treatment. To reduce the variability due to cell death, live cells were selected from the single cell population (Figure 3.25A). Then, mCherry-positive cells were gated (Figure 3.25B) and the proportion of GFP positive cells (Figure 3.25C) was measured to calculate the rate of HAC loss.

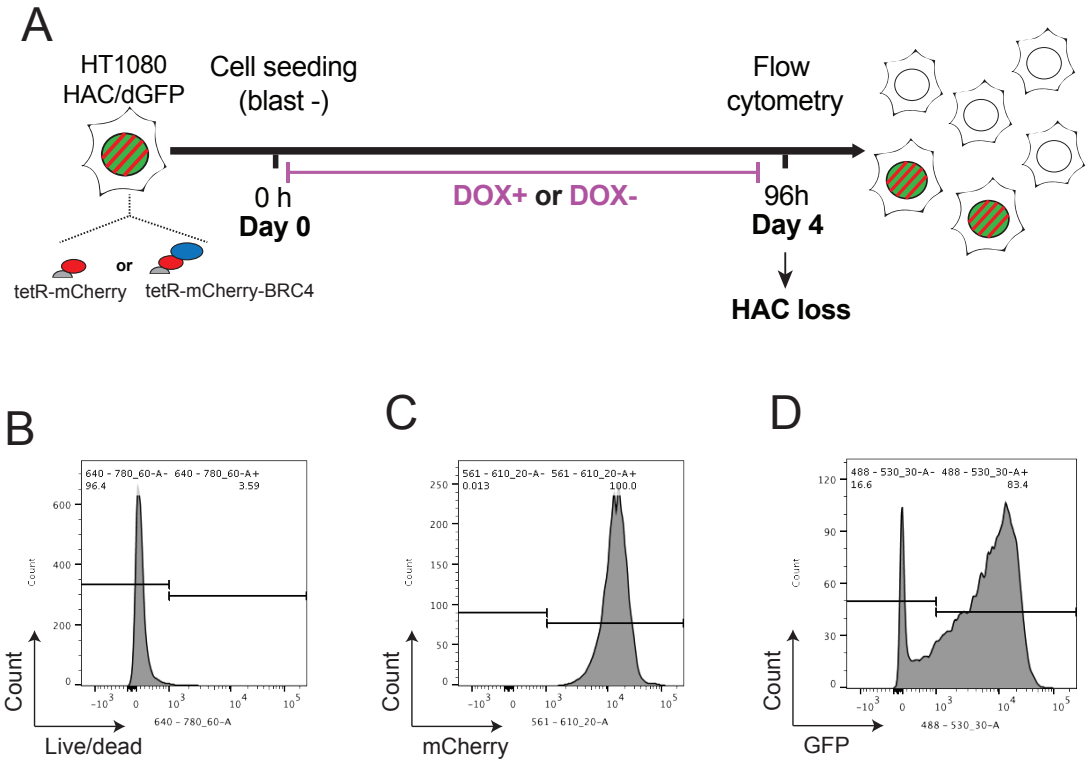


Figure 3.25: **HAC loss analysis with the tetR-mCherry expressing cells**. (**A**) Schematic representation of the protocol of the HAC loss assay with tetR-expressing cell lines. Cells were analysed by flow cytometry at 96 h after seeding. (**B-C-D**) FACS profiles for the analysis of the live mCherry-positive and GFP-positive cells used to calculate the HAC loss. Data shown in this figure were generated by Davide Torre.

To estimate the number of cell divisions, the doubling time of each cell line was calculated from the growth curves (Figure 3.26A-B). Cells were grown for 96 h in presence or absence of DOX and an exponential growth curve was fitted with the data (Figure 3.26C-H). Up to 48 h, a slight reduction in the number of cells was detectable, potentially due to initial cell death after plating. Therefore, I decided to fit the exponential curves from 48 h, when the cellular growth starts to be exponential. After linearisation, the curves were fitted to the data and the doubling time was calculated as described in section 2.6.4. The values of the doubling time were used to calculate the number of cell divisions at 96 h (Table 3.1).

Samples	Doubling Time		Cell divisions at 96 h	
	DOX+	DOX-	DOX+	DOX-
tetR-mCherry cl.9	19.55	24.3	4.9	4.0
tetR-mCherry-BRC4 WT cl.10	15.06	20.76	6.4	4.6
tetR-mCherry-BRC4 M5 cl.3	16.46	15.99	5.8	6

Table 3.1: Doubling times of tetR-mCherry BRC4 constructs in presence (+) and absence (-) of doxycycline (DOX). Doubling times and number of cell divisions were calculated as described in section 2.6.4.

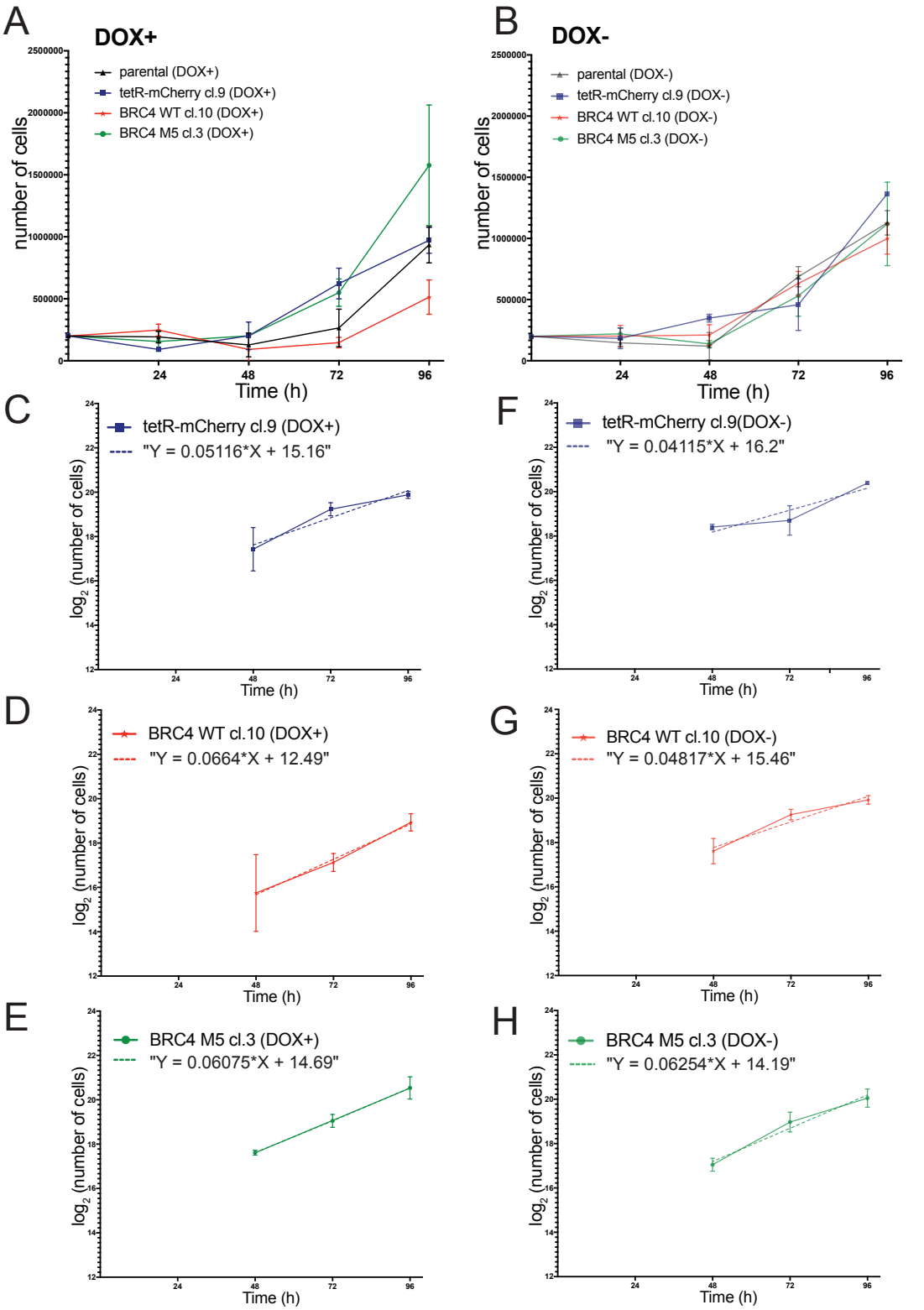


Figure 3.26: **Growth curves of HT1080 HAC-dGFP cells expressing tetR-mCherry-BRC4 constructs**. tetR-mCherry-BRC4 constructs in presence (**A**) and absence (**B**) of DOX (1μg/ml). (**C-H**) Exponential growth curves fitted to the data for each cell line and condition (dashed line, fitted curve). The equations of the fitted curves are written on the graphs. Error bars represent the SD of three technical counts in a single experiment. Data shown in this figure were generated in collaboration with Davide Torre: DT performed the experiment, LR performed the data analysis.

To assess the effect of the tethering of the construct on HAC stability, the rate of HAC loss in the absence of DOX was normalised against the level of HAC loss in the presence of DOX: a rate of HAC loss higher than 1 means that the tethering of the construct to the HAC increased the HAC loss, a rate of HAC loss below one means that the tethering of the construct decreased the HAC loss. If equal to 1, the tethering of the construct did not affect the HAC stability. The tethering of the tetR-mCherry and tetR-BRC4-M5 showed a rate of HAC loss around 1, suggesting that tethering the empty vector and BRC4-M5 did not affect HAC loss. By contrast, cells expressing the tethered BRC4-WT showed a rate of HAC loss higher than 1 and consistently increased the rate of HAC loss compared to the empty vector in three independent experiments (Figure 3.27). This result suggested that the tethering of BRC4 WT impaired the HAC stability.

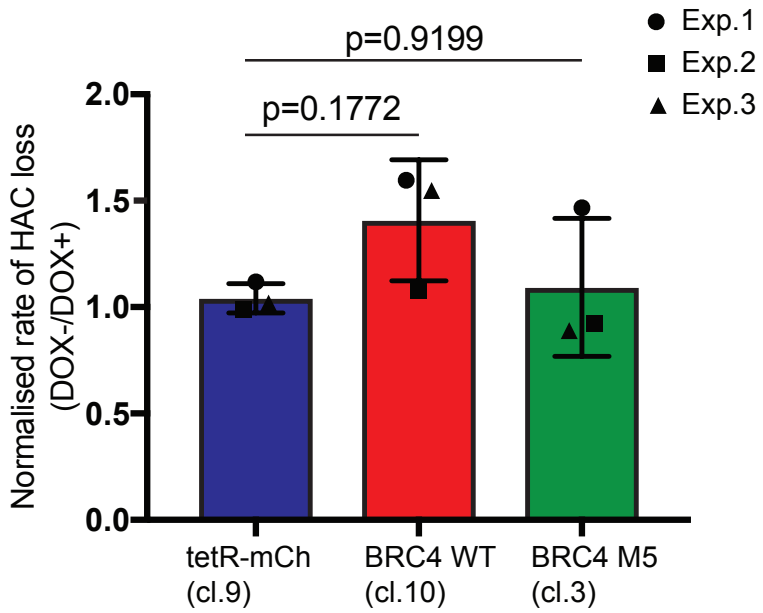


Figure 3.27: **Analysis of the HAC loss at 96 h after seeding**. Effect of tetR-BRC4 construct on the HAC stability. Rate of HAC loss in DOX-free medium was normalised against the value of HAC loss in DOX+ medium. Error bars represent SD of three independent experiments. p-values were calculated using RM one-way ANOVA with *post hoc* Dunnet. Data shown in this figure were generated by Davide Torre.

Preliminary experiments were also performed to assess the effect of tethering the WD40 construct on the HAC stability. The number of cell divisions was calculated using the doubling times calculated from the respective growth curves in the presence and absence of DOX (Figure 3.28A-B). As previously described, exponential growth curves were fitted from 48 h, when cells start to grow (Figure 3.28C-F). The values of the doubling times were used to calculate the number of cell divisions at 96 h (Table 3.2).

Samples	Doubling Time		Cell divisions at 96 h	
	DOX+	DOX-	DOX+	DOX-
tetR-mCherry WD40 cl. 2	19.88	24.5	4.8	3.9
tetR-mCherry-WD40 A1025R cl.3	51.45	24	1.9	4

Table 3.2: Doubling times of tetR-mCherry WD40 constructs in presence (+) and absence (-) of doxycycline (DOX). Doubling times and number of cells divisions were calculated as described in section 2.6.4.

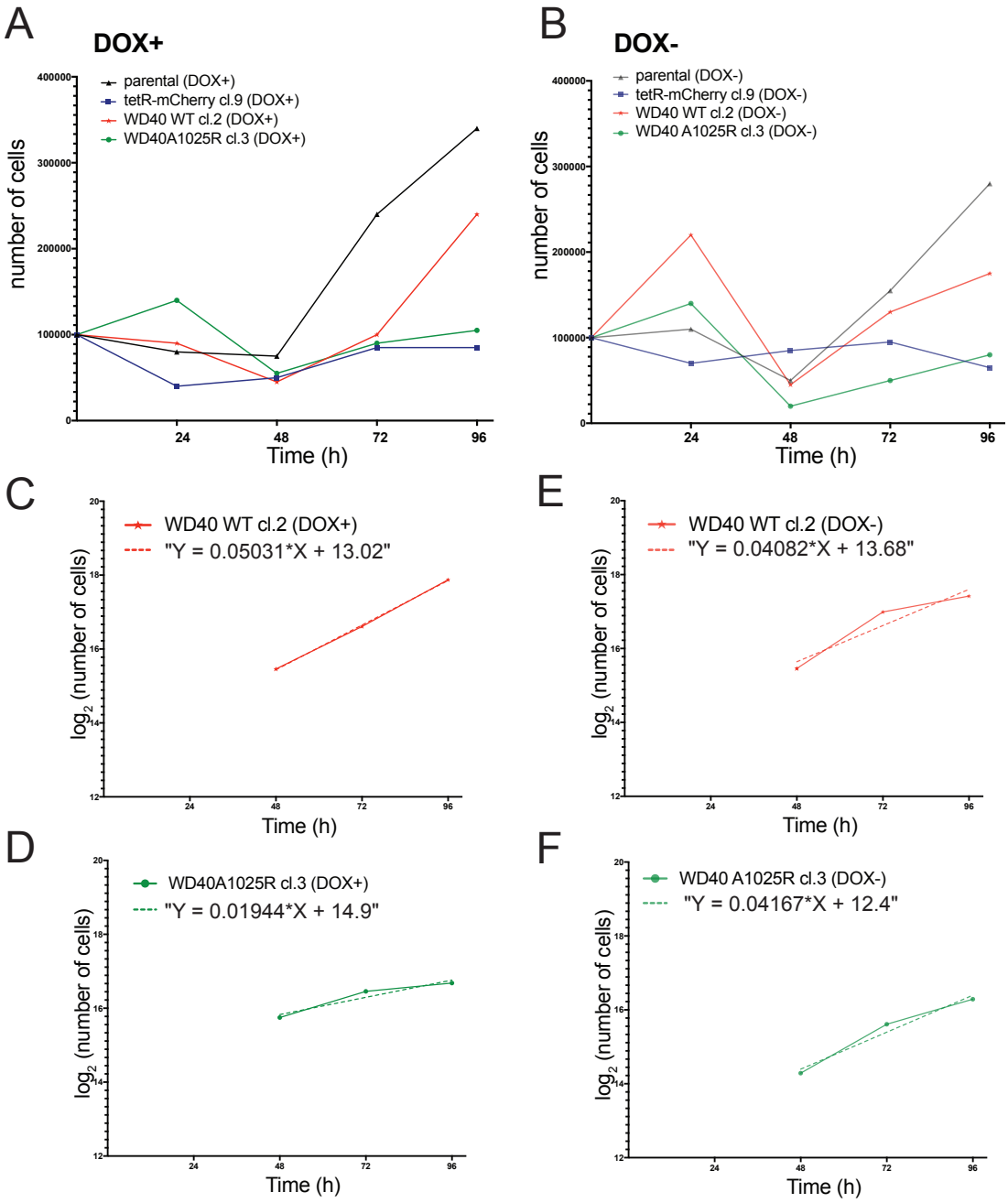


Figure 3.28: **Growth curves of HT1080 HAC-dGFP cells expressing tetR-mCherry-WD40 constructs**. tetR-mCherry-WD40 expressing cells were grown in presence (**A**) and absence (**B**) of DOX ($1\mu g/ml$). (**C-F**) Exponential growth curves fitted on the data for each cell line and condition (dashed line, fitted curve). The equations of the fitted curves were reported on the graphs. Data shown in this figure were generated in collaboration with Davide Torre: DT performed the experiment, LR performed the data analysis.

Preliminary results showed that the tethering of WD40 WT to the HAC did not change the HAC stability compared to the negative control, whereas the tethering of the WD40 A1025R showed reduced level of HAC loss compared to the negative control (Figure 3.29), suggesting that tethering this construct may facilitate the HAC maintenance independently of BRCA2.

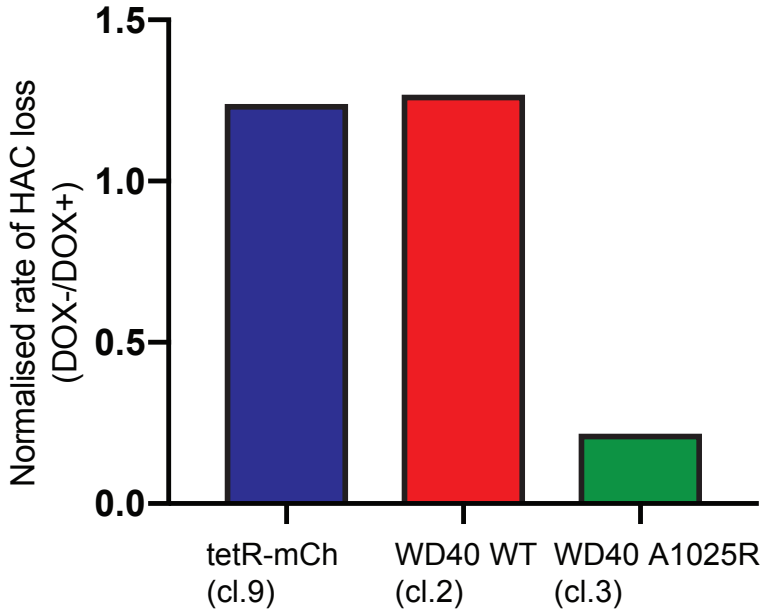


Figure 3.29: **Analysis of the HAC loss at 96 h after seeding**. Effect of tetR-WD40 construct on the HAC stability. Rate of HAC loss in DOX-free medium was normalised against the value of HAC loss in DOX+ medium. A single experiment was performed. Data shown in this figure were generated by Davide Torre.

3.3 Discussion

In this chapter, I investigated the effect of HR proteins, BRCA2, PALB2 and RAD51, on chromosome stability using the alphoid^{tetO} HAC as a model system. The reasons for using this system were to have a model to investigate the function of HR factors at centromeres and, at the same time, to link their effect at centromeres with a powerful quantitative assay to assess chromosomal instability.

3.3.1 Effect of replication stress and B02 treatment on the HAC stability using the alphoid^{tetO} EGFP-HAC

Initial experiments with the alphoid^{tetO} EGFP-HAC showed that replication stress induced by aphidicolin (APH) and hydroxyurea (HU) increased HAC loss; however, no effect was observed upon the inhibition of RAD51 with B02 treatment, suggesting that RAD51 may not be important for HAC maintenance in undamaged conditions. Unexpectedly, B02 treatment in combination with HU showed a reduced level of HAC loss compared to HU treatment alone, suggesting that the inhibition of RAD51 may rescue the HAC stability upon DNA damage. One possible interpretation of these results is that DNA damage induced by replication stress were repaired by RAD51-mediated recombination. Aberrant recombination events may lead to chromosome rearrangements that are detrimental for centromere stability. In accordance with these results, WST-1 assay with B02 and APH treatments showed increased metabolic activity compared to APH treated cells, as a potential consequence of increased cell survival (Figure 3.2B). However, it is important to note that a previous study reported that multiple myeloma cells were arrested in G1 phase upon 1 h of B02 treatment (10 μM) [241]. Thus, it is possible that cells treated with B02 were arrested in G1 phase before they could incorporate replication stress induced by HU. Therefore, in future, it will be necessary to assess the cell cycle profile and the level of DNA damage upon B02 treatment to understand the effect of RAD51 on the HAC stability. Furthermore, during this set of experiments, cells were treated with drugs for 24 hours and subsequently washed

and grown in drug-free medium to allow cell proliferation. Therefore, even if drug treatment arrested the cell cycle during the first 24 hours, cells were then allowed divide and lose the HAC. Despite all cells were growing, it was noted that B02 treated cells were growing slightly slower compared to APH and HU treated cells (but not taxol treated cells) after drug release. Thus, it is possible that B02 treated cells grew slower leading to underestimate the HAC loss. Even if this effect could have a mild consequence on the HAC loss (taxol-treated grew slower than B02 treated cells but they showed increased HAC loss), more traditional methods, such as clonogenic survival assay, could be used in the future to assess the ability of the cells to divide upon B02, HU and APH treatments.

3.3.2 Technical considerations affecting the HAC loss assay

Due to the long half-life of the EGFP protein, the alphoid^{tetO} EGFP-HAC does not allow to study the effect of short-term treatments on the HAC stability. To study the effect of the HR proteins on HAC stability, I made used of the alphoid^{tetO} HAC-dGFP [204]. The HAC loss analysis developed with this system was used in combination with siRNA treatments for the depletion of the HR proteins. The effect of HR protein depletion on HAC loss was relatively small compared to the negative control, and statistically significant differences were not always detectable with three independent experiments. Therefore, the interpretation of the results was based on trends that were consistently observed across different experiments, suggesting that the results were reproducible, and also using different methods, such as FACS and FISH. During the course of the analyses, I noticed that several factors could affect the results of the HAC loss assay:

• **Cell toxicity**. Depletion of certain proteins, such as RAD51 and BRCA2, can be toxic and lead to increased cell death. This reduces the fraction of GFP+/live cells (Q1) in the total cell population (Q1+Q2+Q3+Q4) that is used to calculate the rate of HAC loss (Figure 3.30A). However, because the GFP signal may not be detectable after cell death,

it is not possible to determine if cells die with or without the HAC, leading to an overestimation of HAC loss. This notion was suggested by the observation that samples with increased cell death showed an increase of cells in the GFP-/dead quadrant (Q3). When the fraction of GFP+/live cells (Q1) was assessed in the live cell population only (Q1+Q4) (Figures 3.15 and 3.18), the fraction of cells that die together with HAC loss would not be taken account, resulting in an underestimation of HAC loss. Such an underestimation could indeed occur when cells lose the HAC as well as endogenous chromosomes, leading to a high rate of cell death, as was observed upon double siRNA treatment or a combined treatment of siRNA and APH. To circumvent this problem, FISH analysis was performed to further validate the results (Figure 3.10B). However, this method is laborious and time consuming; it requires the acquisition of large number of data to validate small variations on the HAC loss. Therefore, in future, I propose to assess the HAC loss using the pipeline as represented in Figure A.1. Briefly, initially calculate the HAC loss in the whole cell population including live and dead cells (Q1+Q2+Q3+Q4) (Figure 3.30B.i); if an increase in the cell toxicity is observed (Q2+Q3), the rate of HAC loss should be calculated in the live cell population only (Q1+Q4) (Figure 3.30B.ii). If an increase in HAC loss rate is observed under the this condition, it can be concluded as ”real HAC loss”; even if not, however, it is still possible that the dead cells have lost the HAC. To confirm the result, FISH analysis should be ultimately performed (Figure 3.30B.iii).

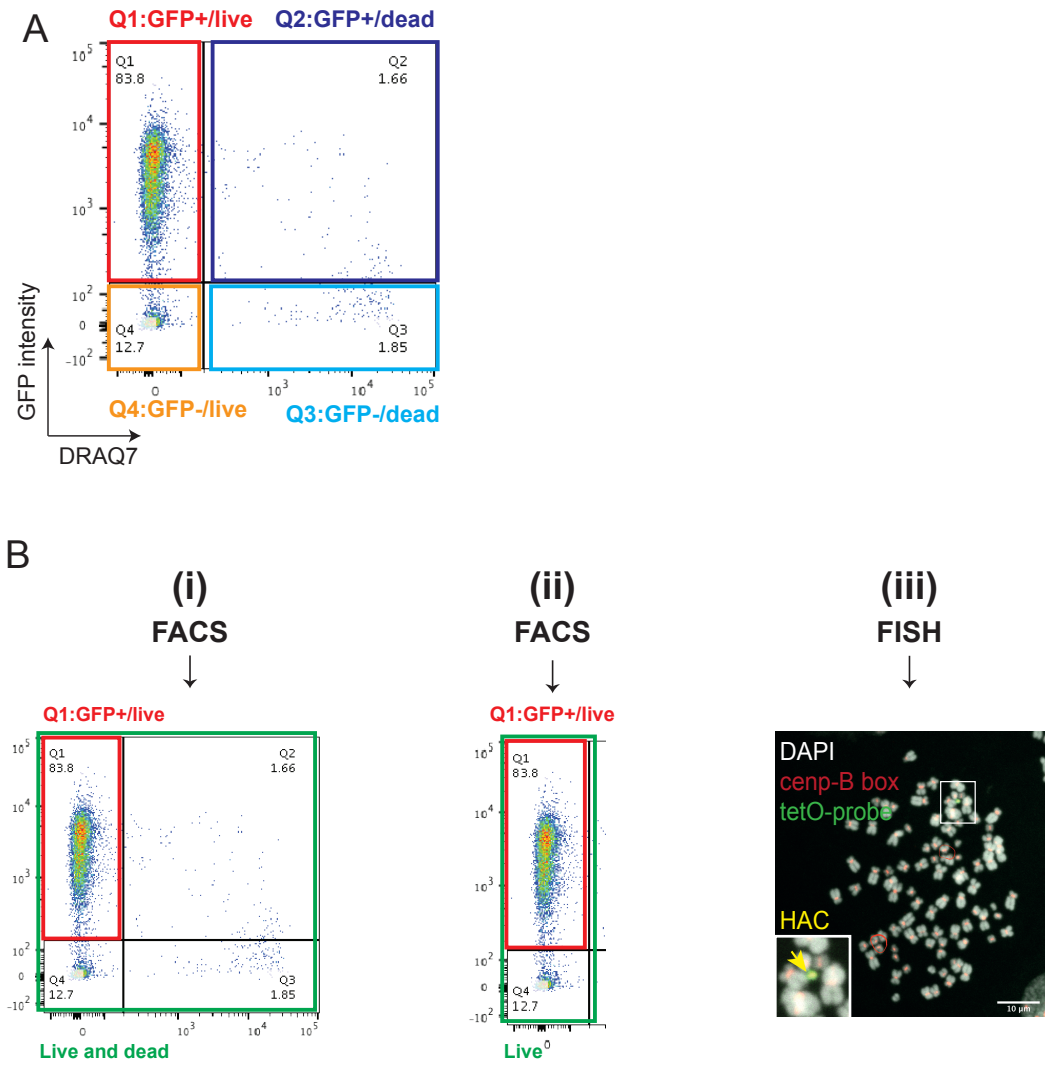


Figure 3.30: **Diagram for the HAC loss analysis.** (**A**) Representative FACS profile of HT1080 HAC-dGFP cells. (**B**) Workflow for the HAC loss analysis.

• **Cell cycle arrest**. Depletion of DNA repair factors and genotoxic stress can activate cell cycle checkpoints. This leads to the accumulation of cells in different stages of the cell cycle and a slow down of cell proliferation. The accumulation of cells in G1-S-G2-early M phase increases the fraction of cells with GFP signal, while the accumulation of cells in late M phase decreases the fraction of cells with GFP signal. For instance, the RAD51 depletion showed increased cells in S/G2 phase, which in turn increased the proportion of GFP+ cells compared to the control cells; whereas BRCA2 depletion showed increased cells in M phase, which could potentially explain the decrease of the

fraction of GFP+ cells compared to the control cells. However, microscopy analyses of BRCA2 depleted cells revealed that these cells were mostly arrested in the early stages of mitosis, when the fluorescent signal is still present. Therefore, the HAC loss in BRCA2 depleted cells was likely to be real chromosome loss and not a consequence of the loss of GFP signal in late mitosis. Furthermore, another consequence of the cell cycle checkpoint activation is slower cell proliferation. When cells undergo fewer cell divisions compared to the negative control, they have less chance to lose the HAC leading to an underestimation of the rate of HAC loss. To solve this problem, a cell proliferation assay was introduced to measure the number of cell divisions.

• **Transfection efficiency and protein depletion**. The level of HAC loss can be also affected by the transfection efficiency of each experiment. To check the efficiency of the transfection, a siRNA targeting GFP was initially used (Figure 3.7). However, high cell toxicity was observed with siGFP. Thus, it was possible that the reduced level of GFP+ cells was partially caused by the cell toxicity. In future, a less toxic siRNA could be designed to accurately assess the transfection efficiency.

3.3.3 BRCA2 depletion increases HAC loss in a HR independent manner in unperturbed cells

The results presented in this chapter showed that depletion of BRCA2 slightly increased HAC loss. Despite the results were not significant (p=0.0675), the trends were consistently observed in different experiments and with different methods (i.e. FACS and FISH), supporting the reproducibility of the result. Based on these observations, I suggest that BRCA2 plays a role to preserve chromosome transmission. Furthermore, the HAC is made from centromeric DNA, thus it is plausible that BRCA2 exerts a function at centromeric regions which is important for their maintenance. However, it is still not clear whether its function is important for the segregation or the replication of the HAC. To understand whether depletion of BRCA2 affects the replication of the HAC, I looked at the number of HACs on the metaphase spread with the fol-

lowing notion: one single HAC dot suggested that the HAC is not replicated, two paired HAC dots suggested that the HAC is fully replicated. However, because the HAC is made by centromeric DNA, which was highly condensed and likely tethered tightly by cohesin during mitosis, it was not possible to clearly distinguish between one or two dots. To assess the level of replication of the HAC upon BRCA2 depletion, real-time PCR of nascent DNA could be performed in future [247]. Moreover, depletion of BRCA2 arrested cells in early mitosis, suggesting that BRCA2 is important to complete this phase of the cell cycle. If BRCA2 is involved in the SAC activation, as has been proposed by Choi et al. [116], the depletion of BRCA2 would lead to a premature anaphase entry, hence faster mitotic progression. However, this was not the case. Thus, I excluded the possibility that the HAC loss was due to a BRCA2 function in the SAC activation. On the other hand, prolonged mitosis may be caused by difficulties in the microtubule-kinetochore attachment, misaligned chromosomes and/or under-replication at centromeres, which need to be addressed before anaphase onset. It is possible that BRCA2 at centromeres may be important for the establishment of kinetochore components through its interaction with the kinetochore components or to ensure the complete replication of the centromeric region.

The combined depletion of PALB2 and BRCA2 showed increased HAC loss compared to BRCA2 or PALB2 depletion alone, suggesting that these two proteins may act on separate pathways. Similarly, BRCA2 and RAD51 depletion showed a small but consistent increase in HAC loss compared to single BRCA2 depletion, supporting the hypothesis that BRCA2 may act on a separate pathway independent of the other HR proteins. The difference between the effect with siBRCA2-siPALB2 and siBRCA2-siRAD51 can be due to a different level of toxicity between these two treatments. It is possible that the HAC loss in the BRCA2-RAD51 siRNA treated cells was underestimated and some of the dead cells had lost the HAC. Moreover, slower cellular growth was observed in siBRCA2-siRAD51 treated cells compared to siBRCA2-siPALB2 treated cells; therefore, it is possible that cells were arrested between G1 and G2 phase, which may reduce the level of HAC loss. In future, the use of a checkpoint inhibitor could be used to force the cells to move into mitosis to assess the effect of siBRCA2-siRAD51

treatment on the HAC maintenance.

Upon APH treatment, depletion of BRCA2 and RAD51 showed an increase in HAC loss, suggesting that both proteins are important for the HAC maintenance under mild replication stress. 0.4 μM APH has been shown to increase the level of DSBs at centromeres [214]. Thus, it is possible that BRCA2 and RAD51 at centromeres mediate an HDR mechanism to repair DSBs. However, their role in the fork protection can not be excluded. The HAC loss assay highlighted the importance of HR only under replicative stress; the single depletion of RAD51 recombinase did not show increased HAC loss under unstressed conditions. Conversely, the results of flow cytometry and FISH analysis showed that RAD51 depletion decreased HAC loss (Figure 3.10). However, the interpretation of the effect of RAD51 on HAC stability needs caution because RAD51 depletion had a dual effect: (1) enrichment of cells in S/G2, which apparently reduces the HAC loss, and (2) increased cell toxicity, but the level of HAC loss in dead cells can not be measured by flow cytometry. However, a single FISH experiment showed that depletion of RAD51 reduced the number of cells without HAC. While this result could support the notion that RAD51 may have a harmful function for the HAC maintenance, it is also possible that RAD51 depleted cells went through fewer cell divisions and had less chance to lose the HAC. If the decreased HAC loss upon RAD51 depletion was caused only by the cell cycle arrest, a similar effect should be obtained with APH treatment, which arrests the cells in S/G2 phase. But this was not the case. Overall, I cannot completely exclude the possibility that RAD51 may have a detrimental function at centromeres in undamaged conditions. Future experiments using FISH analysis with a G2/M checkpoint inhibitor, which forces the cells to enter into mitosis could help in the interpretation of these results.

3.3.4 The effect of the tetR-mCherry expressing cell line on the HAC stability

To further study the function of BRCA2 on HAC stability, cell lines expressing tetR-mCherry constructs fused with the BRC4 and WD40 domains were generated. The WT forms of the constructs showed interactions with RAD51 and BRCA2 respectively, showing that these constructs were able to recruit these proteins at the HAC. At the same time, tetR-mCherry enrichment to the HAC was detectable upon DOX removal, confirming that the tetR-constructs could be artificially tethered to the HAC.

During the generation of the cell lines, 7 clones were generated for the empty vector, 3 for the WD40 A1025R and only one clone for the WD40 WT. WD40 WT cl.2 was the only clone out of 9 clones showing high expression of the mCherry-construct in an homogeneous population. Thus, it is possible that over-expression of WD40 WT is toxic for the cells. However, the WD40 WT cl.2 grew better compared to WD40 A1025R and the empty vector (Figure 3.28). Therefore, it is possible that the WD40 WT cl.2 cells developed secondary mutations, which allowed their survival. Using single cell sorting for the generation of BRC4 cell lines, it was possible to obtain more clones for each cell line. A smaller number of clones was obtained for the BRC4 WT (18) compared to the BRC4 M5 (37), suggesting that BRC WT may be toxic for the cells. Indeed, overexpression of BRC4 WT, but not BRC4 M5, in MCF-7 breast cancer cells has been shown to reduce cellular growth and increase sensitivity to ionising radiation [84].

Tethering of the BRC4 WT to the HAC resulted in increased HAC loss compared to the empty vector, suggesting a detrimental function of the BRC4 construct on HAC stability. BRC4 binds monomeric RAD51 and, through this interaction, assists RAD51 loading onto the ssDNA to form a RAD51 filament that is required to perform the process of strand-invasion during homologous recombination [81] [85] [95] [246] [82]. However, high doses of BRC4 lead to a destabilisation of the RAD51 filament and block the RAD51-mediated recombination activity [87]. Based on these observations, the

tethering of BRC4 WT to the HAC may either lead to the recruitment of RAD51 on the HAC, which could possibly lead to aberrant recombination events at repetitive regions, or a disassembly of RAD51 filaments on the HAC, which might prevent completion of DNA replication. To discriminate between these two hypotheses, the level of RAD51 recruitment to the HAC after the tethering of the tetR-BRC4 WT could be assessed by chromatin immunoprecipitation (ChIP-qPCR). This result may discriminate whether RAD51 has a positive or negative function at centromeres.

Preliminary results conducted with cells expressing tetR-WD40-WT showed no change in the rate of HAC loss compared to the empty vector. One possible interpretation of this result is that endogenous BRCA2 may be already recruited at the HAC to exert its function and its recruitment mediated by the tethering of the tetR-WD40 construct does not change HAC stability. Alternatively, the clone may harbor secondary mutations, which mask the negative impact of BRCA2 tethering on HAC. However, it is also possible that the tethering of WD40 construct improved HAC stability upon replication stress. Unexpectedly, the tethering of WD40 A1025R to the HAC appeared to improve the HAC stability compared to the empty vector in a single experiment. Further repeats need to be done to confirm this observation. WD40 A1025R does not bind BRCA2; however, it may still be able to interact with other DNA repair factors, such as RAD51, RAD51C, XRCC3 [248] [249], which may promote recombination. Moreover, the WD40 domain is one of the most abundant domains in the human proteome and WD40-containing proteins are involved in a wide range of cellular processes, such as cell cycle progression, DNA signalling and repair, chromatin organisation [250]. Therefore, it is also possible that WD40 A1025R, as it is not bound by BRCA2, is able to bind and recruit other factors that have a positive impact on the HAC stability.

All together, the results in this chapter contributed to study the effect of the HR factors at centromeres using the alphoid^{tetO} HAC and link their effect with numerical CIN, i.e., whole-chromosome loss. Using this system it was possible to show that BRCA2 is important for the HAC maintenance and opened up the possibility that BRCA2 plays an HR-independent function at centromeres to support HAC maintenance. Furthermore,

the generation of cell lines expressing tetR-BRC4 constructs showed that the tethering of this BRCA2 fragment is deleterious for the HAC maintenance. The generation of this system could be used in future to further elucidate the function of HR on the HAC stability.

Chapter 4

Investigating the role of BRCA2 at endogenous centromeres

4.1 Introduction

The results in Chapter 3 showed that BRCA2 is required for HAC maintenance (Figure 3.10). This was likely to be independent of its role played with the other HR proteins (i.e., PALB2 and RAD51) in the absence of DNA damage. However, when exposed to replication stress, both BRCA2 and RAD51 appeared to contribute to HAC maintenance. These observations raised the possibility that BRCA2 is important to fine-tune the activity of the HR proteins at centromeres according to the the level of genotoxic stress. During the FISH-based analysis of HAC cells, I also noticed an increase in the number of cells with endogenous centromere breakages upon BRCA2 or PALB2 depletion (Figure 4.1A-B), and that depletion of any HR factors reduced the intensity of FISH probes against endogenous centromeres (Figure 4.1C). These observations suggest that the HR factors are important to prevent centromere rupture and hence their depletion may lead to a shortening of the centromeric repeats.

I additionally noticed that BRCA2 depletion increased the duration of early mitosis in HT1080 HAC-dGFP cells (Figure 3.12). This observation suggested that BRCA2-depleted cells need a longer time before anaphase entry. Notably, a recent study by Feng and Jasin has demonstrated that the level of anaphase bridges and lagging chromosomes was increased upon conditional depletion of BRCA2 in MCF10A cells [117]. These aberrant chromosome structures were predominantly linked with FANCD2 foci, a marker that is often associated with under-replicated regions in mitotic cells, suggesting that anaphase bridges and lagging chromosomes may originate from regions with incomplete replication [117]. A longer G2 phase caused by a short treatment with RO-3306, a CDK1 inhibitor, allowed cells to complete replication and reduced mitotic defects and FANCD2 foci in mitotic cells [117]. Incomplete replication in BRCA2-deficient cells triggered p53 activation in the following G1 phase, leading to G1 arrest, senescence and apoptosis [117]. Finally, they demonstrated that enhanced replication fork protection, enabled by MRE11 depletion, could not restore the normal cell proliferation of BRCA2 deficient cells. Collectively, they suggested that the HR function of BRCA2, rather than its fork protection role, was responsible for the completion of the

replication in S-G2 phase [117]. These observations pose an interesting possibility that at centromeres BRCA2 alleviates replication stress to ensure the completion of DNA replication and promotes successful chromosomal segregation.

In this chapter, I aimed to understand whether the depletion of BRCA2 impaired DNA stability at centromereres. To this end, I assessed whether the depletion of BRCA2 increased the level of DNA damage at centromereres. Remarkably, while doing these experiments, I observed nuclear and chromatin changes upon BRCA2 depletion. Hence, I extended my analysis to understand how such events might affect centromere formation.

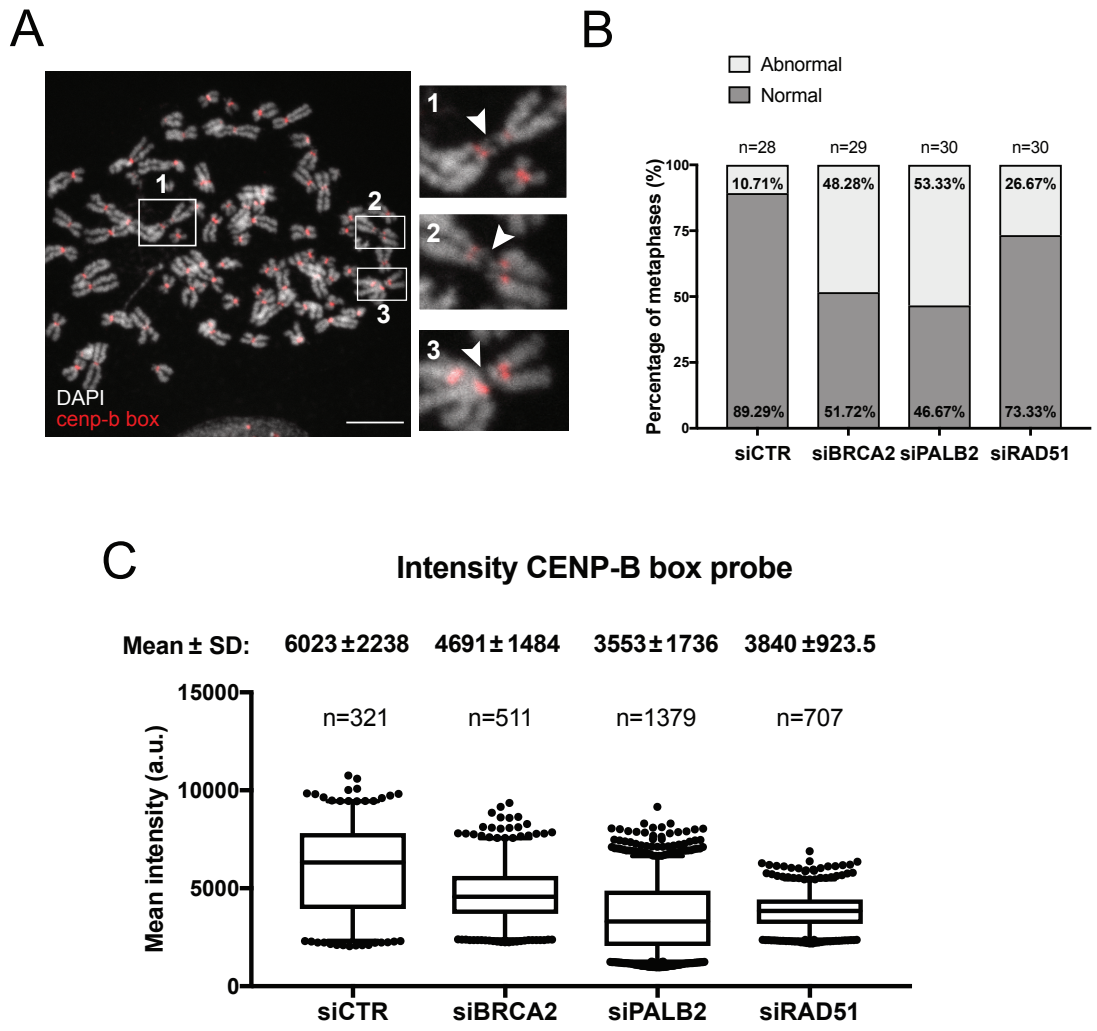


Figure 4.1: **Centromere abnormalities upon HR protein depletion.** (**A**) Fluorescence In-Situ Hybridization (FISH) analysis of HT1080 HAC-dGFP cells.Cells were treated with siRNAs for 72 h. Endogenous centromeres were detected using a CENP-B box probe. Representative picture of abnormal centromeres. Scale bar 10 μm. (**B**) Bar graph represents the percentage of metaphases with at least one abnormal centromere. n represents the number of cells analysed for each condition in a single experiment. (**C**) The intensity of the CENP-B probe at centromeres was measured in 4 cells for siCTR treatment, 6 cells for siBRCA2, 15 cells for siPALB2 and 8 cells for siRAD51 treatment. n represents the number of centromeres analysed for each condition in a single experiment. Mean and SD were reported.

4.2 Results

4.2.1 BRCA2 depletion increases mitotic defects in HeLa cells

Results in section 3.2.2.2 showed that depletion of BRCA2 increased the rate of HAC loss. However, HAC is a small artificial chromosome composed of alphoid repeats and its loss rate is 10-times higher than endogenous chromosomes [203]; thus, the effects observed using this system could be different from endogenous chromosomes. To consolidate the results obtained in Chapter 3, I analysed the mis-segregation of endogenous chromosomes using HeLa cervical cancer cells. These cells are particularly easy to synchronise. Furthermore, the expression of Human Papillomavirus HPV E6 oncogene in HeLa cells leads to p53 degradation [251] [252]; therefore, even in the absence of BRCA2, p53-mediated cell cycle arrest, senescence and apoptosis are not activated. Cells were treated with siRNA, and at 24 h after transfection, they were synchronised using 2 mM thymidine to arrest them in S phase. Subsequently, cells were released into complete medium for 10 hours to enrich mitotic cells (Figure 4.2A). Based on the DNA morphology, cells were classified into three categories: interphase, early mitosis (i.e. prophase and metaphase) and late mitosis (i.e. anaphase and telophase) (Figure 4.2B). BRCA2 depletion increased the number of cells in mitosis with an accumulation in early stages of mitosis. In light of the well-documented function of BRCA2 in DNA repair and replication fork protection in S/G2 phase, this observation was unexpected (Figure 4.2B). In contrast, this result suggested that BRCA2 could be particularly important during early mitosis.

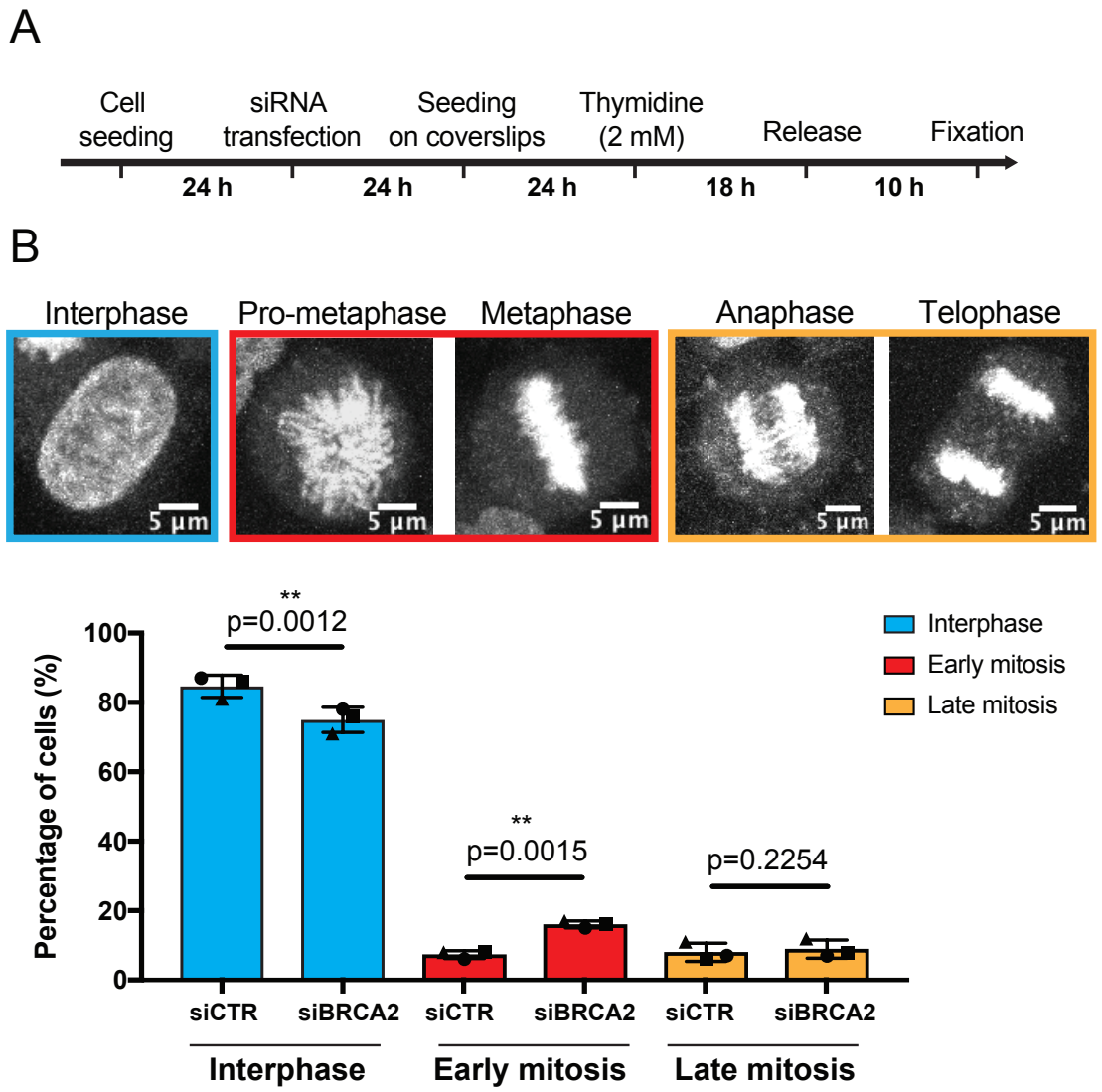


Figure 4.2: **Mitotic index upon BRCA2 depletion in HeLa cells**. (**A**) HeLa Kyoto NFLAP-BRCA2 cells were fixed after siRNA treatment and thymidine block and release. Cells were fixed and stained with DAPI. (**B**) Representative figures of cells in different stages of the cell cycle. Column graph represents the percentage of cells in different stages of the cell cycle after transfection with a non-targeting siRNA (siCTR) and siRNA against BRCA2. About 300 cells were analysed for each condition in each experiment. Mean and SD of three independent experiments. p-values were calculated using paired two-tailed Student t-test.

BRCA2 depletion also led to an increase in the number of cells with late mitotic defects, such as anaphase bridges and lagging chromosomes, compared to control cells (Figure 4.3A). Among different anaphase defects, BRCA2-depleted cells exhibited a modest increase in the number of lagging chromosomes and a more striking increase in the

number of lagging chromosomes compared to untreated cells in a single experiment (Figure 4.3A). In order to assess whether anaphase bridges and lagging chromosomes involved centromeres, anaphase cells were stained with a widely used anti-centromere antibody, ACA (Figure 4.3B). BRCA2 depletion increased the formation of anaphase bridges which were marked by a pair of centromeres in a single experiment (Figure 4.3B).

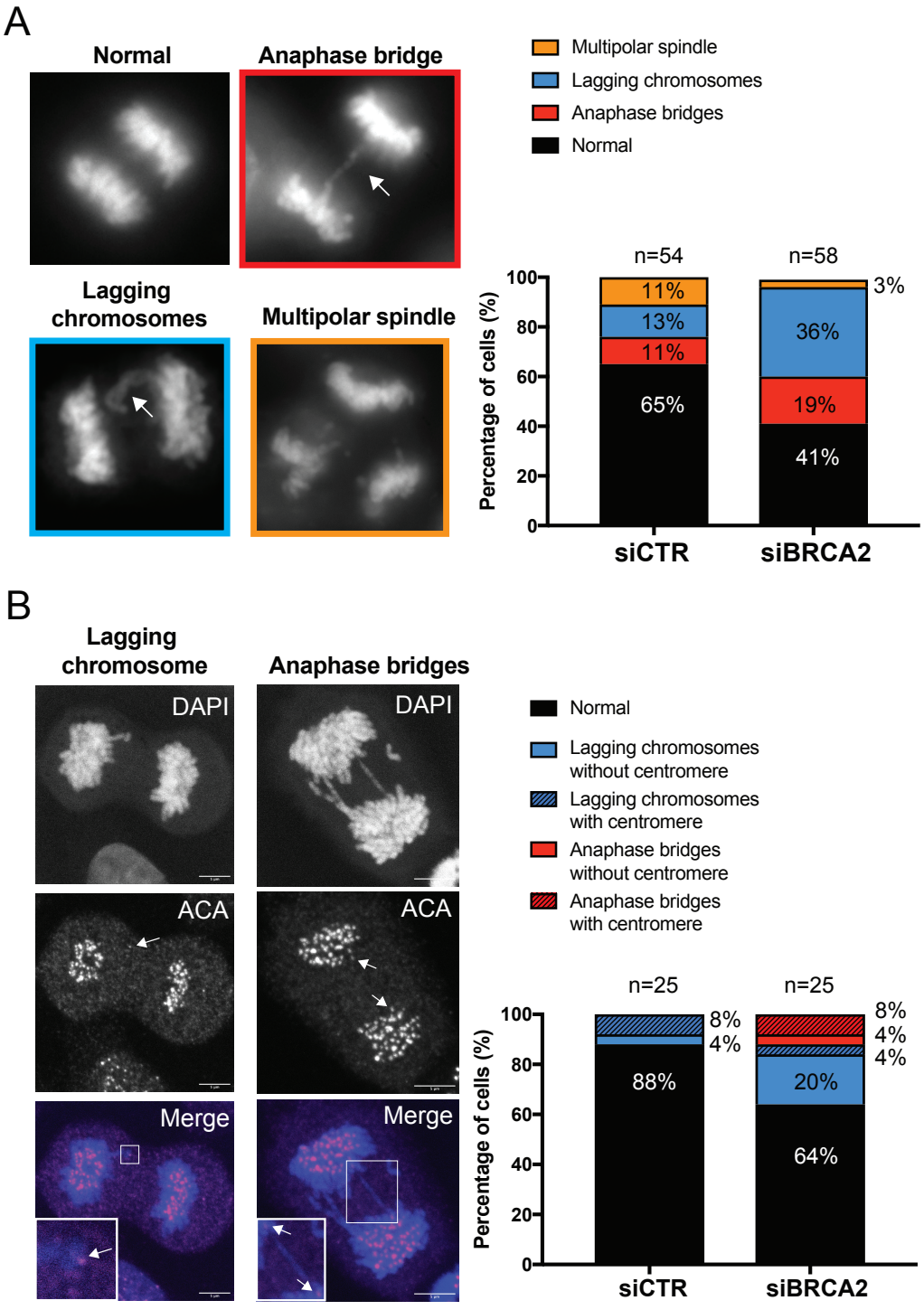


Figure 4.3: **BRCA2 depletion increases mitotic defects**. Cells were treated as described in Figure 4.2A (**A**) Representative images of normal anaphase, anaphase bridges, lagging chromosomes and multipolar spindle. Column graph represents the percentage of mitotic cells in the different categories. n is the number of cells analysed in a single experiment. (**B**) Cells were stained with DAPI and a centromere marker (ACA). Representative images of lagging chromosomes and anaphase bridges with centromeres (white arrow). Column graph represents the number of anaphase cells with normal chromosome segregation, lagging chromosome and anaphase bridges with or without centromeres upon siCTR and siBRCA2 treatment. n is the number of cells analysed for each condition in a single experiment. Scale bar 5 μm.

Chromosome mis-segregation during mitosis can ultimately lead to the formation of micronuclei in interphase cells. Micronuclei can originate from whole-chromosome mis-segregation or small fragments of single chromosomes. In an attempt to distinguish between them, the DAPI-positive bodies were classified into two categories: small and large, based on their area (Figure 4.4B). Depletion of BRCA2 increased the number of micronuclei (Figure 4.4A), particularly, the number of small DAPI-positive bodies, which may originate from fragmented chromosomes (Figure 4.4C). However, this method does not allow to clearly discriminate between whole-chromosomes and chromosome fragments because chromosomes have different size. Overall, these results suggested that the depletion of BRCA2 can lead to chromosomal mis-segregation of endogenous chromosomes, although CIN in BRCA2-depleted cells may be associated chromosome fragmentation rather than whole-chromosome loss.

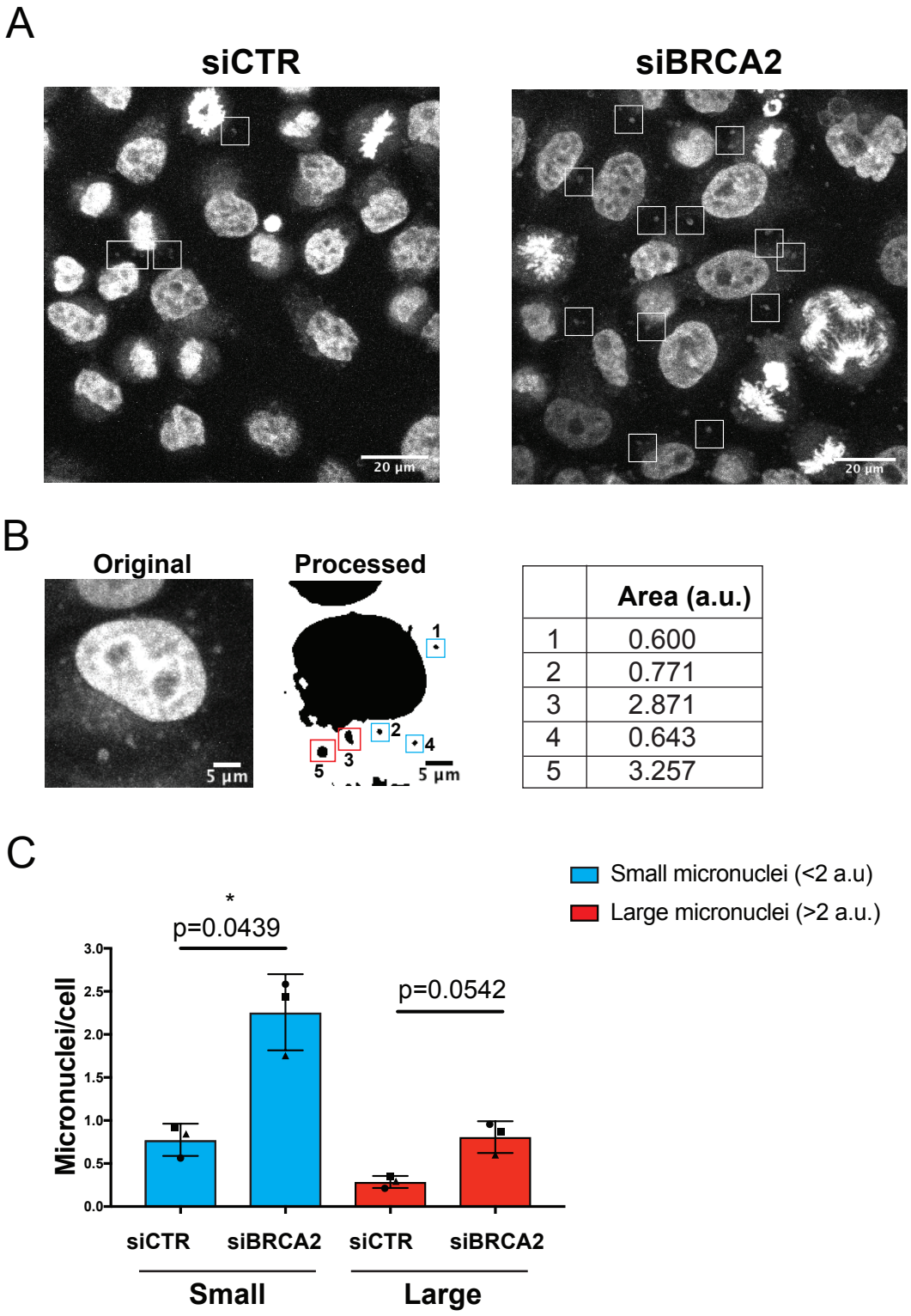


Figure 4.4: **Micronuclei formation upon BRCA2 depletion in HeLa cells**. Cells were treated as described in Figure 4.2A (**A**) Representative images of micronuclei in control (siCTR) and siBRCA2 treated cells. (**B**) Representative images of original and processed images, highlighting small (<2 a.u.) and large (>2 a.u.) micronuclei. a.u.= arbitrary unit. (**C**) Column graph represents the number of micronuclei per cell. About 300 cells were analysed for each condition in each experiment. Mean and SD of three independent experiments. p-values were calculated using paired two-tailed Student t-test.

4.2.2 Effect of replication stress and BRCA2 depletion on centromeric DNA stability

Centromeres form complex secondary structures, which can be difficult to resolve during replication leading to replication errors and fork stalling [131] [253]. The repetitive nature of centromeres serves as a perfect platform for the recombination machinery. In this context, it is possible that BRCA2 is important to protect or repair stalled or collapsed replication forks at centromeres. By contrast, BRCA2 removal could potentially lead to incomplete replication at centromeres, which may result in the formation of anaphase bridges at centromeres in mitosis. In the absence on BRCA2, it is possible that under-replicated regions at centromeres are mechanically broken during mitosis, leaving a DNA break at centromeres in the following G1 phase.

To test whether BRCA2 affects centromeric DNA stability, the colocalisation of γH2AX, a widely used DNA damage marker, and a centromere marker, CENP-C, was analysed by immunofluorescence in the presence or absence of BRCA2. In addition, the colocalisation between γH2AX and CENP-C was assessed upon exposure to a low dose of DNA polymerase inhibitor, aphidicolin (APH) (0.4 μM), which has been shown to induce replication stress at centromeres [214]. At 48 h after transfection, when BRCA2 was fully depleted (Figure 4.12), cells were treated with APH for 24 h and fixed. It was immediately noticeable that colocalisation between γH2AX and CENP-C was not perfect and, in few spots, showed a partial overlap between the two markers. To assess the colocalisation in an unbiased manner, I used the Manders' Colocalisation Coefficient (MCC) [254]. The MCC corresponds to the fraction of signal in one channel that overlaps with the signal in a second channel and it can be used to describe the colocalisation of two signals that do not have a linear correlation [254]. The amount of signal for each channel is estimated based on the intensity values in each pixel [254]. The level of γH2AX signal increased upon BRCA2 depletion or APH treatment, whereas the level of CENP-C signal largely remained unchanged upon different treatments (Figure 4.5A-B-C); thus, the colocalisation was measured as the fraction of CENP-C signal that overlaps with γH2AX signal. The MCC values range from 0 if there is no signal CENP-

C signal that overlaps with γH2AX signal, to 1 if all CENP-C signal colocalises with γH2AX signal. The analysis of the MCC showed that the depletion of BRCA2 did not increase the fraction of CENP-C that overlaps with γH2AX compared to the negative control, meaning that the level of DNA damage at centromeres did not change upon BRCA2 depletion. APH treatment consistently increased the level of DNA damage at centromeres in two independent experiments, but BRCA2 depletion did not exacerbate the phenotype (Figure 4.6).

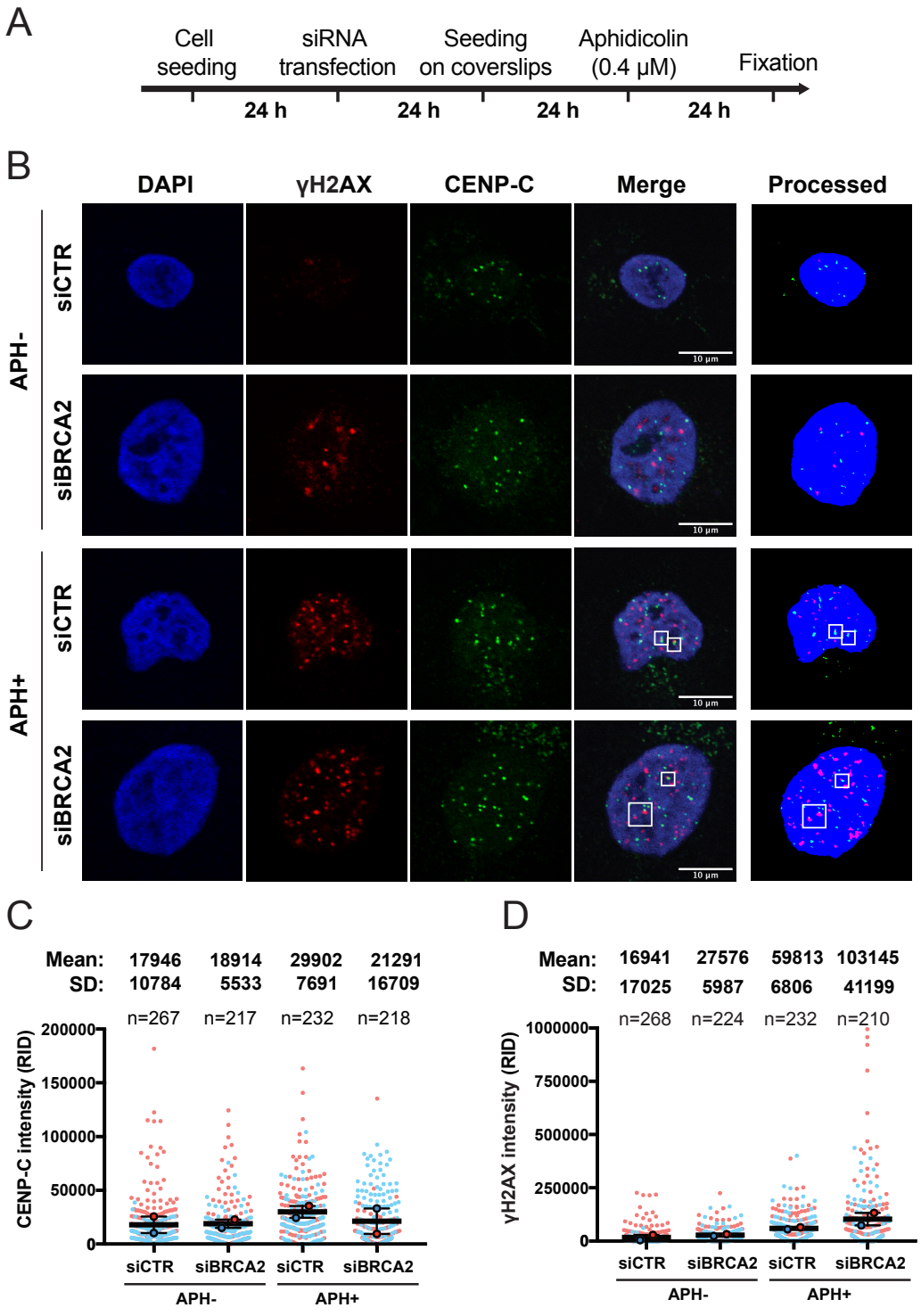


Figure 4.5: **Immunofluorescence (IF) of γH2AX and CENP-C in the presence and absence of BRCA2**.(**A**) Schematic representation of the protocol: HeLa Kyoto NFLAP-BRCA2 cells were treated with non-targeting siRNA (siCTR) and siRNA against BRCA2 (siBRCA2). At 24 h after transfection, cells were seeded on coverslips and let attach for 24 h. Where indicated, cells were treated with aphidicolin (APH) (0.4 μM) to induce replication stress for 24 h before fixation and incubation with antibodies. (**B**) Representative images of the IF experiment using γH2AX and CENP-C antibodies to detect DNA damage and centromeres, respectively. Representative processed images used to measure the MCC are also shown. Sites of colocalisation between the two markers are highlighted in white squares. (**C-D**) CENP-C and γH2AX intensity represented as Raw Integrated Density (RID). Mean and SD of two independent experiments. n represents the number of cells analysed for each condition.

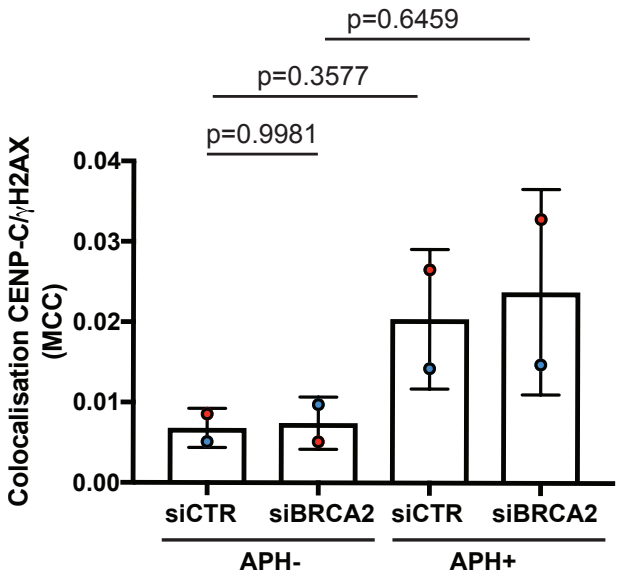


Figure 4.6: **Manders' Colocalisation Coefficient (MCC) between CENP-C and γH2AX in the presence and absence of BRCA2 and APH treatment**. Colocalisation between CENP-C and γH2AX signal was measured by the Manders' Colocalisation Coefficient (MCC). MCC was calculated for 30-40 pictures for each condition. More than 200 cells were analysed in two independent experiments. Column bars represent mean and SD of two independent experiments. p-values were calculated using RM one-way ANOVA with *post hoc* Tukey.

As stated above, γH2AX and CENP-C signals did not show perfect colocalisation but they were often in close proximity, suggesting the possibility that the damage occurred at CENP-C proximal regions. CENP-C defines the region of the kinetochore establishment at centromeres, but does not cover the entire centromeric region. By contrast, CENP-B binds the CENP-B boxes, which are embedded in the α-satellite DNA repeats throughout the centromeric chromatin. Thus, to better define the centromeric chromatin, CENP-B was used as a wider marker to cover the entire centromeric region. Similar to CENP-C signal, CENP-B signal showed less variability compared to the γH2AX signal upon different treatments (Figure 4.7A-B-C). Thus, the fraction of CENP-B that overlapped with the γH2AX signal was measured. Depletion of BRCA2 did not increase the level of γH2AX at CENP-B positive regions compared to the negative control. APH treatment increased the level of damage at CENP-B positive regions in one of the two experiments, but this impact was not exacerbated in BRCA2 depleted cells (Figure 4.8).

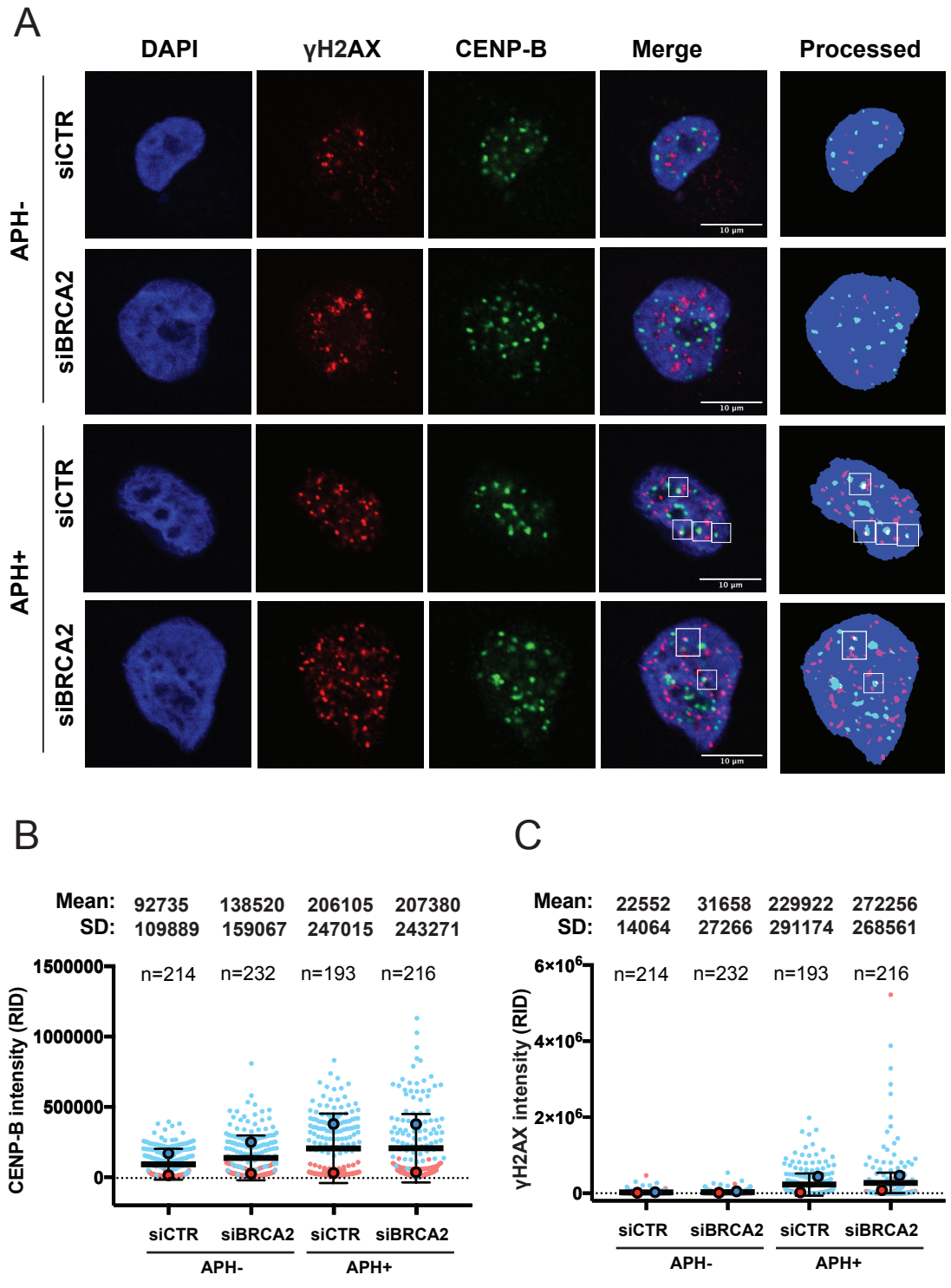


Figure 4.7: **Immunofluorescence (IF) of γH2AX and CENP-B in the presence and absence of BRCA2**. HeLa Kyoto NFLAP BRCA2 cells were treated as described in Figure 4.5A. (**A**) Representative images of the IF experiment using γH2AX and CENP-B antibodies to detect DNA damage and centromeres, respectively. Representative processed images used to measure the MCC are also shown. Sites of colocalisation between the two markers are highlighted in white squares. (**B-C**) CENP-B and γH2AX intensity represented as Raw Integrated Density (RID). Mean and SD of two independent experiments. n represents the number of cells analysed for each condition.

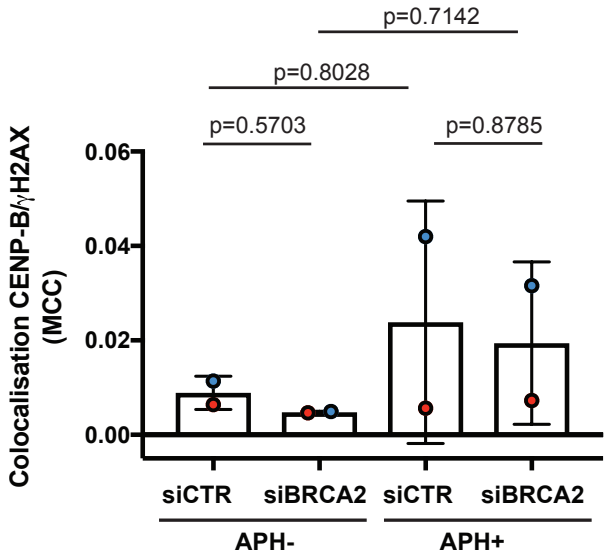


Figure 4.8: **Manders' Colocalisation Coefficient (MCC) between CENP-B and γH2AX in the presence and absence of BRCA2 and APH treatment**. Colocalisation between CENP-B and γH2AX signal was measured by the Manders' Colocalisation Coefficient (MCC). MCC was calculated for 30-40 pictures for each condition. More than 200 cells were analysed in two independent experiments. Column bars represent mean and SD of two independent experiments. p-values were calculated using RM one-way ANOVA with *post hoc* Tukey.

The major drawback of using the MCC to measure colocalisation is to determine what is signal and what is background [254]. In this analysis, CENP-C, CENP-B and γH2AX signals were identified using a standard algorithm (MaxEntropy) of the ImageJ imaging programme, in order to remove non-specific background (processed images in Figure 4.5A, 4.7A). While this method removed any false signal, it may also eliminate some positive signal. Moreover, it was noticed that different methods of thresholding the signal affected the MCC values. Hence, to confirm the results obtained with the MCC, the colocalisation between centromeres and DNA damage was assessed using the proximity ligation assay (PLA). This assay can be used to detect the colocalisation of proteins in the distance of up to 40 nm. The sample is incubated with two antibodies of the two proteins of interest that are crosslinked with two oligos. If the two antibodies are located within 40 nm distance, the two oligos can anneal and amplify the signal producing a fluorescent signal. Thus, each fluorescent dot represents one site of close proximity between the two antibodies. First, each antibody was in-

cubated individually to test the specificity of the signal (Figure 4.9A, Figure 4.10A). Under these conditions, almost no PLA foci were detectable inside the nuclei using CENP-C, CENP-B or γH2AX antibodies alone. Then, CENP-C or CENP-B antibody were incubated with CENP-A antibody to test the efficiency of the assay. Incubation of CENP-A antibody together with CENP-C or CENP-B antibody increased the number of PLA foci inside the nuclei compared to single antibodies, validating that the signal detected was specific (Figure 4.9A, Figure 4.10A). When CENP-C or CENP-B antibody was incubated together with γH2AX antibody, BRCA2 depleted cells did not exhibited increased level of PLA foci compared to control treated cells with either CENP-C and CENP-B antibodies. APH treated cells exhibited a moderately increased number of PLA foci both in siCTR and siBRCA2 treated cells using CENP-C and CENP-B antibodies, depletion of BRCA2 slightly reduced the level of PLA foci compared to siCTR treated cells upon APH treatment. Overall, the PLA analysis corroborated the results previously observed using the MCC.

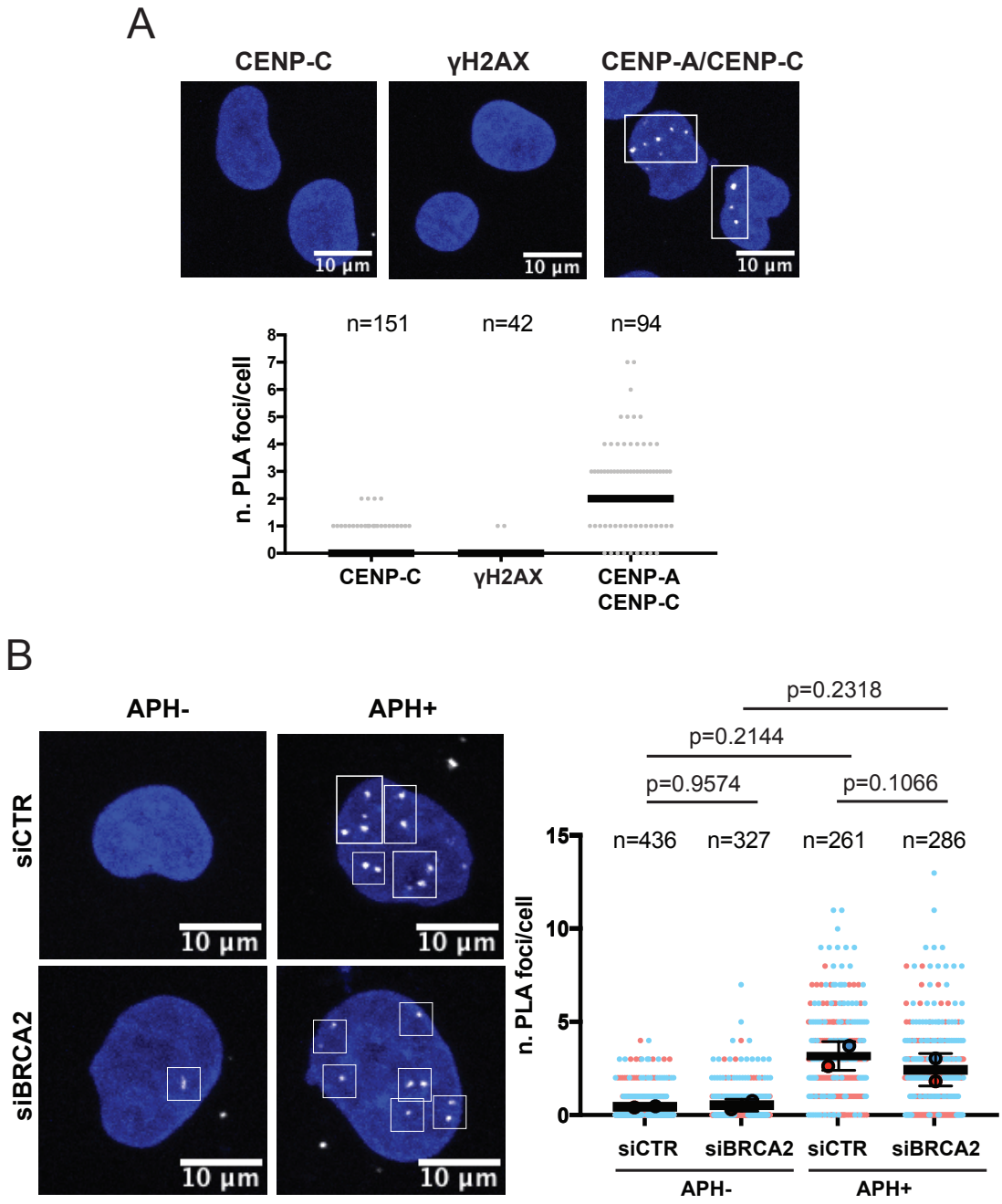


Figure 4.9: **Proximity Ligation Assay (PLA) between CENP-C and γH2AX in the presence and absence of BRCA2**. HeLa Kyoto NFLAP BRCA2 cells were treated as described in Figure 4.5A. (**A**) Cells were incubated with CENP-C and γH2AX antibodies alone (negative controls) and with CENP-A and CENP-C antibodies a positive control to assess the sensitivity of the assay. Scatter plot represents the number of PLA foci per cell in each condition. n is the number of cells analysed in a single experiment. Medians (thick black lines). (**B**) Representative images of PLA assay upon siRNA treatment with non-targeting siRNA (siCTR) and siRNA against BRCA2 combined with aphidicolin treatment (APH) (0.4 μM) to induce replication stress. After fixation, cells were incubated with CENP-C and γH2AX antibodies. Scatter plots represents the number of PLA foci/cell in each condition. Mean and SD of two independent experiments. p-values were calculated using RM one-way ANOVA with *post hoc* Tukey. n represents the number of cells analysed in each condition.

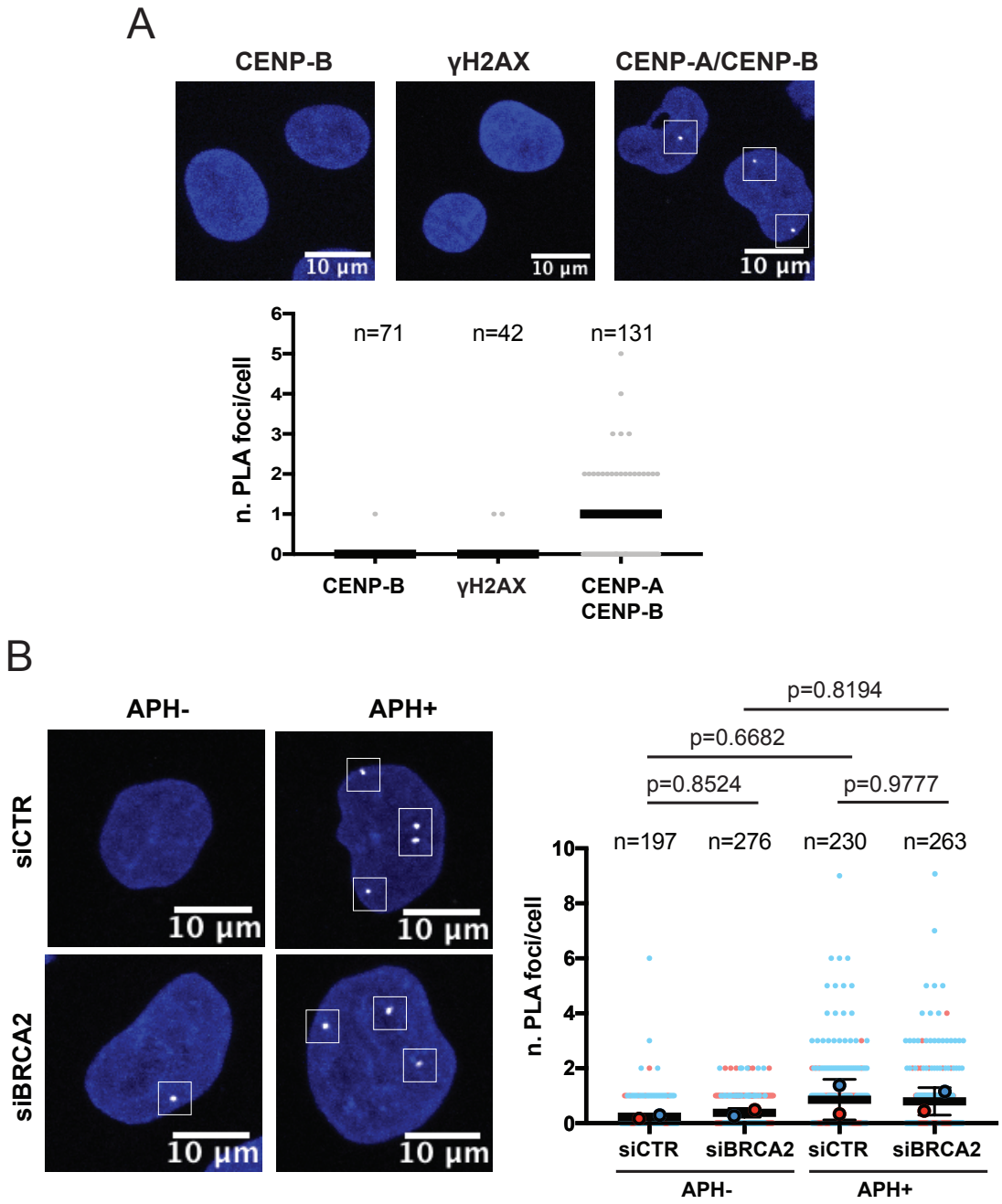


Figure 4.10: **Proximity Ligation Assay (PLA) between CENP-B and γH2AX in the presence and absence of BRCA2**. HeLa Kyoto NFLAP BRCA2 cells were treated as described in Figure 4.5A. (**A**) Cells were incubated with CENP-B and γH2AX antibodies alone (negative controls) and with CENP-A and CENP-B antibodies as a positive control to assess the sensitivity of the assay. Scatter plot represents the number of PLA foci/cell in each condition. n is the number of cells analysed in a single experiment. Medians (thick black lines). (**B**) Representative images of PLA assay upon siRNA treatment with non-targeting siRNA (siCTR) and siRNA against BRCA2 combined with aphidicolin treatment (APH) (0.4 μM) to induce replication stress. After fixation, cells were incubated with CENP-B and γH2AX antibodies. Scatter plots represents the number of PLA foci/cell in each condition. Mean and SD of two independent experiments. p-values were calculated using RM one-way ANOVA with *post hoc* Tukey. n represents the number of cells analysed in each condition.

Finally, I tested whether whether this phenotype could be affected by the cell cycle. An increased number of cells were found in S-G2 phase in siCTR treated cells upon APH treatment (Figure 4.11), whereas siBRCA2 treated cells in combination with APH predominantly accumulated in G1 phase (Figure 4.11). Therefore, it is possible that the reduced number of cells in S-G2 phase in BRCA2 depleted cells compared to siCTR treated cells upon APH treatment partially masked this phenotype. Consistent with previous observations [117], BRCA2 depleted cells exhibited increased cells in G1 phase, and increased p53 and p21 expression (Figure 4.12). This result was rather unexpected as p53 in HeLa cells is considered to be undetectable due to HPV E6 oncoprotein expression that induce p53 proteolysis.

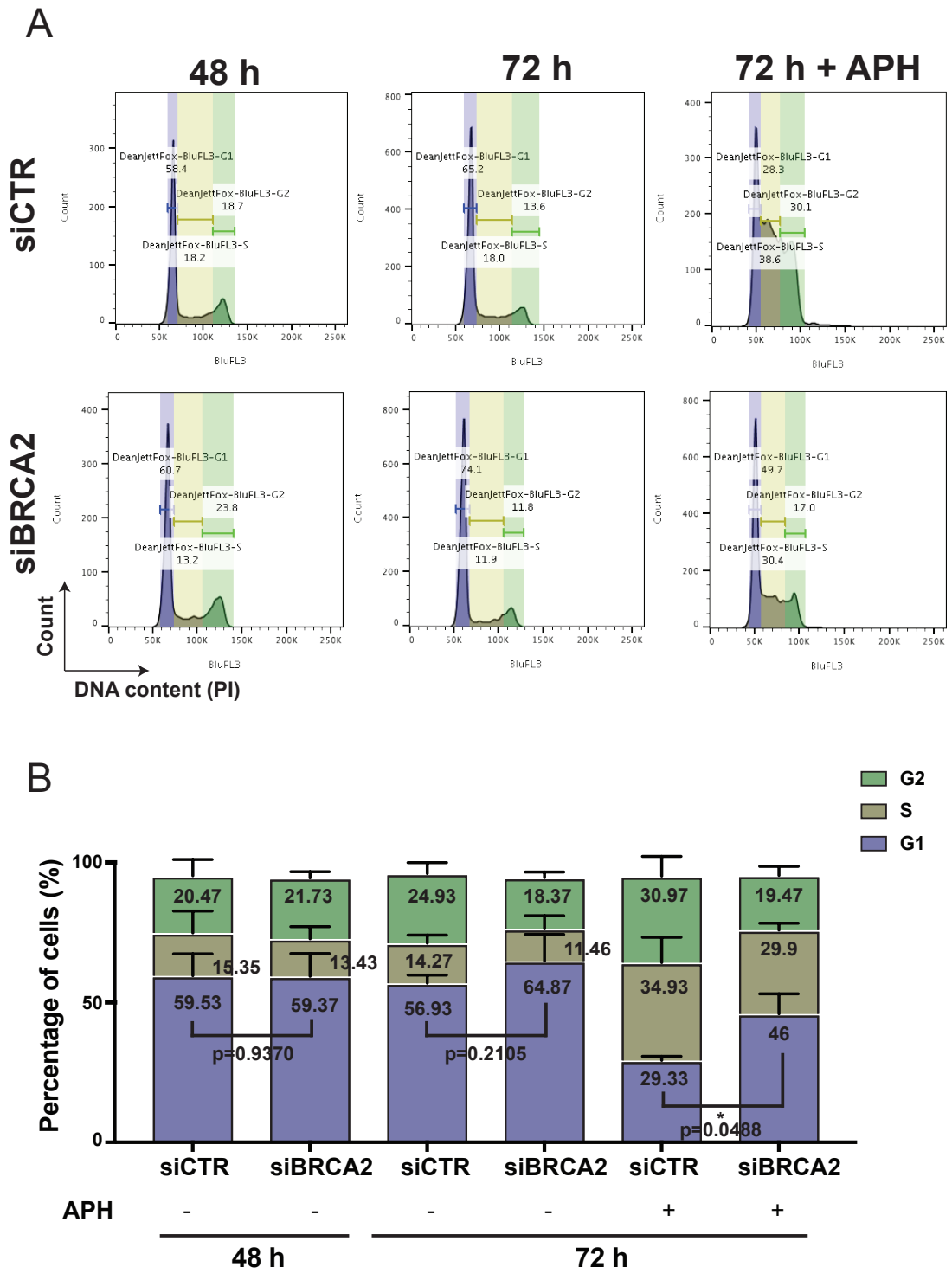


Figure 4.11: **Cell cycle profile upon BRCA2 depletion and APH treatment in HeLa cells.** HeLa Kyoto NFLAP BRCA2 cells were treated as described in Figure 4.5A. (**A**) Histograms represent the cell cycle profile based on propidium iodide (PI) to measure the DNA content. Cell cycle profile was measured after 48 and 72 h after siRNA treatment. (**B**) Percentage of cells in G1-S-G2 phase. Error bars represent SD of three independent experiments. Means were reported on the graph. Statistical analysis was performed between G1 values in siCTR and siBRCA2 treated cells. p-values were calculated using paired two-tailed Student t-test.

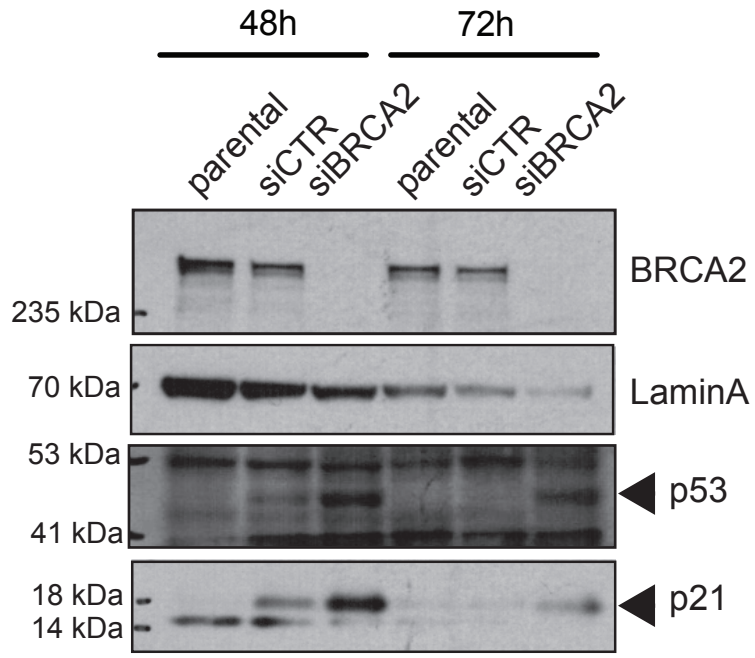


Figure 4.12: **p53 and p21 expression upon BRCA2 depletion in HeLa cells**. Western blot showing protein expression in HeLa Kyoto NFLAP-BRCA2 cells 48 and 72 hours after siRNA treatment with a non-targeting siRNA (siCTR) and siRNA against BRCA2 (siBRCA2). Endogenous proteins were detected using BRCA2 , Lamin A, p53 and p21 antibodies. Lamin A was used as a loading control.

Overall, the results presented in this section showed that, in line with previous observations [214], centromeres were vulnerable to replication stress induced by APH; however, BRCA2 did not appear to be required for the protection of centromeric DNA during replication either in undamaged or replication stress conditions. The long depletion of BRCA2 (72 hours) enriched the cells in G1 compared to control treated cells and showed p53 induction, suggesting that the absence of BRCA2 in mitosis may induce the formation of mitotic errors that arrest cells in the following G1 phase.

4.2.3 Chromatin changes upon BRCA2 depletion

Throughout the IF experiments using the HeLa cells, it was noticed that BRCA2 depletion led to increased nuclear area (Figure 4.13A). This phenotype was mildly detectable at 48 h after siRNA treatment and was more pronounced at 72 h (Figure 4.13B). Similarly, APH treatment slightly increased the nuclear area in siCTR treated cells and fur-

ther increased this phenotype upon BRCA2 depletion (Figure 4.13B). To understand the causes of enlarged nuclear area, I initially wondered whether this phenotype was linked to the different cell cycle stages. By flow cytometry, cells in S-G2 phase appeared slightly bigger compared to cells in G1 phase (Figure 4.14A); however, BRCA2 depleted cells, which are predominantly in G1 phase, showed a bigger nucleus than APH treated cells, which were predominantly in S-G2 (Figure 4.14B). This observation ruled out the possibility that increased the nuclear area upon BRCA2 depletion was a consequence of the accumulation of cells in S-G2 phase.

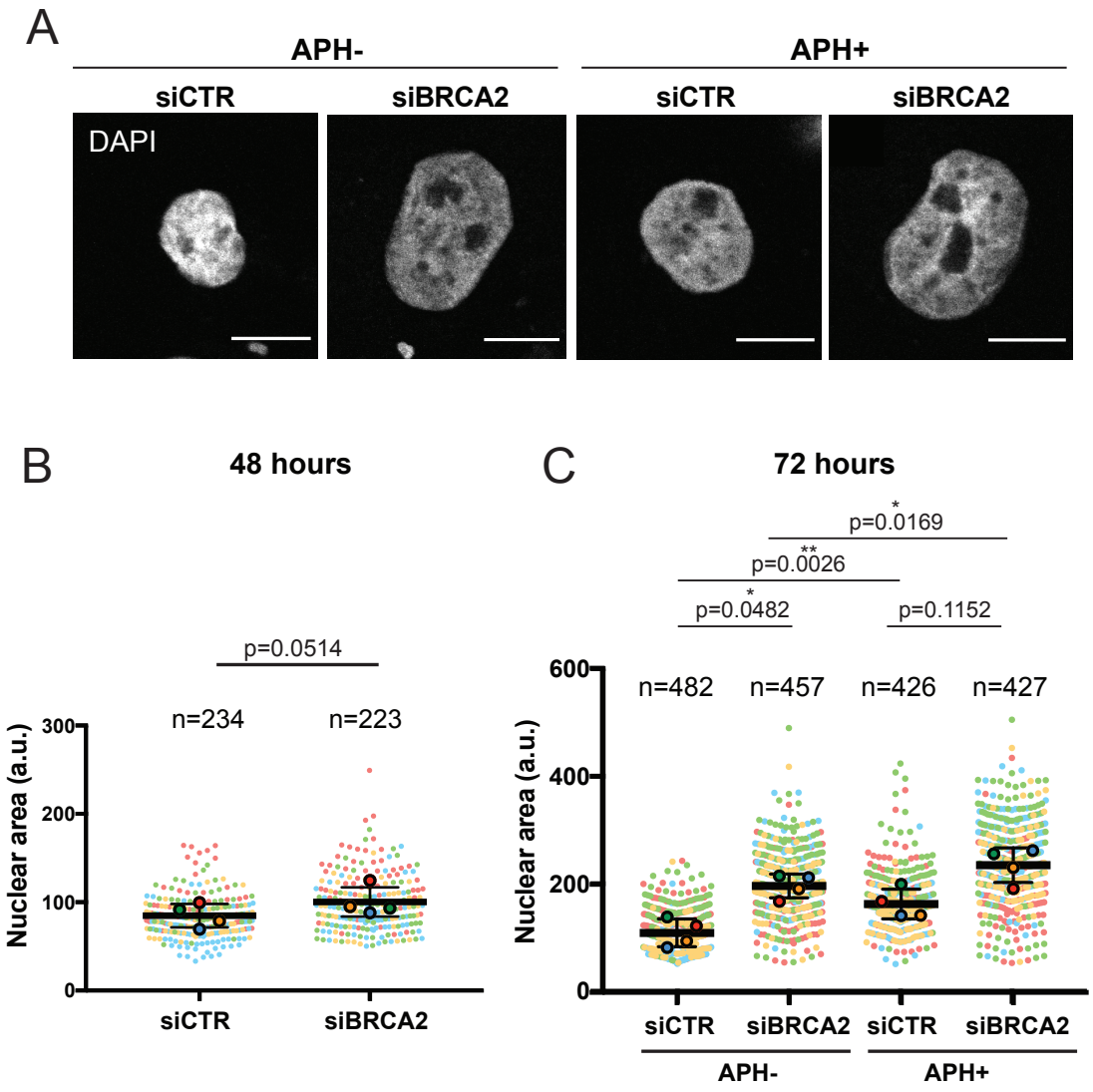


Figure 4.13: **Nuclear expansion upon BRCA2 depletion and APH treatment in HeLa cells**. HeLa Kyoto NFLAP BRCA2 cells were treated as described in Figure 4.5A. (**A**) Representative images of nuclei at 72 h after siRNA treatment with non-targeting siRNA (siCTR) and siRNA against BRCA2 (siBRCA2) and in the presence or absence of aphidicolin treatment (APH). Nuclei were detected by DAPI staining. Scale bar, 10 μm. (**B-C**) Scatter plots represents the average nuclear area at 48 and 72 hours after siRNA treatment. Mean and SD of four independent experiments. p-values were calculated using paired two-tailed Student t-test (B) and RM one-way ANOVA *post hoc* Tukey (C) (*, p-value < 0.05; **, p-value < 0.01). n represents the number of cells analysed.

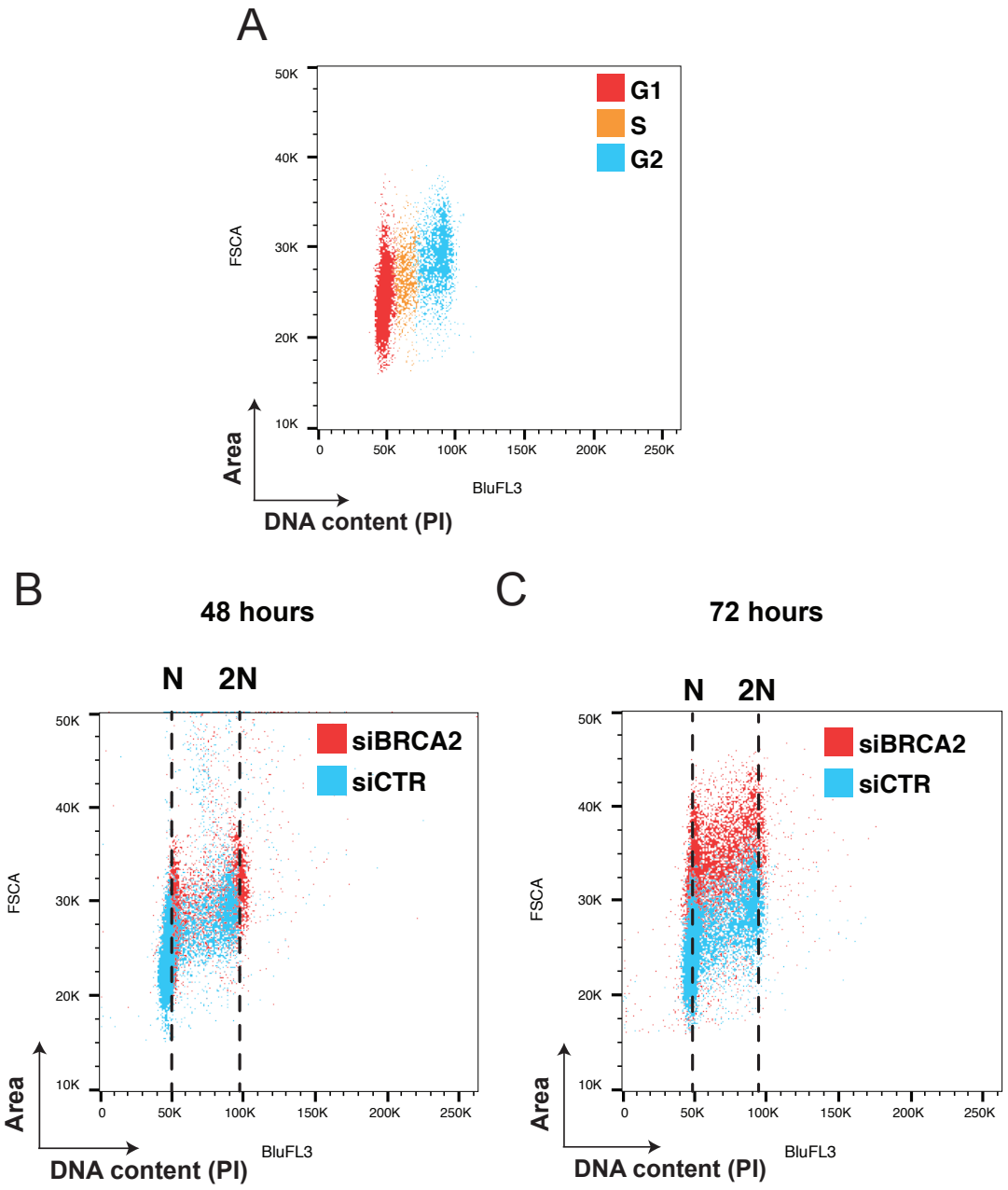


Figure 4.14: **DNA content upon BRCA2 depletion and APH treatment in HeLa cells**. (**A**) Flow cytometry analysis. HeLa Kyoto NFLAP-BRCA2 cells were stained with propidium iodide (PI) to distinguish different stages of the cell cycle (G1, S, G2) (x axis, PI intensity). Cell area was detected based on forward scattering of the light (FSCA). (**B**) DNA content and area at 48 and 72 hours after siRNA treatment with a non-targeting siRNA (siCTR) and siRNA against BRCA2. N = DNA content before replication, 2N = DNA content after replication.

Since BRCA2 leads to chromosome mis-segregation, I next considered that increased nuclear area may be a consequence of increased amount of DNA content due to un-

equal chromosome segregation. However, flow cytometry analysis using a DNA intercalating agent, propidium iodide (PI), which quantifies the DNA content in the cells, showed that, while BRCA2-depleted cells had increased area at 72 h after siRNA treatment, they exhibited no clear change in the amount of DNA content compared to the negative control (Figure 4.13B-C). Therefore, increased nuclear area in BRCA2 depleted cells was unlikely due to increased DNA content.

Nuclear morphology can be also modulated by cellular skeleton components. Formation of nuclear actin filaments (NAF) have been reported to support chromatin remodelling and DNA repair [255]. Here, the formation of NAF was tested using phalloidin, a toxin with a high affinity for F-actin (filamentous) (Figure 4.15A). As previously reported [256], the induction of replication stress induced by APH slightly increased the NAF inside the nucleus compared to control treated cells (Figure 4.15B). Furthermore, the depletion of BRCA2 increased the formation of NAF compared to siCTR treated cells and APH treated cells (Figure 4.15B). These results suggested that BRCA2 depletion lead to increased chromatin mobility.

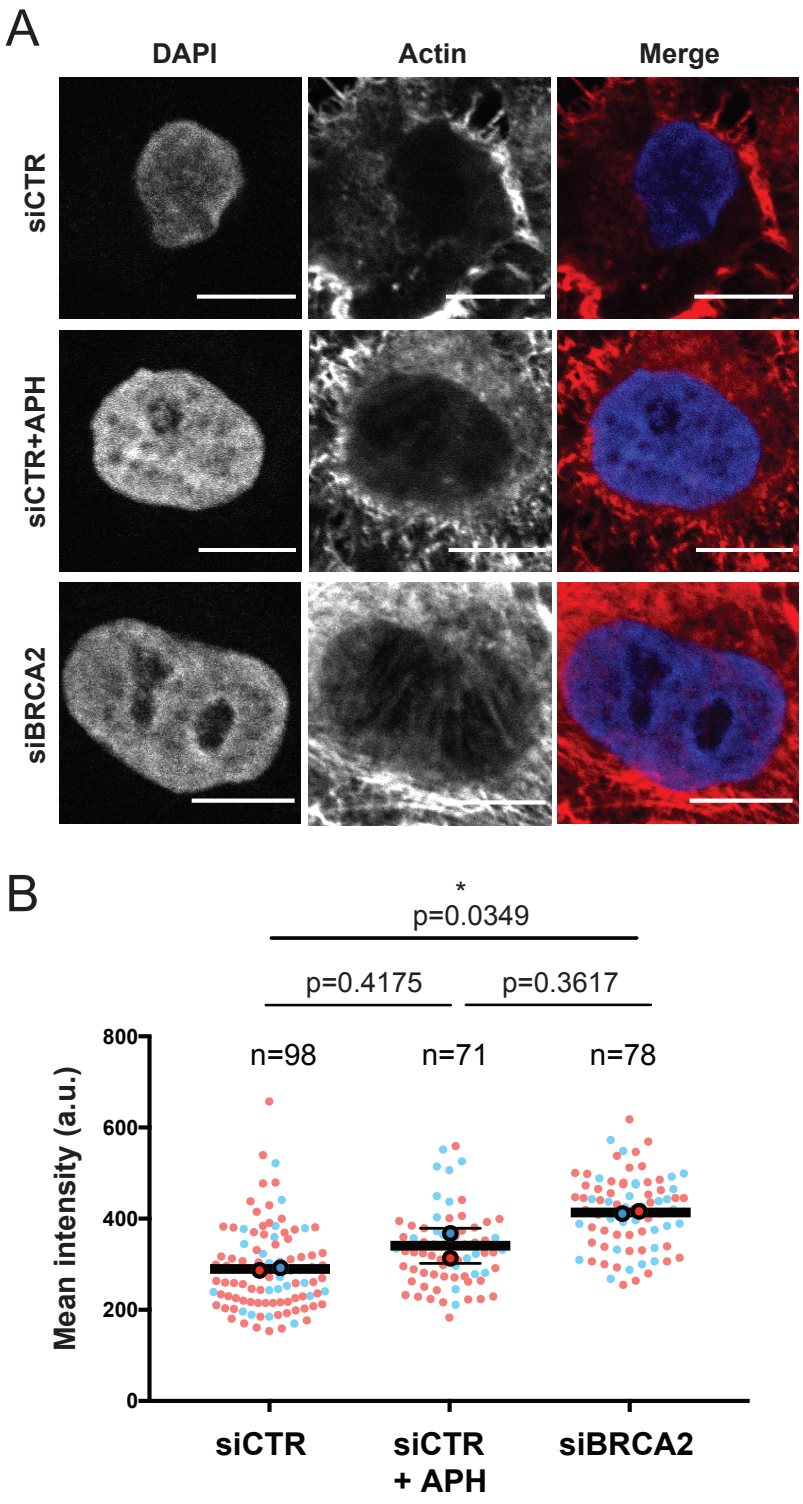


Figure 4.15: **Nuclear actin filaments (NAFs) formation upon BRCA2 depletion and APH treatment in HeLa cells**. HeLa Kyoto NFLAP BRCA2 cells were treated as described in Figure 4.5A. (**A**) Cells were fixed and stained with Phalloidin to detect actin filaments. Scale bar, 10 μm. (**B**) Scatter plots represents the mean intensity of Actin inside the nucleus at 72h after siRNA treatment with a non-targeting siRNA (siCTR) with or without aphidicolin treatment (0.4 μM for 24 h) (APH) and siRNA against BRCA2 (siBRCA2). Mean and SD of two independent experiments. p-values were calculated using RM one-way ANOVA *post hoc* Tukey (*, p-value < 0.05). n represents the number of cells analysed.

Surprisingly, BRCA2 depleted cells also showed increased number of CENP-C, CENP-B and CENP-A foci (Figure 4.16A-B-C). Similarly, a partial increased of CENP-C and CENP-B foci was observed upon APH treatment, suggesting that this phenotype could be associated with replication stress. The number of CENP-A foci was consistently higher compared to the CENP-B foci in siCTR treated and siBRCA2 treated cells (Figure 4.16B-C), suggesting that CENP-A foci can be formed at non-CENP-B regions in interphase cells. Thus, I tested whether BRCA2 depletion increased the formation of ectopic CENP-A formation by co-staining with CENP-A and CENP-B antibodies (Figure 4.17A). BRCA2 depletion almost doubled the number of CENP-B foci per cells and increased the number of CENP-A foci of about one third (Figure 4.17B-C-D). Therefore, BRCA2 depletion predominantly increased the formation of CENP-B foci but not the ectopic CENP-A outside the CENP-B positive regions. During this experiment, an increase in the intensity of CENP-A and CENP-B foci was also observed (Figure 4.17E-F); therefore I tested whether the depletion of BRCA2 led to increased association of the centromeric proteins to the chromatin by cell fractionation and Western blot analysis. This method showed similar levels of CENP-A and CENP-B enrichment in the chromatin fraction in siCTR and siBRCA2 treated cells (Figure 4.18). Interestingly, however, a reduced of CENP-C signal was found in the chromatin fraction. To test the stability of kinetochore components on the chromatin, I additionally blotted with antibodies against several outer kinetochore components. KNL1, ZWINT and DSN1 were similarly associated to the chromatin in siCTR and siBRCA2 treated cells in interphase cells (Figure 4.18). However, these antibodies showed unspecific signal. Therefore, the specificity of the antibodies need to be validated in the future.

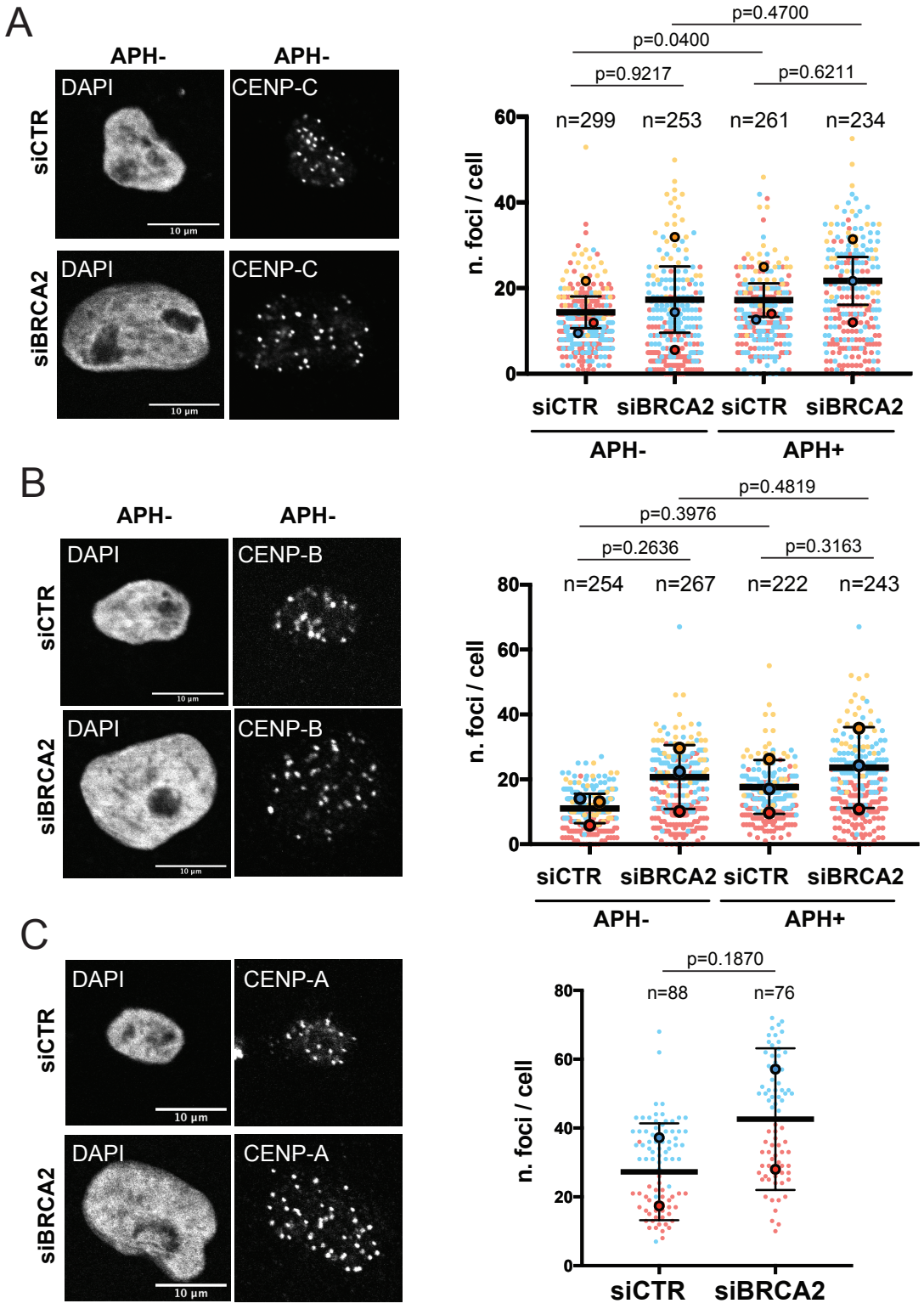


Figure 4.16: **CENPs foci formation upon BRCA2 depleteion and APH treatment**. At 72 h after siRNA treatment, cells were incubated with CENP-C (**A**), CENP-B (**B**), CENP-A (**C**) antibodies. Representative images of cells after siRNA treatment with a non-targeting siRNA (siCTR) and siRNA against BRCA2 (siBRCA2) in the absence of aphidicolin (APH). Scatter plots represent the number of foci per cell. Mean and SD of three (A-B) and two (C) independent experiments. p-values were calculated using RM one-way ANOVA *post hoc* Tukey (*, p-value < 0.05). n represents the number of cells analysed.

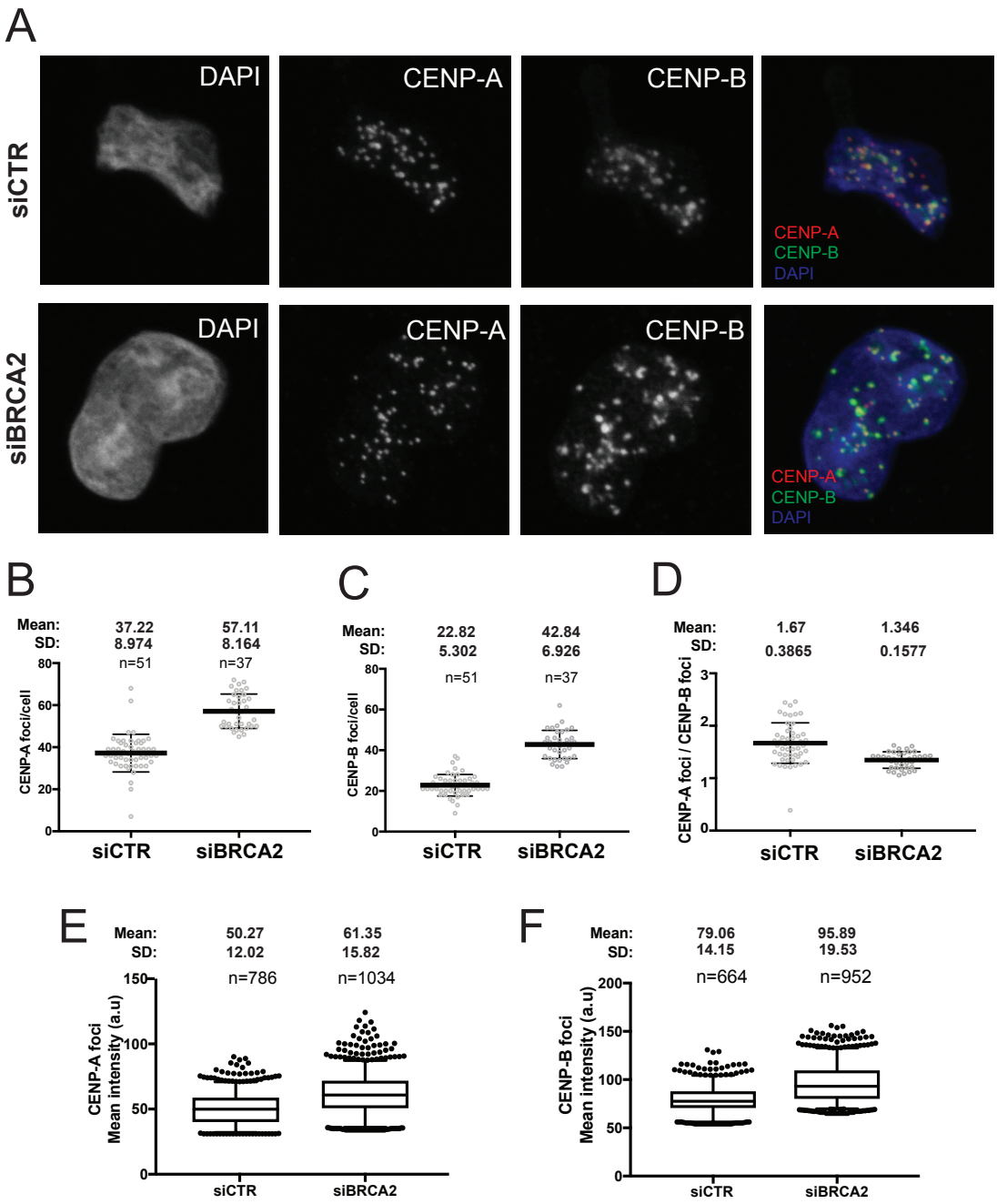


Figure 4.17: **CENP-A and CENP-B foci formation upon BRCA2 depletion in HeLa cells**.(**A**) Representative images of CENP-A and CENP-B staining in HeLa Kyoto NFLAP-BRCA2 cells at 72 h after siRNA treatment with non-targeting siRNA (siCTR) and siRNA against BRCA2 (siBRCA2). (**B-C**) Number of CENP-A and CENP-B foci per cells upon siCTR and siBRCA2 treatment. n represents the number of cells analysed. (**D**) Ratio between CENP-A and CENP-B foci per cell in siCTR and siBRCA2 treated cells. Mean and SD of one single experiment. (**E-F**) Box and whiskers graphs represent the intensity of CENP-A and CENP-B foci. Error bars represent the 5-95% percentile of one single experiments. n represents the number of centromeres analysed.

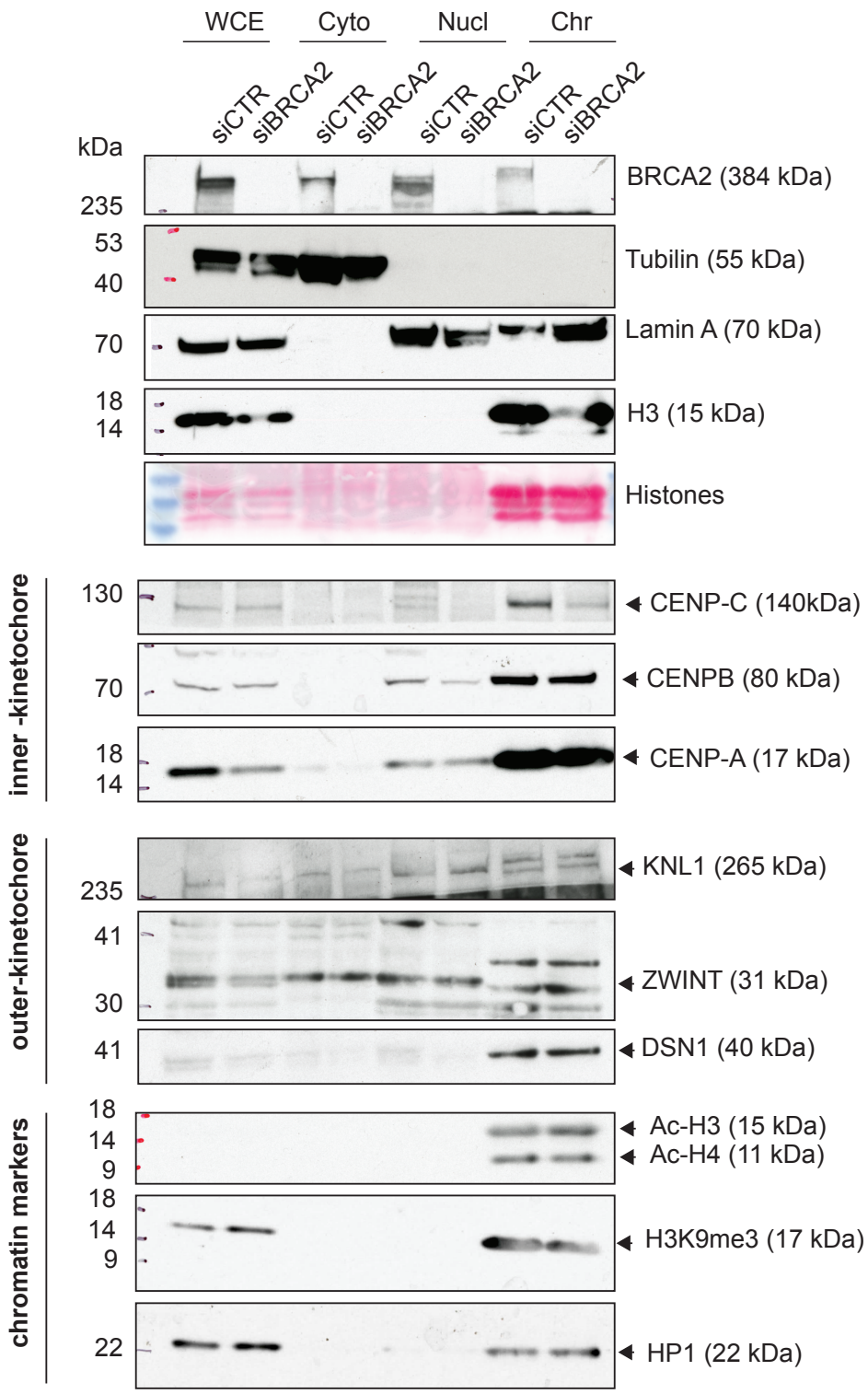


Figure 4.18: **Cellular fractionation analysis upon BRCA2 depletion in HeLa cells**. HeLa Kyoto cell were treated with siRNA against control negative siRNA (siCTR) and siBRCA2. At 72h after siRNA treatment, proteins in different cellular fractions were analysed by Western blot. Whole-cell lysate (WCE), cytoplasmic fraction (cyto), nuclear fraction (nucl), chromatin fraction (chr). Tubulin = marker of cyto. Lamin A = marker of nucl. Histone H3 = marker of chr. Ponceau S staining of histones was shown as loading control. Cellular fractions were incubated with several antibodies for inner- and outer- kinetochore proteins and chromatin markers (Acetylated (Ac) Histone H3 and Histone H4; lysine 9 tri-methylation histone H3 (H3K9me3); heterochromatin protein 1 (HP1))

Finally, I hypothesised that enlarged nuclear area could be caused by the chromatin reorganisation [257]. At the same time, different chromatin status at centromeres can affect the CENP protein association [133]. Open chromatin (euchromatin) correlates with high levels of histone acetylation and occupies a larger nuclear area [258]. At the same time, transcriptional activity and open chromatin at centromeres assist the CENP-A loading and kinetochore formation [234] [172] [259]. By contrast, chromatin condensation may reduce the nuclear area and centromeric heterochromatinisation correlates with reduced CENP-A loading at centromeres and kinetochore formation [234] [260] [166]. To test the chromatin status, BRCA2 depleted cells were stained with euchromatin and heterochromatin markers and the intensity of each marker inside the nucleus was measured by IF. Pan-acetyl Lysine antibody was used to detect histone acetylation as a marker of euchromatin, and lysine 9 tri-methylation histone H3 (H3K9me3) and heterochromatin protein 1 (HP1), which binds H3K9me3, were used as markers of transcriptionally silent heterochromatin. Preliminary experiments showed a small increase of signal detectable with the pan Acetyl-Lysine antibody and no difference with the H3K9me3 antibody (Supplementary Figure 4.19A-B). However, BRCA2 depleted cells showed a consistent increase of HP1 intensity in two independent experiments (Figure 4.20A-B) and formation of HP1 aggregates was found inside the nucleus. However, no enrichment of HP1 was found in the chromatin fraction upon BRCA2 depletion and Histone H3 acetylation was only mildly increased at 72 h after siRNA treatment (Figure 4.18). To test whether heterocromatinisation occurs at centromeres, the intensity of HP1 signal was quantified at CENP-A foci. Depletion of BRCA2 almost doubled the intensity of HP1 signal at CENP-A foci in a single experiment, suggesting a potential heterochromatinisation at centromeres in BRCA2 depleted cells (Figure 4.20B).

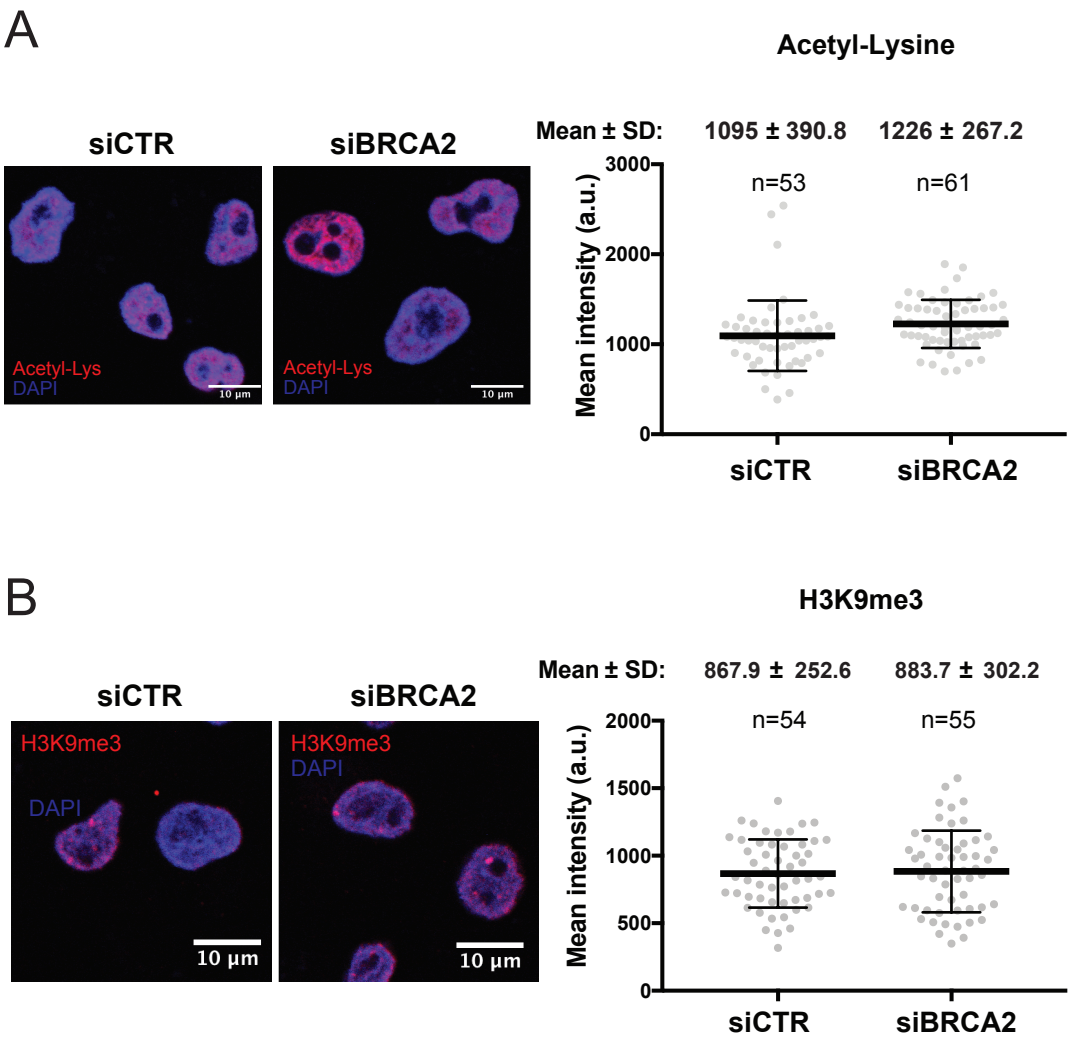


Figure 4.19: **Acetyl-Lysin and H3K9me3 intensity upon BRCA2 depletion in HeLa cells**. (**A-B**) Representative images of HeLa Kyoto NFLAP-BRCA2 cells treated with non-targeting siRNA (siCTR) and siRNA against BRCA2 (siBRCA2) for 48 h. Cells were fixed and stained with pan-Acetyl-Lysine and lysine 9 tri-methylation histone H3 (H3K9me3) antibodies. Scatter plots represent the mean intensity of pan-Acetyl-Lysine signal inside the nucleus. Mean and SD of a single experiment. n represents the number of cells analysed.

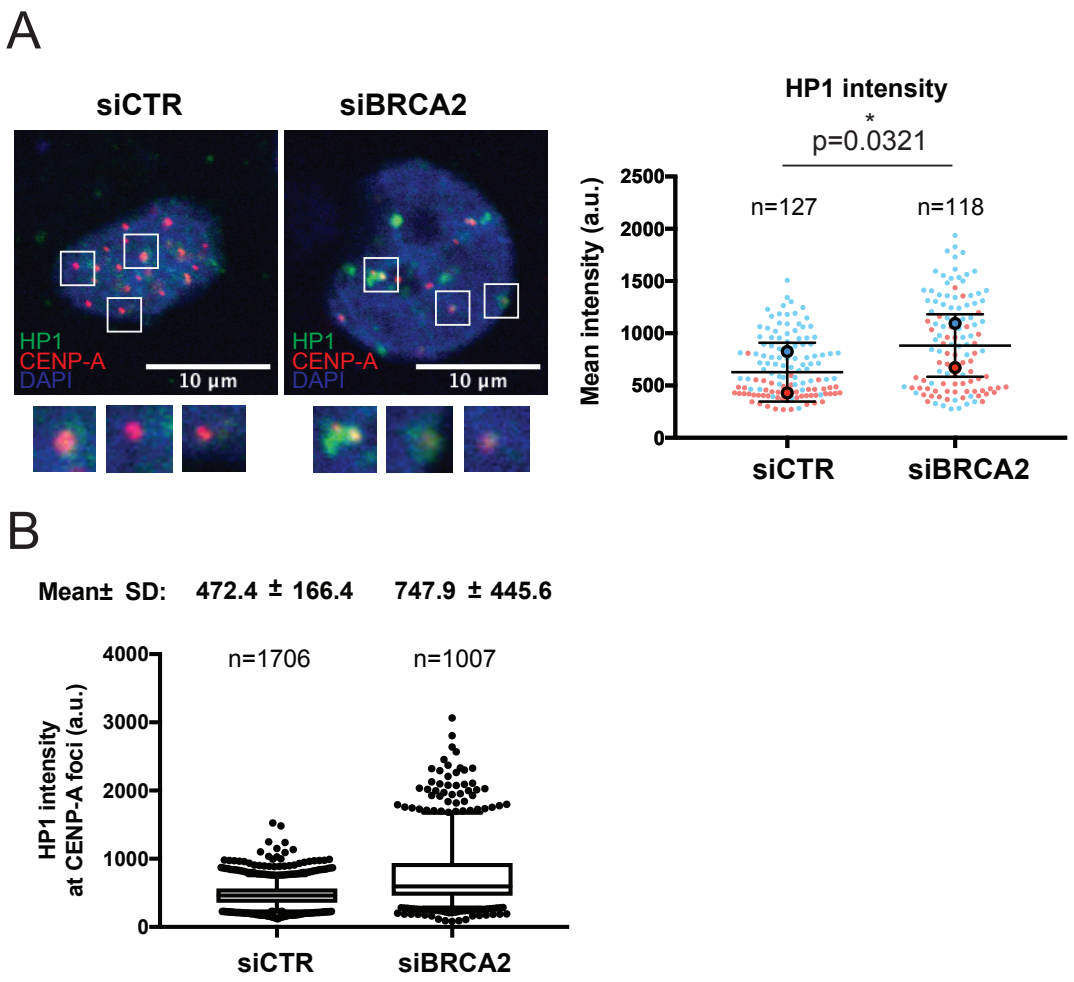


Figure 4.20: **HP1 intensity upon BRCA2 depletion in HeLa cells**. (**A**) Representative images of HeLa Kyoto NFLAP-BRCA2 cells treated with non-targeting siRNA (siCTR) and siRNA against BRCA2 (siBRCA2) for 48 h. Cells were fixed and incubated with heterochromatin protein 1 (HP1) and CENP-A antibodies. Scatter plots represents the mean intensity of HP1 inside the nucleus. Mean and SD of two independent experiments. p-values were calculated using paired two tailed Student t-test (*, p-value $<$ 0.05). n represents the number of cells analysed (**B**) Box and whiskers graphs represent the intensity of HP1 signal at CENP-A foci. Error bars represent the 5-95% percentile of one single experiment. n represents the number of centromeres analysed.

4.3 Discussion

4.3.1 Investigating the role of BRCA2 in centromere DNA stability during replication

In this chapter, I investigated the potential function of BRCA2 at endogenous chromosomes. In line with previous publications, depletion of BRCA2 increased the formation of anaphase bridges, lagging chromosomes, and micronuclei (Figure 4.2, Figure 4.4, Figure 4.3) [107], [116], [117]. BRCA2 depletion increased the formation of small micronuclei and appeared to increase the number of acentric lagging chromosomes, as detected in a single experiment (Figure 4.3, Figure 4.4). The small micronuclei could originate from chromosome fragments upon improper repair of double-strand breaks or chromosome breaks. Also, BRCA2 depletion appeared to increase the formation of anaphase bridges which originate from centromeres, according to a single experiment. Therefore, it is possible that the whole-chromosome loss observed in Chapter 3 is due to HAC fragmentation or unresolved DNA structures at centromeres. In future it would be important to consolidate these results with further replicates. In addition, micronuclei can be stained with centromere markers (i.e., ACA), as previously shown in Tutt et al. [107], to discriminate between whole-chromosome loss and chromosome fragments. Furthermore, it would be interesting to assess whether chromosome mis-segregation in BRCA2 depleted cells affects specific endogenous chromosomes based on the chromosome size or if it affects all chromosomes equally.

Despite the well-documented functions of BRCA2 during replication in DNA repair and fork protection [80], depletion of BRCA2 did not arrest the cells in S/G2 phase but appeared to increase the number of cells in the early stages of mitosis (Figure 4.11). Therefore, it is tempting to speculate that BRCA2 is particularly important during this period of the cell cycle to resolve incomplete events in interphase. During early mitosis, replication could be completed at difficult-to-replicate regions, such as centromeres [118]. At the same time, microtubules bind kinetochores to satisfy the SAC. It remains to be seen whether BRCA2 function in early mitosis is linked to its DNA re-

pair/replication function or to the assembly of kinetochore components. Therefore, in this chapter, I first tested whether BRCA2 depletion led to increased DNA damage at centromeres in the presence or absence of replication stress induced by APH treatment. The colocalisation between a widely used DNA damage/stress marker, γH2AX, and centromeric markers (CENP-C and CENP-B) was assessed using the Manders' colocalisation coefficient (MCC) and the Proximity Ligation Assay (PLA). Both methods showed positive and negative aspects. The IF experiments allowed me to visualise the whole signal coming from both markers, having a better picture of the distribution of the signals inside the cells. However, due to experiment-to-experiment and picture-to-picture variability of the intensity of the signal, it was difficult to identify a consistent method to define the signal-to-noise ratio. This can also vary due to the specificity of the antibodies and the quality of the images. On the other hand, the PLA analysis has a more straightforward readout (i.e., just by counting the foci); however, this assay is only able to generate a fluorescent signal for proteins within 40 nm distance. Perhaps, the amplification of the signal may be also affected by the position and the accessibility of the antibodies. Thus, it is possible that this assay fails to detect all sites in close proximity. Indeed, only few foci were detected even with the positive controls (CENP-C and CENP-A, CENP-B and CENP-A), even if these proteins were shown to interact with each other [176] [142].

Overall, the results of the colocalisation analysis by MCC and PLA consistently showed that replication stress by APH treatment increased γH2AX signal at centromereres, marked by CENP-C and CENP-B with and without BRCA2 (Figure 4.6, Figure 4.8, Figure 4.9, Figure 4.10). However, the depletion of BRCA2 did not increase the γH2AX signal at centromeres. APH treated cells showed a mild decrease of γH2AX signal at centromeres upon BRCA2 depletion at CENP-C positive regions, which could be explained by the reduced number of cells in S-G2 phase compared to APH treated cells alone (Figure 4.11). To further confirm this result, in future, the colocalisation analysis could be performed at different stages of the cell cycle or by combining different cell cycle markers. Furthermore, I cannot exclude the possibility that depletion of BRCA2 leads to DNA damage at centromeres that was undetectable by γH2AX, such

as single-stranded DNA gaps [261]. In the future, different markers could be used to detect single-strand DNA at centromeres, such as RPA or thymidine analogues. Lastly, since γH2AX and CENP were often in close proximity, it is possible that DNA damage was associated to pericentromeres. These are highly packed hetorochromatin regions, which could form complex DNA structures and be "hot-spots" for DNA damage [131].

4.3.2 Depletion of BRCA2 leads to chromatin movement, senescence-like phenotype and abnormal centromere formation

The experiments conducted in section 4.2.3 suggested that BRCA2 depletion leads to increased chromatin dynamics. This idea was supported by the observations of nuclear expansion and increased nuclear actin filament formation (Figure 4.13, Figure 4.14, Figure 4.15). These phenotypes were also observed in APH treated cells, but were even more pronounced in BRCA2 depleted cells. It is possible that these phenotypes were partially associated with replication stress upon BRCA2 depletion. However, BRCA2 depletion did not show increased levels of γH2AX compared to APH treated cells, supporting the idea that chromatin movement upon BRCA2 depletion may be not just a consequence of replication stress. Therefore, it is possible that BRCA2 has a direct function in chromatin dynamics. In the future, chromatin mobility in BRCA2 depleted cells could be further investigated with other methods, such as Fluorescence recovery after photobleaching (FRAP) to explore the dynamics of histones.

Nuclear actin filament (NAF) formation has been shown to allow chromatin decondensation upon mitotic exit [262]. Additionally, it has been shown that NAFs facilitate CENP-A loading in G1 phase [263]. Thus, it is possible that NAFs formation upon BRCA2 depletion may lead to more accessible chromatin regions and facilitate the incorporation of ectopic centromeric proteins. These "extra-centromeres" appeared to be established at CENP-B boxes where also CENP-B can bind (Figure 4.17). A recent study has shown that CENP-B boxes are spread throughout the genome and the CENP-A loading occurred on all of them in G1 phase; however, after replication, CENP-A is

evicted at non-centromeric regions [163]. Based on the previous publication, it remains to be seen whether the ectopic centromere formation in BRCA2 depleted cells leads to functional centromeres in mitotic cells. An alternative explanation of the increased CENP-B foci could be that the BRCA2 depletion leads to chromatin changes, which affect CENP-B binding to the chromatin. It has been shown that demethylation of CpG nucleotides inside the CENP-B box increases CENP-B binding to the chromatin [264] [265]. It is possible that BRCA2 depletion leads to a chromatin reorganisation, which may favour CENP-B binding and centromere formation.

The reduced level of CENP-C in the chromatin fraction by cell fractionation (Figure 4.18) may suggest that CENP-C is less associated with the chromatin. Chromatin fractionation was initially performed using a physiological salt concentration of 150 mM NaCl. Under these conditions no difference was observed in the level of proteins associated with the chromatin between siBRCA2 and siCTR treated cells (data not shown). At 200 mM NaCl, the level of CENP-C association to the chromatin was reduced in BRCA2 depleted cells compared to siCTR (Figure 4.18). Increased salt concentration improves the solubilisation of the chromatin-associated proteins by breaking DNA-protein and protein-protein interactions. One possible interpretation of this result is that upon BRCA2 depletion, CENP-C is less tightly associated to the chromatin and this was only detectable at high salt concentration, in which CENP-C-chromatin interactions had been weaken and hence only a reduced fraction of the protein remained associated to the chromatin. On the other hand, it is also possible that CENP-C is more tightly associated to the chromatin in BRCA2 depleted cells and even at high salt concentration, CENP-C remains tightly bound to the chromatin and only a reduced portion is solubilised in the chromatin fraction. In support of the latter notion, CENP-C was not detectable in the nuclear fraction in BRCA2 depleted cells suggesting that CENP-C could be still associated to the chromatin. To further discriminate between these two hypotheses, one possible avenue could be to perform a titration assay with increasing salt concentrations to test the solubility of CENP proteins in the presence or absence of BRCA2.

It was noted that BRCA2 depleted cells exhibited senescence-like phenotype characterised by G1 arrest, p53 and p21 expression, as previously reported in Feng et al. [117], and increased HP1 signal (Figure 4.11, Figure 4.12, Figure 4.20). However, p53 expression in BRCA2 depleted cells was unexpected as endogenous p53 in HeLa cells is widely considered unexpressed due to the presence of Human Papillomavirus (HPV) E6 oncoprotein that catalyses p53 proteolysis in this cell line. In this context, BRCA2 might act together with HPV E6 to down-regulate p53 and p21, and consequently suppress apoptosis and senescence. Alternatively, BRCA2, through its transactivation activity, may facilitate the HPV E6 expression. Increased HP1 signal in BRCA2 depleted cells could be due to senescence. Senescent cells show increased heterochromatinisation and are characterised by senescence-associated heterochromatin foci (SAHF), which are usually associated with heterochromatin protein 1 (HP1) and lysine 9 trimethylation histone H3 (H3K3me3) [266] [267]. Moreover, in senescent cells, SAHF formation has been described at centromeres, suggesting that centromere heterochromatinisation is linked with senescence [268]. Similarly, preliminary results presented in this chapter have shown that BRCA2 depletion increased HP1 signal at centromeres, marked by CENP-A antibody (Figure 4.20B), which may support the idea of increased heterochromatinisation at centromeres. This experiment needs to be repeated in the future and the level of heterochromatin at centromere could be assessed using different heterochromatin markers (i.e., H3K9me3).

Heterochromatinisation at centromeres has been shown to have a negative impact on centromere and kinetochore formation [234] [260]. CENP-B has been regarded as playing an important role in determining the precise DNA methylation pattern at centromeres. At centromeres, CENP-B promotes *de novo* CENP-A loading, whereas it stimulates heterochromatin formation, preventing CENP-A loading, at α-satellite DNA ectopically integrated on the chromosome arms [167] [168]. Based on these studies, it is plausible that part of the ectopic CENP-B foci observed upon BRCA2 depletion may support the CENP-A loading, whereas others can promote heterochromatinisation. Overall, it remains to be understood whether BRCA2 affects chromatin organisation at centromeres. It would be interesting to understand whether BRCA2 depletion affects

the chromatin status genome-wide or at specific genomic loci, such as centromeres, and whether chromatin reorganisation upon BRCA2 depletion can affect centromere formation. It has been proposed elsewhere that BRCA1, which has been often observed in macromolecular complexes together with BRCA2, was implicated in the silencing of heterochromatin [269] [270]. BRCA1 depletion has been shown to increase heterochromatin transcripts [269]. This notion has been proven also for α-satellite repeats assembled into heterochromatin domains flanking the kinetochore, suggesting a link between BRCA1 deficiency and chromosome mis-segregation [270]. Similarly, it is possible that BRCA2, together with BRCA1, may support heterochromatin silencing.

In the study shown in this chapter, increased H3K9me3 signal was not detectable upon BRCA2 depletion (Figure 4.19B), suggesting that increased HP1 signal may not be associated with increased heterochromatinisation. Apart from its interaction with the heterochromatin, HP1 was described as being localised at sites of DNA damage independently of epigenetic markers [271] [272]. A preliminary experiment in which cells were stained with HP1α and γH2AX did not show increased colocalisation between the two markers, suggesting that increased HP1 signal was not linked with the DNA damage; however, appropriate quantification is needed. Curiously, upon BRCA2 depletion, HP1 signal appeared to form distinct aggregates/foci inside the nucleus (Figure 4.20A). Recent studies from elsewhere also propose that HP1 forms chromatin linkages which drive the formation of droplets of heterochromatin [273] [274] [275]. Thus, it is possible that BRCA2 depletion leads to an HP1 relocation inside the nucleus that confines the heterochromatin at specific areas of the nucleus. Alternatively, HP1-mediated chromatin linkages have been proposed to maintain the nuclear shape [276]. In that study, transient HP1 depletion was associated with reduced nuclear stiffness without affecting the level of heterochromatin inside the nucleus [276]. In the future, it would be interesting to further investigate how BRCA2 depletion leads to HP1 accumulation, and its potential links to cellular senescence, nuclear size, and CENP-A, B and C foci formation. Time-course analyses of HP1 localisation and its dynamics upon BRCA2 depletion may provide further insights into this question.

Chapter 5

Investigating the role of BRCA2 at kinetochores

5.1 Introduction

BRCA2 deficiency has been associated with aberrant chromosome structure and abnormal chromosome number [73] [62] [74]. Mouse embryonic fibroblasts (MEFs) with a targeted truncation at amino-acid 1492 (BRCA2$^{Tr/Tr}$), which results in a transcript containing the first three BRC motifs, showed chromosome abnormalities, such as chromosome breaks, tri-radial and quadri-radial chromosomes, and polyploidy [62]. MEFs carrying a similar BRCA2 truncation after the seventh BRC motif (BRCA2 ^{Tr2014}) undergo micronuclei formation as a result of chromosome mis-segregation [107]. In human cells, CAPAN-1 pancreatic cancer cells, which lack one copy of *BRCA2* and have a 6174delT mutation on the other allele that leads to a premature truncation of the DBD and NLSs, showed several chromosome rearrangements, chromosomal translocations and abnormal chromosome number [74]. While mutations and translocations in BRCA2-deficient cells were proposed to be mainly caused by impaired DNA repair, it is not well known how BRCA2 deficiency is linked with aneuploidy. Several former studies have tried to characterise mitotic functions of BRCA2 as described in section 1.2.3.4; however, none of them fully explain why BRCA2-deficient cells undergo aneuploidy. A recent study has proposed that the HR BRCA2 function in S-G2 phase is responsible of chromosome mis-segregation in mitosis [117]. BRCA2-deficient cells can enter mitosis with under-replicated DNA, which can lead to the formation of lagging chromosome and anaphase bridges [117]. Overall, it is still poorly understood whether aneuploidy in BRCA2-deficient cells is a consequence of the BRCA2 function during replication or is due to an HR-independent function in mitosis.

Unbiased shotgun proteomics studies conducted in the laboratory of Dr. Fumiko Esashi have identified outer-kinetochore proteins as significant BRCA2 binding partners (Figure 5.1A-B). Using asynchronous cells, BRCA2 was found to associate with DSN1 (a component of the MIS12 complex) (Figure 5.1A), as also described elsewhere [277]. When cells were enriched in S-phase, using a double-thymidine block to arrest them at the G1-S boundary and released into S phase for three hours, resultant BRCA2 interactome analyses revealed several components of the MIS12 and KNL1 complexes as

BRCA2 binding partners (Figure 5.1B), suggesting that BRCA2-kinetochore interaction may occur progressively as the cell goes into S phase. Intriguingly, previous studies in the laboratory of Dr. Fumiko Esashi have shown that the PALB2-BRCA2 complex is enriched at transcriptionally active regions, which is mediated through the binding between PALB2 and the histone binding protein MRG15 [278]. The presence of the PALB2-BRCA2 complex at actively transcribed regions was proposed to protect DNA damage induced by the conflict between transcription and replication. This observation posed a possibility that BRCA2 also associates at actively transcribed centromeric regions. Interestingly, when exposed to camptothecin, a topoisomerase I inhibitor, which induces DNA damage at actively transcribed regions, the BRCA2-kinetochore interaction was down-regulated (M. Fournier, unpublished data), suggesting that this interaction was not DNA damage dependent. These results showed for the first time that BRCA2 associates with kinetochore components, which are directly involved in the chromosome segregation.

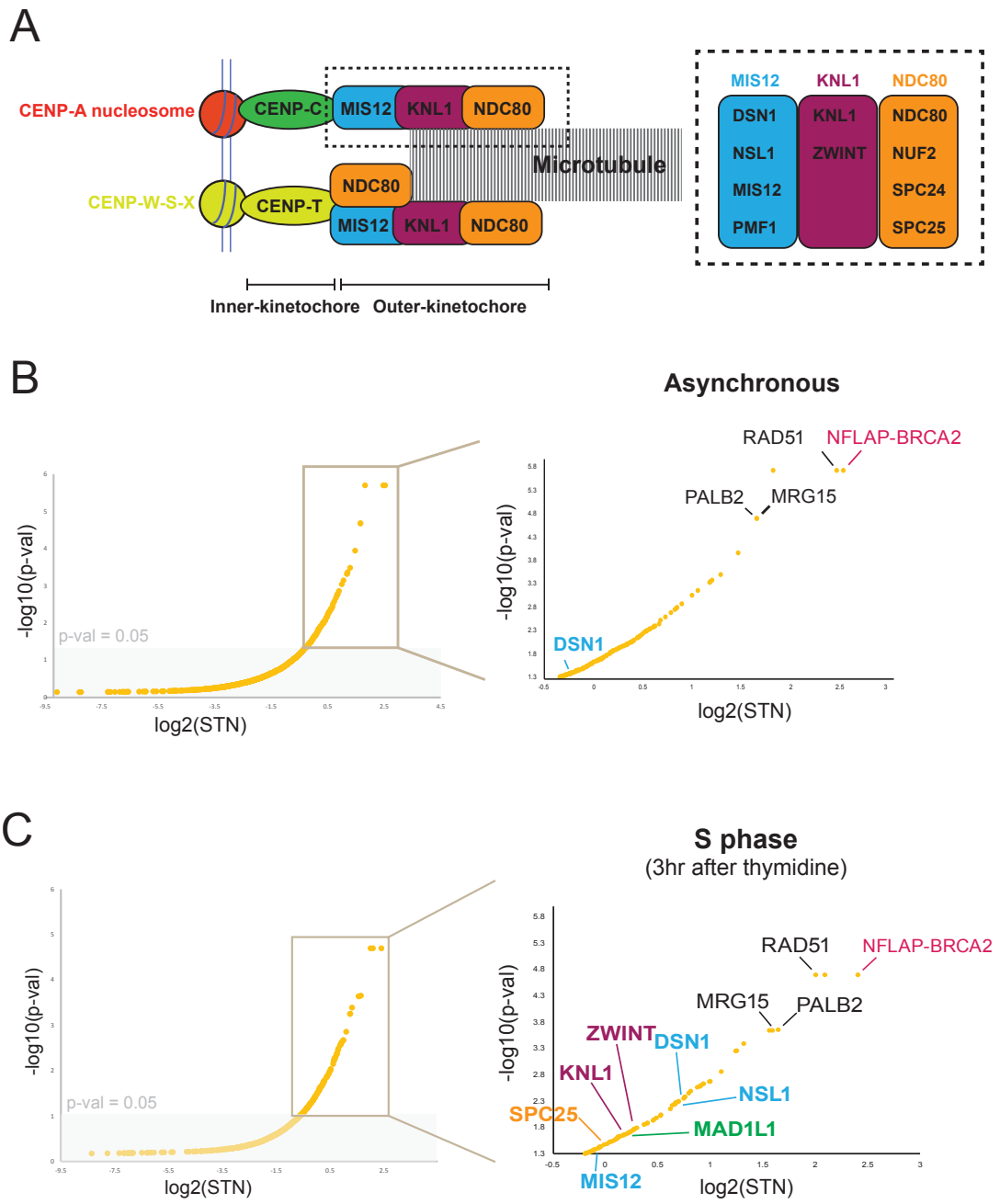


Figure 5.1: **BRCA2 interactome.** (**A**) Schematic representation of kinetochore-associated proteins. (**B-C**) Volcano Plot showing BRCA2 binding partners. HeLa NFLAP-BRCA2 were analysed in untreated conditions (asynchronous) (B) or treated with double thymidine-block and release for 3 hours prior GFP-pull down (C). PLGEM statistical analyses were performed using HeLa-GFP cells as negative control. Graphs on the right represent BRCA2 binding partners after LC/MS-MS analysis of NFLAP-BRCA2 pull-down eluates (n=3, p-value < 0.05). The significance of the enrichment is depicted on the y axis (-log10(p-value) versus the fold enrichment in x axis (log2 STN). Well-known binding partners of BRCA2 (black), Kinetochore proteins (MIS12 complex in light blue, KNL1 complex in purple, NDC80 complex in orange), spindle-assembly checkpoint protein (green) are shown on the graph. Data shown in B and C was generated by Dr. Marjorie Fournier.

Initial experiments using synchronised cultures showed that BRCA2 interaction with KNL1 complex (i.e. KNL1 and ZWINT) occurs predominantly in the S phase and this interaction is progressively reduced in mitosis (Supplementary Figure 5.2). Kinetochore components of the MIS12 and KNL1 complexes start to be recruited at centromeres in S phase [195]. However, only during mitosis, is the full-kinetochore complex stably formed at centromeres [195]. This is in part accomplished after nuclear envelope breakdown, when NDC80, which is normally spatially separated in cytoplasm in interphase, can access centromeres [195]. Additionally, FRAP (Fluorescence Recovery After Photo-bleaching) experiments showed that during interphase, MIS12 association at centromeres was more dynamic, whereas during mitosis this was more stable [196]. Currently, the recruitment of kinetochores at centromeres during mitosis is considered to be mediated by two independent pathways: CENP-C- and CENP-T-dependent mechanisms [199] [183] [185]. In mitotis, the CENP-C-dependent pathway is mediated by phosphorylation of the KMN complex by Aurora B [185], whereas the CENP-T-dependent pathway is facilitated by CDK-mediated CENP-T phosphorylation, which allows the binding to the NDC80 complex [183] [185]. However, it is still not fully understood how the kinetochore components are recruited at centromeres during the cell cycle and how the kinetochore components are assembled at centromeres.

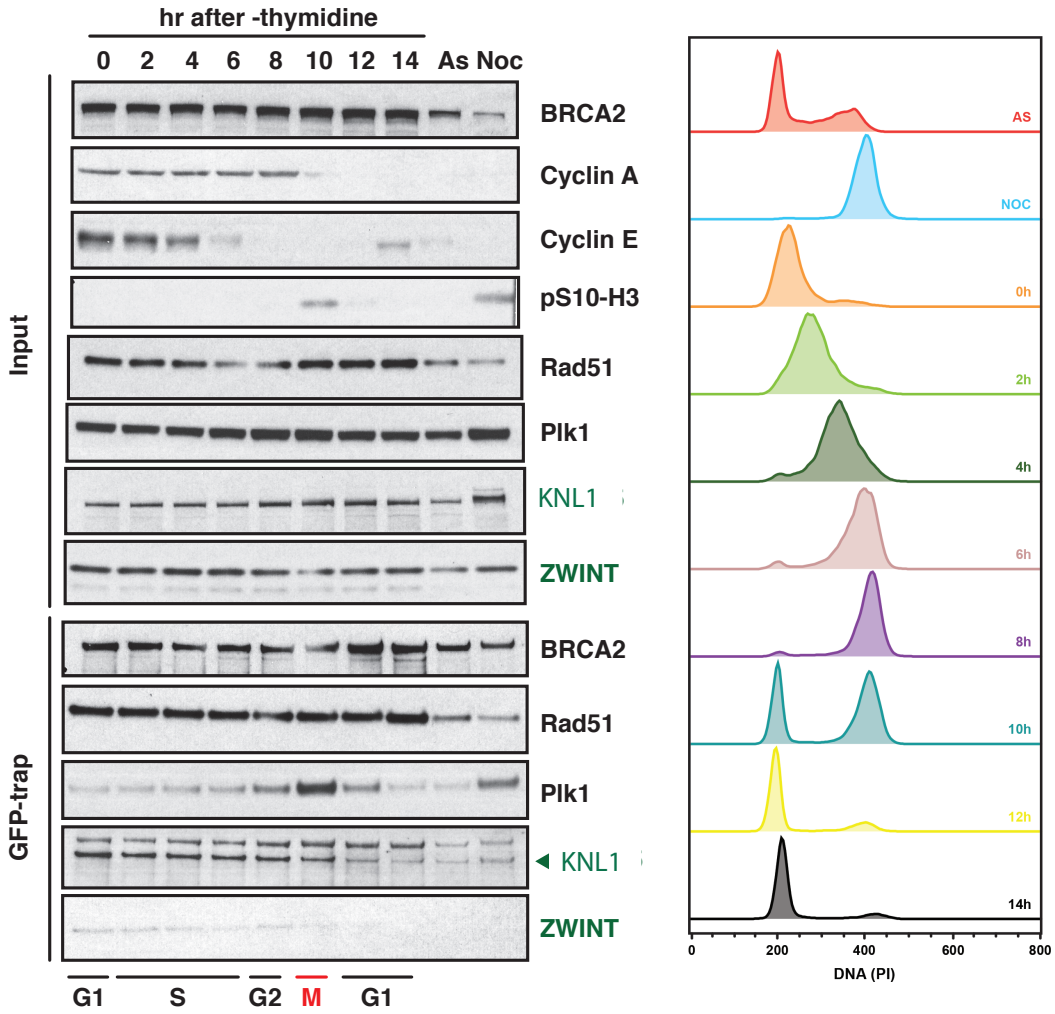


Figure 5.2: **BRCA2 binding partners in synchronised culture**. HeLa NFLAP-BRCA2 cells were synchronised by double thymidine-block release, and BRCA2 kinetochore-binding partners were analyzed (KNL1 and ZWINT). Cell-cycle progression was monitored by cell-cycle markers cyclin E (for G1/S), cyclin A (for S/G2), Plk1 (for S/G2/M), pS10-H3 (for M) and by FACS. Data shown in this figure was generated by Dr. Fumiko Esashi.

Following the mass-spectrometry analysis, I hypothesised that BRCA2 could be recruited at actively transcribed centromeric regions, and through an interaction with kinetochore components could control the timing of chromosome segregation in mitosis. Since BRCA2-kinetochore interaction was enriched in S phase, when kinetochores components start to be recruited at centromeres, I hypothesised that BRCA2 was involved in the recruitment of the kinetochore components at centromeres during this phase of the cell cycle. To this end, I initially aimed to characterise the localisation of

the BRCA2 and kinetochore components during the cell cycle.

5.1.1 The challenge of detecting BRCA2

Endogenous BRCA2 is a nuclear localised protein. Its enrichment in the nuclear fraction was shown by cellular fractionation followed by Western blot in T24 human bladder carcinoma cells [83] and U2OS human osteosarcoma cells [97]. However, the detection of BRCA2 by imaging analysis is still quite challenging. BRCA2 is expressed throughout the cell cycle but its expression is relatively low. In imaging analysis, BRCA2 has been detected under DNA damaged condition [97] [129]. In S phase, BRCA2 forms characteristic nuclear foci, which colocalise with DNA repair proteins (i.e. PALB2 and BRCA1) [97] [83]. Under DNA damage conditions, such as ionising radiation (IR) and ribonucleotide reductase inhibitor, hydroxyurea (HU) treatment, the formation of BRCA2 foci was detectable inside the nucleus and they colocalised with DNA damage marker (γH2AX) [97] [83]. However, the BRCA2 localisation in interphase in unperturbed condition is still poorly described.

Previous studies reported BRCA2 localisation at the midbody in undamaged cells in mitosis [113]; however, this localisation was questioned by the specificity of the antibody [114]. Following studies confirmed the specificity of the antibody following siRNA treatment and BRCA2 localisation at the midbody [115]. However, IF experiments have several limitations. They rely on the specificity of the antibody and they can not be used to study the dynamics of the protein in live cell imaging. The generation of a new cell line expressing GFP-BRCA2 allowed workers to study the cellular localisation of BRCA2 in several studies [114] [116]. HeLa NFLAP-BRCA2 cells carry a bacterial artificial chromosome (BAC) containing the BRCA2 locus, in which the BRCA2 gene is fused to the FLAP-tag at the N terminus (NFLAP) [114]. The tagging cassette consists of a FLAG-epitope and enhanced green fluorescent protein (EGFP). HeLa Kyoto NFLAP-BRCA2 cells were used in the previous mass spectrometry experiments and synchronised cultures after GFP pull-down (Figure 5.1 5.2). Using this cell

line, I tried to visualise BRCA2 in unperturbed conditions in interphase cells. After fixation, however, the GFP-BRCA2 signal appeared quite faint in control-treated cells (Figure 5.3A). Furthermore, it was noticed that the fluorescent signal localised outside the nucleus, likely due to the overexpression of the protein. To verify the specificity of the signal, cells were treated with siRNAs against BRCA2: siBRCA2 treatment showed depletion of the protein by Western blot (Figure 5.3B); however, the GFP signal was only partially reduced inside the nucleus (Figure 5.3C).

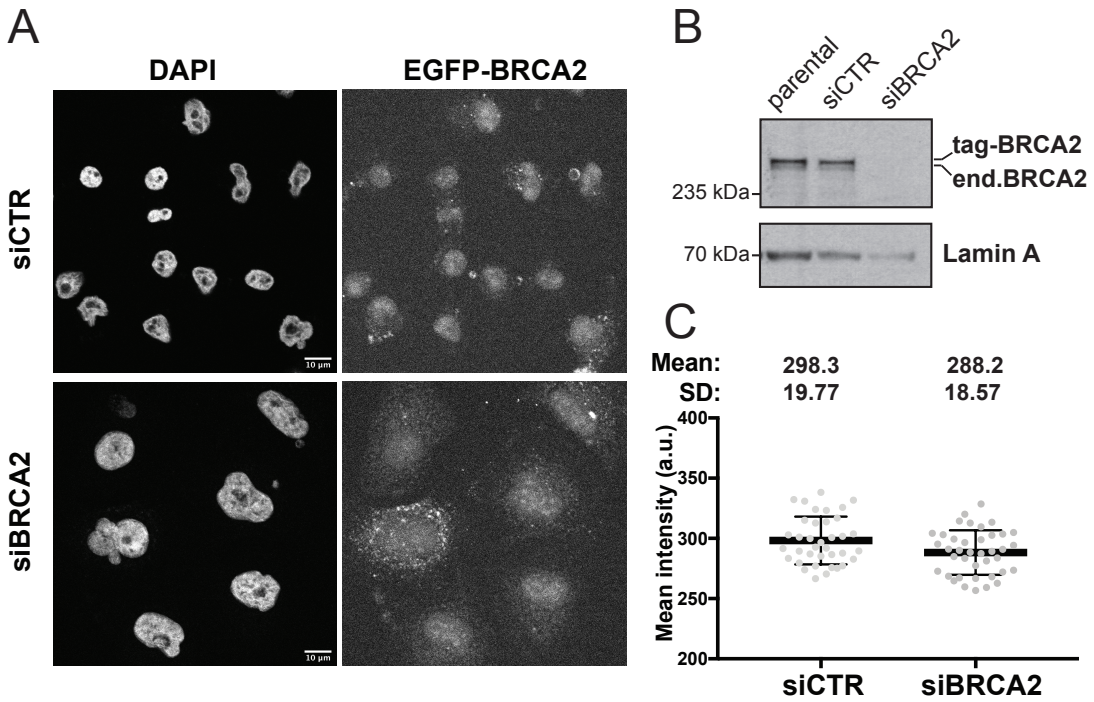


Figure 5.3: **Imaging analysis of HeLa Kyoto NFLAP-BRCA2 cells**. (**A**) Representative images of the GFP-BRCA2 signal. Cells were transfected with non-targeting siRNA (siCTR) and siRNA against BRCA2 (siBRCA2). Cells were fixed in 4% PFA. (**B**) Protein expression was analysed 72 h after siRNA treatment by Western blot using BRCA2 antibodies. Lamin A as a loading control. (**C**) Quantification of EGFP-BRCA2 mean intensity inside the nuclear area. 37 cells were analysed for siCTR, 39 cells were analysed for siBRCA2. Mean and SD of a single experiment.

Due to the difficulties of visualising BRCA2 signal with the existing method, I decided to generate a new CRISPR-modified cell line to enable the detection of the endogenous BRCA2. Using this system, initial experiments were performed to characterise the BRCA2 localisation in damaged and undamaged condition during the cell cycle. Furthermore, BRCA2 was tagged with an auxin-inducible degron (mAID) for the rapid de-

pletion of the protein, which allowed rapid depletion of the protein within few hours.

5.2 Results

5.2.1 Generation of CRISPR-modified cell lines for BRCA2 tagging

In order to generate a new system, which allows to study the localisation and the function of endogenous BRCA2 during the cell cycle, CRISPR-modified cell lines were generated and characterised as a joint effort of several laboratory's members (i.e., Chris Ralf, Fumiko Esashi, Xanita Saayman, Lucia Rampazzo and Marjorie Fournier, Emily Graham and Jacob Wall). The N-terminus of *BRCA2* locus was tagged with an mAID-Halo construct (Figure 5.4A). The mAID tag is a small fragment of the auxin-inducible degron (AID). When exposed to auxin in the medium, mAID-tagged proteins can be recognised by the TIR1-ubiquitin ligase complex, and subsequently rapidly ubiquitinated and degradated by the proteasome within 10-20 min [205]. The Halo tag is a small peptide (33 kDa), which binds synthetic ligands that can be used for imaging and molecular analysis [279]. Clonal cell lines of chromosomally stable human colorectal cancer HCT116 cells expressing mAID-Halo tag were initially generated. The selected positive clone (IV-E6) showed expression of the Halo-construct by Western blot, which is almost completely removed after 2 h with auxin treatment (IAA) (Figure 5.4A). Cells treated with IAA showed reduced survival upon treatment with the DNA damaging agent, mitomycin C (MCC) (Figure 5.4B). This result suggested that the Halo-tag BRCA2 is able to protect the DNA behaving as the endogenous protein. Imaging analysis with several Halo-ligands (i.e. TMR-Direct, Oregon-Green, Janelia Fluor), however, failed to detect BRCA2 inside the nucleus either in undamaged or damaged conditions with IR (Figure 5.4B). Conversely, cells expressing a Halo-tagged sister chromatid cohesin (SCC1) [280], used as positive control, showed visible nuclear staining, suggesting that the protocol used with Halo-ligand successfully permeated the nuclear membrane.

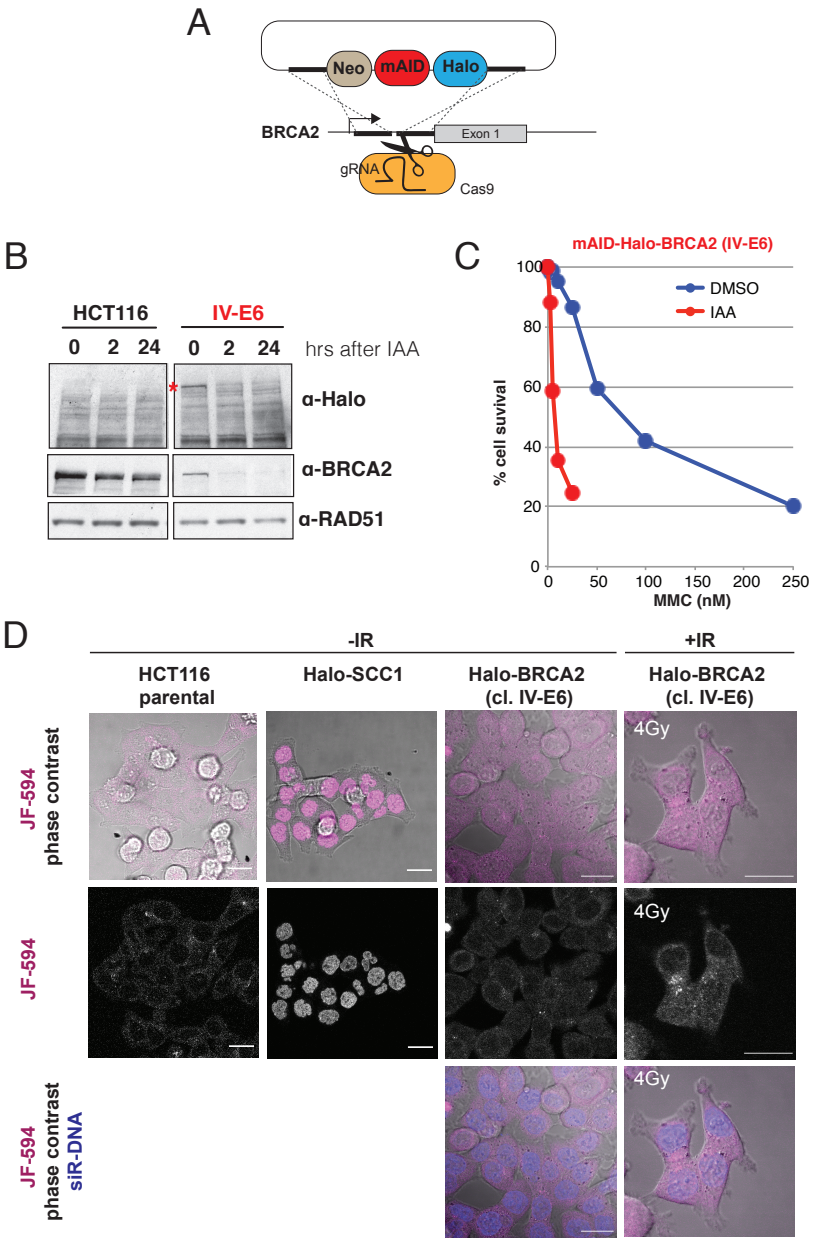


Figure 5.4: **Generation of CRISPR-modified HCT116 mAID-Halo-BRCA2 cell line**. (**A**) Schematic representation of mAID-Halo construct used to generate CRISPR-modified cell lines. Site of cleavage by the Cas9 was directed by a gRNA at the 5'-end of the *BRCA2* locus. The homology arms (black thick lines), fused upstream and downstream of the neo-mAID-Halo construct, allow the homology-directed integration of this construct at the *BRCA2* locus. The DNA break was repaired using Neo-mAID-Halo tag-containing template. Neomycin resistance (Neo) was used for the drug selection. mini-Auxin Inducible Degron (mAID). Halo-tag (Halo). (**B**) Western blot showing protein expression of HCT116 parental cells (black) and mAID-Halo-BRCA2 positive clone (IV-E6, red). Auxin (AII) (0.5 μM). Data shown in C was generated by Dr. Fumiko Esashi. (**C**) Survival assay in cells treated with IAA and DMSO (negative control) upon mitomycin C (MCC) exposure. Data shown in D was generated by Dr. Marjorie Fournier. (**D**) Live cell imaging of mAID-Halo-BRCA2 (IV-E6) using Halo-ligand Janelia Fluor 594. HCT116 parental cell line (negative control). HCT116 Halo-SCC1 (positive control) [280]. IV-E6 in unperturbed and perturbed conditions using ionising radiation (IR) (4Gy). Nuclear BRCA2 foci were not detectable inside the nucleus. Where indicated, nuclei were detected with nuclear staining siR-DNA. Scale bar, 20 μm.

To overcome the problem of staining with the Halo-ligand, I replaced the Halo-tag with a fluorescent tag mNeonGreen (Figure 5.5A). mNeonGreen is a monomeric green fluorescent protein three times brighter than GFP and more stable than EGFP [281]. Thus, it is suitable for confocal microscopy and it can be used to tag proteins with a low level of expression. Furthermore, the neomycin resistance gene was replaced with hygromycin resistance gene. In the first round of CRISPR screening it was noticed that neomycin concentration (700 μg/ml) appeared to kill almost all transfected cells. Thus, it is likely that the low level of expression of neomycin resistance gene, which was under the native BRCA2 promoter, did not confer enough resistance. Following these results, CRISPR screening was done with no or low drug concentration (50 μg/ml hygromycin) and screening was performed using the fluorescence expression by FACS followed by PCR. CRISPR-modified cells were generated in three different backgrounds: parental HCT116 cells, HCT116 cells expressing OsTIR1 under a tetracycline-inducible promoter (Tet) and HCT116 with constitutive expression of OsTIR1 under a CMV promoter. Single cells were selected by single-cell sorting for mNeonGreen positive cells (Figure 5.5B). The growing colonies were screened with two steps of PCR to assess the integration of the full-length construct in both alleles. The first step of PCR was performed using primers flanking the region of integration (primer a and b in Figure 5.5A): Figure 5.5C shows a representative gel, in which several clones were tested. Clones with integration of construct at both alleles showed a single band at around 4,500 Kb (red asterisks). Positive clones were further tested with a combination of other three different primers to assess the integration of the different parts of the constructs (primers: a+c, a+d) and the removal of the backbone plasmid (primers: e+c) (Figure 5.5D). Two positive clones were finally selected: IIE clone, which was generated in parental HCT116 cells; and IIF clone, which was generated in cells expressing OsTIR1 under the CMV promoter. No clones were successfully generated in cells expressing OsTIR1 with Tet promoter. The protein expression of the positive clones was confirmed by Western blot using BRCA2 antibody. mNeonGreen-BRCA2 expressing cells showed a band at higher molecular weight compared to HCT116 parental cells. Upon auxin (IAA) exposure, more than 50% of BRCA2

protein was depleted at two hours after treatment.

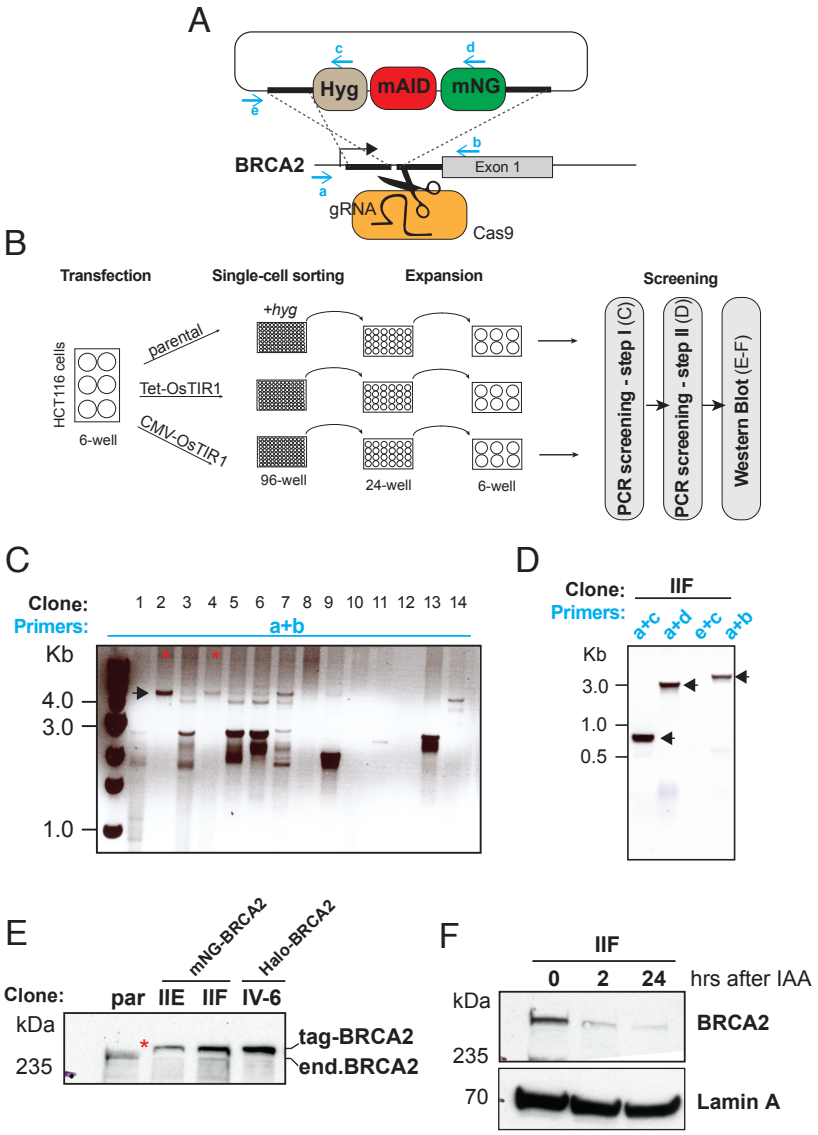


Figure 5.5: **Generation of CRISPR-modified HCT116 mAID-mNeonGreen-BRCA2 cell line**. (**A**) Schematic representation of mAID-mNeonGreen construct used to generate CRISPR-modified cell lines. Site of cleavage by the Cas9 was specified by a gRNA at the 5′-end of the *BRCA2* locus. The homology arms (black thick lines), fused upstream and downstream of the hyg-mAID-mNG construct, allow the homology-directed integration of this construct at the *BRCA2* locus. The DNA break was repaired using Hyg-mAID-mNG tag-containing template. Hygromycin resistance (Hyg). mini-Auxin Inducible Degron (mAID). mNeonGreen-tag (mNG). Primers used for PCR screening in C and D (light blue arrows). (**B**) Schematic representation of the steps for the generation of CRISPR-modified clones. (**C**) Representative gel of electrophoresis of the PCR screening - step I. Genomic DNA was amplified using primers a and b. Positive clones (red asterisks). Expected band is indicated by a black arrow. (**D**) Representative gel of electrophoresis of PCR screening - step II. Genomic DNA using primers sets, a+c, a+d or a+b, to test the integration of the construct and e+c primers to test the removal of the backbone plasmid. Expected bands are indicated by black arrows. (**E**) Western blot of mNG-BRCA2 cell lines: HCT116 parental cell line (par) as negative control, HCT116 parental mAID-mNG-BRCA2 (clone IIE), HCT116 CMV-OsTIR1 mAID-mNG-BRCA2 (clone IIF), HCT116 CMV-OsTIR1 mAID-Halo BRCA2 (clone IV-E6). BRCA2 was detected using anti-BRCA2 antibodies. Tagged BRCA2 is highlighted with red asterisk. (**F**) Protein depletion of mAID-mNG-BRCA2 IIF upon 0, 2, 24 h of auxin treatment (AII) (0.5 μM).

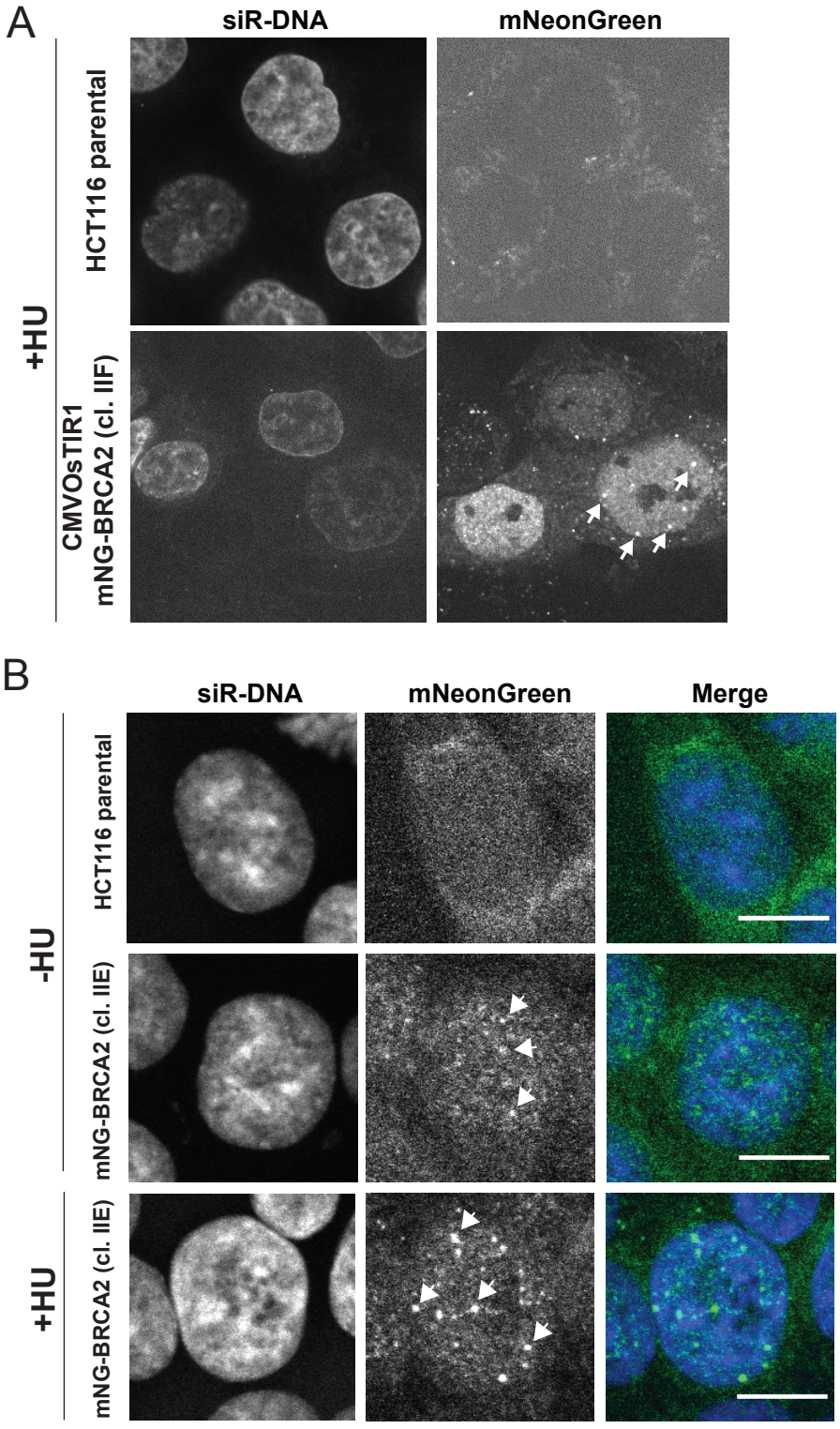


Figure 5.6: **mNeonGreen-BRCA2 localisation in the presence and absence of HU**. (**A**) Live cell imaging of HCT116 CMV-OsTIR1 mAID-mNG-BRCA2 clone IIF upon hydroxyurea (HU) treatment (2 mM for 16 h). siR-DNA was used for nuclear staining. (**B**) Imaging analysis of BRCA2 signal after fixation of HCT116 parental mAID-mNG-BRCA2 clone IIE in the presence and absence of HU (2 mM for 16 h). Arrows indicate BRCA2 foci inside the nucleus. Scale bar, 10 μm.

Imaging analysis revealed that mNeonGreen-BRCA2 was localised in the nucleus and formed foci inside the nucleus upon hydroxyurea (HU) treatment (Figure 5.6A). It was noticed that the fluorescent signal was not homogeneous in the whole population. After fixation, the fluorescent signal inside the nucleus was reduced compared to live cell imaging; however, it was still possible to detect fluorescent signal inside the nucleus compared to the parental cell lines in both unperturbed and perturbed (HU treated) conditions (Figure 5.6B). In unperturbed conditions, the BRCA2 signal inside the nucleus was more faint and diffuse and most of the cells in interphase presented few BRCA2 foci, which partially colocalised with DNA damage marker (γH2AX) (Figure 5.7A). In mitotic cells, BRCA2 did not appear to localise withγH2AX foci (Figure 5.7B). In HU treated cells, increased nuclear BRCA2 foci formation, which mostly colocalised with γH2AX, was detectable. Nonetheless, a few γH2AX-independent BRCA2 foci were detectable (Figure 5.6C).

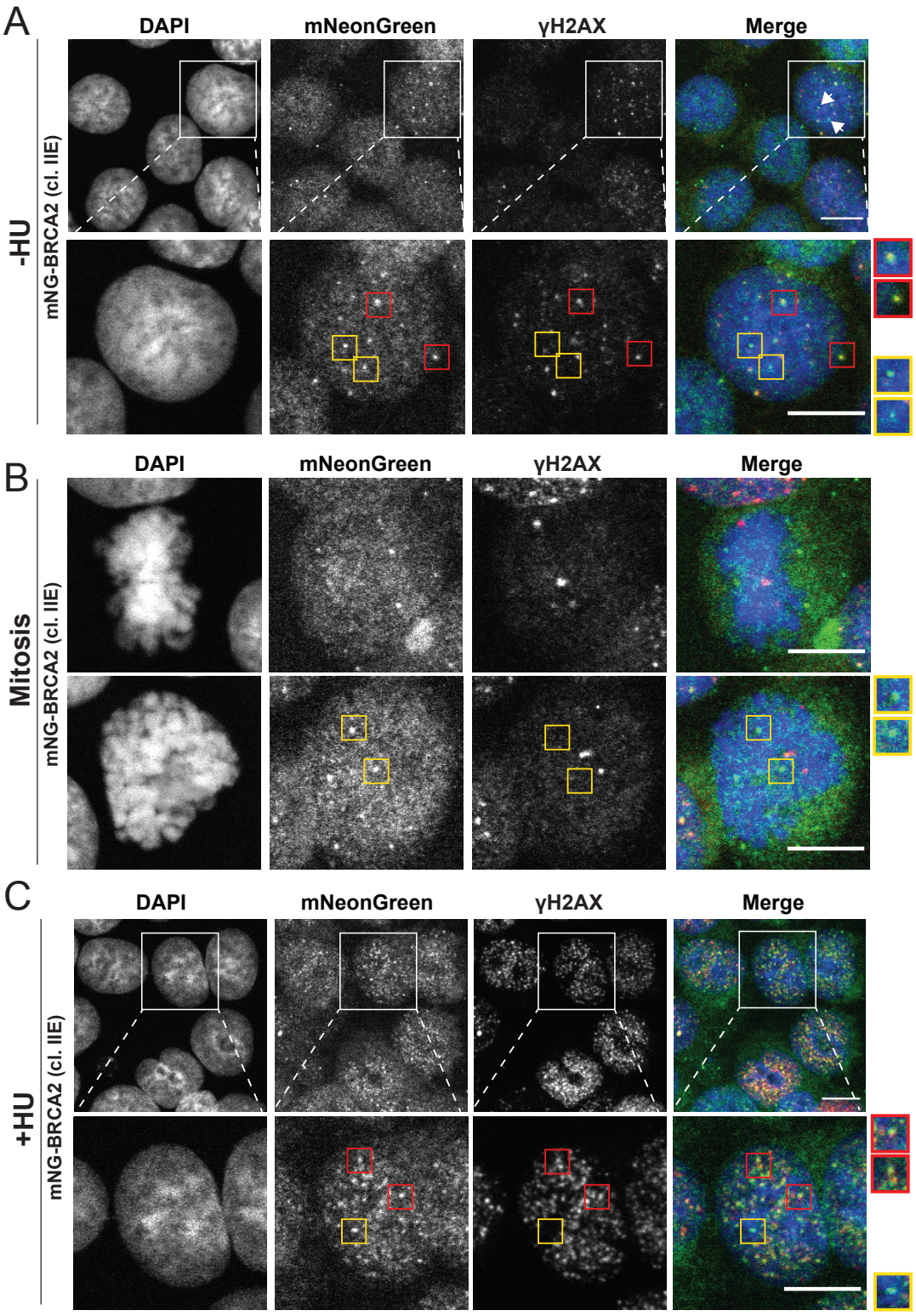


Figure 5.7: **Localisation of mNeonGreen-BRCA2 with DNA damage marker during the cell cycle**. Interphase (**A**) and mitotic (**B**) cells expressing mNeonGreen-BRCA2 (clone IIE) were fixed without and with HU treatment (2 mM for 16 h) (**C**). DNA damage was detected using γH2AX antibody. Nuclear BRCA2 foci which colocalise with γH2AX foci were indicated with red squares. Nuclear BRCA2 foci detected which do not colocalise with γH2AX foci were indicated with yellow squares. Scale bar, 10 μm.

5.2.2 BRCA2 localisation with kinetochore and centromere components during the cell cycle

The CRISPR-modified cell lines were used to assess the BRCA2-kinetochore localisation during the cell cycle. Kinetochore proteins were detected using monoclonal antibodies for human DSN1 and NSL1, kindly provided from Dr. M. Yanagida's laboratory [282] [283]. A few nuclear BRCA2 foci colocalised with DSN1 and NSL1 in interphase cells (Figure 5.8A-B). In mitotic cells, BRCA2 foci were predominantly excluded from chromosomes and were not found to colocalise either with DSN1 or NSL1 antibodies (Figure 5.8). Similarly, ACA antibodies were used to detect centromeres during the cell cycle. Cyclin B staining was used to distinguish cells in G2 phase (Figure 5.9). A few colocalisation of ACA foci and BRCA2 foci were detectable in interphase cells, but not in mitotic cells (Figure 5.9). Only in very rare cases, mitotic cells were found to have one or two BRCA2 foci that colocalised with NSL1 and ACA antibodies. Overall, these results showed that BRCA2 localisation at kinetochores/centromeres (if any) occurs in interphase cells, suggesting that this interaction may be cell-cycle regulated.

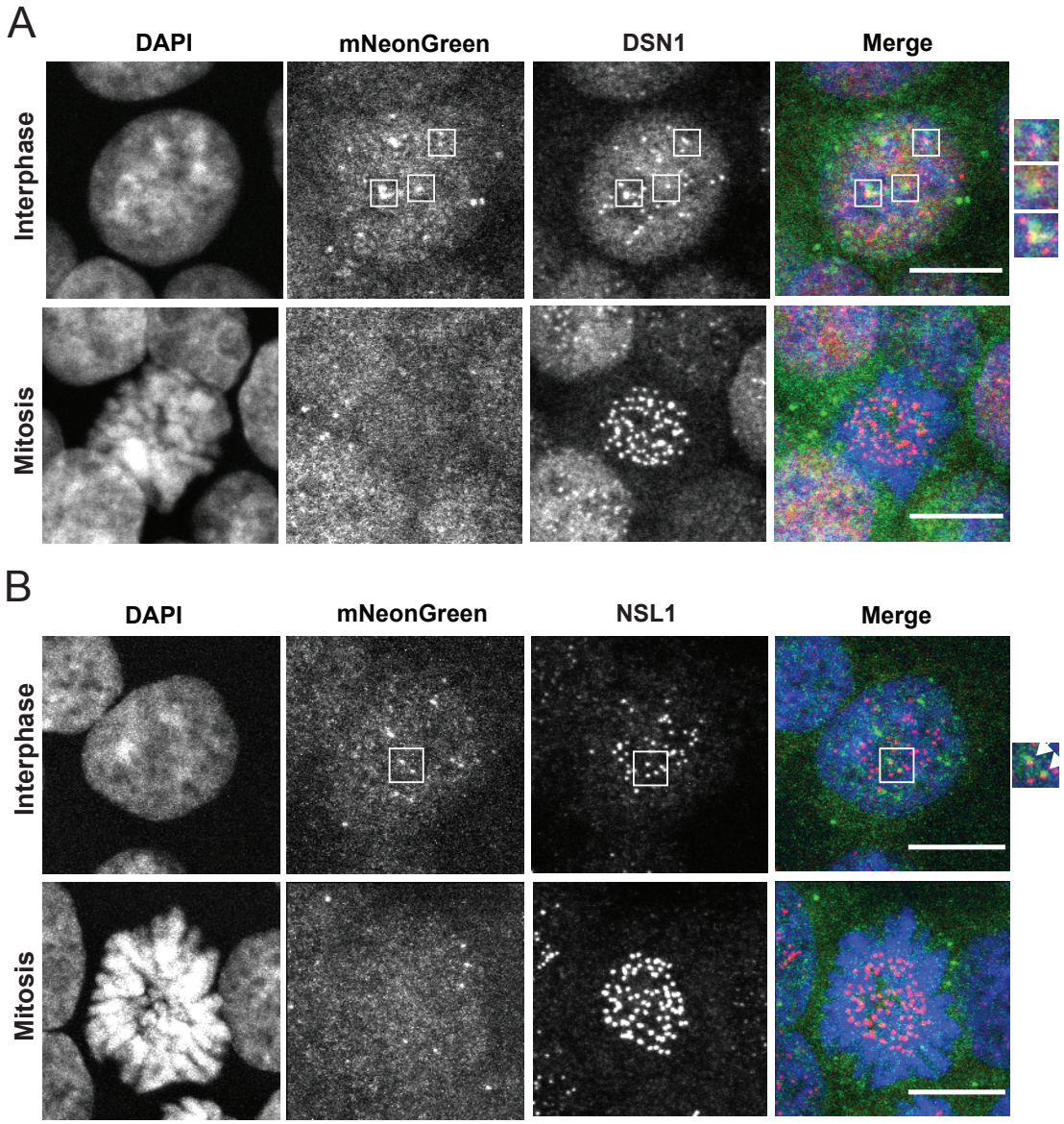


Figure 5.8: **Localisation of mNeonGreen-BRCA2 with MIS12 complex during the cell cycle**. Interphase and mitotic cells expressing mNeonGreen-BRCA2 (clone IIE) were fixed and stained with monoclonal hMIS13 and hMIS14 antibodies to detect DSN1 and NSL1, respectively. Colocalisation of BRCA2 foci and DSN1 and NSL1 foci was indicated with white squares. Scale bar, 10 μm.

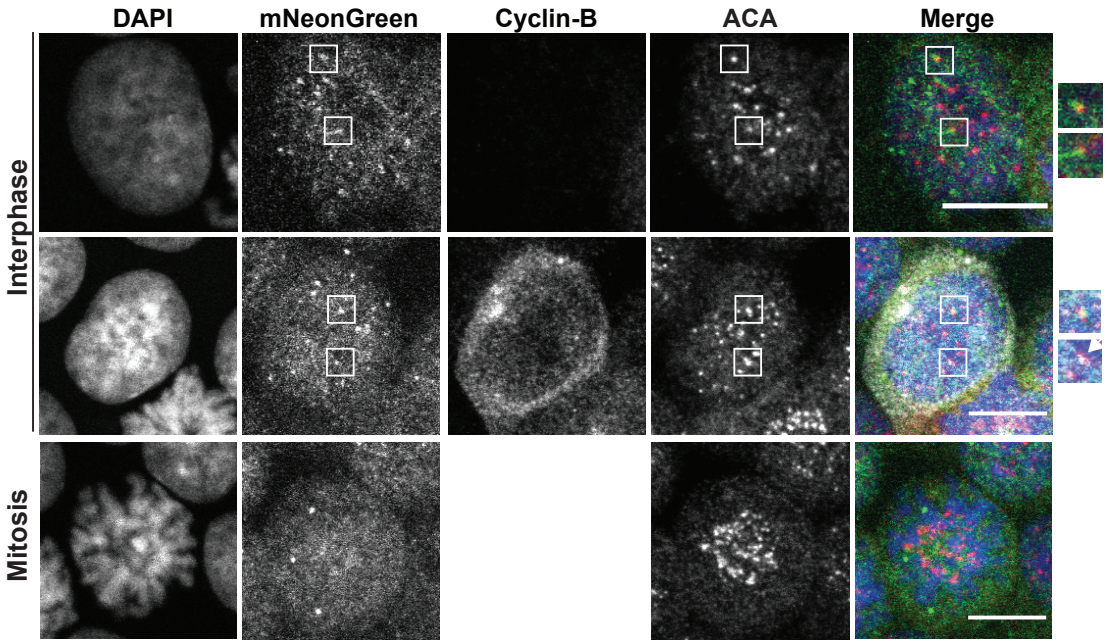


Figure 5.9: **Localisation of mNeonGreen-BRCA2 with centromeres during the cell cycle**. Interphase and mitotic cells expressing mNeonGreen-BRCA2 (clone IIE) were fixed and stained with human-ACA antibody to detect centromeres. Cyclin B was used as a marker of G2 phase. Colocalisation of BRCA2 foci and ACA foci was indicated with white squares. Scale bar, 10 μm.

5.2.3 Effect of BRCA2 depletion on kinetochore recruitment at centromeres

BRCA2 depleted cells showed moderate whole-chromosome loss in Chapter 3. However, depletion of the other HR factors, RAD51 and PALB2, did not show similar chromosome loss suggesting that BRCA2 may have an HR-independent function which is important to maintain chromosomal stability. Furthermore, BRCA2 depletion in HT1080 and HeLa cells led to an increase of the cell population in early mitosis. This is the time of the cell cycle when the SAC is activated allowing microtubules-kinetochores attachment. Thus, I hypothesised that BRCA2 may have an HR-independent function, which is important for the stable establishment of the kinetochore proteins at centromeres. Its depletion may affect kinetochore recruitment and slow down the mitotic progression. As the interaction between BRCA2 and kinetochore-associated proteins appeared to peak in S phase and DSN1 was the most enriched kinetochore-associated proteins in the BRCA2 interactome in S phase (Figure 5.1), I tested whether BRCA2 de-

pletion affected DSN1 recruitment at centromeres in S phase in HeLa NFLAP-BRCA2 expressing cells. The incorporation of a thymidine analogue, 5-Ethynyl-2'-deoxyuridine (EdU), was used to detect cells in S phase (Figure 5.10A). The Pearson's correlation coefficient (PCC) [254] was measured to assess the colocalisation between DSN1 and centromere marker (ACA) in the presence or absence of BRCA2 following siRNA treatment. BRCA2 depleted cells exhibited a similar distribution of DSN1 and ACA signal in S phase both in siCTR and siBRCA2 treated cells. (Figure 5.10A). Moreover, preliminary experiments were performed to detect the kinetochore localisation in mitotic cells in the presence and absence of BRCA2. BRCA2 depleted cells showed similar localisation of DSN1 at centromeres compared to siCTR treated cells (Figure 5.10B).

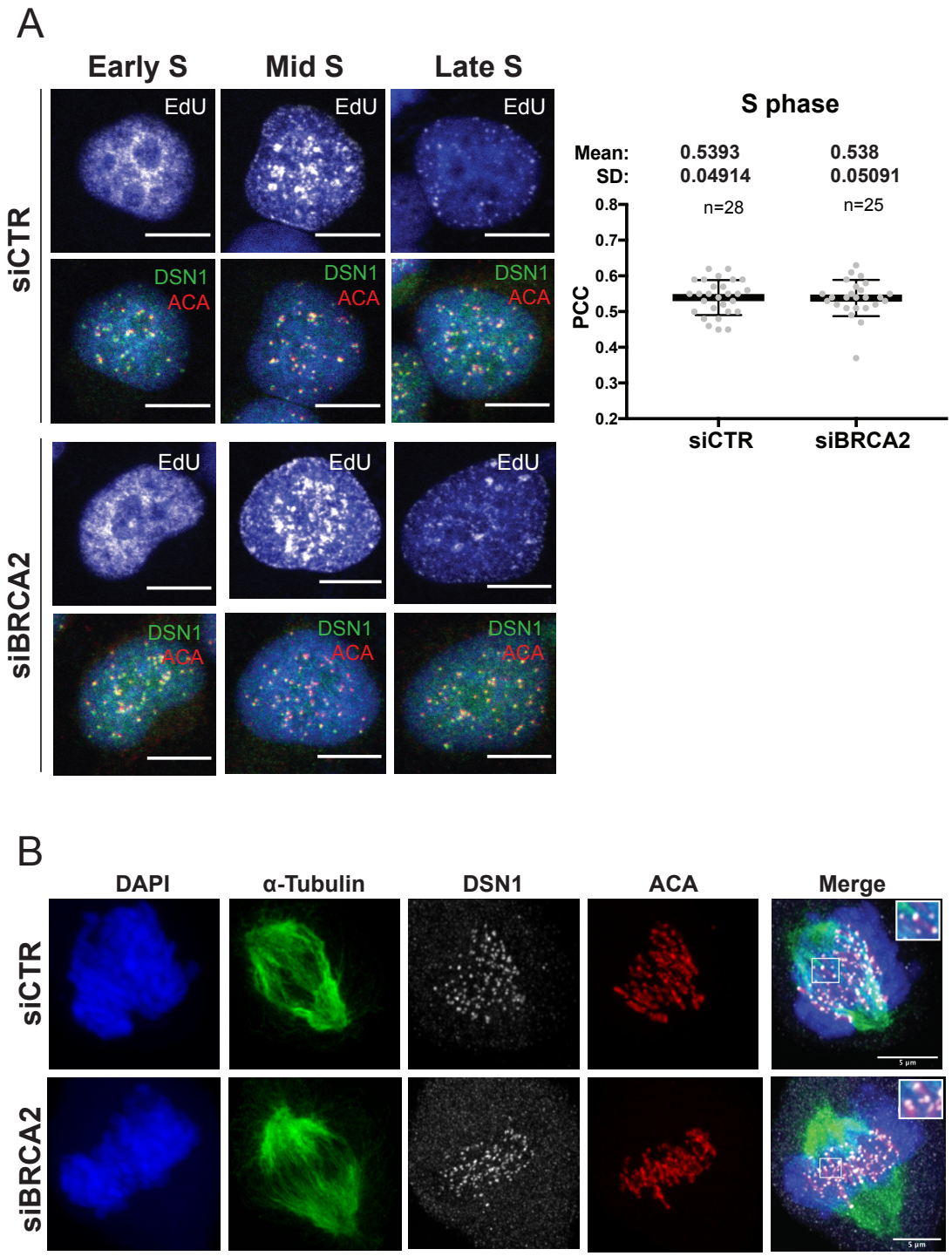


Figure 5.10: **Effect of BRCA2 depletion on DSN1 recruitment at centromeres during the cell cycle**. (**A**) HeLa Kyoto NFLAP-BRCA2 cells were transfected with a non-targeting siRNA (siCTR) and siRNA against BRCA2 (siBRCA2). At 48 h after transfection, cells were incubated with EdU to distinguish cells in S phase. Cells were stained with DSN1 (hMIS13) and ACA antibodies to detect kinetochore and centromeres, respectively. Pearson's colocalisation coefficient (PCC) was used to quantify DSN1-ACA colocalisation in EdU positive cells. n represents the number of cells analysed in a single experiment. Mean and SD were reported on the graph. (**B**) Representative figure of of HeLa NFLAP-BRCA2 cells 48 h after tranfection with siCTR and siBRCA2. Cells were incubated with α-Tubulin, DSN1 and ACA antibodies to detect microtubules, kinetochores and centromeres, respectively.

5.3 Discussion

Experiments conducted in the laboratory of Dr. Fumiko Esashi identified kinetochore-associated proteins as new BRCA2 binding partners in the S phase (Figure 5.1), and this interaction was down-regulated upon DNA damage treatments. These results showed, for the first time, that BRCA2 interacts with cellular components that are directly linked with chromosome segregation and opened up the possibility that the function of BRCA2 at these regions may be independent from its previously well-characterised function in DNA repair. Indeed, some BRCA2 foci were found to localise outside the DNA damage marker in interphase cells (Figure 5.7A-B). However, it is also possible that BRCA2 foci localised at sites of DNA stress which were not detected by the general DNA damage marker, γH2AX. To further confirm the hypothesis that BRCA2-kinetochore interaction occurs independently of DNA damage, in future, it would be beneficial to co-stain HCT116 cells expressing mNeonGreen-BRCA2 with kinetochore and γH2AX antibodies to observe whether BRCA2 and kinetochore foci colocalise independently of the γH2AX foci.

Initial experiments using synchronised cultures have shown that BRCA2-kinetochore interaction occurs predominantly in S phase and it is reduced in mitosis (Figure 5.2). In agreement with this result, some BRCA2 foci were found to have colocalised with DSN1 and NSL1 foci in interphase cells but not in mitotic cells (Figure 5.8A-B). However, the colocalisation was detected only in a few kinetochore foci. This result may suggest that the BRCA2-kinetochore interaction could be a dynamic event or it occurs at specific chromosomes, such as acrocentric chromosomes. Similarly, BRCA2 foci were rarely detectable at centromeres in interphase cells (Figure 5.9). Since kinetochore components of the MIS12 complex can be recruited at centromeres in interphase [195], it is possible that the BRCA2-kinetochore interaction occurs at centromeres. To confirm this hypothesis, mNeonGreen-BRCA2 expressing cells could be co-stained with DSN1/NSL1 and ACA antibodies. Furthermore, to better characterise the time of BRCA2-kinetochore interaction, BRCA2-kinetochore colocalisation can be tested in synchronised cultures and using different cell-cycle markers in IF experiments or gen-

erating stable cell lines expressing fluorescently labelled kinetochore proteins to analyse their localisation in live cell imaging.

The recruitment of the kinetochore components of the MIS12 and KNL1 complexes at centromeres was shown to start in S phase [195]. This appeared to be reduced upon treatment with a CDK inhibitor [195]; however, how the kinetochore components are recruited at centromeres at the right time and space is still not fully understood. In this context, it is possible that BRCA2 may mediate the kinetochore formation at centromeres. One of the hypotheses that I started to investigate in this chapter was whether BRCA2 depletion affects kinetochore localisation of the MIS12 complex at centromeres. Initial experiments showed that BRCA2 depletion did not affect the kinetochore localisation at centromeres in S phase and in mitotic cells (Figure 5.10A-B). However, appropriate quantification of the amount of DSN1 signal at centromeres in mitotic cells needs to be carried out. During these experiments, it was noted that the DSN1 signal was found to correlate slightly less with centromeres in the absence of BRCA2 in cells not stained with EdU (data not shown), suggesting that BRCA2 depletion may affect the MIS12 localisation at centromeres in other cell cycle stages. EdU negative cells could be either in G1 or G2 phase. Further experiments using different cell cycle markers of the G1 and G2 phase could confirm whether BRCA2 depletion affects kinetochore recruitment at centromeres during these phases of the cell cycle. Moreover, localisation of other kinetochore components could be assessed in the future. One of the reasons why BRCA2 depletion did not show any detectable effect on kinetochore localisation at centromeres may be due to the fact that kinetochores are recruited at centromeres through two independent pathways mediated by CENP-C and CENP-T. It is possible that BRCA2 is involved in one of the two pathways and the inhibition of one can be compensated by the other. In the future, it would be interesting to test whether BRCA2 depletion may affect kinetochore localisation in combination with CENP-T or CENP-C depletion.

On the other hand, it is also possible that BRCA2 is not involved in the recruitment but in preventing kinetochore recruitment at centromeres (or other parts of the genome)

before mitosis. According to this hypothesis, it is possible that BRCA2-kinetochore interaction is down-regulated in mitosis to allow the complete kinetochore formation, and BRCA2 removal may possibly favour the kinetochore localisation at centromeres, leading to a stronger association of kinetochore proteins at centromeres. In previous studies, it has been shown that NSL1 binds HP1α in HeLa cells, the heterochromatin protein that is enriched at pericentromeres [283]. Depletion of HP1α by siRNA reduced the level of NSL1 at kinetochores in mitotic cells [283]. In Chapter 4, I showed that BRCA2 depletion increased HP1 signal at centromeres (Figure 4.20). In this context, it is possible that increased HP1 signal in BRCA2 depleted cells may enhance kinetochore recruitment at centromeres.

5.3.1 A new system to study BRCA2 localisation in time and space

To investigate the localisation and function of BRCA2, CRISPR-modified cell lines were generated. Previous methods to detect BRCA2 localisation involved the use of BRCA2 antibodies or the exogenous expression of the fluorescently labelled protein [97] [114]. However, these methods have several limitations: the antibody-based methods cannot be used to study the dynamics of the protein and the accurate detection of the protein depends on their specificity; whereas exogenously expressed proteins could potentially behave differently from endogenous proteins. Moreover, in both these methods, RNAi-mediated protein depletion does not allow us to study the function of the protein within a short-time period.

To tackle these problems, CRISPR-modified cell lines were generated to tag the endogenous BRCA2, such that the detection of the endogenous protein and its rapid depletion could be achieved. Initially, a Halo-tag was introduced at the N-terminus of BRCA2. Despite the fact that Halo-BRCA2 was detectable by Western blot, none of the Halo-ligands tested in these studies (i.e. TMR-Direct, Oregon-Green and Janelia Fluor) were able to detect the BRCA2 signal by imaging analyses. Nevertheless, the protocol appeared to allow efficient detection of the highly-expressed nuclear-localised protein

Halo-SCC1. Thus, it is possible that the level of protein expression may affect the ability to detect Halo-ligands. Moreover, the protocol for Halo-ligand staining requires a step of permeabilisation of the membranes to allow the internalisation of the ligand and several washes for the removal of the unbound molecules. These steps could be more challenging to optimise with proteins that are expressed at a low level and are localised in the nucleus.

The use of the mNeonGreen (mNG) tag, a brighter and more stable tag compared to EGFP, allowed the detection of BRCA2 in live cells and after fixation. mNG-BRCA2 expressing cells were successfully generated in two different backgrounds. Clone IIE was generated in a HCT116 parental cell line and clone IIF was generated in HCT116 cells expressing CMV-OsTIR1. While clone IIF can be used for the rapid depletion of the protein after 2 h of auxin treatment, this was less suitable for imaging analysis due to leakiness of the OsTIR1 system. Indeed, OsTIR1 is under the expression of a CMV promoter, which possibly leads to protein degradation even in the absence of auxin. Furthermore, high cell density/confluency appeared to reduce the expression of mNG-BRCA2. Using clone IIE, the mNG-BRCA2 signal was detected in live cells and after fixation. BRCA2 appeared to be mostly diffused inside the nucleus without DNA damage, and BRCA2 foci were partially localised at DNA damage sites stained by γH2AX.

To the best of my knowledge, the HCT116 mAID-mNeonGreen-BRCA2 cells are the first CRISPR-modified cell line in which endogenous BRCA2 is tagged. These can allow for the rapid depletion of the protein and studies of its localisation. In future, this system could be used to elucidate the function of BRCA2 during the cell cycle and to understand whether its function in G1-S-G2 or M phase is essential for the maintenance of chromosomal stability.

Chapter 6

Discussion and Conclusions

6.1 Summary of thesis

Chromosomal instability (CIN) is one of the most harmful features of cancer cells. Understanding the molecular mechanisms that preserve the transmission of the genetic information encoded in the human chromosomes is essential in order to prevent cancer development and maintain lifelong health and well-being.

The breast cancer 2 gene (*BRCA2*) was discovered to be mutated in patients with a family history of breast cancer [56]. Later on, mutations of the *BRCA2* locus were also found to be associated with other types of cancer, such as prostate, ovary and pancreatic cancer. BRCA2-deficient cancer cells show CIN characterised by alterations in the chromosome structure and number. Structural CIN in BRCA2-deficient cells has been proposed to be caused mainly by impaired DNA repair functions during replication. BRCA2-deficient cancer cells also show abnormal chromosome numbers, micronuclei formation, lagging chromosomes and multipolar spindles. These phenotypes are commonly associated with defects during mitosis. Despite the fact that several functions have been proposed for BRCA2 in mitosis, it is still not fully understood how BRCA2 defects can lead to aneuploidy. More precisely, it is still not clear in which phase of the

cell cycle BRCA2 plays its essential role in preserving chromosomal stability. Despite its well-described function to protect genome integrity during replication, it has been reported that BRCA2 defective cells exhibited G1 arrest followed by apoptosis rather than G2 arrest, highlighting a possible fundamental role of BRCA2 in mitosis. This complexity has resulted in increased attention being given to the topic by the scientific community working in this field. In this context, the work presented in this thesis tries to shed light on these questions. In this thesis, I described previously uncharacterised features of BRCA2-deficient cells. In the following sections, I will discuss the key findings of my research, the questions that still remain open and I will propose some future work to further elucidate the proposed hypotheses.

6.1.1 BRCA2 regulated RAD51-mediated recombination at centromeres

The experiments conducted in Chapter 3 showed that BRCA2 depletion leads to a mild but consistent increase of HAC loss with different techniques (i.e., FACS and FISH). Notably, HAC loss was not consistently observed upon RAD51 and PALB2 depletion in unperturbed cultures. This result led me to form the hypothesis that BRCA2 may play an HR-independent role for the HAC maintenance in undamaged conditions. Surprisingly, RAD51 inhibition by B02 and RAD51 depletion by RNAi did not affect HAC loss. Furthermore, tethering of the BRCA2 fragment (BRC4), which binds RAD51, increased the HAC loss. However, a mild dose of APH treatment increased HAC loss in BRCA2 and RAD51 depleted cells, suggesting a contribution of these proteins upon exposure to replication stress.

One possible interpretation of these results is that BRCA2 may act to fine-tune the RAD51-mediated recombination activity at centromeres during the cell cycle. Recombination may be allowed in the S phase to protect centromeres under a low level of replication stress, but it could be blocked during mitosis, through the phosphorylation of S3291 of the C-terminal region of BRCA2, to avoid deleterious recombination events. In this context, it is possible that the tethering of the BRC4 motif at the alphoid^{tetO} ar-

rays supports undesired RAD51 recruitment at centromeres leading to increased HAC loss. Also, it is possible that the tethering of BRC4, which continuously binds RAD51, to the HAC may reduce the dynamics of RAD51 association to the chromatin. It is important to note, however, that it has been shown that the BRC4 motif has a dose-dependent effect on RAD51 recruitment. A high dose of BRC4 could conversely lead to a displacement of the endogenous RAD51 at the alphoid^{tetO} arrays. To reveal the precise function of RAD51, a key experiment would be to assess the association of RAD51 with the alphoid^{tetO} arrays under the condition where the BRC4 is tethered on the HAC.

6.1.2 Proposed function of BRCA2 as a chromatin linker and structural nuclear protein

An interesting question in the field of centromere biology is how centromeres preserve their genetic stability. These regions are prone to DNA breaks and have been reported to be highly recombinogenic. Thus, I investigated whether BRCA2, one of the key regulators of the HR, was important in order to repair the DNA at centromeres. The experiments conducted in Chapter 4 did not provide evidence that BRCA2-depletion increases DNA damage at centromeres in unperturbed or perturbed conditions, i.e., in the presence or absence of APH. This result led me to hypothesise that BRCA2 may not be involved in DNA repair at centromeres. However, some considerations need to be taken into account. In these experiments, the DNA damage was detected by γH2AX, a general marker of DNA stress. However, it is possible that depletion of BRCA2 at centromeres leads to a different type of stress, which is not detectable by γH2AX. Indeed, ATR, which is widely known to be activated upon replicative stress, is inactive at centromeres in the Xenopus system [213]. Therefore, different types of DNA damage markers should be used to detect the damage at centromeres in the future. Moreover, it is possible that the DNA damage induced during replication in BRCA2 depleted cells might be repaired by other DNA repair pathways, such as NHEJ, to compensate for the BRCA2 deficiency. A precise analysis of the DNA damage at centromeres upon BRCA2

depletion could be performed in combination with the depletion of other DNA repair factors. Alternatively, BRCA2 might play functions unrelated to DNA repair or replication depending on the phase of the cell cycle. This possibility could be addressed by using the newly generated mAID-BRCA2 expressing cells. These cells can be synchronised using different compounds: mevinolin/lovastatin [284], a proteasome inhibitor, can be used to arrest the cells in the G1/S boundary; palbociblib, a CDK4-6 inhibitor, can be used for G1 arrest [285]. After synchronisation, BRCA2 can be removed at different stages of the cell cycle by auxin treatment and the damage can be assessed at centromeres.

During the experiments conducted in HeLa cells, I noticed that long-term depletion of BRCA2 leads to a nuclear expansion together with an increased number of centromere foci. Similar phenotypes, but milder compared to BRCA2 depletion, were observed in APH treated cells suggesting that these characteristics may be a consequence of the replicative stress, which can be induced upon BRCA2 depletion. Curiously, however, BRCA2 depletion showed a reduced level of γH2AX compared to APH treated cells, but a much higher nuclear expansion and nuclear actin filament formation, indicating that the level of DNA damage does not correlate with the nuclear changes. Therefore, it is possible that nuclear changes upon BRCA2 depletion may be not just an indirect effect of replication stress, but BRCA2 may have a more direct function in controlling the chromatin status. For example, depletion of BRCA2 may affect the chromatin compaction inside the nucleus, exposing new accessible chromatin regions for loading of the CENPs proteins (Figure 6.1). However, it still remains to be seen: 1) whether these phenotypes are also found in other cell lines; 2) when nuclear changes start to occur upon BRCA2 depletion in relation with other DNA stress response; 3) whether these phenotypes are a consequence of senescence.

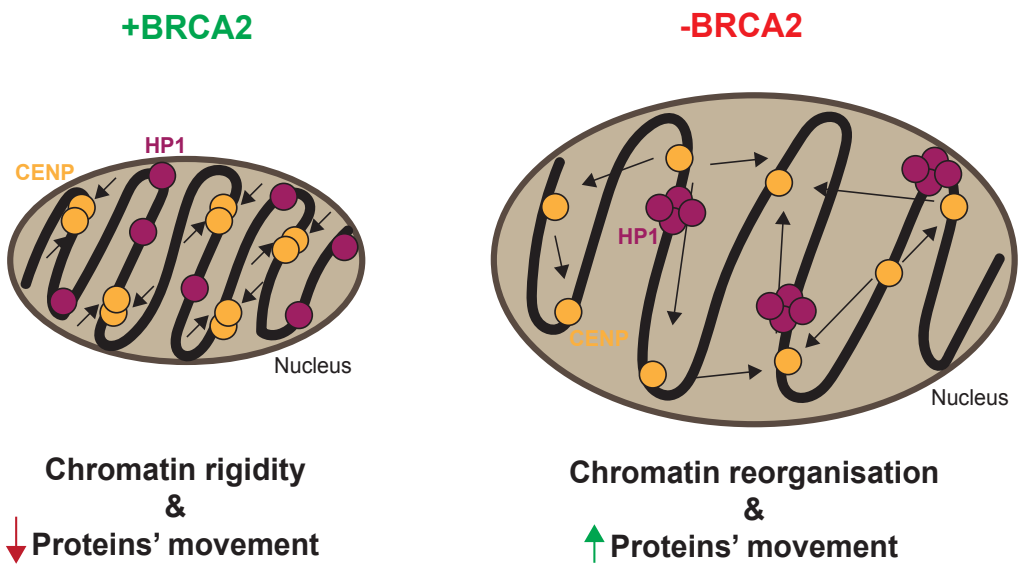


Figure 6.1: **Proposed Model 2.** BRCA2 acts as a chromatin linker and a structural nuclear protein.

BRCA2 depletion did not appear to change the status of euchromatin or heterochromatin as detected by the level of acetylation and H3K9me3. However, increased heterochormatin protein 1 (HP1) was found in BRCA2 depleted cells. HP1 has been said to be involved in the formation of chromatin linkages that drive the generation of droplets of heterochromatin inside the nucleus [273] [274] [275]. The formation of these HP1 linkages has been also proposed to help the maintenance of the nuclear structure of interphase cells and mitotic chromosomes, without affecting the level of heterochromatin [276]. BRCA2 interacts with EMSY, a transcriptional repressor that is associated with HP1 [106]. Through this interaction, it is possible that BRCA2 maintains HP1 localisation at certain regions and assists the formation of HP1 chromatin linkages, which confer nuclear rigidity. Alternatively, BRCA2 depletion may lead to increased chromatin movement and relocation of HP1. This movement may expose more accessible regions for CENP proteins to associate with the chromatin (Figure 6.1). Similarly, it is possible that the depletion of BRCA2 affects the condensation of the chromosomes in mitosis. Hence, its depletion may lead to uncondensed, misaligned chromosomes and longer mitosis. In future, further research may be needed to study nuclear changes and

HP1 dynamics upon BRCA2 depletion.

6.1.3 BRCA2, kinetochores and centromeres

Mass-spectrometry studies conducted in the laboratory of Dr. Fumiko Esashi have shown that BRCA2 interacts with kinetochore-associated proteins in the S phase. This interaction was downregulated upon DNA damage suggesting that the BRCA2-kinetochore interaction is inhibited by DNA damage. In accordance with this result, mNeonGreen-BRCA2 foci were found outside γH2AX foci. BRCA2 foci, albeit limited numbers, were found to colocalise with DSN1, NSL1 and centromere markers in interphase cells, but not in mitosis. It remains to be seen whether BRCA2-kinetochore interaction occurs at centromeres. If this interaction occurs at centromeres, it is possible that BRCA2 assists kinetochore recruitment at centromeres. By contrast, if BRCA2 colocalises with kinetochore proteins outside centromeres, this may suggest that BRCA2 displaces kinetochore proteins at non-centromeric regions. In this way, BRCA2 may possibly act as a regulator of the kinetochore formation at centromeres during the cell cycle. Nevertheless, it is important to note that BRCA2-kinetochore colocalisation was not common inside the cells. This initially led me to think that it was a dynamic event but it is also possible that this interaction occurs only for certain chromosomes. To test this hypothesis, chromosome mis-segregation could be assessed upon BRCA2 depletion using different chromosome markers by FISH analysis.

6.1.4 Development of CRISPR-modified cells for BRCA2 tagging

BRCA2 is a large protein, which likely plays multiple functions depending on the phase of the cell cycle, and consequently, several abnormal phenotypes can be induced by its long-term depletion. My generation of the CRISPR-modified cells may help to dissect this problem and understand the function of BRCA2 at different stages of the cell cycle. Explicitly, synchronised cultures of mAID-BRCA2 expressing cell lines could

be combined with the rapid depletion of BRCA2 by Auxin treatment at different stages of the cell cycle. A subsequent analysis of the mitotic defects may allow a better understanding as to how BRCA2 depletion affects chromosome segregation.

In future, the CRISPR-modified mNeonGreen-BRCA2 cells could be used to study the recruitment of endogenous BRCA2 at sites of DNA damage, kinetochores and centromeres. I believe that this system can be a powerful tool, which could contribute to expanding the knowledge around the dynamic localisation of this protein at every stage of the cell cycle.

6.2 Concluding remarks

Despite having been studied for more than 25 years since its discovery in 1995, it is still unclear how BRCA2 deficiency leads to chromosomal instability (CIN). The work presented in this thesis shows that BRCA2 is important in maintaining the chromosomal stability. The causes that lead to CIN in BRCA2-deficient cells are multiplex. In this thesis, I proposed that BRCA2 may be important in conferring structural rigidity to the chromatin. Further research needs to be done in future to understand the molecular mechanism by which BRCA2 depletion may lead to chromatin mobility. In the meantime, the generation of the CRISPR-modified cell lines is expected to expand the current knowledge about the functions of BRCA2 during the cell cycle.

Appendix A

Supplementary information

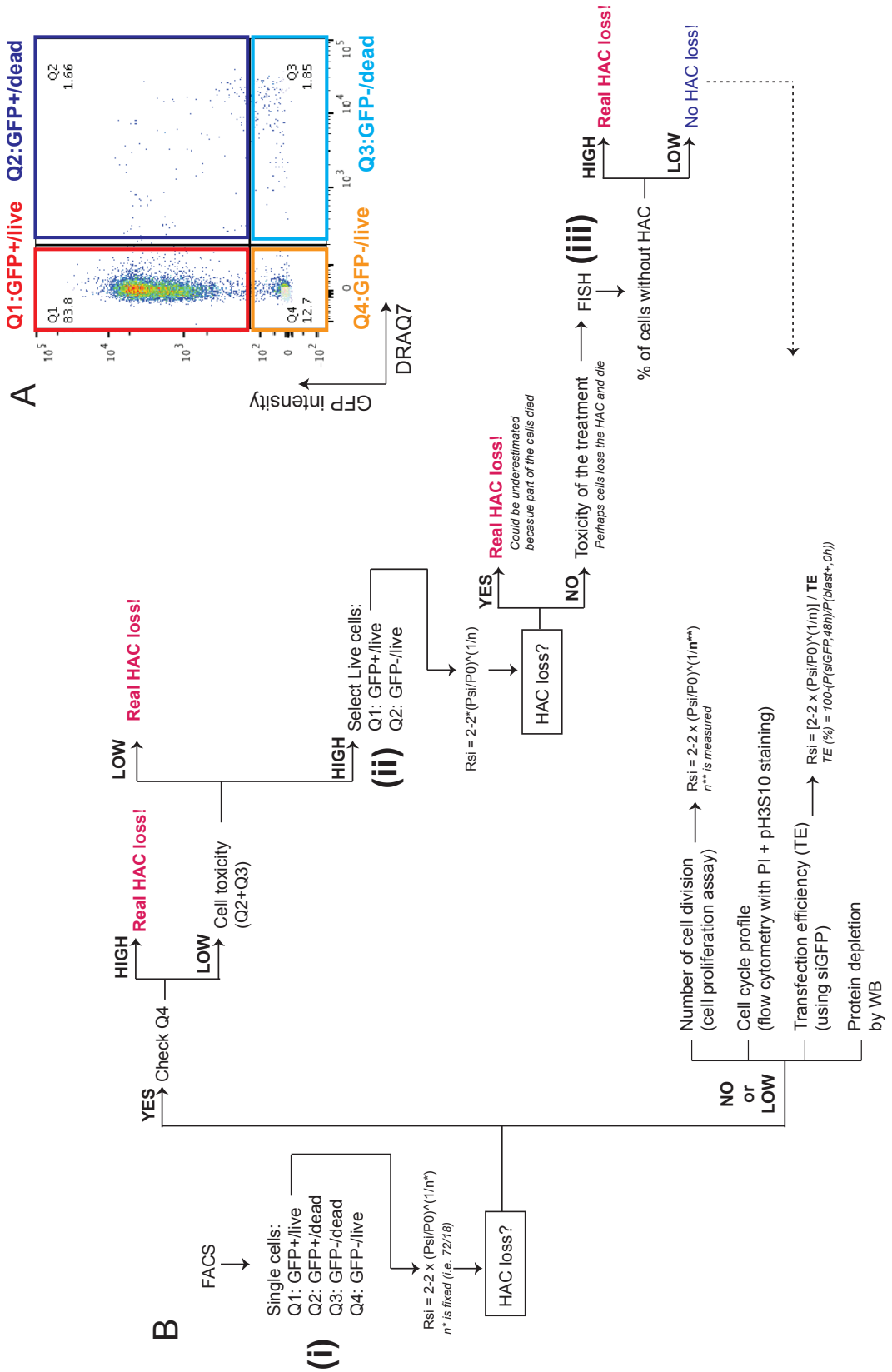


Figure A.1: **Diagram for the HAC loss analysis.** (**A**) Representative FACS profile of HT1080 HAC-dGFP cells. (**B**) Extended workflow for the HAC loss analysis.

A.1 Macros for image analysis

A.1.1 Micronuclei counting

```
run(”Despeckle”);
run(”Median...”, ”radius=2”);
setAutoThreshold(”Mean dark no-reset”);
//run(”Threshold...”);
run(”Convert to Mask”);
run(”Analyze Particles...”, ”size=0.50-20.00 circularity=0.10-1.00 display exclude clear summarize add”);
```

A.1.2 PLA foci counting

```
selectWindow(”MAX_C2-” +name);
run(”Find Maxima...”, ”noise=2000 output=[Single Points]”);
selectWindow(”MAX_C2-” +name+ ” Maxima”);
run(”Divide...”, ”value=255”);
// run(”Set Measurements...”, ”area mean integrated redirect=None decimal=3”);
roiManager(”Measure”);
// run(”Set Measurements...”, ”area integrated redirect=None decimal=3”);
```

A.1.3 Colocalisation analysis

Select nuclear area:

```
selectWindow(name);
run(”Split Channels”);
```

```
selectWindow("C1-"+name);
run("Despeckle");
run("Median...", "radius=2");
run("Auto Threshold", "method=Default");
setOption("BlackBackground", false);
run("Convert to Mask");
run("Dilate");
run("Fill Holes");
run("Erode");
```

Run colocalization analysis of channel 2 and channel 3:

```
selectWindow("C3-"+name);
run("Auto Threshold", "method=MaxEntropy white");
run("Convert to Mask");
run("Erode");
selectWindow("C4-"+name);
run("Auto Threshold", "method=MaxEntropy white");
run("Convert to Mask");
run("Erode");
run("Coloc 2", "channel_1=C3-"+name+"
channel_2=C4-"+name+" roi_or_mask=C1-"+name+" threshold_regression=Costes show_-
save_pdf_dialog display_images_in_result manders'_correlation psf=3 costes_randomi-
sations=10 save=["+dir+"/coloc/"+name+".pdf]");
selectWindow("Log");
saveAs("Text", dir+"/coloc/"+name+".csv");
```

Acknowledgements

And what I might ask you to remember from this talk is that next time you face a problem you can't solve in work or in life, there's a word for what you're going to see: the cloud. And you can go through the cloud not alone but together with someone who is your source of support to say "Yes, and" to your ideas, to help you say "Yes, and" to your own ideas, to increase the chance that, through the wisps of the cloud, you'll find that moment of calmness where you get your first glimpse of your unexpected discovery. - Uri Alon, Professor and Systems Biologist at the Weizmann Institute of Science

I would like to thank all the people who have shared this journey with me. First of all, I want to thank my supervisor, Dr. Fumiko Esashi, for her valuable guidance during this project and for her endless passion and dedication to science, a passion that she constantly shares with her students.

I want to express my heartfelt thanks to my former colleagues Isabel, Marjorie, Jean-Yves, Anthony, Chris, Federico, Kirsten, Sarah, Jedrzej, Brian, Qassi, and my present colleagues Xanita, Emily, Jacob, Arianna and Grace for their many valuable suggestions and for being there with me, on every step of this bumpy journey. In particular, I would like to thank Dr. Vladimir Larionov's and Dr. Natasha Kouprina's laboratory who helped me to start the HAC project and Davide Torre, who preciously contributed to this project with the generation and the characterisation of the HT1080 HAC-dGFP tetR-mCherry-BRC4 cell lines. Furthermore, I would like to thank Lior, Alan and Michal for their technical help with microscopy and flow-cytometry experiments.

I could not have done all this without the support of my closest friends Giulia, Paola, Elena, Mattia, Thomas, Beatriz, Frida, and the unconditional love of my family. Last but not least, all the words of this thesis would not be enough to express my gratitude to Luca, the person who more than everyone, believed in me every single step of the way.

Bibliography

[1] Andrés Aguilera and Belén Gómez-González. "Genome instability: A mechanistic view of its causes and consequences". In: *Nature Reviews Genetics* (2008). ISSN: 14710056. DOI: 10.1038/nrg2268.

[2] Simona Negrini, Vassilis G Gorgoulis, and Thanos D Halazonetis. "Genomic instability — an evolving hallmark of cancer". In: *Nature Reviews Molecular Cell Biology* 11.March (2010), pp. 220–228. DOI: 10.1038/nrm2858.

[3] Theodor Boveri. "Zur Frage der Entstehung maligner Tumoren". In: *Die Naturwissenschaften* (1914). ISSN: 00281042. DOI: 10.1007/BF01503136.

[4] Theodor Boveri. "Concerning the origin of malignant tumours by Theodor Boveri. Translated and annotated by Henry Harris". In: *Journal of Cell Science* (2008). ISSN: 00219533. DOI: 10.1242/jcs.025742.

[5] T. Boveri. *Über mehrpolige Mitosen als Mittel zur Analyse des Zellkerns*. Verhandlungen d. physikal.-medic. Gesellschaft zu Würzburg. Stuber, 1902. URL: https://books.google.co.uk/books?id=WFyimQEACAAJ.

[6] Manfred Dietel. "Boveri at 100: The life and times of Theodor Boveri". In: *The Journal of Pathology* (2014). ISSN: 1096-9896. DOI: 10.1002/path.4410.

[7] Andrew J Holland and Don W Cleveland. "Boveri revisited: chromosomal instability, aneuploidy and tumorigenesis." In: *Nature reviews. Molecular cell biology* 10.7 (2009), pp. 478–87. ISSN: 1471-0080. DOI: 10.1038/nrm2718. arXiv: NIHMS150003. URL: http://www.pubmedcentral.nih.gov/articlerender.fcgi?artid=3154738{\&}tool=pmcentrez{\&}rendertype=abstract.

[8] Karen Crasta et al. *DNA breaks and chromosome pulverization from errors in mitosis*. 2012. DOI: 10.1038/nature10802.

[9] Cheng Zhong Zhang et al. "Chromothripsis from DNA damage in micronuclei". In: *Nature* (2015). ISSN: 14764687. DOI: 10.1038/nature14493.

[10] Philip J. Stephens et al. "Massive genomic rearrangement acquired in a single catastrophic event during cancer development". In: *Cell* (2011). ISSN: 00928674. DOI: 10.1016/j.cell.2010.11.055.

[11] Christoph E. Heilig et al. "Chromosomal instability correlates with poor outcome in patients with myelodysplastic syndromes irrespectively of the cytogenetic risk group". In: *Journal of Cellular and Molecular Medicine* (2010). ISSN: 15821838. DOI: 10.1111/j.1582-4934.2009.00905.x.

[12] Chang Min Choi et al. "Chromosomal instability is a risk factor for poor prognosis of adenocarcinoma of the lung: Fluorescence in situ hybridization analysis of paraffin-embedded tissue from Korean patients". In: *Lung Cancer* (2009). ISSN: 01695002. DOI: 10.1016/j.lungcan.2008.07.016.

[13] Samuel F. Bakhoum et al. "Chromosomal instability substantiates poor prognosis in patients with diffuse large B-cell lymphoma". In: *Clinical Cancer Research* (2011). ISSN: 10780432. DOI: 10.1158/1078-0432.CCR-11-2049.

[14] Sarah L. Thompson, Samuel F. Bakhoum, and Duane A. Compton. "Mechanisms of Chromosomal Instability". In: *Current Biology* 20.6 (2010), R285–R295. ISSN: 09609822. DOI: 10.1016/j.cub.2010.01.034. URL: http://dx.doi.org/10.1016/j.cub.2010.01.034.

[15] Peter S. Linsley et al. "Copy number loss of the interferon gene cluster in melanomas is linked to reduced T cell infiltrate and poor patient prognosis". In: *PLoS ONE* (2014). ISSN: 19326203. DOI: 10.1371/journal.pone.0109760.

[16] Sarah E. McClelland, Rebecca A. Burrell, and Charles Swanton. "Chromosomal instability: A composite phenotype that influences sensitivity to chemotherapy". In: (2009). ISSN: 15514005. DOI: 10.4161/cc.8.20.9690.

[17] Sarah L. Thompson and Duane A. Compton. "Chromosomes and cancer cells". In: (2011). ISSN: 09673849. DOI: 10.1007/s10577-010-9179-y.

[18] Charles Swanton et al. "Chromosomal instability determines taxane response". In: *Proceedings of the National Academy of Sciences of the United States of America* (2009). ISSN: 00278424. DOI: 10.1073/pnas.0811835106.

[19] Therese Wilhelm, Maha Said, and Valeria Naim. "DNA Replication Stress and Chromosomal Instability: Dangerous Liaisons." In: *Genes* 11.6 (2020), pp. 1–35. ISSN: 2073-4425. DOI: 10.3390/genes11060642. URL: http://www.ncbi.nlm.nih.gov/pubmed/32532049.

[20] Rebecca A. Burrell et al. "Replication stress links structural and numerical cancer chromosomal instability". In: *Nature* (2013). ISSN: 14764687. DOI: 10.1038/nature11935.

[21] Lilian Kabeche et al. "A mitosis-specific and R loop-driven ATR pathway promotes faithful chromosome segregation". In: *Science* (2018). ISSN: 10959203. DOI: 10.1126/science.aan6490.

[22] Alberto Ciccia and Stephen J. Elledge. "The DNA Damage Response: Making It Safe to Play with Knives". In: *Molecular Cell* 40.2 (2010), pp. 179–204. ISSN: 10972765. DOI: 10.1016/j.molcel.2010.09.019. URL: http://linkinghub.elsevier.com/retrieve/pii/S1097276510007471.

[23] Anthony Tubbs and André Nussenzweig. *Endogenous DNA Damage as a Source of Genomic Instability in Cancer*. 2017. DOI: 10.1016/j.cell.2017.01.002.

[24] Matteo Berti and Alessandro Vindigni. "Replication stress: getting back on track". In: *Nature Structural & Molecular Biology* 23.2 (2016), pp. 103–109. ISSN: 1545-9993. DOI: 10.1038/nsmb.3163. URL: http://dx.doi.org/10.1038/nsmb.3163.

[25] Michelle K Zeman and Karlene A Cimprich. "Causes and consequences of replication stress". In: 16.1 (2014).

[26] Lee Zou and Stephen J. Elledge. "Sensing DNA damage through ATRIP recognition of RPA-ssDNA complexes". In: *Science* (2003). ISSN: 00368075. DOI: 10.1126/science.1083430.

[27] Ali Jazayeri et al. "ATM- and cell cycle-dependent regulation of ATR in response to DNA double-strand breaks". In: *Nature Cell Biology* (2006). ISSN: 14657392. DOI: 10.1038/ncb1337.

[28] Dana Branzei and Marco Foiani. "Regulation of DNA repair throughout the cell cycle". In: *Nature Reviews Molecular Cell Biology* 9.4 (2008), pp. 297–308. ISSN: 1471-0072. DOI: 10.1038/nrm2351. URL: http://www.nature.com/doifinder/10.1038/nrm2351.

[29] Sandeep Burma et al. "ATM Phosphorylates Histone H2AX in Response to DNA Double-strand Breaks". In: *Journal of Biological Chemistry* (2001). ISSN: 00219258. DOI: 10.1074/jbc.C100466200.

[30] Irene M. Ward and Junjie Chen. "Histone H2AX Is Phosphorylated in an ATR-dependent Manner in Response to Replicational Stress". In: *Journal of Biological Chemistry* (2001). ISSN: 00219258. DOI: 10.1074/jbc.C100569200.

[31] Oscar Fernandez-Capetillo et al. "H2AX: The histone guardian of the genome". In: (2004). ISSN: 15687864. DOI: 10.1016/j.dnarep.2004.03.024.

[32] Fei Zhao et al. *DNA end resection and its role in DNA replication and DSB repair choice in mammalian cells*. 2020. DOI: 10.1038/s12276-020-00519-1.

[33] Mary Ellen Moynahan and Maria Jasin. "Mitotic homologous recombination maintains genomic stability and suppresses tumorigenesis". In: 11.mARCH (2010). DOI: 10.1038/nrm2851. URL: http://dx.doi.org/10.1038/nrm2851.

[34] Christine Richardson and Maria Jasin. "Frequent chromosomal translocations induced by DNA double-strand breaks". In: *Nature* (2000). ISSN: 00280836. DOI: 10.1038/35015097.

[35] Jeremy M. Stark and Maria Jasin. "Extensive Loss of Heterozygosity Is Suppressed during Homologous Repair of Chromosomal Breaks". In: *Molecular and Cellular Biology* (2003). ISSN: 0270-7306. DOI: 10.1128/mcb.23.2.733-743.2003.

[36] Efrem A. H. Neuwirth, Masamitsu Honma, and Andrew J. Grosovsky. "Interchromosomal Crossover in Human Cells Is Associated with Long Gene Conversion Tracts". In: *Molecular and Cellular Biology* (2007). ISSN: 0270-7306. DOI: 10.1128/mcb.01852-06.

[37] Stephanie A. Hagstrom and Thaddeus P. Dryja. "Mitotic recombination map of 13cen-13q14 derived from an investigation of loss of heterozygosity in retinoblastomas". In: *Proceedings of the National Academy of Sciences of the United States of America* (1999). ISSN: 00278424. DOI: 10.1073/pnas.96.6.2952.

[38] Beth Elliott, Christine Richardson, and Maria Jasin. "Chromosomal translocation mechanisms at intronic Alu elements in mammalian cells". In: *Molecular Cell* (2005). ISSN: 10972765. DOI: 10.1016/j.molcel.2005.02.028.

[39] Silvana Mourón et al. "Repriming of DNA synthesis at stalled replication forks by human PrimPol". In: *Nature Structural and Molecular Biology* (2013). ISSN: 15459993. DOI: 10.1038/nsmb.2719.

[40] Sara García-Gómez et al. "PrimPol, an Archaic Primase/Polymerase Operating in Human Cells". In: *Molecular Cell* (2013). ISSN: 10972765. DOI: 10.1016/j.molcel.2013.09.025.

[41] Julie Bianchi et al. "Primpol bypasses UV photoproducts during eukaryotic chromosomal DNA replication". In: *Molecular Cell* (2013). ISSN: 10972765. DOI: 10.1016/j.molcel.2013.10.035.

[42] Ann Liza Piberger et al. "PrimPol-dependent single-stranded gap formation mediates homologous recombination at bulky DNA adducts". In: *Nature Communications* (2020). ISSN: 20411723. DOI: 10.1038/s41467-020-19570-7.

[43] Arnab Ray Chaudhuri et al. "Topoisomerase i poisoning results in PARP-mediated replication fork reversal". In: *Nature Structural and Molecular Biology* (2012). ISSN: 15459993. DOI: 10.1038/nsmb.2258.

[44] Ralph Zellweger et al. "Rad51-mediated replication fork reversal is a global response to genotoxic treatments in human cells". In: *Journal of Cell Biology* (2015). ISSN: 15408140. DOI: 10.1083/jcb.201406099.

[45] Rémy Bétous et al. "Substrate-Selective Repair and Restart of Replication Forks by DNA Translocases". In: *Cell Reports* (2013). ISSN: 22111247. DOI: 10.1016/j.celrep.2013.05.002.

[46] Andrew C. Kile et al. "HLTF's Ancient HIRAN Domain Binds 3' DNA Ends to Drive Replication Fork Reversal". In: *Molecular Cell* (2015). ISSN: 10974164. DOI: 10.1016/j.molcel.2015.05.013.

[47] Marko Vujanovic et al. "Replication Fork Slowing and Reversal upon DNA Damage Require PCNA Polyubiquitination and ZRANB3 DNA Translocase Activity". In: *Molecular Cell* (2017). ISSN: 10974164. DOI: 10.1016/j.molcel.2017.08.010.

[48] Katharina Schlacher et al. "Double-Strand Break Repair-Independent Role for BRCA2 in Blocking Stalled Replication Fork Degradation by MRE11". In: *Cell* 145.4 (2011), pp. 529–542. ISSN: 00928674. DOI: 10.1016/j.cell.2011.03.041. URL: http://linkinghub.elsevier.com/retrieve/pii/S0092867411003758.

[49] Katharina Schlacher, Hong Wu, and Maria Jasin. "A Distinct Replication Fork Protection Pathway Connects Fanconi Anemia Tumor Suppressors to RAD51-BRCA1/2". In: *Cancer Cell* 22.1 (2012), pp. 106–116. ISSN: 15356108. DOI: 10.1016/j.ccr.2012.05.015. arXiv: NIHMS150003. URL: http://dx.doi.org/10.1016/j.ccr.2012.05.015.

[50] Catherine E. Smith, Bertrand Llorente, and Lorraine S. Symington. "Template switching during break-induced replication". In: *Nature* (2007). ISSN: 14764687. DOI: 10.1038/nature05723.

[51] Ranjith P. Anand et al. "Chromosome rearrangements via template switching between diverged repeated sequences". In: *Genes and Development* (2014). ISSN: 15495477. DOI: 10.1101/gad.250258.114.

[52] Bertrand Llorente, Catherine E. Smith, and Lorraine S. Symington. "Break-induced replication: What is it and what is it for?" In: 7.7 (2008), pp. 859–864. ISSN: 15514005. DOI: 10.4161/cc.7.7.5613.

[53] Ralph Scully et al. "DNA double-strand break repair-pathway choice in somatic mammalian cells". In: (2019). ISSN: 14710080. DOI: 10.1038/s41580-019-0152-0.

[54] Jeff M. Hall et al. "Linkage of early-onset familial breast cancer to chromosome 17q21". In: *Science* (1990). ISSN: 00368075. DOI: 10.1126/science.2270482.

[55] D F Easton et al. "Genetic linkage analysis in familial breast and ovarian cancer: results from 214 families. The Breast Cancer Linkage Consortium." In: *American journal of human genetics* (1993). ISSN: 0002-9297.

[56] Richard Wooster et al. "Localization of a breast cancer susceptibility gene, BRCA2, to chromosome 13q12-13". In: *Science* (1994). ISSN: 00368075. DOI: 10.1126/science.8091231.

[57] Richard Wooster et al. "Identification of the breast cancer susceptibility gene BRCA2". In: *Nature* (1995). ISSN: 00280836. DOI: 10.1038/378789a0.

[58] Nasim Mavaddat et al. "Cancer risks for BRCA1 and BRCA2 mutation carriers: Results from prospective analysis of EMBRACE". In: *Journal of the National Cancer Institute* (2013). ISSN: 00278874. DOI: 10.1093/jnci/djt095.

[59] A. Antoniou et al. "Average risks of breast and ovarian cancer associated with BRCA1 or BRCA2 mutations detected in case series unselected for family history: A combined analysis of 22 studies". In: *American Journal of Human Genetics* (2003). ISSN: 00029297. DOI: 10.1086/375033.

[60] Steven A. Narod and William D. Foulkes. "BRCA1 and BRCA2: 1994 and beyond". In: (2004). ISSN: 1474175X. DOI: 10.1038/nrc1431.

[61] Niall G. Howlett et al. "Biallelic inactivation of BRCA2 in Fanconi anemia". In: *Science* (2002). ISSN: 00368075. DOI: 10.1126/science.1073834.

[62] K J Patel et al. "Involvement of Brca2 in DNA repair." In: *Molecular cell* 1.3 (1998), pp. 347–357. ISSN: 10972765. DOI: 10.1016/S1097-2765(00)80035-0.

[63] Ashok R. Venkitaraman. "Cancer susceptibility and the functions of BRCA1 and BRCA2". In: (2002). ISSN: 00928674. DOI: 10.1016/S0092-8674(02)00615-3.

[64] T. Thorslund and S. C. West. "BRCA2: A universal recombinase regulator". In: (2007). ISSN: 09509232. DOI: 10.1038/sj.onc.1210870.

[65] Kathryn P. Pennington et al. "Germline and somatic mutations in homologous recombination genes predict platinum response and survival in ovarian, fallopian tube, and peritoneal carcinomas". In: *Clinical Cancer Research* (2014). ISSN: 10780432. DOI: 10.1158/1078-0432.CCR-13-2287.

[66] Dan Robinson et al. "Integrative Clinical Genomics of Advanced Prostate Resource Integrative Clinical Genomics of Advanced Prostate Cancer". In: *Cell* (2015). ISSN: 1097-4172.

[67] Alexander Liede, Beth Y. Karlan, and Steven A. Narod. "Cancer risks for male carriers of germline mutations in BRCA1 or BRCA2: A review of the literature". In: (2004). ISSN: 0732183X. DOI: 10.1200/JCO.2004.05.055.

[68] Helen Cavanagh and Katherine M.A. Rogers. "The role of BRCA1 and BRCA2 mutations in prostate, pancreatic and stomach cancers". In: (2015). ISSN: 18974287. DOI: 10.1186/s13053-015-0038-x.

[69] Elizabeth M. Kass et al. "Robust homology-directed repair within mouse mammary tissue is not specifically affected by Brca2 mutation". In: *Nature Communications* (2016). ISSN: 20411723. DOI: 10.1038/ncomms13241.

[70] S K Sharan et al. "Embryonic lethality and radiation hypersensitivity mediated by Rad51 in mice lacking Brca2." In: *Nature* 386 (1997), pp. 804–810. ISSN: 0028-0836. DOI: 10.1038/386804a0.

[71] Akira Suzuki et al. "Brca2 is required for embryonic cellular proliferation in the mouse". In: *Genes and Development* (1997). ISSN: 08909369. DOI: 10.1101/gad.11.10.1242.

[72] Jos Jonkers et al. "Synergistic tumor suppressor activity of BRCA2 and p53 in a conditional mouse model for breast cancer". In: *Nature Genetics* (2001). ISSN: 10614036. DOI: 10.1038/ng747.

[73] Veronica P.C.C. Yu et al. "Gross chromosomal rearrangements and genetic exchange between nonhomologous chromosomes following BRCA2 inactivation". In: *Genes and Development* (2000). ISSN: 08909369. DOI: 10.1101/gad.14.11.1400.

[74] M. Grigorova et al. "Possible causes of chromosome instability: Comparison of chromosomal abnormalities in cancer cell lines with mutations in BRCA1, BRCA2, CHK2 and BUB1". In: *Cytogenetic and Genome Research* 104.1-4 (2004), pp. 333–340. ISSN: 14248581. DOI: 10.1159/000077512.

[75] Tina Thorslund et al. "The breast cancer tumor suppressor BRCA2 promotes the specific targeting of RAD51 to single-stranded DNA". In: *Nature Structural and Molecular Biology* (2010). ISSN: 15459993. DOI: 10.1038/nsmb.1905.

[76] Taha Shahid et al. "Structure and mechanism of action of the BRCA2 breast cancer tumor suppressor". In: *Nature Structural and Molecular Biology* (2014). ISSN: 15459985. DOI: 10.1038/nsmb.2899.

[77] Ken Ichi Yano et al. "Nuclear localization signals of the BRCA2 protein". In: *Biochemical and Biophysical Research Communications* (2000). ISSN: 0006291X. DOI: 10.1006/bbrc.2000.2392.

[78] Brian H. Spain et al. "Truncated BRCA2 is cytoplasmic: Implications for cancer-linked mutations". In: *Proceedings of the National Academy of Sciences of the United States of America* (1999). ISSN: 00278424. DOI: 10.1073/pnas.96.24.13920.

[79] Juan S. Martinez, Céline Baldeyron, and Aura Carreira. "Molding BRCA2 function through its interacting partners". In: (2015). ISSN: 15514005. DOI: 10.1080/15384101.2015.1093702.

[80] Amélie Fradet-Turcotte et al. "BRCA2 functions: From DNA repair to replication fork stabilization". In: (2016). ISSN: 14796821. DOI: 10.1530/ERC-16-0297.

[81] Alexander K C Wong et al. "RAD51 Interacts with the Evolutionarily Conserved BRC Motifs in the Human Breast". In: (1997).

[82] Aura Carreira and Stephen C. Kowalczykowski. "Two classes of BRC repeats in BRCA2 promote RAD51 nucleoprotein filament function by distinct mechanisms". In: *Proceedings of the National Academy of Sciences of the United States of America* (2011). ISSN: 00278424. DOI: 10.1073/pnas.1106971108.

[83] Phang Lang Chen et al. "The BRC repeats in BRCA2 are critical for RAD51 binding and resistance to methyl methanesulfonate treatment". In: *Proceedings of the National Academy of Sciences of the United States of America* (1998). ISSN: 00278424. DOI: 10.1073/pnas.95.9.5287.

[84] C. F. Chen et al. "Expression of BRC repeats in breast cancer cells disrupts the BRCA2-Rad51 complex and leads to radiation hypersensitivity and loss of G(2)/M checkpoint control". In: *J Biol Chem* 274.46 (1999), pp. 32931–5. ISSN: 0021-9258 (Print) 0021-9258 (Linking). DOI: 10.1074/jbc.274.46.32931. URL: https://www.ncbi.nlm.nih.gov/pubmed/10551859.

[85] Luca Pellegrini et al. "Insights into DNA recombination from the structure of a RAD51-BRCA2 complex." In: *Nature* (2002). ISSN: 0028-0836. DOI: 10.1038/nature01230.

[86] Aura Carreira et al. "The BRC Repeats of BRCA2 Modulate the DNA-Binding Selectivity of RAD51". In: *Cell* (2009). ISSN: 00928674. DOI: 10.1016/j.cell.2009.02.019.

[87] Vitold E. Galkin et al. "BRCA2 BRC motifs bind RAD51-DNA filaments". In: *Proceedings of the National Academy of Sciences of the United States of America* (2005). ISSN: 00278424. DOI: 10.1073/pnas.0407266102.

[88] Gouri Chatterjee et al. "Distinct binding of BRCA2 BRC repeats to RAD51 generates differential DNA damage sensitivity". In: *Nucleic Acids Research* (2016). ISSN: 13624962. DOI: 10.1093/nar/gkw242.

[89] Haijuan Yang et al. "BRCA2 function in DNA binding and recombination from a BRCA2-DSS1-ssDNA structure". In: *Science* (2002). ISSN: 00368075. DOI: 10.1126/science.297.5588.1837.

[90] Nicola J. Marston et al. "Interaction between the Product of the Breast Cancer Susceptibility Gene BRCA2 and DSS1, a Protein Functionally Conserved from Yeast to Mammals". In: *Molecular and Cellular Biology* (1999). ISSN: 0270-7306. DOI: 10.1128/mcb.19.7.4633.

[91] Anand D. Jeyasekharan et al. "A cancer-associated BRCA2 mutation reveals masked nuclear export signals controlling localization". In: *Nature Structural and Molecular Biology* (2013). ISSN: 15459993. DOI: 10.1038/nsmb.2666.

[92] Weixing Zhao et al. "Promotion of BRCA2-Dependent Homologous Recombination by DSS1 via RPA Targeting and DNA Mimicry". In: *Molecular Cell* (2015). ISSN: 10974164. DOI: 10.1016/j.molcel.2015.05.032.

[93] Owen Richard Davies and Luca Pellegrini. "Interaction with the BRCA2 C terminus protects RAD51-DNA filaments from disassembly by BRC repeats". In: *Nature Structural and Molecular Biology* (2007). ISSN: 15459993. DOI: 10.1038/nsmb1251.

[94] Fumiko Esashi et al. "Stabilization of RAD51 nucleoprotein filaments by the C-terminal region of BRCA2." In: *Nature structural & molecular biology* 14.6 (2007), pp. 468–474. ISSN: 1545-9993. DOI: 10.1038/nsmb1245.

[95] Fumiko Esashi et al. "CDK-dependent phosphorylation of BRCA2 as a regulatory mechanism for recombinational repair." In: *Nature* 434.March (2005), pp. 598–604. ISSN: 0028-0836. DOI: 10.1038/nature03404.

[96] Nabieh Ayoub et al. "The Carboxyl Terminus of Brca2 Links the Disassembly of Rad51 Complexes to Mitotic Entry". In: *Current Biology* (2009). ISSN: 09609822. DOI: 10.1016/j.cub.2009.05.057.

[97] Bing Xia et al. "Control of BRCA2 Cellular and Clinical Functions by a Nuclear Partner, PALB2". In: *Molecular Cell* (2006). ISSN: 10972765. DOI: 10.1016/j.molcel.2006.05.022.

[98] Feng Zhang et al. "PALB2 Links BRCA1 and BRCA2 in the DNA-Damage Response". In: *Current Biology* (2009). ISSN: 09609822. DOI: 10.1016/j.cub.2009.02.018.

[99] Shyng Shiou F Yuan et al. "BRCA2 is required for ionizing radiation-induced assembly of Rad51 complex in vivo". In: *Cancer Research* (1999). ISSN: 00085472.

[100] Mary Ellen Moynahan, Andrew J. Pierce, and Maria Jasin. "BRCA2 is required for homology-directed repair of chromosomal breaks". In: *Molecular Cell* (2001). ISSN: 10972765. DOI: 10.1016/S1097-2765(01)00174-5.

[101] Kalina T. Haas et al. "Single-molecule localization microscopy reveals molecular transactions during RAD51 filament assembly at cellular DNA damage sites". In: *Nucleic Acids Research* (2018). ISSN: 13624962. DOI: 10.1093/nar/gkx1303.

[102] Mikhail Lomonosov et al. "Stabilization of stalled DNA replication forks by the BRCA2 breast cancer susceptibility protein". In: *Genes and Development* (2003). ISSN: 08909369. DOI: 10.1101/gad.279003.

[103] Jonathan Milner et al. "Transcriptional activation functions in BRCA2 [3]". In: (1997). ISSN: 00280836. DOI: 10.1038/386772a0.

[104] Margareta Nordling et al. "A large deletion disrupts the exon 3 transcription activation domain of the BRCA2 gene in a breast/ovarian cancer family". In: *Cancer Research* (1998). ISSN: 00085472.

[105] François Fuks, Jonathan Milner, and Tony Kouzarides. "BRCA2 associates with acetyltransferase activity when bound to P/CAF". In: *Oncogene* (1998). ISSN: 09509232. DOI: 10.1038/sj.onc.1202475.

[106] Luke Hughes-Davies et al. "EMSY Links the BRCA2 Pathway to Sporadic Breast and Ovarian Cancer". In: *Cell* (2003). ISSN: 00928674. DOI: 10.1016/S0092-8674(03)00930-9.

[107] Andrew Tutt et al. "Absence of Brca2 causes genome instability by chromosome breakage and loss associated with centrosome amplification". In: *Current Biology* 9.19 (1999), pp. 1107–1110. ISSN: 09609822. DOI: 10.1016/S0960-9822(99)80479-5.

[108] Xihan Guo et al. "The molecular origins and pathophysiological consequences of micronuclei: New insights into an age-old problem". In: (2019). ISSN: 13882139. DOI: 10.1016/j.mrrev.2018.11.001.

[109] Akira Nakanishi et al. "Interference with BRCA2, which localizes to the centrosome during S and early M phase, leads to abnormal nuclear division". In: *Biochemical and Biophysical Research Communications* (2007). ISSN: 0006291X. DOI: 10.1016/j.bbrc.2007.01.100.

[110] Takayoshi Niwa et al. "BRCA2 interacts with the cytoskeletal linker protein plectin to form a complex controlling centrosome localization". In: *Cancer Science* (2009). ISSN: 13479032. DOI: 10.1111/j.1349-7006.2009.01282.x.

[111] Hui Feng Wang et al. "BRCA2 and nucleophosmin coregulate centrosome amplification and form a complex with the Rho effector kinase ROCK2". In: *Cancer Research* (2011). ISSN: 00085472. DOI: 10.1158/0008-5472.CAN-10-0030.

[112] Sadiya Malik et al. "BRCA2 mediates centrosome cohesion via an interaction with cytoplasmic dynein". In: *Cell Cycle* (2016). ISSN: 15514005. DOI: 10.1080/15384101.2016.1195531.

[113] Matthew J Daniels et al. "Abnormal cytokinesis in cells deficient in the breast cancer susceptibility protein BRCA2." In: *Science (New York, N.Y.)* 306.5697 (2004), pp. 876–9. ISSN: 1095-9203. DOI: 10.1126/science.1102574. URL: http://www.ncbi.nlm.nih.gov/pubmed/15375219.

[114] Sergey Lekomtsev et al. "Evidence that the tumor-suppressor protein BRCA2 does not regulate cytokinesis in human cells." In: *Journal of cell science* 123.Pt 9 (2010), pp. 1395–1400. ISSN: 0021-9533. DOI: 10.1242/jcs.068015.

[115] Gourish Mondal et al. "BRCA2 Localization to the Midbody by Filamin A Regulates CEP55 Signaling and Completion of Cytokinesis". In: *Developmental Cell* 23.1 (2012), pp. 137–152. ISSN: 15345807. DOI: 10.1016/j.devcel.2012.05.008. arXiv: NIHMS150003.

[116] Eunhee Choi et al. "BRCA2 Fine-Tunes the Spindle Assembly Checkpoint through Reinforcement of BubR1 Acetylation". In: *Developmental Cell* 22.2 (2012), pp. 295–308. ISSN: 15345807. DOI: 10.1016/j.devcel.2012.01.009.

[117] Weiran Feng and Maria Jasin. "BRCA2 suppresses replication stress-induced mitotic and G1 abnormalities through homologous recombination". In: *Nature Communications* 8.1 (2017). ISSN: 20411723. DOI: 10.1038/s41467-017-00634-0.

[118] Sheroy Minocherhomji et al. "Replication stress activates DNA repair synthesis in mitosis". In: *Nature* 528.7581 (2015), pp. 286–290. ISSN: 0028-0836. DOI: 10.1038/nature16139. arXiv: nature.vol.342.30nov1989. URL: http://www.nature.com/doifinder/10.1038/nature16139.

[119] María Fernández-Casañas and Kok Lung Chan. "The unresolved problem of DNA bridging". In: (2018). ISSN: 20734425. DOI: 10.3390/genes9120623.

[120] Valeria Naim and Filippo Rosselli. "The FANC pathway and BLM collaborate during mitosis to prevent micro-nucleation and chromosome abnormalities". In: *Nature Cell Biology* (2009). ISSN: 14657392. DOI: 10.1038/ncb1883.

[121] Kok Lung Chan et al. "Replication stress induces sister-chromatid bridging at fragile site loci in mitosis". In: *Nature Cell Biology* (2009). ISSN: 14657392. DOI: 10.1038/ncb1882.

[122] Keiko Yata et al. "BRCA2 Coordinates the Activities of Cell-Cycle Kinases to Promote Genome Stability". In: *CellReports* 7.5 (2014), pp. 1547–1559. ISSN: 2211-1247. DOI: 10.1016/j.celrep.2014.04.023. URL: http://dx.doi.org/10.1016/j.celrep.2014.04.023.

[123] Keiko Yata et al. "Article Plk1 and CK2 Act in Concert to Regulate Rad51 during DNA Double Strand Break Repair". In: *Molecular Cell* 45.3 (2012), pp. 371–383. ISSN: 1097-2765. DOI: 10.1016/j.molcel.2011.12.028. URL: http://dx.doi.org/10.1016/j.molcel.2011.12.028.

[124] Lyuben Tsvetkov and David F. Stern. "Interaction of chromatin-associated Plk1 and Mcm7". In: *Journal of Biological Chemistry* (2005). ISSN: 00219258. DOI: 10.1074/jbc.M413514200.

[125] Kristina Trenz, Alessia Errico, and Vincenzo Costanzo. "Plx1 is required for chromosomal DNA replication under stressful conditions". In: *EMBO Journal* (2008). ISSN: 02614189. DOI: 10.1038/emboj.2008.29.

[126] Tohru Takaki et al. *Polo-like kinase 1 reaches beyond mitosis-cytokinesis, DNA damage response, and development*. 2008. DOI: 10.1016/j.ceb.2008.10.005.

[127] Mathias Uhlén et al. "Tissue-based map of the human proteome". In: *Science* (2015). ISSN: 10959203. DOI: 10.1126/science.1260419.

[128] Antony W. Oliver et al. "Structural basis for recruitment of BRCA2 by PALB2". In: *EMBO Reports* 10.9 (2009), pp. 990–996. ISSN: 1469221X. DOI: 10.1038/embor.2009.126.

[129] Humberto Sánchez et al. "Architectural plasticity of human BRCA2-RAD51 complexes in DNA break repair". In: *Nucleic Acids Research* (2017). ISSN: 13624962. DOI: 10.1093/nar/gkx084.

[130] Kara L McKinley and Iain M Cheeseman. "The molecular basis for centromere identity and function". In: *Nat Rev Mol Cell Biol* 17.1 (2016), pp. 16–29. ISSN: 1471-0072. DOI: 10.1038/nrm.2015.5. URL: http://www.nature.com/nrm/journal/v17/n1/full/nrm.2015.5.html.

[131] V. Barra and D. Fachinetti. "The dark side of centromeres: types, causes and consequences of structural abnormalities implicating centromeric DNA". In: (2018). ISSN: 20411723. DOI: 10.1038/s41467-018-06545-y.

[132] M. Dumont and D. Fachinetti. "DNA Sequences in Centromere Formation and Function". In: *Centromeres and Kinetochores: Discovering the Molecular Mechanisms Underlying Chromosome Inheritance*. Ed. by Ben E. Black. Cham: Springer International Publishing, 2017, pp. 305–336. ISBN: 978-3-319-58592-5. DOI: 10.1007/978-3-319-58592-5_13. URL: https://doi.org/10.1007/978-3-319-58592-5_13.

[133] Oscar Molina et al. "Using human artificial chromosomes to study centromere assembly and function". In: *Chromosoma* (2017). ISSN: 0009-5915. DOI: 10.1007/s00412-017-0633-x. URL: http://link.springer.com/10.1007/s00412-017-0633-x.

[134] William C. Earnshaw and Naomi Rothfield. "Identification of a family of human centromere proteins using autoimmune sera from patients with scleroderma". In: *Chromosoma* (1985). ISSN: 00095915. DOI: 10.1007/BF00328227.

[135] D. K. Palmer et al. "A 17-kD centromere protein (CENP-A) copurifies with nucleosome core particles and with histones". In: *Journal of Cell Biology* (1987). ISSN: 00219525. DOI: 10.1083/jcb.104.4.805.

[136] Kevin F. Sullivan, Mirko Hechenberger, and Khaled Masri. "Human CENP-A contains a histone H3 related histone fold domain that is required for targeting to the centromere". In: *Journal of Cell Biology* (1994). ISSN: 00219525. DOI: 10.1083/jcb.127.3.581.

[137] Emily V Howman et al. "Early disruption of centromeric chromatin organization in centromere protein A (Cenpa) null mice." In: *Proceedings of the National Academy of Sciences of the United States of America* 97.3 (2000), pp. 1148–53. ISSN: 0027-8424. DOI: 10.1073/pnas.97.3.1148. URL: http://www.pubmedcentral.nih.gov/articlerender.fcgi?artid=15551{\&}tool=pmcentrez{\&}rendertype=abstract.

[138] Masashi Ikeno, Hiroshi Masumoto, and Tuneko Okazaki. "Distribution of CENP-B boxes reflected in CREST centromere antigenic sites on long-range α-satellite DNA arrays of human chromosome 21". In: *Human Molecular Genetics* (1994). ISSN: 09646906. DOI: 10.1093/hmg/3.8.1245.

[139] H. Masumoto et al. "A human centromere antigen (CENP-B) interacts with a short specific sequence in alphoid DNA, a human centromeric satellite". In: *Journal of Cell Biology* (1989). ISSN: 00219525. DOI: 10.1083/jcb.109.5.1963.

[140] Yoshinao Muro et al. "Centromere protein B assembles human centromeric α-satellite DNA at the 17-bp sequence, CENP-B box". In: *Journal of Cell Biology* (1992). ISSN: 00219525. DOI: 10.1083/jcb.116.3.585.

[141] Nobutaka Suzuki et al. "CENP-B Interacts with CENP-C Domains Containing Mif2 Regions Responsible for Centromere Localization". In: *Journal of Biological Chemistry* (2004). ISSN: 00219258. DOI: 10.1074/jbc.M306477200.

[142] Daniele Fachinetti et al. "DNA Sequence-Specific Binding of CENP-B Enhances the Fidelity of Human Centromere Function". In: *Developmental Cell* (2015). ISSN: 18781551. DOI: 10.1016/j.devcel.2015.03.020.

[143] Jun ichirou Ohzeki et al. "CENP-B box is required for de novo centromere chromatin assembly on human alphoid DNA". In: *Journal of Cell Biology* (2002). ISSN: 00219525. DOI: 10.1083/jcb.200207112.

[144] Mini Kapoor et al. "The cenpB gene is not essential in mice". In: *Chromosoma* (1998). ISSN: 00095915. DOI: 10.1007/s004120050343.

[145] Ana V. Perez-Castro et al. "Centromeric protein B null mice are viable with no apparent abnormalities". In: *Developmental Biology* (1998). ISSN: 00121606. DOI: 10.1006/dbio.1998.9005.

[146] Damien F. Hudson et al. "Centromere protein B null mice are mitotically and meiotically normal but have lower body and testis weights". In: *Journal of Cell Biology* (1998). ISSN: 00219525. DOI: 10.1083/jcb.141.2.309.

[147] W. C. Earnshaw et al. "Molecular cloning of cDNA for CENP-B, the major human centromere autoantigen". In: *Journal of Cell Biology* (1987). ISSN: 00219525. DOI: 10.1083/jcb.104.4.817.

[148] L. E. Voullaire et al. "A functional marker centromere with no detectable alpha-satellite, satellite III, or CENP-B protein: Activation of a latent centromere?" In: *American Journal of Human Genetics* (1993). ISSN: 00029297.

[149] Theresa W. Depinet et al. "Characterization of neo-centromeres in marker chromosomes lacking detectable alpha-satellite DNA". In: *Human Molecular Genetics* (1997). ISSN: 09646906. DOI: 10.1093/hmg/6.8.1195.

[150] Owen J. Marshall et al. "Neocentromeres: New Insights into Centromere Structure, Disease Development, and Karyotype Evolution". In: (2008). ISSN: 00029297. DOI: 10.1016/j.ajhg.2007.11.009.

[151] Patrick Heun et al. "Mislocalization of the drosophila centromere-specific histone CID promotes formation of functional ectopic kinetochores". In: *Developmental Cell* (2006). ISSN: 15345807. DOI: 10.1016/j.devcel.2006.01.014.

[152] María José Mendiburo et al. "Drosophila CENH3 is sufficient for centromere formation". In: *Science* (2011). ISSN: 10959203. DOI: 10.1126/science.1206880.

[153] Meghan C. Barnhart et al. "HJURP is a CENP-A chromatin assembly factor sufficient to form a functional de novo kinetochore". In: *Journal of Cell Biology* (2011). ISSN: 00219525. DOI: 10.1083/jcb.201012017.

[154] Lars E T Jansen et al. "Propagation of centromeric chromatin requires exit from mitosis". In: *Journal of Cell Biology* 176.6 (2007), pp. 795–805. ISSN: 00219525. DOI: 10.1083/jcb.200701066.

[155] Dani L. Bodor et al. "Assembly in G1 phase and long-term stability are unique intrinsic features of CENP-A nucleosomes". In: *Molecular Biology of the Cell* (2013). ISSN: 10591524. DOI: 10.1091/mbc.E13-01-0034.

[156] Daniel R. Foltz et al. "Centromere-Specific Assembly of CENP-A Nucleosomes Is Mediated by HJURP". In: *Cell* (2009). ISSN: 00928674. DOI: 10.1016/j.cell.2009.02.039.

[157] Elaine M. Dunleavy et al. "HJURP Is a Cell-Cycle-Dependent Maintenance and Deposition Factor of CENP-A at Centromeres". In: *Cell* (2009). ISSN: 00928674. DOI: 10.1016/j.cell.2009.02.040.

[158] Yohta Fujita et al. "Priming of Centromere for CENP-A Recruitment by Human hMis18α, hMis18β, and M18BP1". In: *Developmental Cell* (2007). ISSN: 15345807. DOI: 10.1016/j.devcel.2006.11.002.

[159] Takeshi Hayashi et al. "Mis16 and Mis18 are required for CENP-A loading and histone deacetylation at centromeres". In: *Cell* (2004). ISSN: 00928674. DOI: 10.1016/j.cell.2004.09.002.

[160] Ben Moree et al. "CENP-C recruits M18BP1 to centromeres to promote CENP-A chromatin assembly". In: *Journal of Cell Biology* (2011). ISSN: 00219525. DOI: 10.1083/jcb.201106079.

[161] Silvia Dambacher et al. "CENP-C facilitates the recruitment of M18BP1 to centromeric chromatin". In: *Nucleus* (2012). ISSN: 19491042. DOI: 10.4161/nucl.18955.

[162] Elaine M. Dunleavy, Geneviève Almouzni, and Gary H. Karpen. "H3.3 is deposited at centromeres in S phase as a placeholder for newly assembled CENP-A in G phase." In: *Nucleus (Austin, Tex.)* (2011). ISSN: 19491042. DOI: 10.4161/nucl.2.2.15211.

[163] Yael Nechemia-Arbely et al. "DNA replication acts as an error correction mechanism to maintain centromere identity by restricting CENP-A to centromeres". In: *Nature Cell Biology* (2019). ISSN: 14764679. DOI: 10.1038/s41556-019-0331-4.

[164] Beth A. Sullivan and Gary H. Karpen. "Centromeric chromatin exhibits a histone modification pattern that is distinct from both euchromatin and heterochromatin". In: *Nature Structural and Molecular Biology* (2004). ISSN: 15459993. DOI: 10.1038/nsmb845.

[165] Susana Abreu Ribeiro et al. "A super-resolution map of the vertebrate kinetochore". In: *Proceedings of the National Academy of Sciences of the United States of America* (2010). ISSN: 00278424. DOI: 10.1073/pnas.1002325107.

[166] Jun-ichirou Ohzeki et al. "Breaking the HAC Barrier: Histone H3K9 acetyl/methyl balance regulates CENP-A assembly". In: *The EMBO Journal* 31.10 (2012), pp. 2391–2402. ISSN: 0261-4189. DOI: 10.1038/emboj.2012.82. URL: http://dx.doi.org/10.1038/emboj.2012.82.

[167] Teruaki Okada et al. "CENP-B Controls Centromere Formation Depending on the Chromatin Context". In: *Cell* (2007). ISSN: 00928674. DOI: 10.1016/j.cell.2007.10.045.

[168] Koichiro Otake et al. "CENP-B creates alternative epigenetic chromatin states permissive for CENP-A or heterochromatin assembly". In: *Journal of Cell Science* (2020). ISSN: 14779137. DOI: 10.1242/JCS.243303.

[169] F. Lyn Chan et al. "Active transcription and essential role of RNA polymerase II at the centromere during mitosis". In: *Proceedings of the National Academy of Sciences of the United States of America* (2012). ISSN: 00278424. DOI: 10.1073/pnas.1108705109.

[170] Delphine Quénet and Yamini Dalal. "A long non-coding RNA is required for targeting centromeric protein A to the human centromere". In: *eLife* (2014). ISSN: 2050084X. DOI: 10.7554/eLife.03254.

[171] Silvana Rošić, Florian Köhler, and Sylvia Erhardt. "Repetitive centromeric satellite RNA is essential for kinetochore formation and cell division". In: (2014). ISSN: 15408140. DOI: 10.1083/jcb.201404097.

[172] Jan H Bergmann et al. "Epigenetic engineering shows H3K4me2 is required for HJURP targeting and CENP-A assembly on a synthetic human kinetochore." In: *The EMBO Journal* 30.2 (2011), pp. 328–340. ISSN: 0261-4189. DOI: 10.1038/emboj.2010.329. URL: http://dx.doi.org/10.1038/emboj.2010.329{\%}5Cnpapers2://publication/doi/10.1038/emboj.2010.329.

[173] Iain M. Cheeseman and Arshad Desai. "Molecular architecture of the kinetochore-microtubule interface". In: (2008). ISSN: 14710072. DOI: 10.1038/nrm2310.

[174] Marion E. Pesenti, John R. Weir, and Andrea Musacchio. "Progress in the structural and functional characterization of kinetochores". In: 37 (2016), pp. 152–163. ISSN: 1879033X. DOI: 10.1016/j.sbi.2016.03.003.

[175] Kathryn Kixmoeller, Praveen Kumar Allu, and Ben E. Black. "The centromere comes into focus: from CENP-A nucleosomes to kinetochore connections with the spindle". In: *Open Biology* (2020). ISSN: 2046-2441. DOI: 10.1098/rsob.200051.

[176] Christopher W. Carroll, Kirstin J. Milks, and Aaron F. Straight. "Dual recognition of CENP-A nucleosomes is required for centromere assembly". In: *Journal of Cell Biology* (2010). ISSN: 00219525. DOI: 10.1083/jcb.201001013.

[177] Hidenori Kato et al. "A conserved mechanism for centromeric nucleosome recognition by centromere protein CENP-C". In: *Science* (2013). ISSN: 10959203. DOI: 10.1126/science.1235532.

[178] Samantha J. Falk et al. "CENP-C reshapes and stabilizes CENP-A nucleosomes at the centromere". In: *Science* (2015). ISSN: 10959203. DOI: 10.1126/science.1259308.

[179] Emanuela Screpanti et al. "Direct binding of Cenp-C to the Mis12 complex joins the inner and outer kinetochore". In: *Current Biology* (2011). ISSN: 09609822. DOI: 10.1016/j.cub.2010.12.039.

[180] Marcin R. Przewloka et al. "CENP-C is a structural platform for kinetochore assembly". In: *Current Biology* (2011). ISSN: 09609822. DOI: 10.1016/j.cub.2011.02.005.

[181] Kerstin Klare et al. "CENP-C is a blueprint for constitutive centromere-associated network assembly within human kinetochores". In: *Journal of Cell Biology* (2015). ISSN: 15408140. DOI: 10.1083/jcb.201412028.

[182] Arsen Petrovic et al. "Structure of the MIS12 Complex and Molecular Basis of Its Interaction with CENP-C at Human Kinetochores". In: *Cell* 167.4 (2016), 1028–1040.e15. ISSN: 10974172. DOI: 10.1016/j.cell.2016.10.005. URL: http://dx.doi.org/10.1016/j.cell.2016.10.005.

[183] Karen E. Gascoigne et al. "Induced ectopic kinetochore assembly bypasses the requirement for CENP-A nucleosomes". In: *Cell* (2011). ISSN: 00928674. DOI: 10.1016/j.cell.2011.03.031.

[184] Tatsuya Nishino et al. "CENP-T provides a structural platform for outer kinetochore assembly". In: *EMBO Journal* (2013). ISSN: 02614189. DOI: 10.1038/emboj.2012.348.

[185] Florencia Rago, Karen E. Gascoigne, and Iain M. Cheeseman. "Distinct organization and regulation of the outer kinetochore KMN network downstream of CENP-C and CENP-T". In: *Current Biology* (2015). ISSN: 09609822. DOI: 10.1016/j.cub.2015.01.059.

[186] Pim J. Huisin'T Veld et al. "Molecular basis of outer kinetochore assembly on CENP-T". In: *eLife* (2016). ISSN: 2050084X. DOI: 10.7554/eLife.21007.

[187] Emily a Foley and Tarun M Kapoor. "Microtubule attachment and spindle assembly checkpoint signalling at the kinetochore." In: *Nature reviews. Molecular cell biology* 14.1 (2013), pp. 25–37. ISSN: 1471-0080. DOI: 10.1038/nrm3494. arXiv: NIHMS150003. URL: http://www.pubmedcentral.nih.gov/articlerender.fcgi?artid=3762224{\&}tool=pmcentrez{\&}rendertype=abstract.

[188] Susan L. Kline et al. "The human Mis12 complex is required for kinetochore assembly and proper chromosome segregation". In: *Journal of Cell Biology* (2006). ISSN: 00219525. DOI: 10.1083/jcb.200509158.

[189] Chikashi Obuse et al. "A conserved Mis12 centromere complex is linked to heterochromatic HP1 and outer kinetochore protein Zwint-1". In: *Nature Cell Biology* (2004). ISSN: 14657392. DOI: 10.1038/ncb1187.

[190] Daniel A. Starr et al. "HZwint-1, a novel human kinetochore component that interacts with HZW10". In: *Journal of Cell Science* (2000). ISSN: 00219533.

[191] Hongmei Wang et al. "Human Zwint-1 specifies localization of Zeste White 10 to kinetochores and is essential for mitotic checkpoint signaling". In: *Journal of Biological Chemistry* 279.52 (2004), pp. 54590–54598. ISSN: 00219258. DOI: 10.1074/jbc.M407588200.

[192] Geert J.P.L. Kops et al. "ZW10 links mitotic checkpoint signaling to the structural kinetochore". In: *Journal of Cell Biology* 169.1 (2005), pp. 49–60. ISSN: 00219525. DOI: 10.1083/jcb.200411118.

[193] Iain M. Cheeseman et al. "The Conserved KMN Network Constitutes the Core Microtubule-Binding Site of the Kinetochore". In: *Cell* 127.5 (2006), pp. 983–997. ISSN: 00928674. DOI: 10.1016/j.cell.2006.09.039.

[194] Ronnie R. Wei, Jawdat Al-Bassam, and Stephen C. Harrison. "The Ndc80/HEC1 complex is a contact point for kinetochore-microtubule attachment". In: *Nature Structural and Molecular Biology* (2007). ISSN: 15459993. DOI: 10.1038/nsmb1186.

[195] Karen E. Gascoigne and Iain M. Cheeseman. "CDK-dependent phosphorylation and nuclear exclusion coordinately control kinetochore assembly state". In: *Journal of Cell Biology* 201.1 (2013), pp. 23–32. ISSN: 00219525. DOI: 10.1083/jcb.201301006.

[196] Peter Hemmerich et al. "Dynamics of inner kinetochore assembly and maintenance in living cells". In: *Journal of Cell Biology* 180.6 (2008), pp. 1101–1114. ISSN: 00219525. DOI: 10.1083/jcb.200710052.

[197] Soonjoung Kim and Hongtao Yu. "Multiple assembly mechanisms anchor the KMN spindle checkpoint platform at human mitotic kinetochores". In: *Journal of Cell Biology* (2015). ISSN: 15408140. DOI: 10.1083/jcb.201407074.

[198] Mi Sun Kwon et al. "CENP-C is involved in chromosome segregation, mitotic checkpoint function, and kinetochore assembly". In: *Molecular Biology of the Cell* (2007). ISSN: 10591524. DOI: 10.1091/mbc.E07-01-0045.

[199] Tetsuya Hori et al. "CCAN Makes Multiple Contacts with Centromeric DNA to Provide Distinct Pathways to the Outer Kinetochore". In: *Cell* (2008). ISSN: 00928674. DOI: 10.1016/j.cell.2008.10.019.

[200] Pablo Lara-Gonzalez, Frederick G. Westhorpe, and Stephen S. Taylor. "The spindle assembly checkpoint". In: (2012). ISSN: 09609822. DOI: 10.1016/j.cub.2012.10.006.

[201] Andrea Musacchio. *The Molecular Biology of Spindle Assembly Checkpoint Signaling Dynamics*. 2015. DOI: 10.1016/j.cub.2015.08.051.

[202] Sushama Sivakumar and Gary J. Gorbsky. *Spatiotemporal regulation of the anaphase-promoting complex in mitosis*. 2015. DOI: 10.1038/nrm3934.

[203] S Y Lee, S Rozenzhak, and P Russell. " H2A-Binding Protein Brc1 Affects Centromere Function in Fission Yeast". In: *Molecular and Cellular Biology* 33.7 (2013), pp. 1410–1416. ISSN: 0270-7306. DOI: 10.1128/MCB.01654-12. URL: http://mcb.asm.org/cgi/doi/10.1128/MCB.01654-12.

[204] M. Liskovykh et al. "A novel assay to screen siRNA libraries identifies protein kinases required for chromosome transmission". In: *Genome Res* 29.10 (2019), pp. 1719–1732. ISSN: 1549-5469 (Electronic) 1088-9051 (Linking). DOI: 10.1101/gr.254276.119. URL: https://www.ncbi.nlm.nih.gov/pubmed/31515286.

[205] Toyoaki Natsume et al. "Rapid Protein Depletion in Human Cells by Auxin-Inducible Degron Tagging with Short Homology Donors". In: *Cell Reports* 15.1 (2016), pp. 210–218. ISSN: 22111247. DOI: 10.1016/j.celrep.2016.03.001.

[206] Mathew E. Sowa et al. "Defining the Human Deubiquitinating Enzyme Interaction Landscape". In: *Cell* (2009). ISSN: 00928674. DOI: 10.1016/j.cell.2009.04.042.

[207] Jean Yves Bleuyard et al. "ChAM, a novel motif that mediates PALB2 intrinsic chromatin binding and facilitates DNA repair". In: *EMBO Reports* (2012). ISSN: 1469221X. DOI: 10.1038/embor.2011.243.

[208] H. S. Lee et al. "Effects of Anticancer Drugs on Chromosome Instability and New Clinical Implications for Tumor-Suppressing Therapies". In: *Cancer Res* 76.4 (2016), pp. 902–11. ISSN: 1538-7445 (Electronic) 0008-5472 (Linking). DOI: 10.1158/0008-5472.CAN-15-1617. URL: https://www.ncbi.nlm.nih.gov/pubmed/26837770.

[209] H. J. Motulsky. "GraphPad Statistics Guide". In: (Accessed 2020). URL: http://www.graphpad.com/guides/prism/7/statistics/index.htm.

[210] K G Ten Hagen et al. "Replication timing of DNA sequences associated with human centromeres and telomeres." In: *Molecular and Cellular Biology* (1990). ISSN: 0270-7306. DOI: 10.1128/mcb.10.12.6348.

[211] Sergei M. Mirkin. "Expandable DNA repeats and human disease". In: (2007). ISSN: 14764687. DOI: 10.1038/nature05977.

[212] Junhua Zhao et al. "Non-B DNA structure-induced genetic instability and evolution". In: (2010). ISSN: 1420682X. DOI: 10.1007/s00018-009-0131-2.

[213] Antoine Aze et al. "Centromeric DNA replication reconstitution reveals DNA loops and ATR checkpoint suppression". In: *Nature Cell Biology* 18.6 (2016), pp. 684–691. ISSN: 1465-7392. DOI: 10.1038/ncb3344. URL: http://www.nature.com/doifinder/10.1038/ncb3344{\%}5Cnhttp://www.ncbi.nlm.nih.gov/pubmed/27111843{\%}5Cnhttp://www.nature.com/doifinder/10.1038/ncb3344.

[214] Nicola Crosetto et al. "Nucleotide-resolution DNA double-strand break mapping by next-generation sequencing". In: *Nature Methods* 10.4 (2013), pp. 361–365. ISSN: 15487091. DOI: 10.1038/nmeth.2408. arXiv: NIHMS150003.

[215] Anne Helmrich et al. "Transcription-replication encounters, consequences and genomic instability". In: (2013). ISSN: 15459993. DOI: 10.1038/nsmb.2543.

[216] Rodrigo Bermejo, Mong Sing Lai, and Marco Foiani. "Preventing Replication Stress to Maintain Genome Stability: Resolving Conflicts between Replication and Transcription". In: (2012). ISSN: 10972765. DOI: 10.1016/j.molcel.2012.03.001.

[217] Andrés Aguilera and Tatiana García-Muse. "R Loops: From Transcription Byproducts to Threats to Genome Stability". In: (2012). ISSN: 10972765. DOI: 10.1016/j.molcel.2012.04.009.

[218] Natalay Kouprina et al. "A new generation of human artificial chromosomes for functional genomics and gene therapy". In: *Cellular and Molecular Life Sciences* 70.7 (2013), pp. 1135–1148. ISSN: 1420682X. DOI: 10.1007/s00018-012-1113-3.

[219] John J Harrington et al. "Formation of de novo centromeres and construction of first-generation human artificial microchromosomes". In: *Nature Genetics* 15.4 (1997), pp. 345–355. ISSN: 1546-1718. DOI: 10.1038/ng0497-345. URL: https://doi.org/10.1038/ng0497-345.

[220] Christine J. Farr et al. "Telomere-associated chromosome fragmentation: Applications in genome manipulation and analysis". In: *Nature Genetics* (1992). ISSN: 15461718. DOI: 10.1038/ng1292-275.

[221] K. E. Brown et al. "Dissecting the centromere of the human Y chromosome with cloned telomeric DNA". In: *Human Molecular Genetics* (1994). ISSN: 09646906. DOI: 10.1093/hmg/3.8.1227.

[222] R. Heller et al. "Mini-chromosomes derived from the human Y chromosome by telomere directed chromosome breakage". In: *Proceedings of the National Academy of Sciences of the United States of America* (1996). ISSN: 00278424. DOI: 10.1073/pnas.93.14.7125.

[223] Walter Mills et al. "Generation of an ~2.4 Mb human X centromere-based minichromosome by targeted telomere-associated chromosome fragmentation in DT40". In: *Human Molecular Genetics* (1999). ISSN: 09646906. DOI: 10.1093/hmg/8.5.751.

[224] Motonobu Katoh et al. "Construction of a novel human artificial chromosome vector for gene delivery". In: *Biochemical and Biophysical Research Communications* (2004). ISSN: 0006291X. DOI: 10.1016/j.bbrc.2004.06.145.

[225] Y. Kazuki et al. "Refined human artificial chromosome vectors for gene therapy and animal transgenesis". In: *Gene Therapy* (2011). ISSN: 09697128. DOI: 10.1038/gt.2010.147.

[226] Karla A. Henning et al. "Human artificial chromosomes generated by modification of a yeast artificial chromosome containing both human alpha satellite and single-copy DNA sequences". In: *Proceedings of the National Academy of Sciences of the United States of America* (1999). ISSN: 00278424. DOI: 10.1073/pnas.96.2.592.

[227] Masashi Ikeno et al. "Generation of human artificial chromosomes expressing naturally controlled guanosine triphosphate cyclohydrolase I gene". In: *Genes to Cells* (2002). ISSN: 13569597. DOI: 10.1046/j.1365-2443.2002.00580.x.

[228] N. Kouprina et al. "Cloning of human centromeres by transformation-associated recombination in yeast and generation of functional human artificial chromosomes". In: (2003). ISSN: 03051048. DOI: 10.1093/nar/gkg182.

[229] Nobutaka Suzuki et al. "Human artificial chromosomes constructed using the bottom-up strategy are stably maintained in mitosis and efficiently transmissible to progeny mice". In: *Journal of Biological Chemistry* (2006). ISSN: 00219258. DOI: 10.1074/jbc.M603053200.

[230] Daniela Moralli et al. "A novel human artificial chromosome gene expression system using herpes simplex virus type 1 vectors". In: *EMBO Reports* (2006). ISSN: 1469221X. DOI: 10.1038/sj.embor.7400768.

[231] Mohammad A. Mandegar et al. "Functional human artificial chromosomes are generated and stably maintained in human embryonic stem cells". In: *Human Molecular Genetics* (2011). ISSN: 09646906. DOI: 10.1093/hmg/ddr144.

[232] Daniela Moralli and Zoia L. Monaco. "Developing de novo human artificial chromosomes in embryonic stem cells using HSV-1 amplicon technology". In: *Chromosome Research* (2015). ISSN: 15736849. DOI: 10.1007/s10577-014-9456-2.

[233] Natalay Kouprina et al. "Human artificial chromosome-based gene delivery vectors for biomedicine and biotechnology." In: *Expert opinion on drug delivery* 11.4 (2014), pp. 517–35. ISSN: 1744-7593. DOI: 10.1517/17425247.2014.882314. URL: http://www.ncbi.nlm.nih.gov/pubmed/24479793.

[234] Megumi Nakano et al. "Inactivation of a Human Kinetochore by Specific Targeting of Chromatin Modifiers". In: *Developmental Cell* 14.4 (2008), pp. 507–522. ISSN: 15345807. DOI: 10.1016/j.devcel.2008.02.001. URL: http://dx.doi.org/10.1016/j.devcel.2008.02.001.

[235] Natalay Kouprina et al. "Organization of synthetic alphoid DNA array in human artificial chromosome (HAC) with a conditional centromere". In: *ACS Synthetic Biology* 1.12 (2012), pp. 590–601. ISSN: 21615063. DOI: 10.1021/sb3000436. arXiv: NIHMS150003.

[236] Yuichi Iida et al. "Human Artificial Chromosome with a Conditional Centromere for Gene Delivery and Gene Expression". In: *DNA Research* 17.5 (Aug. 2010), pp. 293–301. ISSN: 1340-2838. DOI: 10.1093/dnares/dsq020. eprint: https://academic.oup.com/dnaresearch/article-pdf/17/5/293/1012113/dsq020.pdf. URL: https://doi.org/10.1093/dnares/dsq020.

[237] Natalay Kouprina et al. "Human artificial chromosome (HAC) for measuring chromosome instability (CIN) and identification of genes required for proper chromosome transmission". In: *Experimental Cell Research* 387.2 (2020), p. 111805. ISSN: 0014-4827. DOI: https://doi.org/10.1016/j.yexcr.2019.111805. URL: http://www.sciencedirect.com/science/article/pii/S0014482719306937.

[238] Arun Mouli Kolinjivadi et al. "Smarcal1-Mediated Fork Reversal Triggers Mre11-Dependent Degradation of Nascent DNA in the Absence of Brca2 and Stable Rad51 Nucleofilaments". In: *Molecular Cell* (2017). ISSN: 10974164. DOI: 10.1016/j.molcel.2017.07.001.

[239] Rémi Buisson et al. "Breast Cancer Proteins PALB2 and BRCA2 Stimulate Polymerase η in Recombination-Associated DNA Synthesis at Blocked Replication Forks". In: *Cell Reports* 6.3 (2014), pp. 553 –564. ISSN: 2211-1247. DOI: https://doi.org/10.1016/j.celrep.2014.01.009. URL: http://www.sciencedirect.com/science/article/pii/S2211124714000102.

[240] F. Huang et al. "Inhibition of homologous recombination in human cells by targeting RAD51 recombinase". In: *Journal of Medicinal Chemistry* 55.7 (2012). ISSN: 00222623. DOI: 10.1021/jm201173g.

[241] David A. Alagpulinsa, Srinivas Ayyadevara, and Robert Joseph Shmookler Reis. "A Small-Molecule Inhibitor of RAD51 Reduces Homologous Recombination and Sensitizes Multiple Myeloma Cells to Doxorubicin". In: *Frontiers in Oncology* 4 (2014), p. 289. ISSN: 2234-943X. DOI: 10.3389/fonc.2014.00289. URL: https://www.frontiersin.org/article/10.3389/fonc.2014.00289.

[242] Sarah R. Hengel, M. Ashley Spies, and Maria Spies. "Small-Molecule Inhibitors Targeting DNA Repair and DNA Repair Deficiency in Research and Cancer Therapy". In: *Cell Chemical Biology* 24.9 (2017), pp. 1101 –1119. ISSN: 2451-9456. DOI: https://doi.org/10.1016/j.chembiol.2017.08.027. URL: http://www.sciencedirect.com/science/article/pii/S2451945617303252.

[243] Jin Akagi et al. "Real-time cell viability assays using a new anthracycline derivative DRAQ7®". In: *Cytometry Part A* (2013). ISSN: 15524922. DOI: 10.1002/cyto.a.22228.

[244] Isabel E. Wassing and Fumiko Esashi. "RAD51: Beyond the break". In: *Seminars in Cell and Developmental Biology* (2020). ISSN: 10963634. DOI: 10.1016/j.semcdb.2020.08.010.

[245] Thomas W. Glover et al. "DNA polymerase α inhibition by aphidicolin induces gaps and breaks at common fragile sites in human chromosomes". In: *Human Genetics* (1984). ISSN: 03406717. DOI: 10.1007/BF00272988.

[246] M. K. Shivji et al. "A region of human BRCA2 containing multiple BRC repeats promotes RAD51-mediated strand exchange". In: *Nucleic Acids Res* 34.14 (2006), pp. 4000–11. ISSN: 1362-4962 (Electronic) 0305-1048 (Linking). DOI: 10.1093/nar/gkl505. URL: https://www.ncbi.nlm.nih.gov/pubmed/16914443.

[247] Indri Erliandri et al. "Replication of alpha-satellite DNA arrays in endogenous human centromeric regions and in human artificial chromosome". In: *Nucleic Acids Research* (2014). ISSN: 13624962. DOI: 10.1093/nar/gku835.

[248] J. Y. Park et al. "Breast cancer-associated missense mutants of the PALB2 WD40 domain, which directly binds RAD51C, RAD51 and BRCA2, disrupt DNA repair". In: *Oncogene* (2014). ISSN: 14765594. DOI: 10.1038/onc.2013.421.

[249] Rémi Buisson et al. "Cooperation of breast cancer proteins PALB2 and piccolo BRCA2 in stimulating homologous recombination". In: *Nature Structural and Molecular Biology* (2010). ISSN: 15459993. DOI: 10.1038/nsmb.1915.

[250] Matthieu Schapira et al. "WD40 repeat domain proteins: A novel target class?" In: (2017). ISSN: 14741784. DOI: 10.1038/nrd.2017.179.

[251] F Hoppe-Seyler and K Butz. "Repression of endogenous p53 transactivation function in HeLa cervical carcinoma cells by human papillomavirus type 16 E6, human mdm-2, and mutant p53." In: *Journal of Virology* (1993). ISSN: 0022-538X. DOI: 10.1128/jvi.67.6.3111-3117.1993.

[252] V. Band et al. "Enhanced degradation of p53 protein in HPV-6 and BPV-1 E6-immortalized human mammary epithelial cells". In: *EMBO Journal* (1993). ISSN: 02614189. DOI: 10.1002/j.1460-2075.1993.tb05833.x.

[253] Claudia M.B. Carvalho and James R. Lupski. "Mechanisms underlying structural variant formation in genomic disorders". In: (2016). ISSN: 14710064. DOI: 10.1038/nrg.2015.25.

[254] Raphael Kopan et al. "A practical guide to evaluating colocalization in biological microscopy". In: *Am J Physiol Cell Physiol* 46202.300 (2011), pp. 723–742. ISSN: 0363-6143. DOI: 10.1152/ajpcell.00462.2010..

[255] Verena Hurst, Kenji Shimada, and Susan M. Gasser. "Nuclear Actin and Actin-Binding Proteins in DNA Repair". In: (2019). ISSN: 18793088. DOI: 10.1016/j.tcb.2019.02.010.

[256] Noa Lamm et al. "ATR and mTOR regulate F-actin to alter nuclear architecture and repair replication stress". In: *bioRxiv* (2018). DOI: 10.1101/451708.

[257] Predrag Jevtić et al. "Sizing and shaping the nucleus: Mechanisms and significance". In: (2014). ISSN: 09550674. DOI: 10.1016/j.ceb.2014.01.003.

[258] Allison B. Chambliss et al. "Simultaneously defining cell phenotypes, cell cycle, and chromatin modifications at single-cell resolution". In: *FASEB Journal* (2013). ISSN: 15306860. DOI: 10.1096/fj.12-227108.

[259] Jan H. Bergmann et al. "Epigenetic engineering: Histone H3K9 acetylation is compatible with kinetochore structure and function". In: *Journal of Cell Science* (2012). ISSN: 00219533. DOI: 10.1242/jcs.090639.

[260] Stefano Cardinale et al. "Hierarchical inactivation of a synthetic human kinetochore by a chromatin modifier". In: *Molecular Biology of the Cell* (2009). ISSN: 10591524. DOI: 10.1091/mbc.E09-06-0489.

[261] Nicholas J. Panzarino et al. "Replication gaps underlie BRCA deficiency and therapy response". In: *Cancer Research* (2021). ISSN: 15387445. DOI: 10.1158/0008-5472.CAN-20-1602.

[262] Christian Baarlink et al. "A transient pool of nuclear F-actin at mitotic exit controls chromatin organization". In: *Nature Cell Biology* (2017). ISSN: 14764679. DOI: 10.1038/ncb3641.

[263] Chenshu Liu, Ruijun Zhu, and Yinghui Mao. "Nuclear Actin Polymerized by mDia2 Confines Centromere Movement during CENP-A Loading". In: *iScience* (2018). ISSN: 25890042. DOI: 10.1016/j.isci.2018.10.031.

[264] Arthur R. Mitchell et al. "Epigenetic control of mammalian centromere protein binding: Does DNA methylation have a role?" In: *Journal of Cell Science* (1996). ISSN: 00219533.

[265] Yoshinori Tanaka, Hitoshi Kurumizaka, and Shigeyuki Yokoyama. "CpG methylation of the CENP-B box reduces human CENP-B binding". In: *FEBS Journal* (2005). ISSN: 1742464X. DOI: 10.1111/j.1432-1033.2004.04406.x.

[266] Rugang Zhang et al. "Formation of macroH2A-containing senescence-associated heterochromatin foci and senescence driven by ASF1a and HIRA". In: *Developmental Cell* (2005). ISSN: 15345807. DOI: 10.1016/j.devcel.2004.10.019.

[267] Rugang Zhang, Wei Chen, and Peter D. Adams. "Molecular Dissection of Formation of Senescence-Associated Heterochromatin Foci". In: *Molecular and Cellular Biology* (2007). ISSN: 0270-7306. DOI: 10.1128/mcb.02019-06.

[268] Kayoko Maehara, Kohta Takahashi, and Shigeaki Saitoh. "CENP-A Reduction Induces a p53-Dependent Cellular Senescence Response To Protect Cells from Executing Defective Mitoses". In: *Molecular and Cellular Biology* (2010). ISSN: 0270-7306. DOI: 10.1128/mcb.01318-09.

[269] Quan Zhu et al. "BRCA1 tumour suppression occurs via heterochromatin-mediated silencing". In: *Nature* (2011). ISSN: 00280836. DOI: 10.1038/nature10371.

[270] Artem V. Kononenko et al. "A portable BRCA1-HAC (human artificial chromosome) module for analysis of BRCA1 tumor suppressor function". In: *Nucleic acids research* (2014). ISSN: 13624962. DOI: 10.1093/nar/gku870.

[271] Céline Baldeyron et al. "HP1α recruitment to DNA damage by p150CAF-1 promotes homologous recombination repair". In: *Journal of Cell Biology* (2011). ISSN: 00219525. DOI: 10.1083/jcb.201101030.

[272] Nabieh Ayoub et al. "HP1-β mobilization promotes chromatin changes that initiate the DNA damage response". In: *Nature* (2008). ISSN: 14764687. DOI: 10.1038/nature06875.

[273] Adam G. Larson et al. "Liquid droplet formation by HP1α suggests a role for phase separation in heterochromatin". In: *Nature* (2017). ISSN: 14764687. DOI: 10.1038/nature22822.

[274] Amy R. Strom et al. "Phase separation drives heterochromatin domain formation". In: *Nature* (2017). ISSN: 14764687. DOI: 10.1038/nature22989.

[275] S. Sanulli et al. "HP1 reshapes nucleosome core to promote phase separation of heterochromatin". In: *Nature* (2019). ISSN: 14764687. DOI: 10.1038/s41586-019-1669-2.

[276] Amy R Strom et al. "HP1α is a chromatin crosslinker that controls nuclear and mitotic chromosome mechanics". In: *bioRxiv* (2020).

[277] Edward L. Huttlin et al. "The BioPlex Network: A Systematic Exploration of the Human Interactome". In: *Cell* (2015). ISSN: 10974172. DOI: 10.1016/j.cell.2015.06.043.

[278] Jean-Yves Bleuyard et al. "MRG15-mediated tethering of PALB2 to unperturbed chromatin protects active genes from genotoxic stress". In: *Proceedings of the National Academy of Sciences* 114.29 (2017), p. 201620208. ISSN: 0027-8424. DOI: 10.1073/pnas.1620208114. URL: http://www.pnas.org/lookup/doi/10.1073/pnas.1620208114.

[279] Christopher G. England, Haiming Luo, and Weibo Cai. "HaloTag Technology: A Versatile Platform for Biomedical Applications". In: *Bioconjugate Chemistry* (2015). ISSN: 15204812. DOI: 10.1021/acs.bioconjchem.5b00191.

[280] E. Miron et al. "Chromatin arranges in filaments of blobs with nanoscale functional zonation". In: *bioRxiv* (2019).

[281] Nathan C. Shaner et al. "A bright monomeric green fluorescent protein derived from Branchiostoma lanceolatum". In: *Nature Methods* (2013). ISSN: 15487091. DOI: 10.1038/nmeth.2413.

[282] Tomomi Kiyomitsu, Chikashi Obuse, and Mitsuhiro Yanagida. "Human Blinkin/AF15q14 Is Required for Chromosome Alignment and the Mitotic Checkpoint through Direct Interaction with Bub1 and BubR1". In: *Developmental Cell* (2007). ISSN: 15345807. DOI: 10.1016/j.devcel.2007.09.005.

[283] Tomomi Kiyomitsu et al. "Inner centromere formation requires hMis14, a trident kinetochore protein that specifically recruits HP1 to human chromosomes". In: *Journal of Cell Biology* (2010). ISSN: 00219525. DOI: 10.1083/jcb.200908096.

[284] Sonia Javan Moghadam-Kamrani and Khandan Keyomarsi. "Synchronization of the cell cycle using lovastatin". In: *Cell Cycle* (2008). ISSN: 15514005. DOI: 10.4161/cc.6364.

[285] Eleanor Wendy Trotter and Iain Michael Hagan. "Release from cell cycle arrest with Cdk4/6 inhibitors generates highly synchronized cell cycle progression in human cell culture". In: *Open Biology* (2020). DOI: 10.1098/rsob.200200.